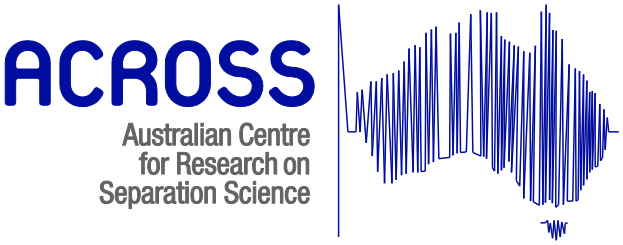

RELATING STARCH STRUCTURE IN BREAKFAST CEREALS AND RICE TO THEIR DIGESTIBILITY

Presented by:

Matthew Paul Van Leeuwen

Master of Science (Honours) Medicine

Principal Supervisor: Prof. Jens Coorssen[1,2]

Co-Supervisors: Dr Marion Gaborieau[2,3], Dr Patrice Castignolles[3], Dr Rachelle Ward[4]

[1] Western Sydney University (WSU), School of Medicine

[2] WSU, Molecular Medicine Research Group (MMRG)

[3] WSU, School of Science and Health, Australian Centre for Research On Separation Science (ACROSS)

[4] NSW Department of Primary Industries

Western Sydney University
2016

Acknowledgements

I would like to acknowledge my family, friends and associates that made this Master's thesis possible. Bear with me as I attempt to make this emotional tribute, one of only a few I expect to make in my lifetime.

First I would like to acknowledge my supervisors who have guided me along in my journey. Prof. Jens Coorssen, my primary supervisor, who's support allowed me the opportunity to undertake this research as well as providing insightful discussion and extensive encouragement in my research endeavours. Despite a busy schedule he always managed to stay on top of whatever I threw his way. I would also like to thank my co-supervisors, Dr Marion Gaborieau and Dr Patrice Castignolles, who have gone above and beyond in their efforts to teach and guide me during my Master's research. Their dedication and commitment to the research and support of not only myself but an entire group of postgraduates and undergraduates is a testament to their passion for research and improving the lives of others. I am grateful for the opportunity to work with you both.

To my parents, Lee Anne and Leonard, thank you for your unwavering support in all my endeavours over the last 24 years and encouraging me to do my best in all that I attempt. Thank you for providing for and supporting me throughout the years with a seemingly unlimited supply of cooked food, frozen food, and reheated food. Maybe one day the freeloading money pit will move out.

To my wife, Penny, you have had to put up with a lot of crap over the past 4+ years but the fact that we are getting married seems to indicate that it didn't faze you, I'll take that as my cue to continue being a pain...out of love of course. Your positivity and incessant smiling kept me positive and on track, while your relaxed attitude also forced me to take breaks when it was clear (though not to me) that a break was what I needed. Thank you also for the constant supply of beverages of the caffeinated and carbonated variety and a steady supply of late night dinner deliveries when I was stuck working with no food and an empty wallet. I look forward to the years to come together.

To the 1.11 crew, Joel, Alison and Michelle. After forcing my way into the office, a healthy competition blossomed as to who was the best, who was the worst and who was looking at whom. Most would argue that Joel (best buddy) is in fact the worst (but also the self-proclaimed best), Michelle was the best and that everyone was in fact looking at Alison. Looking past our disruptive yet productive workspace, each of you has had a positive impact in my time during my Master's. Joel the worst, thank you for your help in almost everything separation based, including the construction of advanced filtering apparatus, understanding the dreams of mathematicians (dispersity) and the multiple restarts of my CE experiments. Congratulations, you now have experience with another 'water soluble' polysaccharide. Michelle the best, former leader of the DC faction, thank you for the opportunity to start my research journey as your student. We both moved on to the characterisation of starch as the basis of our respective Master's projects. This may have been a poor decision on our part, sugars seem to be much more behaved. Despite this, working alongside you was an excellent experience. Alison, the former group leader whom we are all looking at, thank you for not only the science and research based assistance you have provided but also the much appreciated supply of healthy snacks, including chocolate, cookies, chips and Bistek Tagalog. You also taught me the correct storage position for micropipettes and you were my number one unpaying IT client…though I do not thank you for this. To all of 1.11, despite the seemingly questionable interactions some may observe from us, the 1.11 crew has truly made my experience the best I could have hoped for.

I would like to thank Ric and Tim, the two workhorses keeping the advanced materials characterisation facility (AMCF) running. They have both been extremely helpful in training me in both the practical and theoretical aspects of the instruments that were made available as well as providing insightful discussions on how I could enrich my research through other characterisation techniques.

I would like to thank Rachelle and Laura, who have been very helpful with insightful discussions into the characterisation and digestibility of starch. As part of the Department of Primary Industries (Yanco, NSW, Australia) they also provided the rice samples explored in this work, allowing me the opportunity to work on unique samples produced from specialized breeding programs making my results all the more interesting.

I would like to thank Jitendra and Elliot from the Bragg Institute at ANSTO for their help, discussion and expertise in everything scattering and diffraction. They were instrumental (ha!) in the success of my research grant application to run SAXS experiments at ANSTO and provided exceptional guidance whenever I had questions. They were extremely helpful in the art of peak fitting during my candidature. My experience working at ANSTO was fantastic and I am hopeful of the opportunity to do it again in the future.

Thank you to J.Lee, my fellow DC faction member and Maëlie, my partner in XRD. Thankyou also to the many other members of the Parramatta macromolecular characterisation who have made my experience...interesting including, Coco, Thibaut, Lucie, Melissa, Aaron, Adam, JBL, Michael Jimmy Bob Stan Lee and Elizabeth.

Statement of Authentication

The work presented in this thesis is, to the best of my knowledge and belief, original except as acknowledged in the text. I hereby declare that I have not submitted this material, either in full or in part, for a degree at this or any other institution.

.....

Matthew Paul Van Leeuwen

2016

Research Output of Thesis

Publication from research training:

1. Separation of amylose and amylopectin using capillary electrophoresis, MP Van Leeuwen, JJ Thevarajah, R Ward, P Castignolles, M Gaborieau, in preparation.
2. Determination of the distributions of degrees of acetylation of chitosan. JJ Thevarajah, MP Van Leeuwen, H Cottet, P Castignolles, M Gaborieau, International Journal of Biological Macromolecules (IF 3.1, top 20 % in Polymer Science), 2017, **95**, p. 40-48
3. Quantification of sugars in breakfast cereals using capillary electrophoresis, MR Toutounji, MP Van Leeuwen, JD Oliver, AK Shrestha, P Castignolles, and M Gaborieau, *Carbohydrate Research* (IF 1.8, top 45 % of Applied Chemistry), 2015, **408**: p. 134-141.

Oral presentations as presenter:

1. Molecular characterisation of starch by NMR and FT-IR spectroscopies, and X-ray diffraction, **M Van Leeuwen**, M Toutounji, J Mata, E Gilbert, A Shrestha, L Pallas, R Ward, P Castignolles, M Gaborieau, 2015 International Chemical Congress of Pacific Basin Societies (Pacifichem), Honolulu, USA, December 2015.
2. Capillary electrophoresis of carbohydrates: from the quantification of sugars in breakfast cereals to the characterisation of starch in rice, **MP Van Leeuwen**, MR Toutounji, JR Coorssen, P Castignolles, M Gaborieau, Royal Australian Chemical Institute (RACI) Annual Honours and Master-by-Research Student Presentation Evening, Sydney, Australia, November 2015.
3. Molecular characterisation of starch by NMR and FT-IR spectroscopies, and X-ray diffraction, **M Van Leeuwen**, M Toutounji, J Mata, E Gilbert, A Shrestha, L Pallas, R Ward, P Castignolles, M Gaborieau, Australian Centre for Research on Separation Science (ACROSS) Gathering, Hobart, Australia, July 2015.

Posters as presenter:

1. (Supra)molecular characterization of starch in rice by NMR and SAXS, M Toutounji, **M Van Leeuwen**, J Mata, E Gilbert, L Pallas, R Ward, P Castignolles, M Gaborieau, *Sydney Surface and Soft Stuff meeting (SASSY)*, Kensington, Australia, June 2016.
2. Characterisation of branching in starch using capillary electrophoresis, **MP Van Leeuwen**, JJ Thevarajah, JR Coorssen, M Gaborieau, P Castignolles, *(Solid-state) NMR and Polymers Symposium*, Kensington, Australia, April 2016.
3. Quantification of sugars in breakfast cereals using capillary electrophoresis, M Toutounji, **M Van Leeuwen**, J Oliver, A Shrestha, M Gaborieau, P Castignolles, *Pacifichem*, Honolulu, USA, December 2015.
4. Quantification of sugars in breakfast cereals using capillary electrophoresis with direct UV detection, **MR Toutounji**, **MP Van Leeuwen**, JD Oliver, AK Shrestha, M Gaborieau, P Castignolles, *Virtual Symposium on Applied Separation Science (VSASS)*, online, May 2015.

5. Characterisation of starch by solid-state NMR, FT-IR spectroscopy and X-ray diffraction, **M Van Leeuwen**, **M Toutounji**, A Shrestha, R Wuhrer, J Mata, E Gilbert, P Castignolles, M Gaborieau, *6th UWS NMR, MRI and Diffusion Symposium*, Campbelltown, Australia, March 2015.

Oral presentations presented by others:

1. Pushing FFF further with a second dimension of capillary electrophoresis, **JD Oliver**, KP Bierbaum, MP Van Leeuwen, AR Maniego, M Gaborieau, P Castignolles, N Delaunay, SKR Williams, *FFF of branched polymers: 18th international symposium on field- and flow-based separations*, Dresden, Germany, May 2016.
2. Starch structure and digestibility in rice and breakfast cereals, MR Toutounji, MP Van Leeuwen, J Mata, AK Shrestha, L Pallas, R Ward, EP Gilbert, P Castignolles, **M Gaborieau**, *65th Australian Cereal Chemistry Conference (AGSA 2015)*, Coogee, Australia, September 2015.
3. Quantification of sugars in breakfast cereals using capillary electrophoresis with direct UV detection, **MR Toutounji**, MP Van Leeuwen, JD Oliver, AK Shrestha, M Gaborieau, P Castignolles, *AGSA 2015*, Coogee, Australia, September 2015.
4. Probing molecular dynamics and structure in polysaccharides with spectroscopy in the solid state, JJ Thevarajah, MR Toutounji, MP Van Leeuwen, J Mata, EP Gilbert, MJ Gidley, HW Spiess, R Graf, P Castignolles, **M Gaborieau**, *35th Australasian Polymer Symposium (35APS)*, Gold Coast, Australia, July 2015.

Posters presented by others:

1. (Supra)molecular characterization of starch in rice by NMR and SAXS, **M Toutounji**, Matthew Van Leeuwen, Jitendra Mata, Elliot Gilbert, Laura Pallas, Rachelle Ward, Patrice Castignolles, Marianne Gaborieau, *(Solid-state) NMR and Polymers Symposium*, Kensington, Australia, April 2016.
2. Characterisation of branching in starch using capillary electrophoresis, M Van Leeuwen, **I Thevarajah**, J Coorssen, M Gaborieau, P Castignolles, *RACI Polymer Research Symposium*, University of New South Wales, Sydney, Australia, November 2015.

Professional Societies/Groups:

1. Chair of student organizing committee, Royal Australian Chemical Institute (RACI) Research and Development Topics Conference, 2016
2. Australasian Grain Science Association, 2015 - Present
3. Golden Key International Honour Society, 2012 - Present
4. Royal Australian Chemical Institute – Member (2015 - present) and Western Sydney University student representative for NSW Analytical and Environmental chemistry group (2016 - present)
5. European Polysaccharide Network of Excellence, 2015 - Present
6. Molecular Medicine Research Group, Western Sydney University, 2013 - Present

7. Australian Centre for Research on Separation Science, 2013 - Present
8. Society of Academic Research, Western Sydney University community group, 2014 - 2015

Attended Conferences/Meetings with no presentations:

1. Australasian Polymer Summer School, University of Queensland, February 2016
2. Molecular Medicine Research Group Annual Meeting, Western Sydney University, Campbelltown, September 2015
3. 65th Australian Cereal Chemistry Conference, Coogee, Australia, September 2015

Awards/Competitive Grants:

1. 2016: Small angle X-ray scattering equipment time grant from Australian Nuclear Science and Technology Organisation: Matthew Van Leeuwen, Marianne Gaborieau, Elliot Gilbert, Jitendra Mata. 5 days – AUD 6,900
2. 2015: Graduate student travel grant from Molecular Medicine Research Group: Matthew Van Leeuwen. AUD 2,000

Table of Contents

Table of Tables

Table of Figures

Table of Abbreviations

μ	Electrophoretic mobility
μ_m	Moment-average electrophoretic mobility
μ_w	Weight-average electrophoretic mobility
μ_z	Electrophoretic mobility of the z^{th} molecule
AACCI	American Association of Cereal Chemists International
Am	Amylose
Ap	Amylopectin
AsFlFFF	Asymmetric flow field-flow fractionation
ATR	Attenuated total reflectance
ATR-FTIR	Attenuated total reflection Fourier-transform infrared
BMI	Body mass index
BS	Background subtraction
C^*	Critical polymer concentration
CE	Free solution capillary electrophoresis
CE-CC	Capillary electrophoresis in the critical conditions
CI	Crystalline index
CI_{1047}	Crystalline index from the ratio of peak heights at 1047 and 1022 cm^{-1}
CI_{995}	Crystalline index from the ratio of peak heights at 995 and 1022 cm^{-1}
CP-MAS NMR	Cross-polarization magic-angle-spinning nuclear magnetic resonance
D	Dispersity
$D(1,0)$	Dispersity calculated as the ratio of first and zeroth order moments divided by the ratio of zeroth and negative first order moments of the distribution

$D(2,0)$	Dispersity calculated as the ratio of the second and first order moments divided by the ratio of first and zeroth order moments of the distribution
$D(3,0)$	Dispersity calculated as the ratio of third and second order moments divided by the ratio of second and first order moments of the distribution
DAD	Diode array detector
DB	Average degree of branching
DMSO	Dimethyl sulfoxide
DNA	Deoxyribonucleic acid
DPI	Department of Primary Industries
EOF	Electroosmotic flow
FSANZ	Food Standards Australia New Zealand
FSD	Fourier self-deconvolution
FTIR	Fourier-transform infrared
GI	Glycaemic index
GL	Glycaemic load
GPC	Gel permeation chromatography
HH	Head house
HPLC	High performance liquid chromatography
IA-CE	Iodine affinity capillary electrophoresis
k_{ad}	Rate of adsorption
k_{de}	Rate of desorption
LC-CC	Liquid chromatography in the critical conditions
l_d	Length to detector
LiBr	Lithium bromide
l_t	Total length
MALS	Multi angle light scattering
NaOH	Sodium hydroxide

NMR	Nuclear magnetic resonance
NSW	New South Wales
OECD	Organisation for Economic Co-operation and Development
PAA	Poly(acrylic acid)
PNaA	Poly(sodium acrylate)
$\boldsymbol{q}$	Scattering vector
R^2	Correlation coefficient
RDS	Rapidly digestible starch
RH	Relative humidity
RI	Refractive index
rpm	Revolutions per minute
RS	Resistant Starch
RSD	Relative standard deviation
RT	Room temperature
SANS	Small angle neutron scattering
SAXS	Small angle X-ray scattering
SDev	Dispersity of the electrophoretic mobility distribution calculated as the standard deviation taking the weight-average electrophoretic mobility as a reference
SDS	Slowly digestible starch
SEC	Size exclusion chromatography
T	Temperature
t_{eof}	Migration time of EOF
t_m	Migration time
UV	Ultraviolet
UV-Vis	Ultraviolet and visible light
V	Voltage

$W(\mu)$	Weight distribution of electrophoretic mobility
WHO	World Health Organisation
XRD	Powder X-ray diffraction

Abstract

Grain based food products are rich in the complex carbohydrate starch and represent a major source of dietary energy for the majority of the world's population. These products play a significant role in digestive health, making them ideal targets for weight management and the prevention and management of obesity related illnesses such as type 2 diabetes and cardiovascular disease. Understanding the digestibility of grain products and improving their dietary quality is important for improving dietary management. However, the complex matrices of these products have resulted in poorly understood digestibility mechanisms.

This project aims to characterise starch structure in grain foods to improve our understanding of their digestibility. In this work starches were employed as model samples with which to set up and optimise characterisation methods. Rice flour samples were then characterised. Rice has a relatively simple composition (90 % starch) allowing for a less complex model with which to understand the relationship between starch structure and functional properties of starch such as digestibility. Breakfast cereals were also explored, allowing for an investigation into the characterisation of starch in a more complex sample matrix.

Starch has multiple hierarchical structural levels on both the molecular and supramolecular level that need to be understood to comprehend the various models for starch digestibility. This has involved the mastering of a variety of techniques to characterise different structural levels of starch. Free solution capillary electrophoresis (CE) was employed in characterising the molecular of starch structure through the determination of amylose content and the investigation of heterogeneity of branching. The supramolecular structure of starch must also be characterised, with supramolecular arrangements introducing steric factors to digestibility. Both short- and long-range crystallinity were explored by a variety of techniques. Short-range order was investigated by Fourier-transform infrared (FTIR) spectroscopy, while long-range order was explored using X-ray diffraction (XRD) and small angle X-ray scattering (SAXS).

CE is a powerful separation technique that has been shown to be useful for the separation of amylose and amylopectin, the two macromolecular components of starch, by taking advantage of iodine binding and visible light detection. The amylose content of starch has been

linked with digestive properties; therefore, accurate characterisation is an important step in understanding digestive properties. Separation approaches overcome the interference caused by overlapping absorbance bands in traditional approaches, allowing for a more accurate quantification. Previous applications of the CE method in the literature had employed non-ideal dissolution conditions, introducing inaccuracy into analysis. In this thesis the incorporation of improved dissolution conditions in the methodology was explored. A reduced sample concentration was found to be ideal, reducing aggregation. The use of anhydrous DMSO with the addition of a hydrogen bond disruptor, as well as high dissolution temperatures were also determined to be essential in obtaining a complete dissolution thus allowing for accurate characterisation.

Using a new methodology developed by our research team, the heterogeneity of branching in starch was also explored by CE, assessing the broadness of resulting electrophoretic mobility distributions through the value of their dispersity. Results using this methodology indicated an extremely high degree of heterogeneity of branching in starch. Further optimisation of the separation method will allow the heterogeneity of amylose and amylopectin to be investigated independently.

The determination of short-range order by FTIR spectroscopy is based on the ratio of infrared bands; however, the assignments of these bands are poorly understood. In this work, the improvement of spectral resolution, and the correlation of crystalline index values with published crystallinity values were explored. Transmission mode FTIR spectra measured at cryogenic temperatures yielded the best resolution of the peaks of interest with deconvolution also yielding slight improvements to spectral resolution. The influence of improved spectral resolution on the determined crystalline index was highly variable. Crystalline index values had a loose correlation with published crystallinity values in some cases; however, as a measure of crystallinity, this method was deemed to be suitable in cases where only an estimate is required. The determination of long-range order by XRD was also explored, investigating the influence of data processing and software packages in peak fitting approaches for crystallinity determinations. The different algorithms that the software packages employed impacted on the peak fitting, baseline fitting and resulting crystallinity determinations.

SAXS has proven to be a valuable tool in the analysis of lamellar structures in starch. The relation between lamellar structure of maize starches and amylose content was explored. A

decrease in the relative amount and size of semi-crystalline structure was observed with increasing amylose content. This trend is similar to those found in the literature in other plant starches. The same trend between varying amylose content and semi-crystalline structural features was also observed in rice flour for the first time. Degree of branching (as measured by another member of our research team) was also investigated in relation to other structural features. Degree of branching showed a trend with varying amylose content as well as a relationship with semi-crystalline structure. These relationships are expected to rely heavily on the amylose content itself and also on the branching structure of the amyloses present.

In conclusion, the starch structure is complex and every structural level influences digestive properties. A number of characterisation methods were explored in this work, aiming to develop a set of tools that may be used in understanding how starch structure at different levels relates to digestibility. Identifying the links between starch structure and digestibility creates opportunities for applications within the food industry to alter the digestion rates of foods and food ingredients. These relationships may then be used in more efficiently producing healthier food products to combat the issue of rising obesity rates and associated illnesses.

Chapter 1 Introduction - Carbohydrates in society

1.1 The need to study carbohydrates

Grain based foods are a major component of the modern human diet, and have been a dietary staple for thousands of years. A major staple for two-thirds of the world population, rice is an important crop in the nutrition intake of the global population. Rice is comprised primarily of starch and water along with small amounts of proteins and lipids [1]. In the industrial era of today, the modern interpretation of grain based foods has become that of the highly processed variety, keeping up with the demand required by a growing population as well as matching the desires of the market for easy and palatable foods. Grains are harvested and modified to produce many of the foods we as a global society are now accustomed to. An example of this industrial trend is the proliferation of grain breakfast cereals in Western societies. These breakfast cereal products make use of grains that have been processed by milling and heat treatments, which are then made more palatable by additives such as sugars for sweetening. These breakfast cereals are a common form in which people consume grains in Western nations. In Australia, breakfast cereals are consumed by 50 % of the adult population who consume breakfast at least five days a week [2]. The proliferation of modified grain based products can also be seen in their use as filler materials or thickening agents in not only food products such as sauces, soups but even in other industrial applications such as paints and cosmetics. In these cases, processing and modifications offer unique starch properties ideal for multiple end uses.

In the last 3 decades, significant changes in the industrial practice of food processing have increased dependence on highly processed grain based foods. This has coincided with factors such as reduced physical activity levels to result in Australia being declared as an obese nation, fuelling the global obesity epidemic [3, 4]. Carbohydrate rich foods and their influence on weight gain [5, 6], and insulin resistance [7] have been widely studied. Classification of the major

dietary carbohydrates is shown in Table 1. Rice and breakfast cereals are carbohydrates rich foods comprised primarily of sugars and starch, the two main carbohydrates contributing to energy intake. Consumption of rice and breakfast cereals is widespread. Their impact on key health factors such as cardiovascular and digestive health make them an ideal target to address the obesity epidemic and associated chronic diseases.

Table 1 The major dietary carbohydrates (adapted from [8, 9])

Class (DP)[a]	**Subgroup**	**Examples**
Sugars (1-2)	Monosaccharide	Glucose, Fructose, Galactose
	Disaccharides	Sucrose, Lactose, Maltose
	Polyols	Sorbitol, Xylitol, Lactitol
Oligosaccharides (3-9) (short-chain carbohydrates)	Malto-oligosaccharides (α-glucans)	Maltodextrins
	Non-α-glucan oligosaccharides	Raffinose, Fructo oligosaccharides, Polydextrose
Polysaccharides (≥10)	Starch (α-glucans)	Amylose, amylopectin, modified starches
	Non-starch polysaccharides	Cellulose, Hemicellulose, Plant gums

[a] Degree of polymerization or number of sugar units

Starch structure plays an important role in the quality and digestive properties of grain based foods [10]. In this study, the structure of starch is characterised in rice varieties with the aim to develop and compare a variety of characterisation techniques to appreciate the diversity of starch structures and their role in digestibility. If a diversity of characteristics can be identified and are capable of explaining a key consumer driver, there is a certain opportunity to employ these techniques in a rice breeding program. With rice as an unprocessed model these techniques were also applied to breakfast cereals, testing the suitability of characterisation techniques to processed foods that have undergone both chemical and physical modification. Understanding the digestibility of such products requires characterisation of all components in the food; however, this work focussed only on the starch component. Measuring starch digestibility is a point of contention in the scientific community

with pros and cons for both *in vivo* and *in vitro* methods available. There is the reality of error in digestibility studies by any method, and this is exacerbated in *in vivo* testing with person-to-person variation. The number of repeats and high cost associated with obtaining a statistically relevant dataset by *in vivo* methods makes *in vitro* alternatives a more attractive option[10, 11]. The repeatability and low cost of *in vitro* methods makes them ideal for comparative analysis in investigating digestibility. This thesis aims to contribute to the application of analytical techniques to the characterisation of starch, and the subsequent correlation of starch properties with not only the preparative conditions of samples but also their digestive properties obtained by *in vitro* analysis.

1.2 Research in carbohydrate foods

1.2.1 Obesity

The concept of overweight and obesity are defined by the World Health Organisation (WHO) as abnormal or excessive fat accumulation that may impair health [3]. Body mass index (BMI) values are commonly used in the determination of obese populations, with individuals whose BMI values are above 25 considered overweight and those greater than 30 considered obese. Over the last three decades the prevalence of obesity has rapidly increased to the point that the World Health Organisation classified obesity as a global epidemic in 1997 [12], followed by classification as a disease in 2013 by the American Medical Association [13].

Global obesity rates have been rising rapidly over the last few decades (Figure 1). Australian surveys reveal a trend of increasing rates of obesity and overweight in both the adult and child populations. Overweight and obesity in adults has risen from 56 % in 1995 to 63 % in 2011-12 [14]. In the child population, 19-23 % of children and adolescents were overweight or obese in 1995-97 [15], which has risen slightly to 25 % in 2011-12 [14].

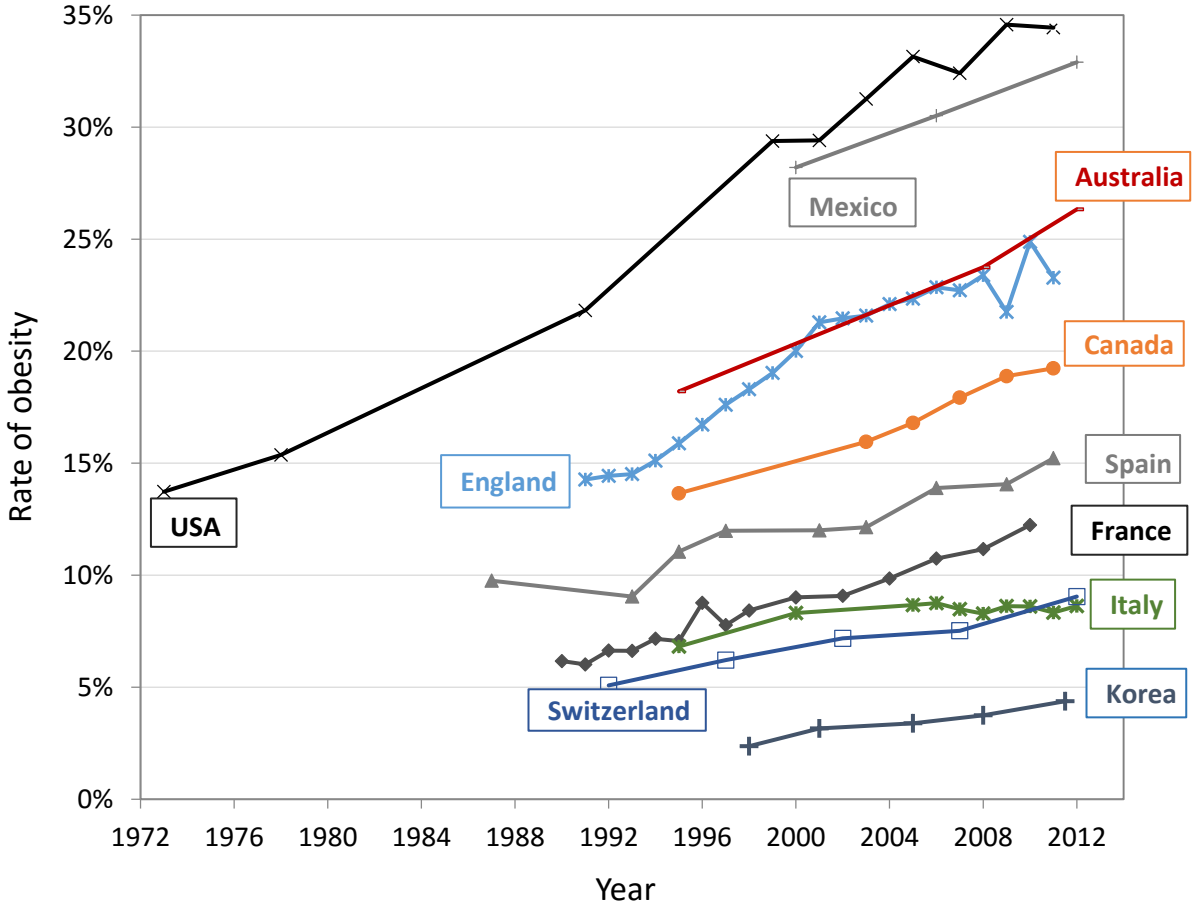

Figure 1 Age- and gender-adjusted rates of obesity using the 2005 Organisation for Economic Co-operation and Development (OECD) standard population [4]

Negative health consequences associated with obesity have been widely studied. These vary from non-fatal medical conditions such as skin problems and arthritis which can affect an individual's lifestyle, to increased risks factors for conditions such as cardiovascular disease, type 2 diabetes and even premature death [12, 16]. With the rising rates of obesity worldwide, dietary management must be improved and preventative measures put in place to force a change in this trend. One opportunity to counter these increasing rates, and reduce the risk of an unhealthy population, could involve improving the dietary quality of foods and reducing the energy intake in the broad population. Alternatively, other approaches could also be successful in achieving a similar outcome such as increased activity, though this can be limited by other health factors.

1.2.2 Nutrient intake, weight management and obesity

From a nutritional perspective, weight gain typically occurs when energy intake exceeds energy expenditure through both physical activity and basal metabolism. When excess energy is introduced into the body, it accumulates in the body as adipose tissue. This energy balance is complex and is also significantly affected by a number of other factors such as genetic, environmental and social influences [5, 6]. The most significant causes of this energy imbalance are seen in the form of excess food intake, as well as lack of physical activity [16]. Genetic influences play a seemingly smaller role; while more than 400 genes have been associated with bodyweight regulation, there are few people worldwide for whom obesity is a result of genetic mutation [16].

Food can be generally broken down into three macronutrients: protein, carbohydrates and fats/lipids. In recent times and as a result of modern life, the consumption of carbohydrate rich foods has drastically increased because they are readily available and accepted as part of the 'average' diet [17]. The 'healthy' carbohydrate rich foods based on whole grains such as breads, pasta and rice are a source of both digestible and indigestible carbohydrates. 'Unhealthy' or highly processed foods such as potato chips, confectionary and pastries tend to have greater energy and nutrient densities than 'healthy' products. This availability of such energy dense foods is likely a contributing factor in the obesity epidemic, though increasing carbohydrate consumption may also play a role. Excess carbohydrate intake has been shown to affect the levels of and sensitivity to insulin, a hormone that regulates blood glucose levels in the bloodstream. This can result in raised blood glucose levels and increased storage of excess energy as fat, indicating that this passive increase in carbohydrate intake is a possible factor in the current obesity epidemic [7].

1.3 The biopolymer: Starch and its structure

1.3.1 Nutritional definitions of starch

Carbohydrates are a major component of the human diet, providing the body with a means of easily digestible energy along with a range of health benefits, as well as potential health risks [18]. Starch is the main dietary carbohydrate. Starch is a highly abundant polysaccharide acting as the primary energy intake for humans, and as a major energy storage system in photosynthesising plants [19].

In the context of digestion and the human diet, starch is categorised in three fractions according to their rate of digestion; rapidly digestible starch (RDS), slowly digestible starch (SDS) and resistant starch (RS) [20]. The proportion of these starch fractions and their proportions within starch-based foods play a significant role in digestive properties and health benefits of the food. RDS is quickly digested to glucose, with complete digestion within 20 minutes of consumption. A high proportion of RDS is common in highly processed foods such as breads and cakes. SDS has a slower digestion rate and is defined as being completely digested between 20 and 120 minutes. RS defines the starch and starch degradation products resisting digestion in the small intestine and fermenting in the large intestine after 120 minutes [21, 22].

Four types of RS have been identified, categorised according to their chemical and physical characteristics. RS type 1 is a physically inaccessible starch found in unprocessed starchy foods. RS type 2 refers to native resistant starch granules. RS type 3 refers to retrograded starch. RS type 4 is highly modified starch. The types and quantity of these types of RS in starchy products vary depending on a number of factors, especially processing which plays a major role in type 1 and type 4 fractions. RS is considered a constituent of dietary fibre and carries a number of health benefits such as improved glycaemic and insulinaemic responses, improved bowel health [21], promoting bowel regularity [23] and prevention of colorectal cancer [24]. Fermentation of these RS fractions produce a number of by-products, including short chain fatty acids which are important in colonic health, aiding the maintenance of cells lining the colon, and increasing colonic blood flow [25].

The term 'available carbohydrates' was coined to describe the amount of digestible carbohydrates contained in a portion, and includes both starch (RDS and SDS) and soluble sugars. Importantly available carbohydrates do not include the indigestible carbohydrates (RS), namely fibres and other polysaccharides such as that from plant cell walls[26]. This is an important concept in many methods that measure digestibility, and offers a way to implement a standardisation of nutrient intake with which to compare different carbohydrate rich foods.

1.3.2 Glycaemic control and satiety

The proportions of the various forms of 'nutritional' starch in a food contribute to the rate of starch digestion as measured by the blood glucose level of an individual. This is known as the glycaemic response. In the digestion of carbohydrates, the monomer unit, glucose, is released into the bloodstream and via insulin the glucose is then used by the body for energy. The rate of carbohydrate digestion depends on the nature of the starch and quantity of available carbohydrates. '

The concept of glycaemic index (GI) was introduced as a way to classify carbohydrate-containing foods according to their postprandial impact on blood glucose levels [27]. The GI is defined as the total glycaemic response 2 hours immediately (RDS plus SDS) after intake of a test food (usually 50 g available carbohydrates), and is expressed relative to an equal carbohydrate quantity of white bread or glucose. Currently *in vivo* GI measurements are limited to 10 healthy individuals, making measurements expensive, with individual error and so questionable statistical significance. GI measures the amount of glucose released into the bloodstream in a given time however does not provide information on the rate of this release and thus does not accurately describe the total glycaemic effect of a food. Glycaemic load (GL) was introduced in 1997 in an attempt to quantify the overall glycaemic response for a typical portion of food [28, 29]. GL is calculated by multiplying the total available carbohydrate in a serving by the GI value.

The glucostatic theory of satiety postulates that these glycaemic and insulinaemic responses from carbohydrates are the main regulators of satiety [30]. This theory states that the high glycaemic response triggered by a high GI meal, followed by a hypoglycaemic period, will trigger hunger and decrease satiety compared to a low GI meal, thus contributing to

overeating. This can be detrimental to health, increasing risk of developing type 2 diabetes, cardiovascular disease and hyperglycaemia in people living with type 1 diabetes [31].

The slower glucose release from SDS increases satiety by reducing spikes in blood glucose and insulin levels [32]. This slower glucose release has also been associated with a better metabolic control through a stable blood glucose level, beneficial in weight management [33] and has been shown in animals to play a role in the prevention of type 2 diabetes [34, 35]. Consumption of foods with higher proportions of SDS is recommended across the entire population with studies showing markers of insulin resistance were reduced regardless of evidence of insulin resistance [36, 37].

It has been suggested that RS and by extension fibre content has a stronger impact on satiety than GI by adding bulk to the diet, producing viscosity and slowing release of nutrients during digestion [38]. Further studies have shown that both short [39] and long term satiety [40] are increased with the addition of fibre source to a meal. Thus the inclusion of a fibre source in a meal is predicted to be beneficial in weight management through better controlled satiety, having potential in the reduction of overall energy intake.

It is important to maintain a healthy balance of these starch fractions within the diet to realise the health benefits that they provide. Consumer and health professional knowledge of the role of different carbohydrate types on glycaemic control and satiety are an important management tool to minimise the proliferation of obesity and impact of chronic diseases on the population.

1.3.3 (Supra)molecular structure of starch

Starch has a complex molecular and supramolecular structure consisting of 6 hierarchical structural levels (Figure 2), all of which are subject to variation due to chemical and/or physical modifications, botanical origins, genotype and growing conditions [41]. The molecular structure of starch is simple in terms of chemical composition, comprising of only glucose units, but becomes more complex with the branching seen in the macromolecules that comprise starch; amylose and amylopectin (Figure 2, level 1-2). The complexity of the supramolecular structure of starch is apparent, ranging from single and double helices to semicrystalline packing structures and repeating semi-crystalline lamellae (Figure 2, level 3-6)[41]. Structural order in starch is often referred to in terms of short and long-range order. Short

range order refers to the formation of helices by amylose and amylopectin, and long-range order refers to the formation of crystallites seen in the semi-crystalline lamellar structure of starch. The crystalline structures seen in starch are further defined depending on their specific crystalline packing structure, given the terms A-type polymorphs, primarily found in cereal starches and B-type polymorphs, observed in tubers and high amylose starches. A- and B-type crystalline polymorphs differ in their packing arrangements of double helices within the starch granule, where A-type polymorphs comprise double helices packed with space group B2 in a monoclinic unit cell, and B-type polymorphs comprising double helices packed with space group $P6_1$ in a hexagonal unit cell [41]. A third C-type polymorph is also observed, defined as a combination of A- and B-type polymorph.

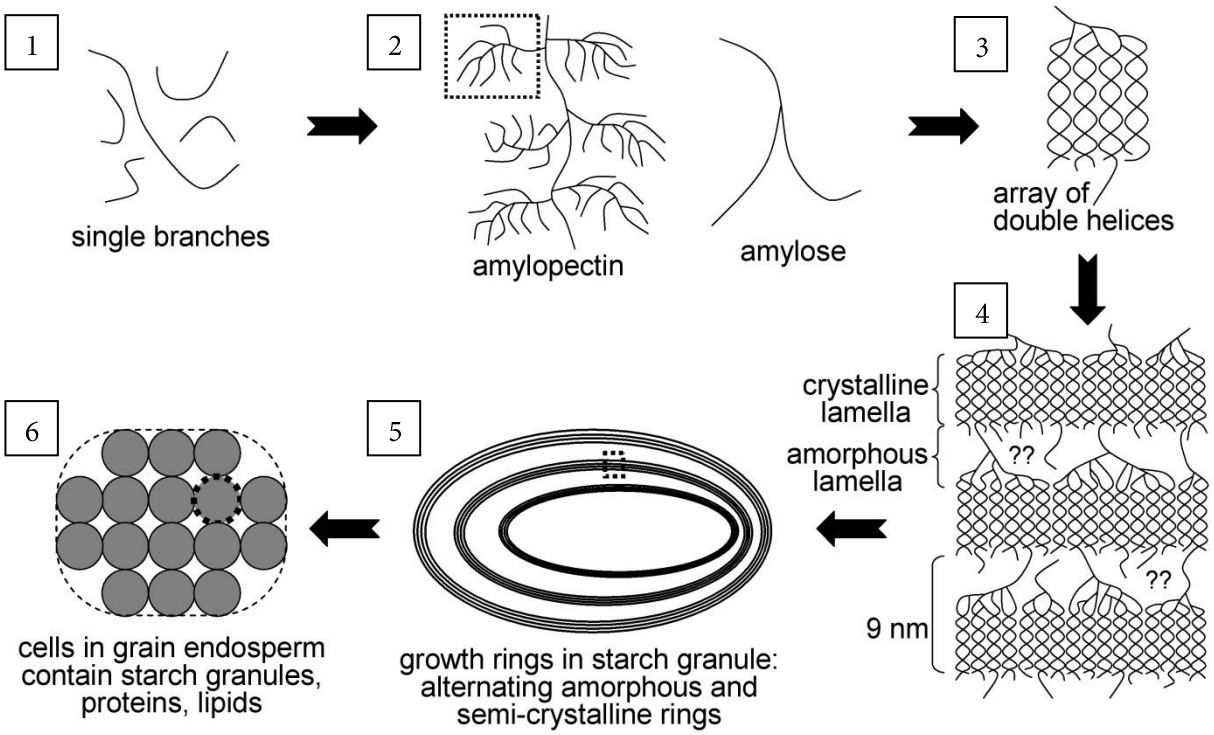

Figure 2 The six structural levels of starch (adapted from Gaborieau and Castignolles [42])

Starch is structurally defined as a glucose homopolymer, with differences in amylose and amylopectin primarily observed in their spatial arrangements and branching nature. Amylose is a slightly branched polymer of glucose monomer units linked by α(1-4) glycosidic links with a small fraction of long branches off the main chain linked by α(1-6) glycosidic linkages (Figure 3) [18, 41]. The helical structure of amylose is generally very dense, reducing its susceptibility to enzyme attack and thus contributing to its reduced digestibility. Amylose is

usually a minor component of starch in plants [41] and is identified as contributing to the amorphous phase of starch [43].

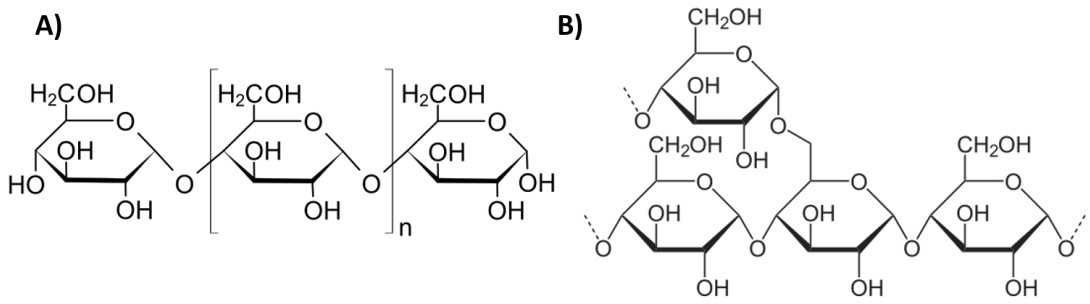

Figure 3 Chemical structure of amylose and amylopectin A) Structure of linear section B) Structure of branching point [44]

Amylopectin is a highly branched polymer with a similar structure to amylose, comprising linear chains of glucose units joined by α(1-4) glycosidic links and branches attached to the main chain by α(1-6) glycosidic links (Figure 3). Amylopectin differs from amylose primarily in the fraction of branched chains as well as chain length of the linear segments. Branched chains are attached by α(1-6) glycosidic links with a degree of branching of 4 to 5 %, a measure of the number of branching points per glucose unit, meaning branching occurs approximately every 24 glucose units [18, 41]. Branching occurs not only on the initial polymer chain but also on the branches themselves, allowing for a high degree of branching following a classification system of A-, B- and C-type chains (Figure 4) [41].

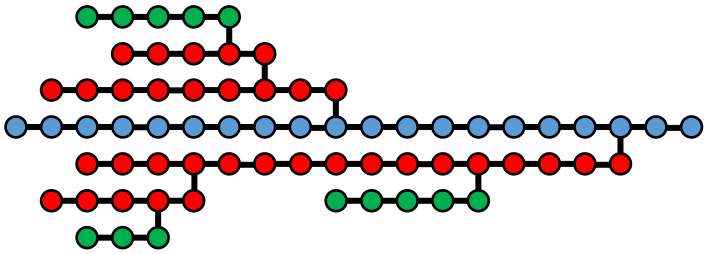

Figure 4 Branching nature of amylopectin; blue – c chain, red – b chain, blue – a chain [44]

A-type chains are outer chains linked by their reducing end through α(1-6) glycosidic linkages to an inner chain, these inner chains are referred to as B-type, defined as a chain bearing other chains as branches. C-type chains are a single chain per molecule that carries all branches [41]. This highly branched and open conformation of amylopectin would theoretically allow for increased access for enzymes, resulting in increased digestion rates as opposed to the more enzyme resistant amylose. Amylopectin is generally found as a major component of

starch in plants and constitutes the crystalline phase forming double helices and ordered supramolecular conformations within the starch granule.

1.3.4 Functional properties of starch

The physicochemical properties of starches play a major role in the determination of its suitability for particular end-uses. Properties such as amylose content, molar mass distribution, branching and molecular order impact on its physical and chemical characteristics, determining its end-use suitability. The physicochemical properties of starch can be greatly affected by a range of factors. Manufacturing methods can potentially cause degradation of intermolecular bonds between starch molecules by cooking (gelatinization), or enhanced crystallinity through formation of amylose helices (retrogradation) by storage[45]. Genetic modification and growing conditions can also affect the physicochemical determinants of starch quality. These factors can substantially affect the molecular and supramolecular structure within the starch granules, thus affecting their physicochemical properties.

Enzyme accessibility is affected by: the differences in amylose content, short-range molecular order such as helix formation, and long-range structural order in the lamellar level between starch samples as a result of modifications. Access of enzymes plays a major role in the digestive properties of starch, so variations to that access by structural alterations are likely to impact on the digestive properties [46].

From a public health perspective, it is important to investigate the ways in which digestive properties of starch can be improved. The ability to monitor and change these digestive characteristics would be an effective tool in the management of diabetes, cardiovascular disease and obesity. Thus, it is important to investigate the structural elements within the complex supramolecular and molecular structure of starch, and the effect this structural variance has on digestive properties. This would allow for investigation into the relationships these properties have with the glycaemic response. Determination of such a relationship would allow development of a possible alternative or complementary technique to current *in vivo* and *in vitro* testing. Such an alternative approach would provide faster and cheaper analysis for large scale testing. While the development of such techniques may not replace human testing, it would provide a valuable set of pre-screening tools for processes such

as grain breeding or quality control programs. Streamlining production of such improved consumer products through fast and efficient characterisation of molecular structure is what will likely result in the greatest impact.

1.4 Australian rice

1.4.1 Grain structure

Rice consists of many different structural layers on the granular scale [47]. Rice is comprised primarily of edible fruit enclosed in a protective covering referred to as the hull (lemma and palea, Figure 5). Underneath the hull are a number of fibrous layers often referred to as the bran, and in some rice products this is left partially intact. The layers that constitute the bran layer are the pericarp and seed-coat [48]. The pericarp and seed-coat are the primary layers in which pigments are stored. The partial retention of these layers is what gives coloured rices their unique appearance. In white rice this bran layer is removed by mechanical abrasion in the whitening process [48]. Below the bran layer are the aleurone cell layer and the embryo cells, where the majority of lipids and proteins are stored in the rice grain [1]. Finally, the inner endosperm of the grain consists of starchy endosperm cells, packed with amyloplasts containing starch granules. This starchy endosperm is characterised by two distinct regions, the subaleurone layer and the central region. The subaleurone layer is typified by the higher amount of proteins than starch. The subaleurone layer consists of small oval shaped starch granules surrounded by membrane proteins. The central region is primarily composed of large starch granules (3 to 9 μm in size), with a smaller amount of protein bodies present and arranged in highly compact polyhedral shapes [1, 48].

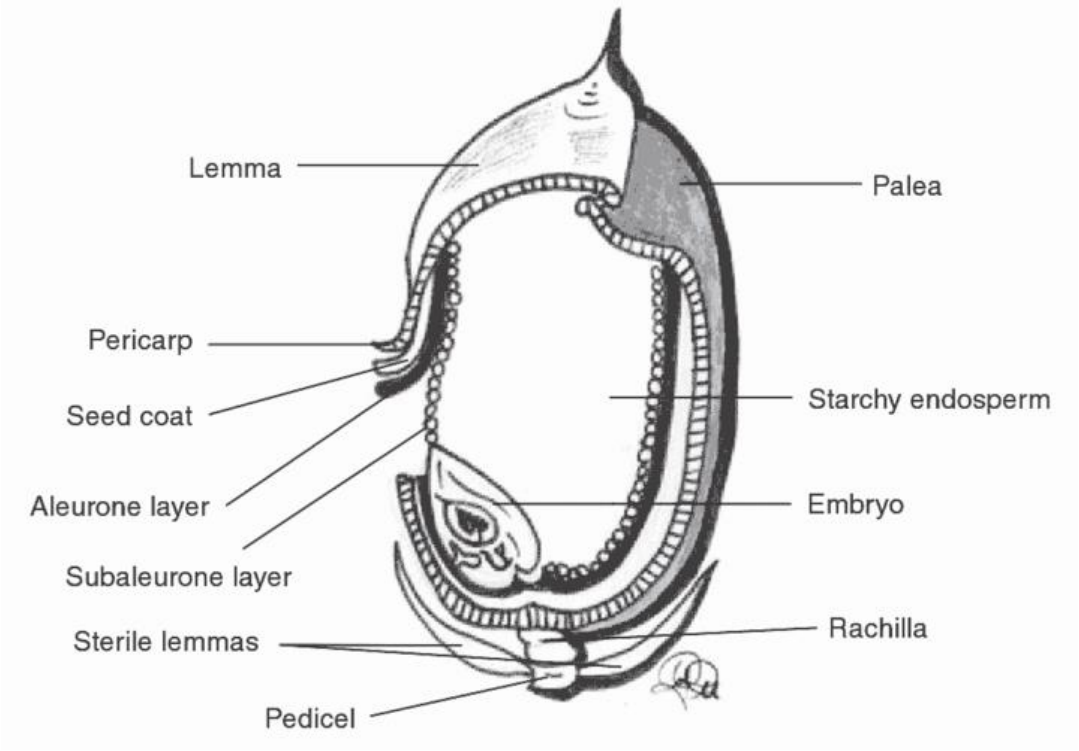

Figure 5 Longitudinal section of the rice grain [1]

Milling is an important process in preparing grains for consumption. However, unlike other cereal grains, rice requires no further processing past milling or polishing. Rice processing starts with the dehulling of the rough rice, which is the removal of the hard, protective outer coating of the rice grain. At this stage some rice products are sold as is, or go further to a whitening process. The whitening process is used to remove the bran layer of the rice grain (pericarp, seed-coat and nucellus). The removal of this layer is what gives rice its white colour. In some cases this layer is left on to either preserve the colour or to maintain a higher fibre content. Whitening is often done by either friction or abrasion based processes. Following this process is a polishing step which further removes the aleurone and subaleurone layers and results in a grain that is primarily composed of the inner starchy endosperm.

Milled rice has a simple composition, consisting primarily of starch (~90 % w/w) [48]. Other components such as lipids and proteins are the other most significant components of starch. Lipids constitute about 1 % of the total weight. This can vary greatly between waxy (containing less than 1 % of amylose[41]) and non-waxy (with higher amylose contents) varieties. Proteins are typically in the form of storage proteins, leftover from starch synthesis and account for between 4 and 18 % of the total weight. This has been shown to vary significantly

from one variety to another [48]. Of these components, the starch content of rice grains is likely to play an important role in the functional properties of the product [47].

In responding to the rise rate of obesity globally a relevant study is required to develop tools that can combat this epidemic. The widespread consumption of rice grains makes it an ideal target to study. Investigating the digestive properties of rice is important in develop tools and knowledge for dietary management. The digestive properties of rice are likely to be heavily influenced by the arrangement and proportions of starch within the grain. The structural properties of the starch itself are also expected to play an important role in the digestibility of rice.

1.4.2 Australian rice varieties

The first record of rice cultivation in Australia was in 1906 when 200 acres of land on the Murray River was allocated by the Victorian government to Isaburo Takasuka, a former Japanese Parliamentarian [49]. Despite floods and droughts, Takasuka managed to produce a crop for commercial sale in 1914. Commercial production of rice then began in 1924 in the Murrumbidgee Irrigation Area. Today, the majority of the rice industry is located in the same south eastern area of Australia, with over 1500 farm businesses operating in the Murrumbidgee Valley of New South Wales (NSW) and the Murray Valley of NSW and Victoria (Figure 6). These areas are ideal due to their large areas of flat land, irrigation infrastructure through immediate access to the Murray-Darling river system, and heavy clay soils [50]. The Australian rice industry is known for producing high quality rice, and doing so with a one of the greatest efficiencies worldwide. It uses 50 % less water per kilogram of rice than the global average. This is important because of the dependence of the rice industry on available water. Water in the area is allocated yearly with priority given to towns, livestock and permanent plantings. Unlike permanent plantings, rice production has water allocated last, and thus is turned on or off depending on the available water.

Figure 6 Rice growing areas in Australia [51]

Rice belongs to the genus *Oryza*, containing 22 to 25 recognised species of which only *Oryza sativa* (Asian Rice) and *Oryza glaberrima* (African Rice) are cultivated [52]. *Orzya sativa* is grown worldwide, in contrast to *Oryza glaberrima* which is grown only in West Africa. The most common species consumed is *Oryza sativa*, comprised of 3 subspecies; *indica*, *japonica* and *javanica*. These subspecies evolved as a result of selective breeding for desired quality traits and adaptation to different ecological systems.

There is about 100,000 rice varieties, though only a very small proportion of these are widely cultivated [1]. In Australia almost all rice grown is of the *japonica* variety, suited to subtropical and temperate climates. *Japonica* is also found in California, Egypt, Japan and China [53]. All Australian rice varieties are the result of rice breeding to ensure a stable product that meets domestic and international market preferences. The most common varieties grown in Australia are outlined in Table 2. Australian rice is of very high quality and has been very successful in international markets with the *Opus* variety being developed for Japanese style cuisine and *Reiziq* finding popularity in the Middle East as a premium product [53].

Table 2 Most common varieties of rice grown in Australia [53]

Name	Description
Amaroo	Semi-dwarf medium grain, high yielding
Reiziq	Semi-dwarf medium grain, but a longer grain than Amaroo and more appealing to Middle East consumers
Quest	New semi-dwarf medium grain, short season
Jarrah	Semi-dwarf medium grain, short season
Koshihikari	Tall-strawed 'Japanese quality' short grain, low yielding
Opus	Semi-dwarf 'Japanese quality' short grain, higher yielding than *Koshihikari*
Illabong	Semi-dwarf '*arborio*', medium grain
Langi	Semi-dwarf long grain, soft cooking
Doongara	Semi-dwarf long grain, hard cooking for premium markets
Kyeema	Tall strawed 'fragrant' long grain, low yielding

Climate plays an important role in the production of rice and in the starch structure within the rice grain. While its contribution to the global rice market is minor, Australia is the world leader in water use efficiency and development of high quality rice varieties. Development of robust rice varieties that maintain a level of quality in varied environments is important, especially when taking into account factors such as climate change which could impact greatly on the rice industry. Along with maintaining and developing adaptability of rice, it is also important to enhance their end use properties, such as digestibility. This is especially important in the growing obesity epidemic.

Development of new rice varieties takes many years, with rice breeders working through thousands of breeds every year. It is therefore important to streamline the determination of the properties of these grains and to efficiently cull the candidates. In the determination of digestive properties, *in vivo* GI testing is currently the market standard; however, *in vivo* methods are expensive and time consuming making them ill-suited for high volume breeding programs. Application of *in vitro* methods is an alternative to *in vivo* methods which may be viable, though the cost of enzymes and time may still be significant factors. The development

of advanced analytical techniques that can probe the structural properties fast and efficiently and relate these properties to digestive properties is thus important. Developing such relationships could allow for the application of fast characterisation techniques as pre-screening tools in the breeding process, allowing either faster development cycles or better development of specific attributes.

1.4.3 Glycaemic properties

The digestion and intestinal absorption of starch from rice is near complete, higher than that of other cereals such as wheat and tubers [54]. However, the rate of digestion of rice is dependent on a number of factors ranging from structural characteristics such as amylose content to cooking method and preparative procedures. Preparative procedures such as washing of rice impact the texture of cooked rice and this has been attributed to the leaching of loose surface starch [55]; however, effects on digestibility are likely to be insignificant. Various studies have revealed the way rice properties can be affected by various cooking procedures. Steaming yielded higher SDS and lower RDS compared to pressure cooking, boiling and straining [56]. RS also varied depending on the cooking method [57]. The degree of cooking can also impact the digestive properties, with significant differences in digestibility kinetics observed between cooked and uncooked rice [58]. However, no significant differences were observed between partially cooked and completely cooked rice samples, suggesting a smaller role of cooking time after gelatinization has occurred. Storage after cooking is also an important factor, with storage at low temperatures affecting textural characteristics, [55] as well increased fractions of SDS and RS with increasing storage time [59]. Therefore, the way in which rice is prepared plays an important role in the final digestive properties.

Rice is generally classified as a high GI food, and a link between amylose content and GI is often referenced [11, 60]. A study investigating the correlation of amylose content with *in vitro* GI of a large variety of rice samples found that samples with higher amylose contents had a lower predicted GI than those with lower amylose contents [11]. Amylose content is often a quality that is modified in breeding according to product design due to its influence on textural characteristics. While amylose content is agreed to have some effect on GI, other structural features of starch within rice can also impact on the digestive properties. Developing a solid understanding of the expected response to macromolecular conformations and amylose

content would allow a way to distinguish between rices based on digestive properties without the expensive and time consuming methods of *in vivo* and *in vitro* testing.

As a natural product, rice varies greatly in grain quality and properties according to genetic makeup [61], environmental influences [47, 62], and processing [63-65]. As a result, it is important that all these factors are taken into account when investigating and comparing different varieties. The variability of rice grains with seasons and geography makes development and maintenance of quality difficult. Fast characterisation methods would be helpful in streamlining these processes.

1.5 Australian breakfast cereals

Breakfast cereals are a widely popular choice of breakfast food for Australians, with 1 in 2 people who eat breakfast choosing a breakfast cereal for this meal [2]. The high rates of consumption in Australia make rice an ideal target to investigate the current high prevalence rates of obesity and other diet related diseases. Breakfast cereals, like most food products, are composed of a variety of components, including various carbohydrates, lipids, proteins and minerals. The heterogeneity of this matrix can make analysis of individual components difficult[66].

The range of components, their quantities and structural arrangements all impact significantly on the digestive properties of breakfast cereals. Understanding these digestive properties and how they relate to specific characteristics is therefore difficult. Factors such as the sugar composition, structure of starch components or the lipid profile are such characteristics that could impact the digestive properties. All of these characteristics are determined by the manufacturing processes, and so vary greatly between different products to match consumer preference.

1.5.1 Processing

Breakfast cereals are a processed grain food consisting of two basic types: hot, requiring cooking, and ready-to-eat, usually consumed with cold milk. Manufacturing and processing of breakfast cereals can vary greatly from one product to another, with 12 defined categories that can be used to identify by general manufacturing processes [67]. The categories are named as follows: 1) Flaked cereals and extruded flakes, 2) Gun-puffed whole grains, 3) Extruded gun-

puffed cereals, 4) Shredded whole grains, 5) Extruded and other shredded cereals, 6) Oven-puffed cereals, 7) Granola cereals, 8) Extruded expanded cereals, 9) Baked cereals, 10) Compressed flake biscuit, 11) Muesli–type products, and 12) Filled bite-sized shredded wheat. Within these defined categories, the processing involved will differ to produce unique products. These differences will affect digestive properties, and so assigning a digestive characteristic to a manufacturing process would not be accurate.

Many of the modifications and processing stages involved in manufacturing aim to create a palatable product with a suitable shelf life, and many of the benefits of the original grains are lost or stripped away to achieve this. Removing the hull, or degerming, is a common step in improving the stability of products. The hull of cereals and grains is a source of unsaturated fats, but these can quickly make a product go rancid and so degerming removes these oil-containing components to improve stability [68]. However, the majority of fibrous content is also found in this layer, and so fibre content is severely reduced by this process.

Refining grains results in a product that is easier to prepare, and more attractive in texture and appearance to consumers. However, the processing of whole grains in cereal productions removes many of the nutritional benefits associated with these grains. In Australia this has been countered by the fortification of cereals and cereal products with a variety of vitamins and minerals such as thiamine and folic acid as part of the Australian Food Standards Code, Food Standards Australia New Zealand (FSANZ) Code 1.3.2 [69]. Addition of thiamine and folic acid has been introduced as a mandatory fortification in products composed of cereals (Standard 2.1.1) [70]. FSANZ codes also allow for voluntary fortification of other vitamins and minerals including Vitamin A, B6, C, and E, as well as calcium and iron. Voluntary fortifications are often incorporated into products to target certain niche health markets. Addition of fibre to cereal products has become common, done in response to the growing emphasis on fibre intake. However fibre is loosely defined, with soluble/insoluble and digestible/indigestible types available and each having their own specific health benefits [71].

Along with the fortification of nutritionally beneficial components, manufacturers also make use of sugars, lipids and flavours to enhance a product's taste, texture and appearance. In many cereals, colours and flavours have been added to create a unique product such as CocoPops®, a sweet chocolate flavoured puffed rice cereal. Achieving certain textures and

product stability can also have a significant impact on the nutritional values, with the addition of sucrose as a both sweetener and for protection from moisture being common [68].

The extensive processing modification of cereals in the manufacturing of breakfast cereals, as well as the addition and fortification of sugars and other vitamins and minerals, make the analysis of starch within the breakfast cereal matrix challenging.

1.5.2 Effect of processing on digestibility

One of the most significant contributing factors to the digestibility of starchy foods is their starch content and structure. During manufacture, different types of treatment such as heat, mechanical stress or dehydration can significantly impact the starch structure. This can result in alterations to the accessibility of digestive enzymes, potentially making it a determinant factor for the rate of digestion.

Processing steps in manufacturing are employed for a variety of reasons. Thus, the ways and extent to which digestibility is affected by manufacturing processes is highly variable. A significant step in any processing flow is the preparation and cooking of the grains. A number of techniques are employed to create products to meet a variety of cultural and consumer preference for taste and texture. These cooking techniques alone can have a significant influence on the digestive profile of the end product. Pressure cooking impacts the starch hydrolysis in other plant based products, reducing the RS fraction and increasing the RDS fraction [72]. This is likely to increase the rate of digestion and yield a greater glycaemic response. Extrusion cooking was also found to increase the soluble and total RS fractions across all temperatures, with insoluble RS fractions being more dependent on variety than on extrusion processing [73]. Thus, extrusion may reduce the digestibility of starchy products. The impact of baking on resistant starch in commercial ingredients has also been studied. The low moisture environment in contrast extrusion and pressure cooking introduces a very different mechanism. One study found that RS fractions were unaltered from raw ingredients by baking, but were decreased when fried [22]. The additional thermal stresses were the suggested driver for this difference.

Thus the cooking process has a significant effect on the digestibility of starch through changes in the RDS, SDS and RS fractions. RS components appear to be most directly affected, being disrupted by stresses associated with processing and breaking down into more digestible

starch fractions. In breakfast cereals, starch fractions may be affected in similar ways, increasing the overall digestibility. The molecular and supramolecular structure of starch dictates the structure of these fractions and their proportions in starch. Thus, the starch structure may be used as a tool to predict these fractions in starch and allow further investigation into the role starch structure plays in the structural stability against processing stresses.

1.6 Conclusion

In a world where the digestibility of starchy grain foods is not completely understood, investigation into the role of starch structure in digestion and the effects of processing is essential. Characterising the molecular and supramolecular structure of starch is complex due to its hierarchal structure, and further complicated in many food samples by the presence of proteins, lipids and various other components. However, characterising this structure will prove valuable in the investigation of starch properties and their digestive mechanisms. Analysis of such samples requires robust and specific methods and techniques.

The aim of this work is to characterise the molecular and supramolecular structure of starch in rice and breakfast cereals, and investigate how these properties relate to digestibility. Chapter 2 focuses on the molecular characterisation of starch by free solution capillary electrophoresis (CE). This work covers the robust separation of amylose and amylopectin, and the subsequent characterisation of the molecular heterogeneity due to branching. Chapter 3 focuses on the supramolecular characterisation of starch by spectroscopic approaches. Investigating the order within the semi-crystalline structure of starch can yield insight into the influence of enzyme accessibility. Short range order was investigated by Fourier-transform infrared (FTIR) spectroscopy and long range order investigated by X-ray powder diffraction (XRD). The size and arrangement of semi-crystalline lamellae within starch may also give understanding into digestive process, and has been investigated by small angle X-ray scattering (SAXS). Chapter 4 will discuss the role of starch structure in rice digestibility, focusing on the semi-crystalline lamellar structure by SAXS and average degree of branching (*DB*) by solution state ^{1}H nuclear magnetic resonance (NMR) spectroscopy.

Chapter 2 Characterisation of the molecular structure of amylose and amylopectin using iodine-affinity capillary electrophoresis

2.1 Background

This chapter focuses on the separation and characterisation of amylose and amylopectin in starch by free solution capillary electrophoresis (CE). These macromolecules represent the molecular level of structure in starch (levels 1-2 of Figure 2). Amylose and amylopectin differ in their branching structures; however, not all amylose and amylopectin molecules are the same. Each rather exists as a family of molecules with similar overall branching structure (Figure 7), but distributions of actual branching topologies and sizes. The distributions of branching structures can make defining amylose and amylopectin as separate molecules difficult, due to possible overlap of their individual distributions of branching structures.

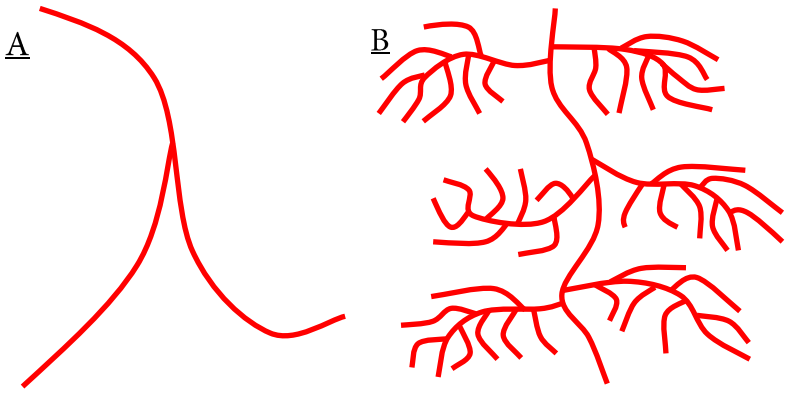

Figure 7 Illustration of the general branching structure of A) Amylose and B) Amylopectin

In the literature, the relative proportions of amylose and amylopectin are commonly described in terms of the 'amylose content' or 'amylose-to-amylopectin ratio'. In this work, the term 'amylose content' will be used to describe these relative proportions.

The branching structure of starch and relative proportions of amylose and amylopectin in starch play an important role in the supramolecular structure of starch, and by extension influence many of the physicochemical properties of starch. Therefore, it is important to characterise the relative proportions and branching structures of these molecules to understand these properties and how starches and starch-based products can be designed with specific properties such as reduced digestibility.

2.1.1 Determination of amylose content

Amylose and amylopectin in cereal starches have traditionally been quantified by taking advantage of iodine binding procedures with detection by amperometric, potentiometric and spectrophotometric techniques. The most popular techniques used in the quantification of amylose and amylopectin in starch samples are spectrophotometric approaches, using the distinct absorption profiles of the two iodine bound macromolecules. The complexation of amylose and amylopectin with iodine yields an altered colorimetric profile with a maximum absorption at 620 and 540 nm, respectively [74, 75]. The closeness of these absorption maxima result in overlapping absorption bands commonly causing interference in colorimetric methods [76]., These overlapping absorption bands can lead to overestimation of amylose content, requiring correction processes such as multi-wavelength processing [77].

The iodine binding property of amylose and amylopectin allows a simple detection method using UV-Vis absorbance, thus making it a viable technique to use in conjunction with a wide range of separation techniques. Successful separation of the iodine complexes of these macromolecules would remove the issues associated with interfering absorbance bands. Thus, a more accurate determination of amylose content can be made, opening ways to further characterise these components.

2.1.2 Industry standard analysis: Liquid chromatography

The industry standards in food and starch analysis, high performance liquid chromatography (HPLC) and size exclusion chromatography (SEC, also known as gel-permeation chromatography, GPC), provide established methods with which to characterise

food samples [78]. These techniques are extensively applied in the determination of molar mass distributions in starch samples [79], and subsequent relation of the distributions to other processes such as digestion [80]. HPLC and SEC work on the principle of separation of components based on molecular attributes. In conventional HPLC, the interactions that cause separation depend on the employed column with modes such as normal phase (polar retention) and reverse phase (non-polar retention). In SEC this separation is a result of the difference in hydrodynamic radius (the size of the molecule in solution) [81, 82]. Following separation, a wide array of detectors can be applied in the analysis of separated components.

In the analysis of starch, the commonly used detection methods involve pairing HPLC or SEC with multi angle light scattering (MALS) and refractive index (RI) detectors [83, 84], UV detectors [84], and also fluorescent detectors [85]. The use of these methods is however hampered by the sample preparation, requiring the solubilisation of starch, as well as the isolation of starch from the sample matrix [86]. Incomplete dissolution and conditions of dissolution of starch samples have a significant impact on analysis results [84]. A common solvent for starch dissolution is dimethyl sulfoxide (DMSO) with varying water content [83, 87], though dissolution in anhydrous DMSO is much faster [88]. Due to the difficulties in starch dissolution, degradation processes such as random chain cleaving by acid hydrolysis are often employed to reduce the molecular size and produce soluble starch [86]. This approach can be used in the determination of starch content by hydrolysis with enzymes in acidic conditions [89]; however, it obscures any other features of starch. Selective cleaving approaches can also be used in the analysis of starch fragments but this does not necessarily improve solubility. These approaches reveal the chain length distributions of the linear fragments after the selective debranching at the α(1-6) linkages by the enzyme treatments. Debranching approaches only provide information on the level 1 structure in starch (Figure 2).

Popular separation methods of analysis for starch components rely on the extraction of amylose and amylopectin components from the sample matrix prior to separation. Thus the preparatory work is tedious. Along with this, HPLC and SEC systems are not particularly robust in regards to the sample. The complex sample matrices and incomplete dissolutions can be damaging to the stationary phase, incurring significant replacement and running costs [90]. Incomplete dissolution as a result of sample preparation also significantly affects analysis,

as it is not truly representative of the original sample. Despite these limitations, an abundance of literature is available on starch characterisation by such techniques [79, 86, 91].

2.1.3 Capillary electrophoresis: An emerging technology

2.1.3.1 Principle of free solution capillary electrophoresis (CE)

Free solution capillary electrophoresis (CE) is a high resolution separation technique [92] in which separation of molecules is based on their charge-to-friction ratio as opposed to the separation by molecular size in (capillary) gel electrophoresis. In CE, a capillary tube is first filled with a background electrolyte. Then the sample is injected at one end of the capillary. Background electrolyte reservoirs are placed at both ends of the capillary and an electric field is applied. Analytes are separated according to their electrophoretic velocity relative to the electroosmotic flow (EOF) of the background electrolyte, yielding an apparent velocity within the capillary (Figure 8).

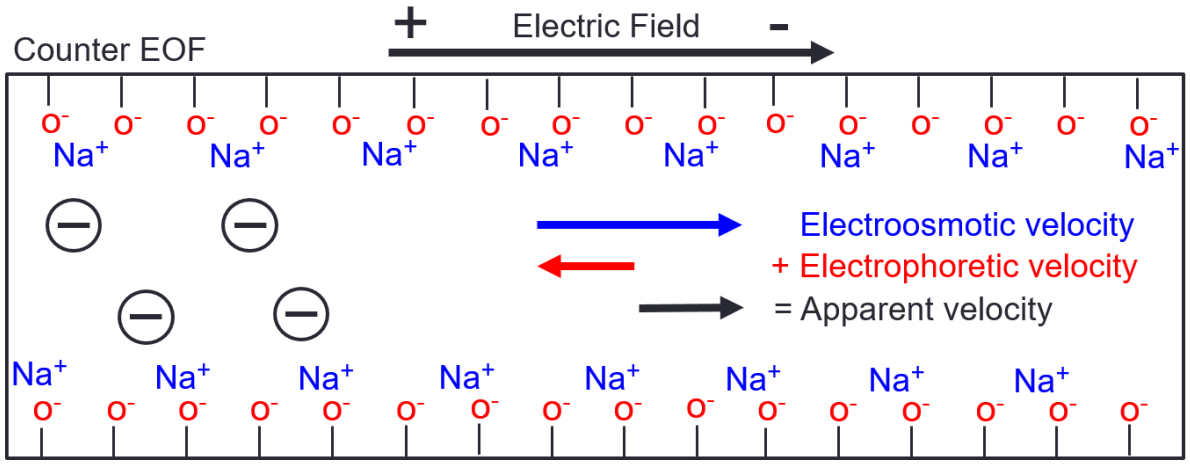

Figure 8 Separation mechanism in CE (counter-EOF mode); EOF – Electroosmotic flow (velocity)

CE offers a significantly higher resolution power when compared to traditional gel electrophoresis, and also shows greater simplicity, versatility, lower operating costs and the possibility of direct sample injection without complex sample pre-treatment [93, 94]. The resilience of fused silica capillaries allows for the use of an extensive variety of buffers, cleaning

solutions and samples which can be injected without negatively affecting the system. The ability for direct injection of samples lends CE an advantage in potential employment in the industrial sector, where simple methods, low operating costs and faster analysis times are desired in routine analysis [95, 96].

CE inherently has a low sample requirement, and thus can suffer from poor sensitivity if the methodology is not optimised [97, 98]. These small sample requirements are ideal in situations where sample quantities are limited or restricted. Where sensitivity is low as a result of extremely dilute samples, several methods are available that can improve sensitivity, such as electrophoretic pre-concentration, micelle based pre-concentration and stacking [97, 98]. The automation and parallelization of CE has the potential for fast, large scale and high throughput analysis at a lower relative cost than competing techniques such as HPLC and SEC.

2.1.3.2 Application of CE to sugar quantification

CE is a useful technique in food analysis to separate sugars extracted from breakfast cereals [66] and to separate carbohydrate and sugar components in complex fermentation matrices [90, 99, 100]. CE is not just limited to qualitative analysis. With the use of calibration curves, CE can also be used in the quantitative analysis of known components, such as mono- and disaccharides in breakfast cereals [66]. Improved quantitative determination of carbohydrates in CE versus HPLC has been reported in fermentation mixtures, with CE showing a higher recovery of the separated analytes[90].

The robustness of CE is advantageous in the analysis of complex samples such as food products, allowing for direct analysis with minimal sample preparation (no filtration) in contrast to HPLC/SEC which often requires tedious sample preparation. Add to this CE's low running costs, resilient and relatively inexpensive capillaries and excellent sample recovery, and CE looks to be a promising alternative to HPLC/SEC [90, 99] for charged analytes such as carbohydrates.

2.1.3.3 Application of CE to starch characterisation

In the analysis of starch by liquid chromatography, a complete separation of amylose and amylopectin is not always obtained. SEC often yields poor resolution between the signals of components [84, 91, 102, 103]. HPLC cannot separate the components. Flow field-flow fractionation can separate amylose and amylopectin, yielding an improved peak resolution compared to SEC [104]. In contrast, CE has become an invaluable tool in the analysis of polymers, particularly biopolymers, where it has been extensively used in separation of DNA and proteins, among others [100, 101]. CE is able to completely separate starch components, amylose and amylopectin, through iodine binding [105]. In this work iodine affinity CE (IA-CE) as reported by Herrero-Martinez et al. [105] has been employed to separate and quantify the main starch components, amylose and amylopectin (Figure 9). In this method iodine binding takes place within the capillary, with the iodine solution incorporated into the background electrolyte. The method is reliable giving detection limits of the order of 0.1 $g \cdot L^{-1}$. The proposed method was applied to the quantitative determination of the amylose content in commercial starches. Irrespective of the differences in solubility of amylopectin between sources, determination of the amylose content ratio could be made using this method.

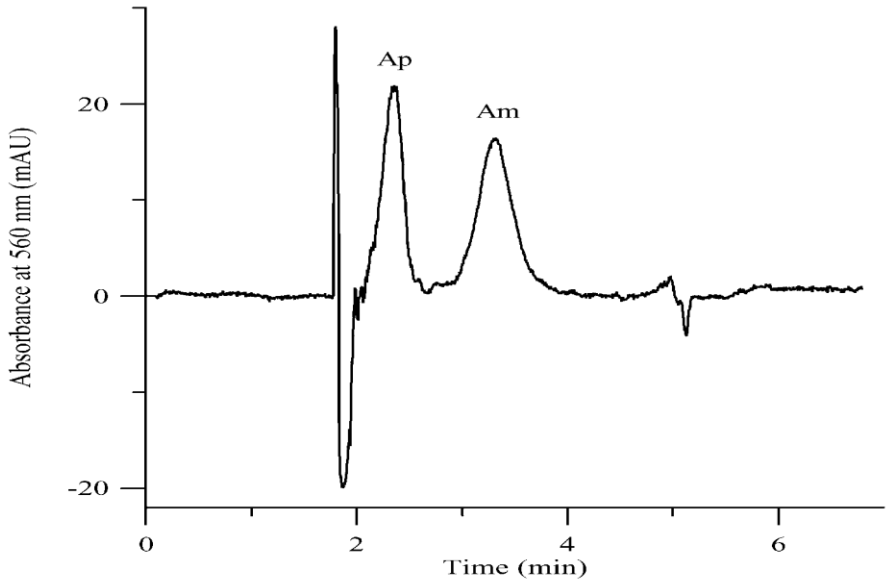

Figure 9 Electropherogram of Corn starch, Ap – Amylopectin; Am - Amylose adapted from Herrero-Martinez et al. [105]. Analytes were injected hydrodynamically for 2 s at 3400 Pa. Separation was performed at 20 kV using an extended light path capillary (37 cm x 75 µm i.d. x 375 µm i.d., bubble factor 3.0). Analytes were prepared at a concentration of 5 to 10 $g \cdot L^{-1}$.

Separation and sample preparation conditions were based on previously reported methodologies [106], and then modified according to Hong et al. [107]. Various background electrolytes were compared, with 1.2 mM I_2 and 7.2 mM KI reported as the optimal concentrations of iodine components in the buffer. Sample preparation for quantitative studies required the solubilisation of starch, and thus required heating due to the poor solubility of starch. This type of treatment could potentially impact on structural features due to starch degradation, and thus yield results that are not representative. A recent study on starch dissolution showed that the dissolution employed in the work of Herrero-Martinez et al. [105] is not optimal, with the presence of water in DMSO slowing the rate of starch dissolution [88]. A solution of 0.05 to 5 % lithium bromide in anhydrous DMSO was optimal [108], especially in the case of high amylose starches where high lithium bromide concentrations are essential for complete dissolution [108]. Lithium salts have been shown to facilitate better solubility of polysaccharides through strong interactions between Li^+ ions and the solvent. Li^+ ions are believed to facilitate enhanced solubility by interaction with hydroxyl groups on the polysaccharide. The interaction of Li^+ with the solvent leaves a relatively strong anion which can interrupt hydrogen bonding [109, 110]. As a result of incomplete dissolution of a starch sample, it is likely that the results of this work are not representative of the whole sample. Along with this, complications can also arise due to phospholipids and fatty acids forming complexes with the amylose chains [111]. Complex food samples very often contain lipids along with a variety of other components which can make direct analysis difficult. In the analysis of starches rather than grain flours there are no other interacting species present and thus this is not a factor in analysis. Further, in the case of rice flours and their very low lipid content, competing iodine binding reactions are also unlikely to play a major role in of the formation of the starch-iodine complex.

In this chapter the separation of amylose and amylopectin by CE has been explored. Dissolution conditions were explored in determining the optimal conditions for analysis. These optimal conditions were then employed in investigating the potential adsorption to the capillary wall, as well as the effect of incubation time on iodine binding in different solvents. Characterisation of the heterogeneity of branching was then investigated, taking advantage of the separation mechanism of polyelectrolytes separating in the critical conditions (discussed in Section 2.3.2.2) [100]. By transforming the resulting electropherograms from migration time

to electrophoretic mobility (μ), a weight distribution of electrophoretic mobilities can be obtained. Heterogeneity of branching can then be investigated using a new methodology to calculate the dispersity of these electrophoretic mobility distributions [112].

2.2 Materials and methods

2.2.1 Materials

Milli-Q® quality (Millipore, Bedford, MA, USA) water was used throughout the analysis. Sodium hydroxide pellets (NaOH), glacial acetic acid, and anhydrous sodium acetate were from Ajax Chemicals (Auburn, NSW, Australia). Analytical grade potassium iodide was from Chem-Supply Pty Ltd (Gillman, SA, Australia). Analytical grade iodine was from Univar (Downers Grove, IL, USA). Dimethyl sulfoxide (DMSO) ≥ 99.5 % (dried over molecular sieves) and lithium bromide (LiBr) ≥ 99 % (both stored in a desiccator) were from Sigma-Aldrich (Castle Hill, NSW, Australia). Millipore Millex-LCR hydrophilic poly(tetrafluoroethylene), hydrophilic PTFE 0.45 μm filters (sample filtration) and poly(ether sulfone), PES 0.22 μm filters (buffer filtration) were from Millipore (Bedford, MA, USA).

Three types of commercial maize starches with different amylose contents (Waxy maize (3.4 % amylose), Regular maize (24 % amylose) and Gelose 80 (83 % amylose)) [113] were from Penford Australia Limited (Lane Cove, NSE, 2066, Australia). Amylose content was determined by the spectrophotometric iodine binding method and reported by Tan et al. [113]. Waxy corn (S9679, Batch: SLBJ1581V), potato amylose (A0512, Batch: 070M7025V), potato amylopectin (A8515, Batch: 049K3775V), Corn (S4126, Batch: MKBQ4397V) and Rice starches (S7260, Batch: BCBP5455V) were from Sigma Aldrich (Castle Hill, NSW, Australia).

2.2.2 Methods

Samples were prepared at a concentration of 1 g·L^{-1} in anhydrous DMSO containing 0.05 % w/w LiBr at 80 °C with shaking at 300 rpm in an Eppendorf Thermomixer C (North Ryde, NSW, Australia) for at least 8 hours unless otherwise indicated. Where DMSO is described with a percentage of lithium bromide it is referred to as 'DMSO with % LiBr' with units of % w/w. Where DMSO is described as 90 % DMSO, this refers to a mixture of 90 %

DMSO and 10 % water with units of % v/v. From this point forward optimal dissolution conditions will refer to the conditions of Schmitz et al. [108], preparing at 80 °C with shaking at 300 rpm in a thermomixer for at least 8 hours in anhydrous DMSO with 0.05 % w/w LiBr at a starch concentration of 1 $g{\cdot}L^{-1}$.

For CE separations, 20 mM acetic acid buffer (7.3 mM acetic acid and 12.7 mM sodium acetate) with 7.2 mM potassium iodide and 1.2 mM iodine metal was prepared according to Herrero-Martinez et al. [105]. The buffer was titrated to a pH of 5.0 by 1 M NaOH. The buffer was prepared on the day of use, sonicated for 10 min to ensure complete dissolution of iodine and degassing, and then filtered with a Millipore poly(ether sulfone)(PES) membrane filter (0.22 μm). The 1 M NaOH was prepared on the day of use.

Separations were performed on an Agilent 7100 CE (Agilent Technologies Waldbronn, Germany) with a Diode Array Detector (DAD) monitoring at 560 nm at a bandwidth of 20 nm. The total capillary length was 37.0 cm (28.5 cm effective length), using fused-silica capillaries including a standard (75 μm i.d.) (Polymicro, Phoenix, AZ, USA) and an extended light-path capillary (75 μm i.d., bubble factor: 2.7) (Agilent Technologies). The capillary was preconditioned before use by flushing (950 mbar) with 1 M NaOH (4 min), 0.1 M NaOH (4 min), water (4 min) and running buffer (12 min). All injections were preceded by flushing (950 mbar) the capillary with 1 M NaOH (24 s) (82 % of capillary volume) and running buffer (2 min). Then the sample was injected hydrodynamically by applying 17 mbar of pressure for 4 s (0.25 % of capillary volume), followed by injection of running buffer by applying 5 mbar of pressure for 5 s. All separations were performed at +20 kV (ramped from 0 kV over 1 min) and 25 °C unless specified. Data was acquired using Chemstation A10.01 [114] and plotted, integrated and μ calculated using OriginPro 9.0 [115]. Raw data was corrected as shown in Section 2.3.2.1, transforming the electropherograms into weight-distributions of electrophoretic mobilities. In figures where the caption does not specify that it has been normalised, this is not a true weight-distribution of electrophoretic mobilities, and is done to allow for investigation into differences in peak areas in relation to sample concentration.

Pressure mobilisation experiments involved preconditioning and sample injection as described for capillary electrophoresis experiments. After sample injection, an internal pressure of 13 mbar was applied, with mixing of the analyte in the background electrolyte done by ramping up the voltage to 20 kV over 1 min, down to -20 kV over 2 min, and back up to 0

kV over 1 min [116]. Corrections are applied to the UV absorbance, taking into account the analyte velocity through the detection window. Absorbance is corrected according to Equation 2 found in Section 2.3.2.

The CE hardware and capillary were validated for each experiment by separation of a standard oligoacrylate solution in sodium borate buffer[117]. The standard was qualitatively compared to previous separations for repeatability of electroosmotic flow and μ of oligoacrylate components.

2.3 Results and discussion

2.3.1 Dissolution

In the analysis of polymers in solution, there are a number of important factors to consider. Complete dissolution is essential to completely analyse the original sample, because incomplete solution results in loss of sample information or inaccurate characterisation. The impact of concentration, temperature, solvent and filtration on the separation of amylose and amylopectin by CE has been investigated here. Literature dissolution conditions are also directly compared to assess their impacts on the separation, employing the dissolution conditions of Herrero-Martinez et al.[105] as well as the improved conditions reported by Schmitz et al. [108].

2.3.1.1 Effect of sample concentration

Aggregation is a major problem in solutions of very large polymers, and is governed by the 'critical polymer concentration' (C^*). This concentration is the point at which the domains occupied by the polymer molecules in solution begin to overlap [118]. At this point, polymer molecules begin interacting with each other, and begin behaving differently from individual molecules in a dilute solution. In some cases, this overlap of phases can result in aggregation or precipitation. This can be detrimental to a wide range of techniques and detection methods, especially in spectrophotometric detection, as strong scattering effects can occur. Large aggregates are also detrimental in the application of chromatography techniques involving particulate stationary phases as filtration is often required. In these cases, sample filtration is successful in removal of these aggregates; however, the removal of these aggregates also

implicitly means a loss of sample, yielding an analysed sample not representative of the original one.

To counter this aggregation phenomenon, distancing the concentration from the critical polymer concentration by reducing the sample concentration is ideal. However, this is often difficult as the C^* for very large polymers is usually very small and sometimes below the detection limit. In these cases, reducing the sample concentration is still beneficial in minimising aggregation and so should be employed where possible. In the analysis of starch, a very large biopolymer, the C^* value is likely to be very low and extremely variable [81] with both amylose and amylopectin having very large and variable reported average molar mass, with a tendency to form very large aggregates. Sample concentration thus becomes a very important factor. In this work, the impact of concentration on the separation of amylose and amylopectin by the method of Herrero-Martinez et al.[105] was explored.

The samples were first prepared as reported by Herrero-Martinez et al. [105], by heating the sample to 100 °C for 1 h in a solvent made of 90 % DMSO and 10 % water v/v (90 % DMSO) (Figure 10). Sample concentrations of 10 $g{\cdot}L^{-1}$ as reported[105] and 1 $g{\cdot}L^{-1}$ were compared. Samples prepared at higher concentrations exhibited significant occurrence of sharp peaks on the amylopectin peak. In CE these large sharp peaks are typical of light scattering effects caused by large particles, and so are likely the results of aggregates forming in solution. At 10 $g{\cdot}L^{-1}$ the presence of aggregates in starch solution was expected, and was likely compounded by the use of 90 % DMSO as the dissolution solvent as opposed to anhydrous DMSO.

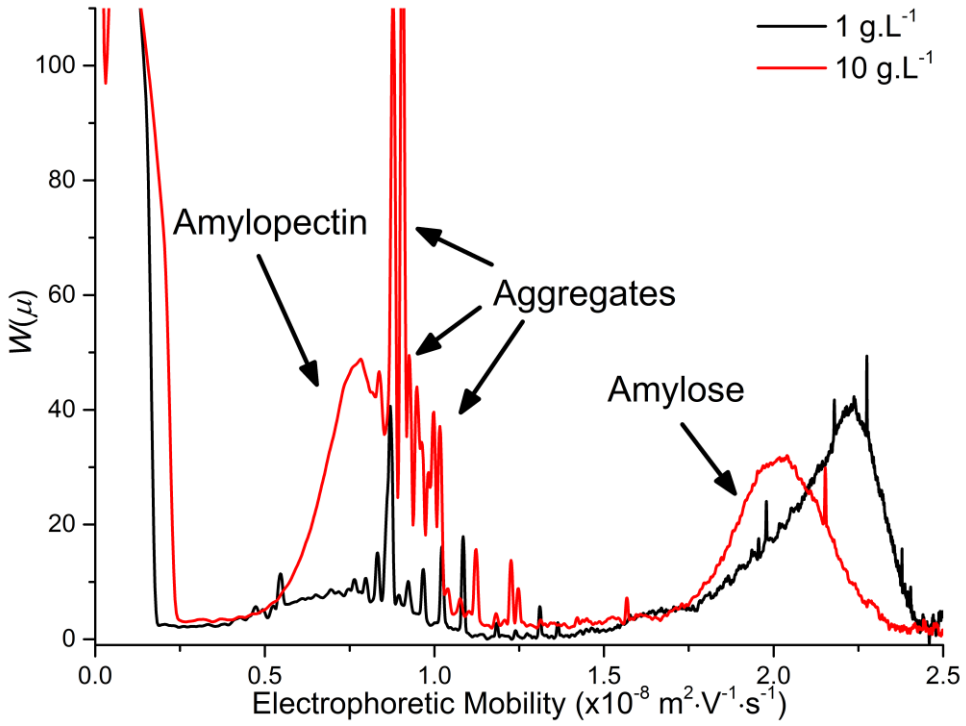

Figure 10 Weight-distributions of electrophoretic mobilities of Rice starch prepared according to Herrero-Martinez et al.[105], varying only concentration (90 % DMSO). The amylopectin peak is over the range 0.5 to 1.25 (× 10^{-8} $m^2 \cdot V^{-1} \cdot s^{-1}$) and the amylose peak over the range of 1.5 to 2.5 (× 10^{-8} $m^2 \cdot V^{-1} \cdot s^{-1}$).

However, using the improved dissolution conditions (Section 2.3.1.2.1) aggregates were still observable at a sample concentration of 10 $g.L^{-1}$ (Figure 11). Their presence had a significant effect on peak area (Figure 10 and Figure 11). The false increases in peak area of amylopectin relative to amylose is likely to cause inaccuracies in the both the quantification of these components and any other further characterisation through bias to greater peak areas. However, at a sample concentration of 1$g.L^{-1}$ in the optimal conditions no aggregation was observed (Figure 11). This is in contrast to the conditions in Figure 10 where aggregation was observed at both 1 and 10 $g.L^{-1}$.

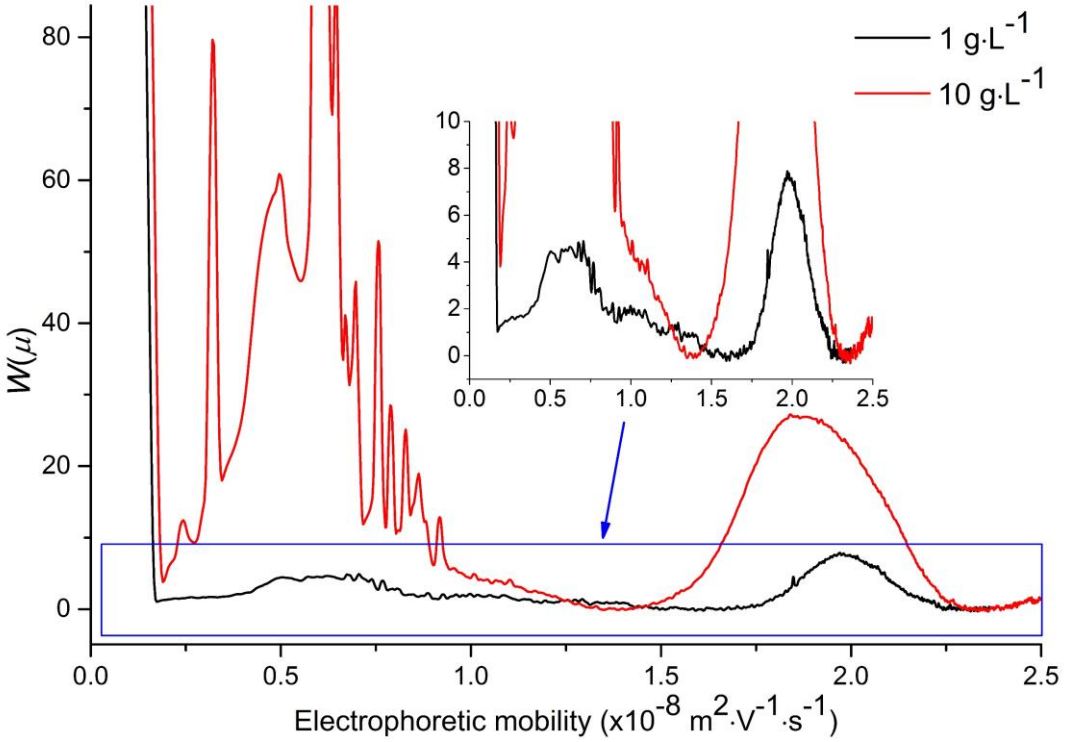

Figure 11 Weight-distributions of electrophoretic mobilities of Rice starch prepared in optimal conditions (Section 2.2.2), varying only concentration. The amylopectin peak is over the range of 0.5 to 1.25 ($\times 10^{-8}$ $m^2 \cdot V^{-1} \cdot s^{-1}$) and the amylose peak over the range of 1.5 to 2.25 ($\times 10^{-8}$ $m^2 \cdot V^{-1} \cdot s^{-1}$).

Exploring further the impact of sample concentration, electropherograms at 1 $g \cdot L^{-1}$ were scaled up by a factor of 10 to a relative concentration of 10 $g \cdot L^{-1}$ (Figure 12). The disparity in relative peak area of amylose and amylopectin was significant, with the scaled trace yielding larger peak areas for amylose and amylopectin, as well as a shift in the relative peak area ratio of the two. No significant differences in viscosity were observed in pressure mobilisation experiments (discussed in Section 2.3.2.3), with 1 $g \cdot L^{-1}$ and 10 $g \cdot L^{-1}$ sample solutions yielding very similar migration times (Figure 34), thus injection volumes are likely very similar and no bias should be observed. Lower observed peak areas at 10 $g \cdot L^{-1}$ should then indicate either a reduced concentration and thus an incomplete dissolution; or a non-linear scaling of absorbance with concentration. A calibration curve would be required to discriminate between the two.

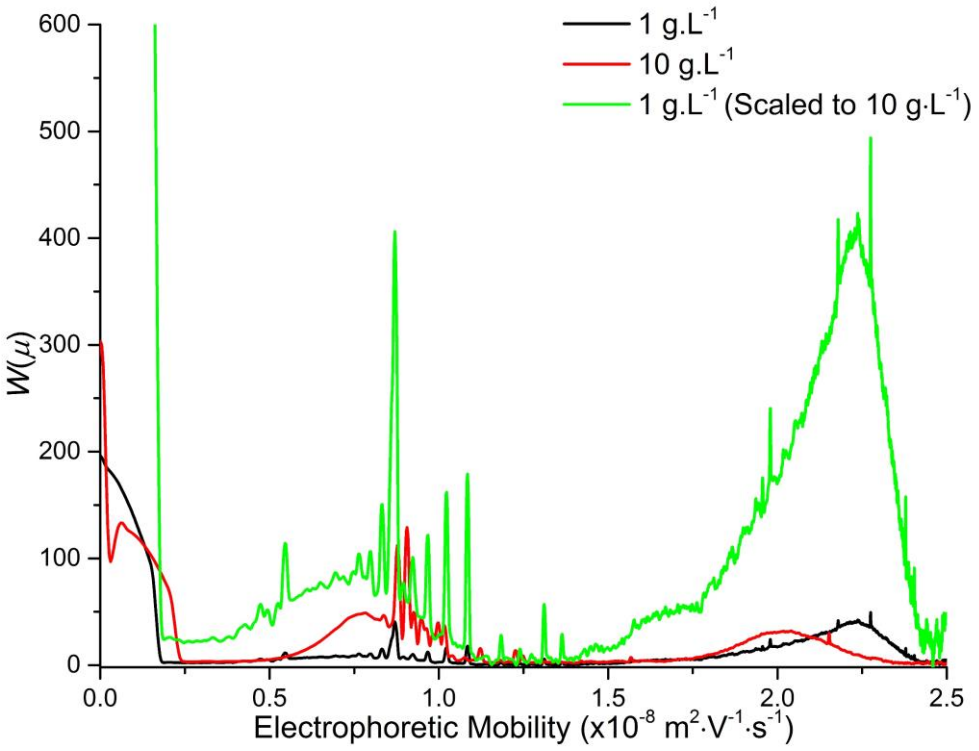

Figure 12 Weight-distributions of electrophoretic mobilities of Rice starch prepared according to Herrero-Martinez et al.[105] with varying concentrations. The amylopectin peak is over the range of 0.5 to 1.25 (× 10^{-8} $m^2 \cdot V^{-1} \cdot s^{-1}$) and the amylose peak over the range of 1.5 to 2.5 (× 10^{-8} $m^2 \cdot V^{-1} \cdot s^{-1}$).

These results indicated that 10 $g \cdot L^{-1}$ is too high in the analysis of starch solutions due to the effects of aggregation and its subsequent impact on analysis. However, further problems were also observed in the form of repeatability. With such a high concentration and the presence of large aggregates, separations appeared to yield poor repeatability of both μ and peak area even after filtration, removing the majority of aggregates and particles that may cause scattering effects (Figure A1 and Figure A2). Comparatively, 1 $g \cdot L^{-1}$ samples yielded an improved repeatability in both mobility and peak area. The electrophoretic mobility at the peak maximum of amylopectin and amylose respectively had an RSD of 7.3 % and 0.92 % for 1 $g \cdot L^{-1}$ (n = 3 for 4 different samples), whereas 14 % and 6.9 % were observed for filtered 10 $g \cdot L^{-1}$ samples (n = 17 for 2 different samples). Peak area of amylopectin and amylose respectively had an RSD of 19 % and 15 % for 1 $g \cdot L^{-1}$ (n = 3 for 4 different samples) and, 50 % and 17 % for filtered 10 $g \cdot L^{-1}$ samples (n = 17 for 2 different samples). Repeatability of electrophoretic mobility is typically in the range of 1 to 2 % RSD [100]. In the case of starch samples at 1 $g \cdot L^{-1}$, RSD values were reasonably close to this range, indicating a good repeatability of electrophoretic mobility. In assessing the RSDs associated with unfiltered 10

g·L^{-1} samples, a significant data set of visually repeatable data could not be obtained and so this sample preparation has been excluded.

From these results, the use of concentrations above 1 g·L^{-1} should be avoided due to increased aggregation and poor repeatability. In the analysis of starch solutions and polymer solutions in general, lower concentrations are almost always preferred due to the aforementioned problems associated with higher concentrations. The sensitivity of CE is sufficient to allow the sample concentration to be reduced, while still retaining the sensitivity required to quantitatively characterise both amylose and amylopectin. Further results will focus primarily on samples prepared at 1 g·L^{-1}, while also including results at 10 g·L^{-1} for comparison.

2.3.1.2 Effect of dissolution solvent

Solvent plays an important role in any dissolution, with good solubility in a given solvent required to obtain a complete dissolution. Starch molecules experience strong hydrogen bonding, and a solvent is required that can overcome these intermolecular forces and disperse the starch molecules. DMSO is a strong polar solvent widely employed as the solvent of choice for starch dissolutions. Its strong polar intermolecular forces allow DMSO to overcome that in starch. However, intermolecular bonding is not always overcome by these forces, especially in the formation of dense amylose helices and some types of resistant starch, and so the addition of hydrogen bond disruptors such as lithium bromide is often employed to enhance dissolution [108].

Common also is the employment of DMSO solvents where a proportion of water is added. Typically, the ratio is 10 % water to 90 % DMSO in units of % v/v. This 90 % DMSO solution has been employed in the dissolution of starch for many years, with claims that the addition of water results in a superior solvent with faster and more complete dissolution. This stems from studies in dissolution analysis by polarised optical microscopy where misinterpretation of results suggested that dissolution was directly related to the loss of crystallinity observed [88]. Often the assumption was that if the solution was transparent or clear, then the dissolution was complete; however, this is not the case. In the dissolution of starch several studies have explored the extent of dissolution of starch. One study with ^{1}H NMR determined that dissolution of starch is faster in 'dry' DMSO vs 'wet' DMSO[88]. 'Dry' DMSO

refers to anhydrous DMSO that has been dried over molecular sieves, while 'wet' DMSO refers to any undried DMSO. Further, the dissolution pathways for both these solvents was also suggested to be vastly different [88]. Dissolution by DMSO with water caused swelling and bursting of starch granules, as well as initiating gelatinisation within the sample [108]. This would lead to a sample appearing to be completely dissolved, when in fact it was not. Dissolution using an anhydrous DMSO followed a mechanism whereby the starch granule was taken into solution layer by layer [108]. In another study investigating the extent of starch dissolution, the addition of a hydrogen bond disruptor (LiBr) in anhydrous DMSO was determined to be essential in the dissolution of high amylose starches, yielding a greater extent of dissolution[108].

Therefore, it is important to ensure the solvent employed is optimal to yield results representative of the sample. Here, different solvents were employed using different sample preparation procedures to assess the impact of the dissolution solvent on the separation and dissolution of amylose and amylopectin in starch. The work of Herrero-Martinez et al. [105] employed DMSO with 10 % water, a dissolution solvent known to slow dissolution kinetics. Therefore the impact of solvent on separation was explored, comparing the DMSO with 10 % water employed by Herrero-Martinez et al. [105] to the optimal anhydrous DMSO both with and without the hydrogen bond disruptor (LiBr) reported by Schmitz et al. [108]. These three solvents were compared through a number of experiments, each employing different dissolution methods including magnetic stirring at room temperature and dissolution at high temperature with shaking.

2.3.1.2.1 Comparison of solvents (magnetic stirring, room temperature)

Preparation of samples by magnetic stirring at room temperature has been explored as a comparative procedure, being reported in the literature as viable for qualitative analysis [105]. However, for quantitative assessment, literature describes high temperatures as essential [105]. Magnetic stirring places external stress on the starch granules and molecules, and has the potential to impact on the starch structure by degradation due to shear forces. For this reason, magnetic stirring is often not used [119].

Differences between the solvents were observed when prepared at 10 $g \cdot L^{-1}$ with magnetic stirring; however, the change in peak area did not indicate the use of anhydrous DMSO with

LiBr to be the better solvent(Figure 13 and Figure 14). Instead, 90 % DMSO gave the greatest peak area for both amylopectin and amylose with the addition of LiBr dramatically reducing amylose peak area for Rice starch (Figure 13). A shoulder peak at higher mobilities of the amylose peak with the addition of LiBr indicates further differences in the dissolution. The sharp peaks indicative of amylopectin aggregates were observed in all solvents, likely a result of the higher concentration used.

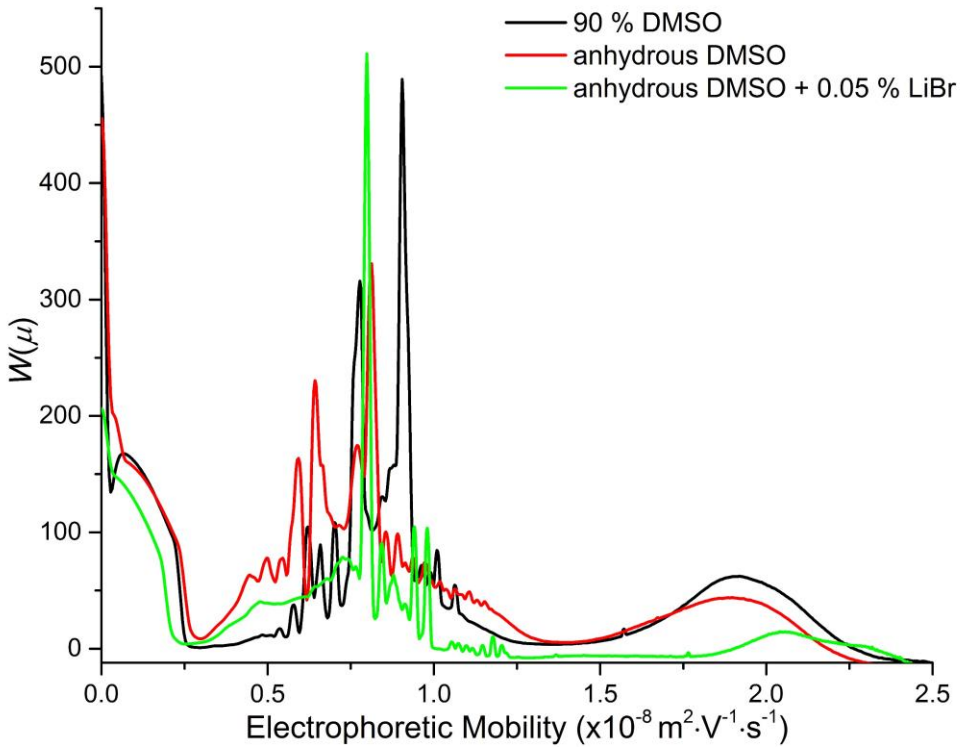

Figure 13 Weight-distributions of electrophoretic mobilities of Rice starch prepared in different solvents at 10 g·L^{-1} by magnetic stirring at room temperature. The amylopectin peak is over the range of 0.25 to 1.25 (× 10^{-8} m^2·V^{-1}·s^{-1}) and the amylose peak over the range of 1.5 to 2.5 (× 10^{-8} m^2·V^{-1}·s^{-1}).

With the addition of LiBr, an additional peak was also observed in Corn starch (Figure 14), which was not observed in dissolution by other solvents. This could indicate another population of slightly branched amylose chains. Further, taking the peak width as an indication of the distribution of mobilities of different structures, the change of dissolution solvent caused variations in the distribution of both amylose and amylopectin.

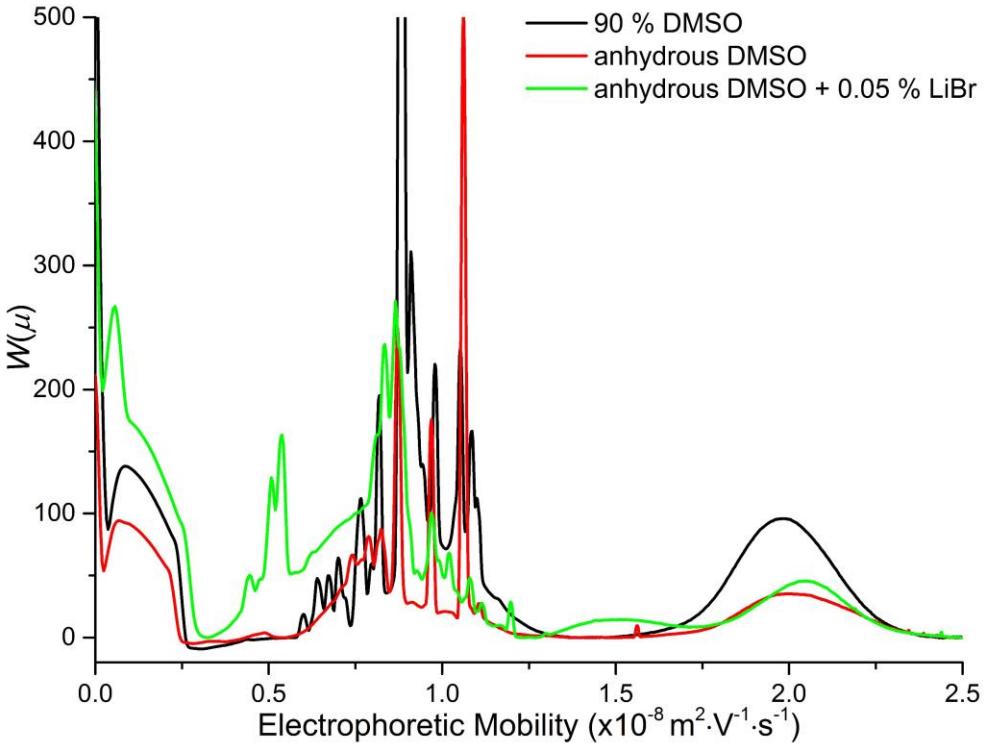

Figure 14 Weight-distributions of electrophoretic mobilities of Corn starch prepared in different solvents at 10 g·L^{-1} by magnetic stirring at room temperature. The amylopectin peak is over the range of 0.25 to 1.25 (×10^{-8} m^2·V^{-1}·s^{-1}) and the amylose peak over the range of 1.5 to 2.5 (× 10^{-8} m^2·V^{-1}·s^{-1}).

For anhydrous DMSO dissolution solvents with LiBr, narrower peak widths were observed in Rice starch for both amylose and amylopectin (Figure 15), and a larger peak width of amylopectin in Corn starch (Figure 14). If it is assumed that dissolution is faster in anhydrous DMSO with LiBr as expected, then it may be posited that the longer time that starch molecules spend in solution gives more opportunity for shear degradation to occur. This may explain the additional populations seen in the amylose peak (1.25 to 1.75 × 10^{-8} m^2·V^{-1}·s^{-1}, Figure 14). Alternatively, this additional population could also be directly related to a more complete dissolution.

Solvents were then compared at a starch concentration of 1 g·L^{-1} with magnetic stirring at room temperature to investigate the impact of the lower sample concentration. Clear differences were observed between the solvents under these dissolution conditions. In the separation of amylose and amylopectin in Rice starch (Figure 15) the analytes in 90 % DMSO yielded a clear separation of the two components; however, the sharp peaks indicative of aggregation on the amylopectin peak suggested limitations in the dissolution. The aggregation seen at 1 g·L^{-1} (Figure 14) is still significantly less pronounced than was observed at 10 g·L^{-1} (Figure 13). Comparatively, in Rice starch samples prepared in both anhydrous DMSO and

with the addition of LiBr, signs of aggregation disappeared (Figure 15). Significant variations were also observed in the amylose peak area and its apparent peak width. In 90 % DMSO, amylose appeared as a single peak with slight tailing, while in anhydrous DMSO with and without the addition of LiBr the main amylose peak was preceded by a shoulder peak (1 to 1.75 $\times$ 10^{-8} $m^2 \cdot V^{-1} \cdot s^{-1}$, Figure 15). This shoulder peak blurs the separation between amylose and amylopectin and is likely indicative of an additional population of amyloses with varying structures. This may be a result of greater extent of dissolution of dense helical amyloses structures or resistant starches. Following this additional population is the disparity in peak area. With the addition of LiBr the peak area of amylose decreased, intuitively suggesting a lesser amount of amylose present especially when compared to anhydrous DMSO alone (Figure 15). The reason for this is not completely understood. It is expected that it arises as a result of factors such as variation in injection volume due to viscosity differences or the presence of aggregates of amylose. In regards to the latter, the lack of large sharp peaks apparently discounts aggregates; however, smaller aggregates may still be present that do not manifest in large sharp peaks.

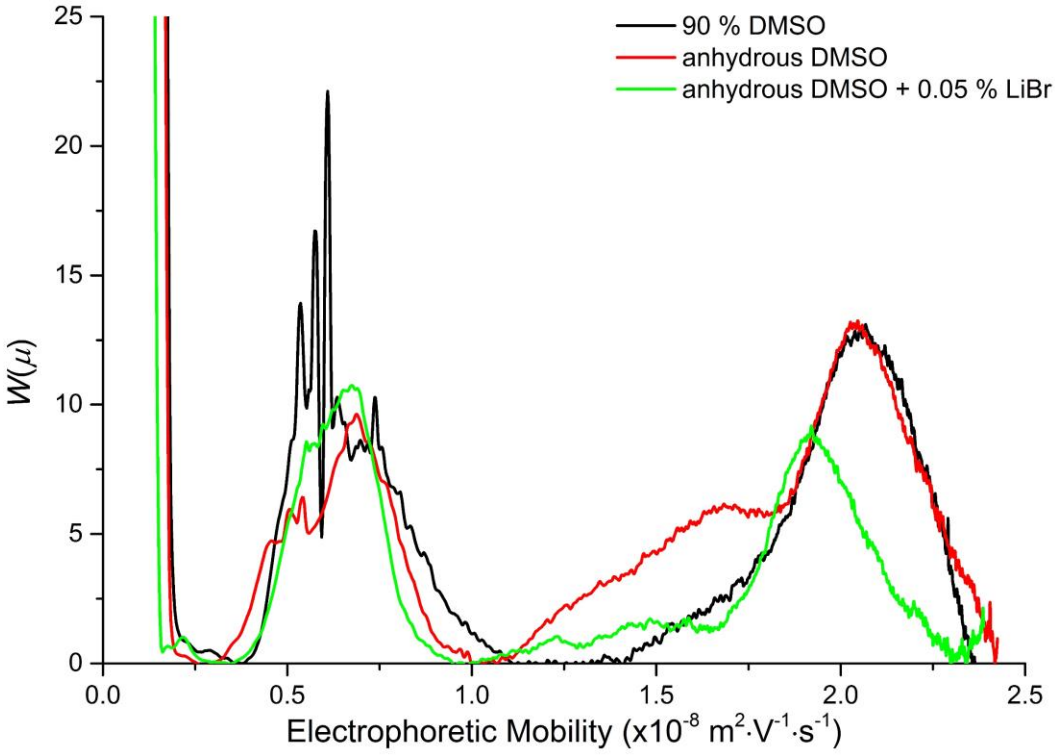

Figure 15 Weight-distributions of electrophoretic mobilities of Rice starch prepared in different dissolution solvents at 1 $g \cdot L^{-1}$ by magnetic stirring at room temperature. The amylopectin peak is over the range of 0.25 to 1.1 ($\times$ 10^{-8} $m^2 \cdot V^{-1} \cdot s^{-1}$) and the amylose peak over the range of 1.2 to 2.5 ($\times$ 10^{-8} $m^2 \cdot V^{-1} \cdot s^{-1}$).

In the separation of amylose and amylopectin in Corn starch differences in the use of different solvents were again observed. In 90 % DMSO, Corn starch (Figure 16) yielded a clear separation of both amylose and amylopectin. Signs of aggregations were present on amylopectin (Figure 16); however, was less pronounced than at a sample concentration of 10 $g \cdot L^{-1}$ (Figure 14). In contrast to results presented on Rice starch (Figure 15), signs of aggregation on amylopectin were present in all solvents tested. In anhydrous DMSO these sharp aggregation peaks occurred primarily at the peak maximum. Additionally the amylopectin peak was observed to be significantly narrower. With the addition of LiBr these sharp aggregate peaks were shifted to the shoulder of amylopectin (0.25 to 0.6×10^{-8} $m^2 \cdot V^{-1} \cdot s^{-1}$, Figure 16), appearing in similar fashion to those in 90 % DMSO (Figure 16). In the case of Corn starch then, Figure 16 shows that dissolution solvent did not impact significantly on the presence of aggregates; however, variation in peak shape and peak area of both amylose and amylopectin were observed. The presence of aggregates of amylopectin made it difficult to compare the peak areas due to their unpredictable effects. However, in the qualitative comparison of amylose peaks, similar trends were observed as in Rice starch with an additional population of amylose appearing in anhydrous DMSO solvent and with the addition of LiBr (Figure 16). Additionally, peak areas appeared to increase with the addition of LiBr; however, this was not quantitatively assessed.

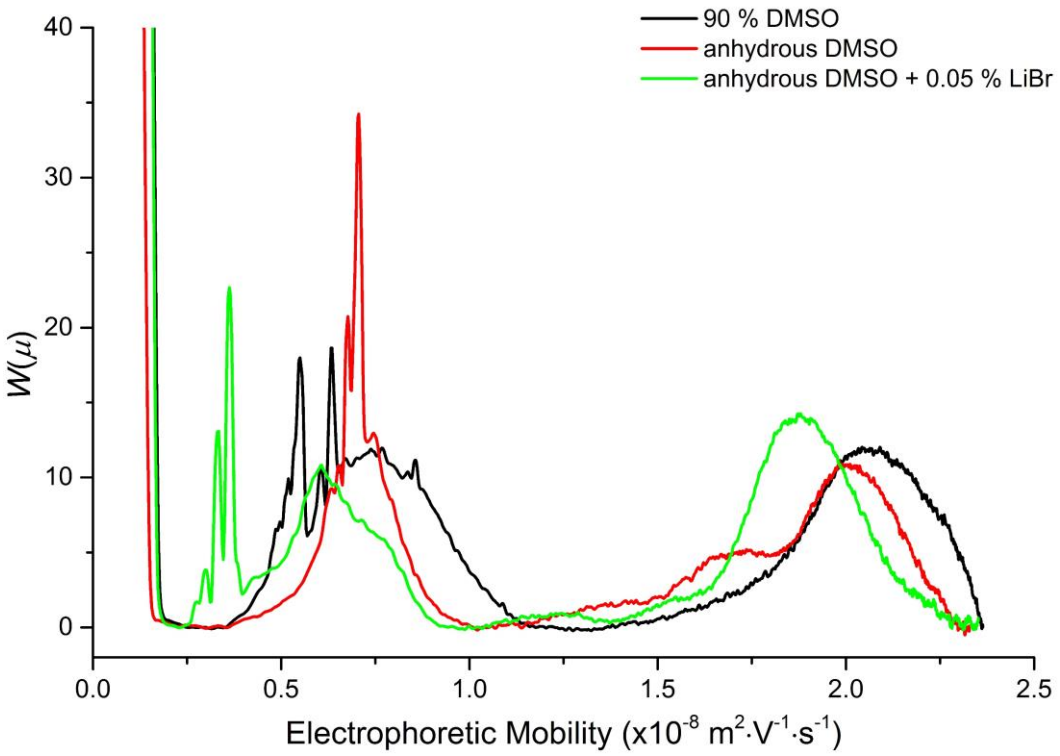

Figure 16 Weight-distributions of electrophoretic mobilities of Corn starch prepared in different solvents at 1 g·L^{-1} by magnetic stirring at room temperature. The amylopectin peak is over the range of 0.25 to 1.0 (× 10^{-8} m^2·V^{-1}·s^{-1}) and the amylose peak over the range of 1.25 to 2.5 (× 10^{-8} m^2·V^{-1}·s^{-1}).

The dissolution solvents tested here have been determined in the literature to have both different dissolution mechanisms and different dissolution kinetics [108]. Experimentation employing these solvents in a standard preparation procedure allowed investigation into how they will impact on the separation of amylose and amylopectin. These results showed that by employing an anhydrous DMSO with or without LiBr, additional populations are observed in the amylose peak, possibly a result of a more complete dissolution of more resistant starch molecules. Further, signs of aggregation of amylopectin appeared reduced in the use of these anhydrous DMSO solvents.

Lower concentrations with magnetic stirring yielded a significant reduction in the presence of aggregates, highlighting again the benefits of reduced sample concentration in reducing aggregation and the associated problems that aggregates can bring in detection. However, the tendency of magnetic stirring to induce sample degradation through shear forces makes it unsuitable in the dissolution of starch which is required for its accurate characterisation [119]. Therefore, magnetic stirring was replaced by shaking in a thermomixer except in cases where magnetic stirring is specified for comparative purposes.

2.3.1.2.2 Comparing dissolution conditions of Hererro-Martinez et al. [105] and Schmitz et al. [108] (shaking, high temperature)

In both the quantification of amylose and amylopectin by Herrero-Martinez et al. and the investigation of optimal dissolution conditions by Schmitz et al. [108], the use of high temperatures with shaking was employed to enhance dissolution.

Here the dissolution conditions employed by Herrero-Martinez et al. [105] and Schmitz et al. [108] have been directly compared, with concentrations modified to 1 g·L^{-1}. This allows for a direct investigation into the influence of improving dissolution conditions on the separation of amylose and amylopectin. Dissolution conditions of Herrero-Martinez et al. [105] involved the heating of sample solution to 100 °C for 1 h, using 90 % DMSO as a dissolution solvent. In contrast the conditions described by Schmitz et al.[108] indicated the use of anhydrous DMSO as the solvent with addition of 0.05 to 5 % LiBr and mixing at 80 °C for at least 8 hours improving the dissolution of resisting starch components. In this work, dissolution time was at least 8 h, up to a maximum of 16 h before injection. A LiBr concentration 0.05 % w/w was employed. All samples were prepared at 1 g·L^{-1} and placed in a thermomixer at the specified temperature with shaking at 300 rpm for the specified time. The sample was allowed to cool down for 1 to 2 h before injection. Therefore, data presented here is representative of cooled samples and any effects that may occur as a result. In SEC, cooling of the sample solution before injection negatively affected repeatability [84]. Therefore the repeatability of cooled samples will be explored in Section 2.3.1.3.

In the separation of Rice starch prepared with different dissolution conditions (Figure 17), the quantitative conditions of Herrero-Martinez et al. [105] showed a loss of signal in the amylopectin peak, as compared to the Schmitz et al. [108] conditions. This in stark contrast to the previous results, where amylopectin was clearly detected (Section 2.3.1.2.1). The amylopectin signal loss is likely a result of the unpredictable effects of cooling on the dissolution. However, comparing the results of this preparation directly to the improved conditions of Schmitz et al. [108], there was a clear increase in peak area of both amylose and amylopectin. This increased peak area in the optimal dissolution conditions suggests a higher concentration of starch and

thus that a more complete dissolution of starch has occurred. Similar to results presented in Figure 15, aggregation is still seen in all cases. In the comparison of optimal conditions with and without LiBr, the addition of LiBr increased the peak area of amylose and reduced signs of aggregation in amylopectin, suggesting a comparatively improved dissolution versus anhydrous DMSO alone.

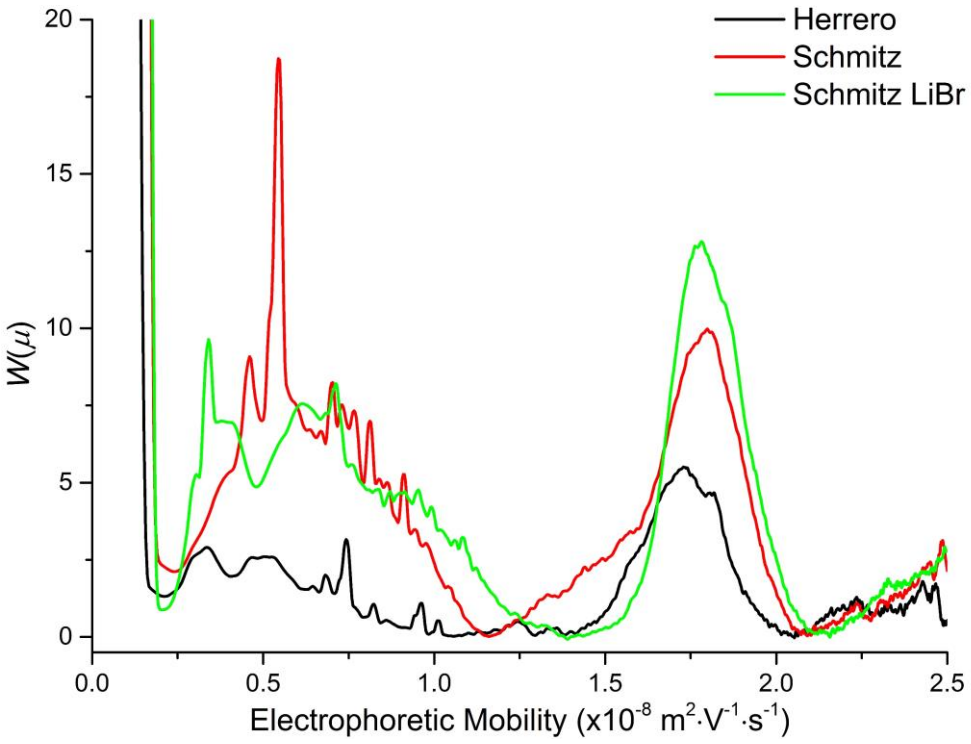

Figure 17 Weight-distributions of electrophoretic mobilities of Rice starch prepared according to different methodologies; Herrero-Martinez et al. [105], Schmitz et al. with (0.05 %) and without LiBr [108]. The amylopectin peak is over the range of 0.25 to 1.25 (× 10^{-8} $m^2 \cdot V^{-1} \cdot s^{-1}$) and the amylose peak over the range of 1.25 to 2.0 (× 10^{-8} $m^2 \cdot V^{-1} \cdot s^{-1}$).

In the separation of amylose and amylopectin in Corn starch that has been prepared in different dissolution conditions (Figure 18), differences observed were very similar to those found in Rice starch (Figure 17). Again the conditions of Herrero-Martinez et al. [105] yielded a comparatively lower peak area in amylopectin suggesting reduced concentration, despite its more soluble nature. These results may hint at limitations in the repeatability of preparation in such conditions. Comparison of optimal conditions with and without LiBr again exhibited the same effects as in Rice starch, with an apparent increase of peak area in amylose with the addition of LiBr; however, aggregation of amylopectin did not appear to be influenced by LiBr as in Rice starch.

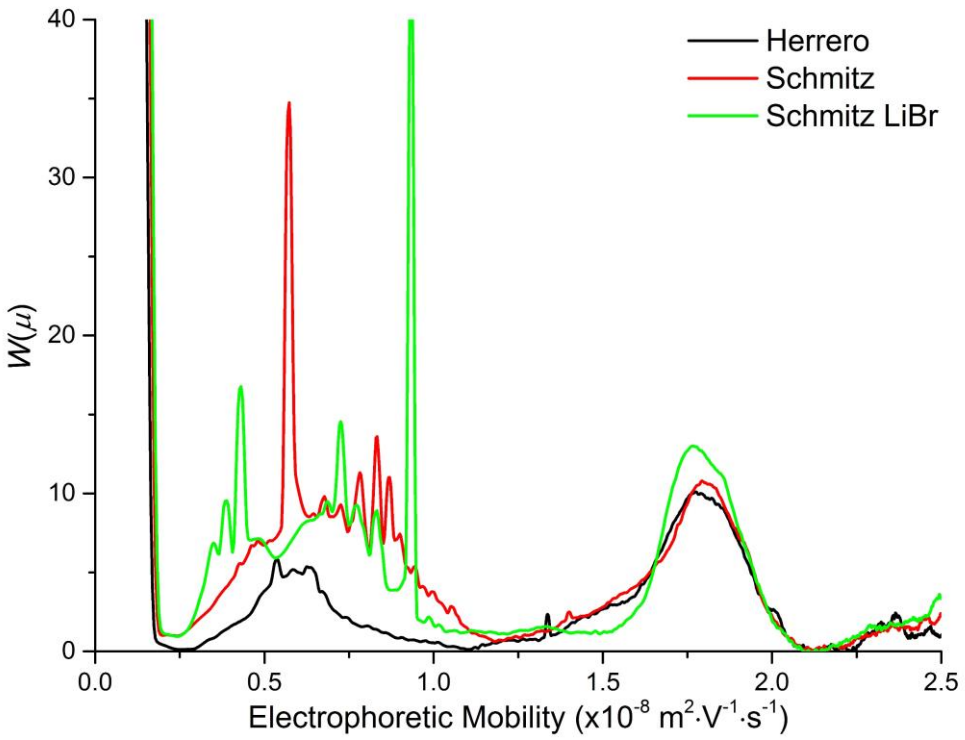

Figure 18 Weight-distributions of electrophoretic mobilities of Corn starch prepared according to different methodologies ; Herrero-Martinez et al.[105], Schmitz et al. with (0.05 %) and without LiBr [108]. The amylopectin peak is over the range of 0.5 to 1.25 (× 10^{-8} $m^2 \cdot V^{-1} \cdot s^{-1}$) and the amylose peak over the range of 1.25 to 2.1 (× 10^{-8} $m^2 \cdot V^{-1} \cdot s^{-1}$).

In comparing the dissolution conditions of both Herrero-Martinez et al. [105] and the improved conditions of Schmitz et al. [108], the improved conditions consistently yielded an increase in the apparent amylose peak area, suggesting an increased concentration. The lack of an additional population in the amylose peak as compared to those observed in the previous section (1 to 1.75 × 10^{-8} $m^2 \cdot V^{-1} \cdot s^{-1}$, Figure 15 and Figure 16) suggest also that heating to 100 °C for 1 h is either not sufficient for complete dissolution, or the higher temperatures employed incite some kind of degradation in the starch. Aggregation was still present in samples prepared under the optimal conditions, and may be related to the cooling of samples between dissolution and injection.

2.3.1.3 Effect of temperature

Solubility is sensitive to temperature, making it an important factor to consider in any dissolution. Dissolution of starch is difficult. Therefore the use of high temperatures is essential in improving solubility and obtaining the most complete dissolution possible. Unfortunately, starch is also quite sensitive to temperature, and so temperatures are limited by the point at which degradation or sample changes begin to occur, e.g. gelatinisation. Gelatinisation is

needed when starch is dissolved in water or DMSO/water mixtures, and is the primary mechanism of dissolution in such solvents. However in anhydrous DMSO gelatinisation does not occur. Maintaining solutions at dissolution temperature has been shown to improve repeatability and reproducibility in the separation of starch by SEC [84]. Therefore, the impact of temperature was investigated, with dissolution completed at 80 °C and 300 rpm in a thermomixer, and solution temperature at the time of injection varied.

Maintaining high temperatures of the solution is important for the solution stability, especially in cases where solubility is poor. To investigate this, separations were performed whereby samples were maintained at their dissolution temperature, in this case 80 °C, after their dissolution. After injection, sample vials were removed from the instrument and placed back in the high temperature environment to re-equilibrate until the next injection.

Indications of improved repeatability were initially observed in samples prepared at 10 $g{\cdot}L^{-1}$ when the dissolution temperature was maintained (Figure 19), with poor repeatability occurring as a result of letting the solution cool. Cooling also appeared to impact on the separation itself, yielding large variation in electropherograms between different temperatures (Figure 19 and Figure 20).

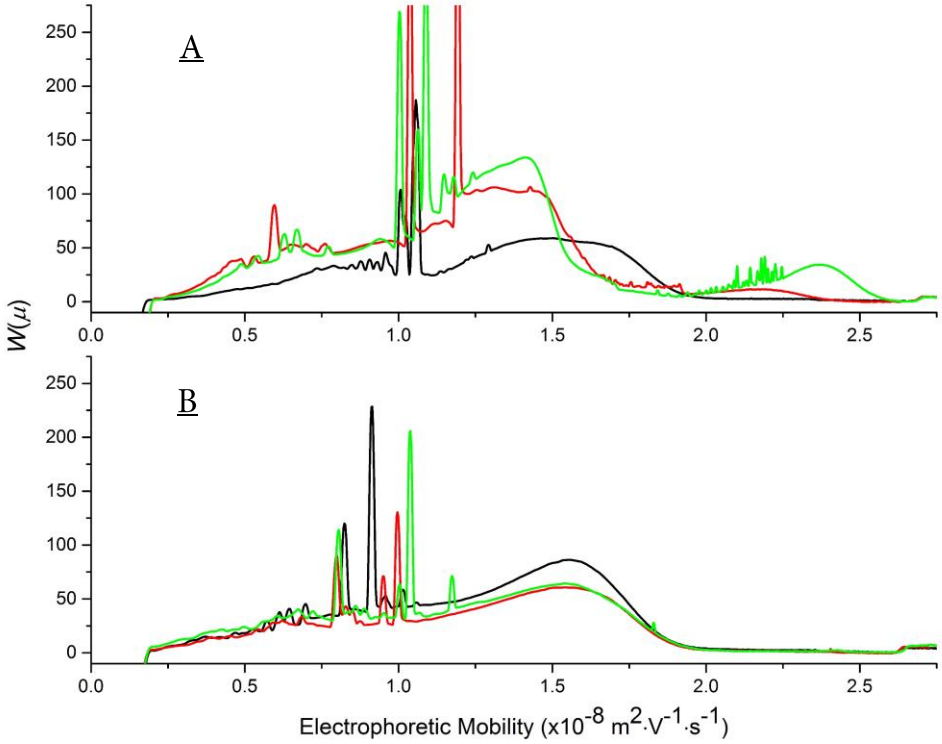

Figure 19 Weight-distributions of electrophoretic mobilities for repeat CE experiments (black – first, red – second and green – third) of Gelose 80 prepared in optimal conditions at 10 g·L^{-1}, A) After cooling and B) While stored at dissolution temperature.

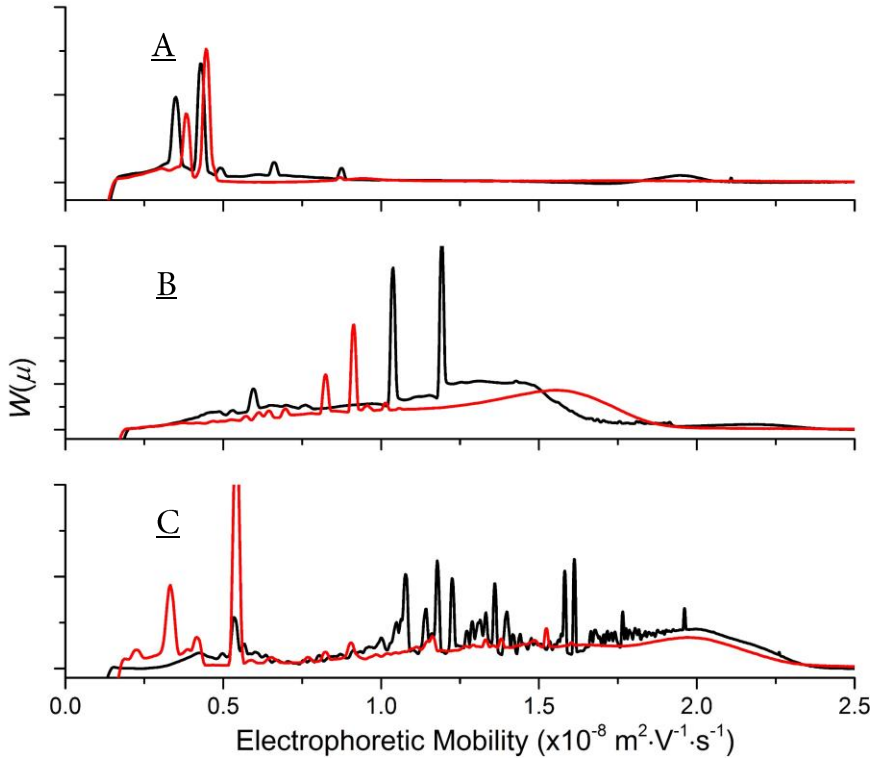

Figure 20 Weight-distributions of electrophoretic mobilities of A) Waxy maize, B) Gelose 80 and C) Regular maize prepared in optimal conditions at 10 g·L^{-1}. Samples were injected after cooling (black) and while stored at dissolution temperature (red).

These results showed that at higher concentrations (10 $g \cdot L^{-1}$) maintaining a high solution temperature right up to the point of separation is essential, providing a more repeatable and accurate separation of the amylose and amylopectin components.

To enable a more streamlined method of maintaining the solution at high temperature, a circulating water bath was used to heat the instrument vial tray to the maximum allowable temperature of 60 °C. While lower than the dissolution temperature, this was done to determine its viability in improving throughput and method simplification.

Keeping all vials at 60 °C yielded poor repeatability of the separation, as well as limited sensitivity in the detection for both amylose and amylopectin (Figure 21). Separations also appeared inconsistent with previous experiments either at high temperature or cooled (Section 2.3.1.3) or at high and low sample concentrations (Section 2.3.1.1). These poor results are hypothesised to be a result of the buffer instability and instrument design. The CE instrument used holds both buffers and samples in the same vial tray, meaning that both the buffer solutions and sample solutions were equilibrated to 60 °C. The stability of the buffer at these temperatures has not been explored, though the disparity in results from buffers conditioned at room temperature and at higher temperatures indicates an instability at higher temperatures. This may be related to the acetic acid/acetate equilibrium (buffer) itself or the iodine/potassium iodide equilibrium impacting the separation and/or the iodine complexation. The latter is more likely, as higher temperatures may lead to the volatilization of I_2 or an increase in I_2 reactions.

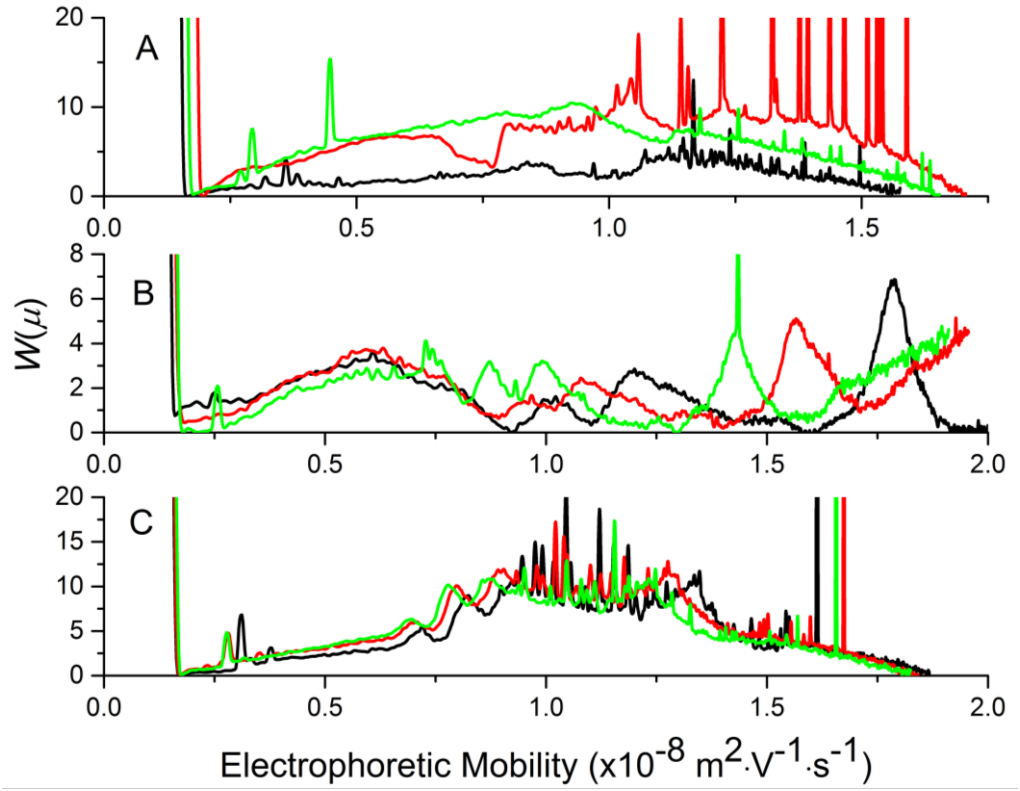

Figure 21 Weight-distributions of electrophoretic mobilities of A) Waxy maize, B) Regular maize and C) Gelose 80 prepared in optimal conditions at 1 g·L^{-1} and left at 60 °C in CE instrument for experiment duration. Black, red and green lines represent repeat separations.

Negative effects of solution cooling were also observed at lower concentrations (1 g·L^{-1}) when prepared in improved dissolution conditions (Figure 22). Repeatability at 1 g·L^{-1} whether the solution was cooled or not was quite similar, though differences were observed in the separation of amylose and amylopectin. Figure 22 illustrates the variation in both peak area and mobility when samples were allowed to cool. The variation observed was not as significant as seen at higher concentrations, though it is still evident. This reduction in peak area was investigated in relation to total cooling time to determine if this disparity was a result of variation in cooling times; however, no trend was observed and the phenomena appears to be sample specific in contrast to other samples where a general reduction in peak area was observed with cooling (Figure 22). In the case of Waxy corn, the separation appeared unaffected by cooling, yielding almost identical amylose and amylopectin peaks.

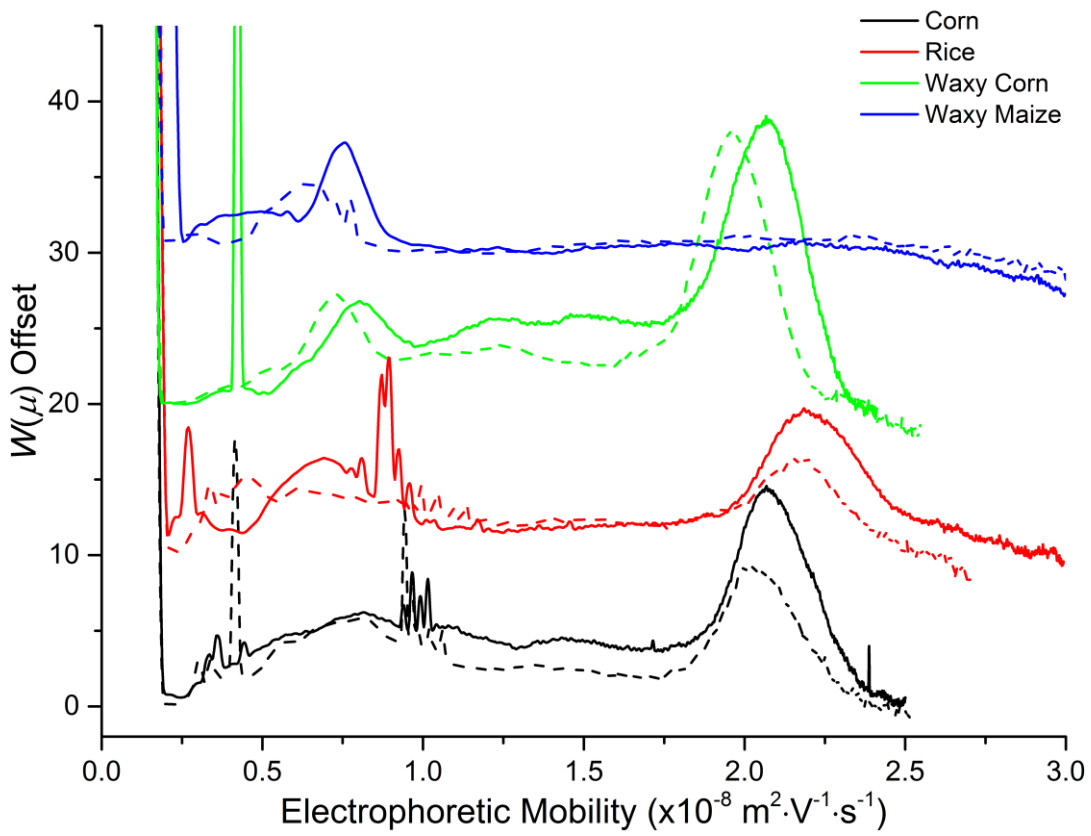

Figure 22 Weight-distributions of electrophoretic mobilities of starch samples prepared in optimal conditions at 1 g·L^{-1}. Samples were injected after cooling (dashed line) or stored at dissolution temperature until injection (solid line). The amylopectin peak is over the range of 0.25 to 1.0 (× 10^{-8} m^2·V^{-1}·s^{-1}) and the amylose peak over the range of 1.75 to 2.5 (× 10^{-8} m^2·V^{-1}·s^{-1}).

However, cooling was also observed to have other significant effects in some samples. In the case of potato amylopectin, cooling had a dramatic effect on the separation, with additional peaks at higher mobilities appearing in a repeatable manner (Figure 23). This sample was prepared with a higher concentration of LiBr (5 % w/v) in the solvent, and so the role of this in the repeatability of either hot or cooled starch solutions is unclear. However, amylopectin is more soluble than amylose, with the addition of LiBr only important in cases of high amylose content. Therefore, dissolution should not vary to such a degree as suggested here, and this poor repeatability may be contributed to by either the temperature or an alternative role that Li^+ and Br^- ions may play in the separation. Further separations of samples prepared in this 5 % LiBr solvent showed similar disparity between hot and cooled samples. This will be discussed further in Section 2.3.2.

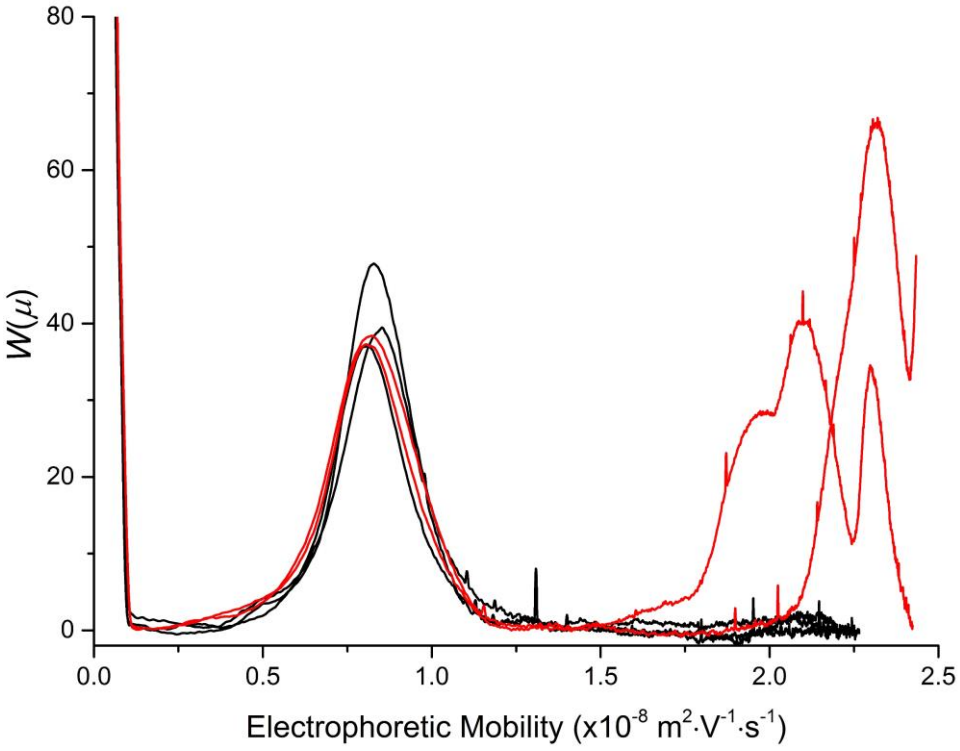

Figure 23 Weight-distributions of electrophoretic mobilities of potato amylopectin prepared in optimal conditions at 1 g·L^{-1}. Samples were injected after cooling (red) or stored at dissolution temperature until injection (black).

2.3.1.4 Effect of filtration

The presence of large particulates and aggregates is important in the chromatography field, and much is done to minimise their presence. The inclusion of these large particulates directly impacts on components such as stationary phases and pumping systems leading to premature wear. To counter this, almost all HPLC methods filter everything that is introduced into the system. This process has become so commonplace with time that it is now commonly applied without second thought and assumed to be the correct procedure regardless of sample. As such many publications focused on chromatography do not even mention or detail any filtration process involved in their work.

Over time the characterisation of starch has evolved as new discoveries and advancements are made in the dissolution and characterisation of starch. Filtration has stubbornly remained common, even with the knowledge that filtration is impacting the sample by removing large particles as intended and has the potential to cause shear degradation [120]. This is important as amylose solutions are not affected by filtration [121], but solutions containing amylopectin are prone to shear degradation [122]. The lack of a stationary phase

makes CE especially resilient to larger particles removing the need for filtration. Its robust nature has been shown in many studies such as the study of plant fibres [90], direct detection of minerals in zucchini [94], and the quantification of sugars in breakfast cereals[66].

Starch filtration can be damaging to the original starch sample, with the potential to alter the composition with respect to amylose and amylopectin proportions within the sample, as well as possibly degrading the chains themselves. The removal of large particles as intended also has a significant impact, as these large particles are also a key component of the starch itself and are essential to its complete characterisation.

Herrero-Martinez et al.[105] prepared samples under the same conditions which yielded very different separation profiles to those found in this work. Especially apparent is the lack of aggregation being seen in amylopectin by Herrero-Martinez et al. [105] . Filtration is such a common procedure in chromatography that it is sometimes not mentioned in the preparative procedure. It was hypothesised that the difference observed between the results obtained here and those published by Herrero-Martinez et al.[105] arise from sample filtration for the published results. Here the effect of filtration on the separation and detection of amylose and amylopectin is explored.

A comparison of filtered and unfiltered samples is presented in Figure 24 and Figure 25. A hydrophilic PTFE filter membrane was employed due to its chemical compatibility with the solvents used, and ideal interactions with the naturally hydrated starch samples. These samples were prepared in the dissolution conditions described in Herrero-Martinez et al. [105], heated to 100 °C and shaken at 300 rpm in a thermomixer for 1 h using 90 % DMSO as the solvent to compare with past results. Samples were prepared at 1 $g{\cdot}L^{-1}$ due to better response in the presence of aggregates, as discussed earlier (Section 2.3.1.1).

In Rice starch (Figure 24), filtration had a significant impact on the detected components. In unfiltered samples, both amylose and amylopectin peaks were observed, consistent with previous separations; however, after filtration there was a complete loss of amylopectin. Additionally, the peak area of amylose was reduced.

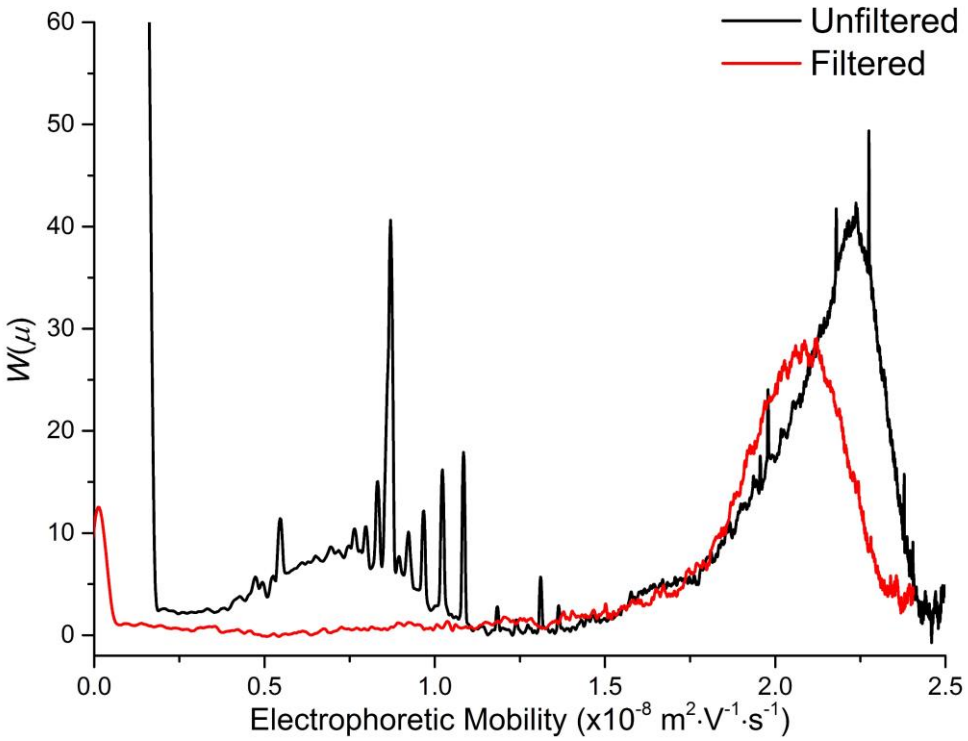

Figure 24 Weight-distributions of electrophoretic mobilities of Rice starch both filtered and unfiltered at 1 g·L^{-1} (prepared following Herrero-Martinez et al. [105]). The amylopectin peak is over the range of 0.25 to 1.25 (× 10^{-8} m^2·V^{-1}·s^{-1}) and the amylose peak over the range of 1.25 to 2.5 (× 10^{-8} m^2·V^{-1}·s^{-1}).

A similar trend was also observed in Corn starch (Figure 25), with loss of both amylose and amylopectin in the filtered sample compared to the unfiltered sample. In this case filtration had a more significant effect, with a weak, broad peak appearing covering the typical mobility range of amylose and amylopectin. This may occur as a result of degradation due to filtration, or may be explained by sample loss. However, the apparent loss of amylose is counterintuitive, as the filtration of amyloses should be possible [121] and so amylose should still be seen in the final solution. Degradation of amylopectin by shear forces may have created a distribution of structures of degradation products, and may explain the seemingly continuous distribution of amylose and amylopectin observed (Figure 25). However, the comparatively low peak area and signal-to-noise ratio indicate that this distribution cannot be representative of the whole sample, suggesting a major sample loss.

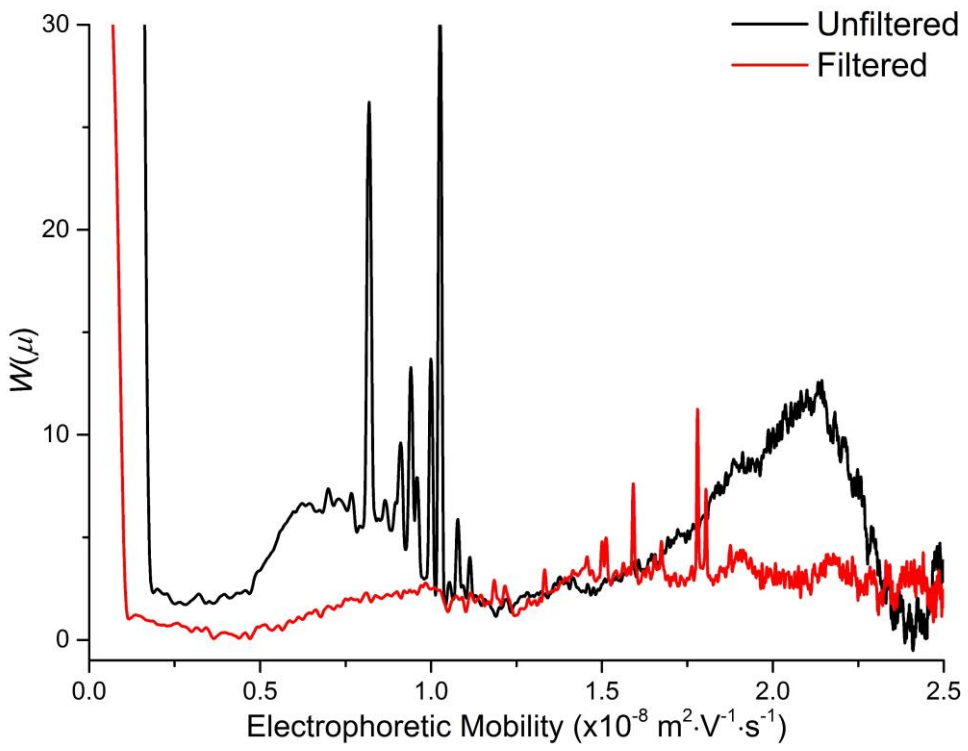

Figure 25 Weight-distributions of electrophoretic mobilities of Corn starch both filtered and unfiltered at 1 g·L^{-1} (prepared following Herrero-Martinez et al. [105]). The amylopectin peak is over the range of 0.25 to 1.25 (× 10^{-8} m^2·V^{-1}·s^{-1}) and the amylose peak over the range of 1.25 to 2.5 (× 10^{-8} m^2·V^{-1}·s^{-1}).

Figure 24 and Figure 25 show that filtration has significant negative effects on the separation of amylose and amylopectin. In both cases the presence of amylopectin was severely impacted by filtration, in agreement with the notion that amylopectin cannot be filtered and is susceptible to shear degradation when filtered. Additionally, amylose is affected also by filtration. Amylose can be filtered [121]; however, our results indicate that amylose is also affected, with an apparent loss of amylose observed in both rice (Figure 24) and corn (Figure 25) starches. Therefore, it is concluded that starch filtration has a significant impact on both the composition and structure of the original starch sample. When characterisation representative of the original sample is desired, filtration should be avoided.

Further investigations into the effect of filtration was done, comparing samples prepared in the optimal conditions (1 g·L^{-1}) to those prepared as described in Herrero-Martinez et al. [105] (10 g·L^{-1}) with an additional filtration step. As discussed earlier, filtration has a detrimental effect on amylose and amylopectin. So here a comparison of the optimal conditions determined earlier in this section (Section 2.3.1) to those presented by Herrero-Martinez et al. [105] is made.

Figure 26 compares these two for Rice starch. Significant differences were observed in peak area and peak shapes, with filtered Rice starch showing a much lower peak area of amylopectin, especially considering the 10-fold higher concentration. The presence of two peaks in the mobility zone of amylopectin (0.25 to 1.5 × 10^{-8} $m^2 \cdot V^{-1} \cdot s^{-1}$) also suggests that some degradation or sample modification has occurred. When comparing the peak areas of amylose in both preparation procedures, peak area was greater in filtered conditions; however, the greater solution concentration indicated a significant sample loss from filtration, in agreement with the trend observed in previous cases in this section.

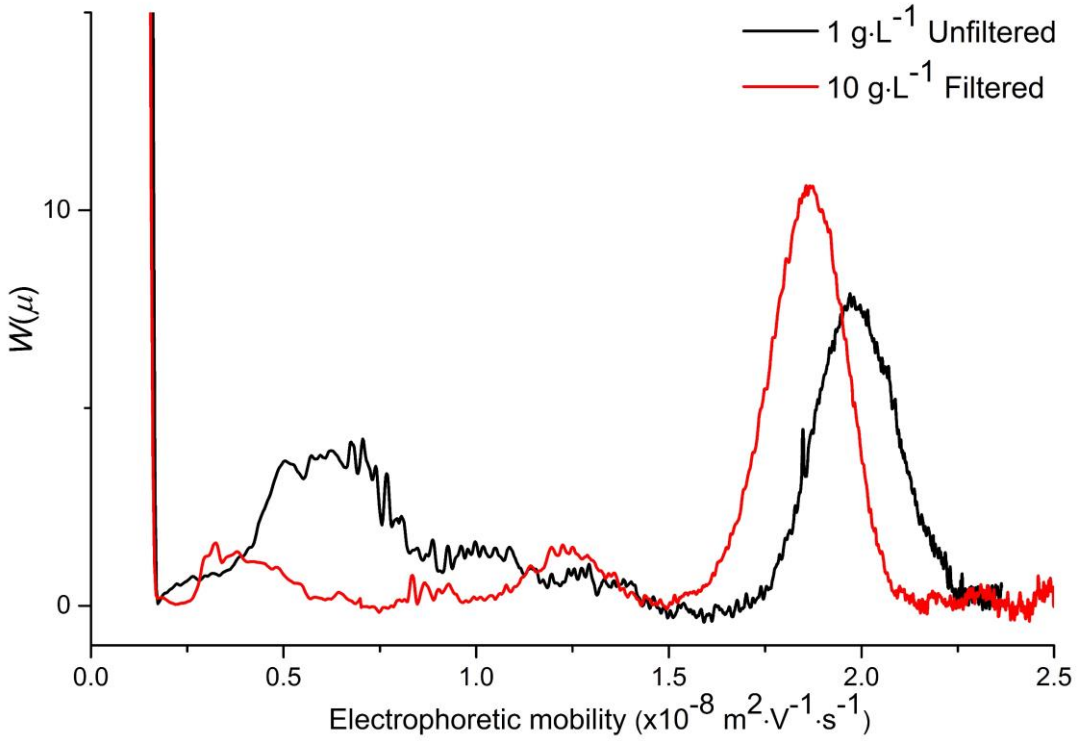

Figure 26 Weight-distributions of electrophoretic mobilities of Rice starch at 1 g·L^{-1} without filtration (prepared in optimal conditions) and at 10 g·L^{-1} with filtration (prepared following Herrero-Martinez et al.[105]). The amylopectin peak is over the range of 0.25 to 1.25 (× 10^{-8} $m^2 \cdot V^{-1} \cdot s^{-1}$) and the amylose peak over the range of 1.5 to 2.25 (× 10^{-8} $m^2 \cdot V^{-1} \cdot s^{-1}$).

In an additional experiment, the stability of filtered starch samples prepared by magnetic stirring at room temperature was explored. This experiment aimed to determine the aggregation kinetics of a filtered starch solution, and whether aggregation increases with storage time after filtration. Filtered starch solutions were repeatedly injected over time to investigate how the separation and composition of amylose and amylopectin evolved with storage time (Figure A1 and Figure A2). The electropherograms of Rice starch revealed no trend in peak area, mobility or aggregation (Figure A1). Fluctuations in these observed properties occurred randomly, indicating either an inherent range of error in the method, or

high variability or heterogeneity within the sample solution itself (Figure 27). The fact that the three types of mobility varied in the same way indicates that the variations in mobility and peak area are affecting the highly branched and lesser branched components in a similar fashion. When taking into account the qualitative observations of aggregation (Figure A1), it may also be noted that there is no effect of branching on aggregation.

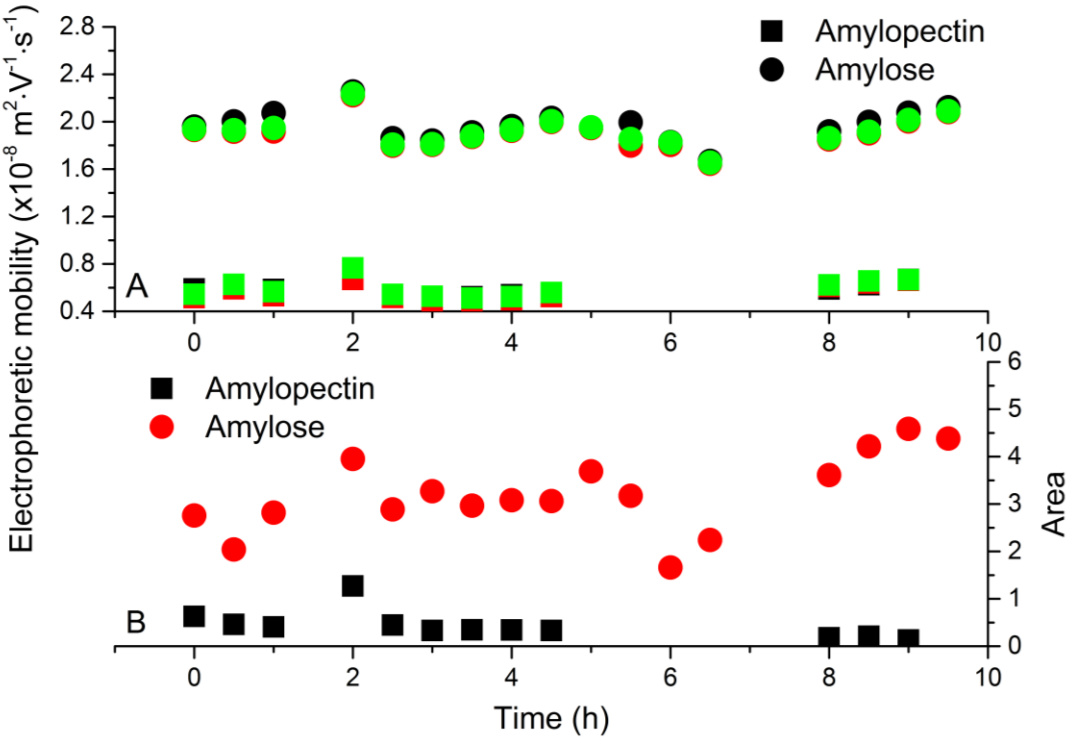

Figure 27 Peak parameters of amylose and amylopectin from electropherograms of Rice starch in Figure A1 showing: A) Evolution of μ at the maximum (black), moment-average μ (red) and weight-average μ (green) with time; and B) Evolution of peak area with time. Calculation of moment-average and weight-average μ is shown in Section 2.3.3.1

The same experiment performed on Corn starch (Figure A2) gave similar results, with a random variation in peak area and mobility with increasing storage time (Figure 28). As discussed previously, this could be attributed to method error or sample heterogeneity. Additionally, the same conclusion may be drawn from the similarity of the different types of mobility (Figure 28), indicating that no effect of branching is seen on aggregation.

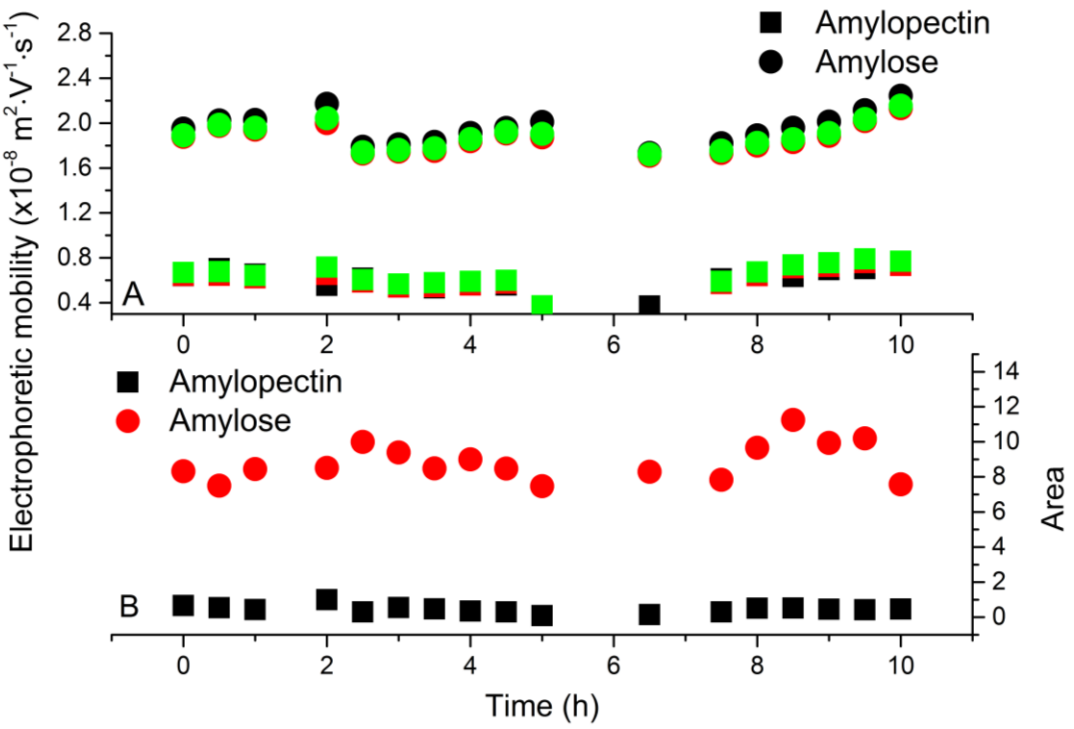

Figure 28 Peak parameters of amylose and amylopectin from electropherograms of Corn starch in Figure A2 showing: A) Evolution of μ at the maximum (black), moment-average μ (red) and weight-average μ (green) with time; and B) Evolution of peak area with time. Calculation of moment-average and weight-average μ is shown in Section 2.3.3.1

The stability of the filtered samples over time was investigated to probe the conditions employed by Herrero-Martinez et al. [105], specifically determining if filtration was the reason no signs of aggregation were observed. Initial results indicated a lack of aggregation; however, significant loss of amylopectin was also observed. The type of filter employed likely plays a significant role in this, and while the filter employed in this work resulted in the loss of amylopectin in the sample other filters may not lead to this. The significant reduction of aggregates is similar to what is observed in the results of Herrero-Martinez et al.[105], and so it was determined that filtration was likely employed in their work. The effect of sample aging was then investigated to determine if this also played a role in the lack of aggregation seen in the results of Herrero-Martinez et al. [105]. No correlation was found; however this did allow for some insight into the variability of this method with filtration.

In this section the impact of filtration on starch dissolution was assessed through its impact on the separation of amylose and amylopectin in CE. Filtration has a significant detrimental effect on the concentration of both amylose and amylopectin regardless of their initial concentration. Aggregates were removedin some cases of filtration; however, this was also accompanied by a loss of most of the amylopectin. Additionally, the effect of filtration on

amylose content was more significant than sometimes assumed. Filtration of amylose is believed to be possible; however, my results suggested that while amylose survives filtration in most cases, the final concentration is likely impacted yielding a lower final concentration. Therefore, it was concluded that filtration of starch samples should be avoided.

2.3.2 Separation

In separation of analytes by CE two properties are required. First, a net charge to the analytes is required. Second, a way to detect the analytes is needed. In the separation of amylose and amylopectin these properties are not natively occurring. However, taking advantage of the well-studied and documented iodine binding phenomenon, both a charge and characteristic absorbance are obtained in starch [74]. The mechanism of complexation is not explored in this work, with the methodology being adapted from the work of Herrero-Martinez et al. [105], modifying only the dissolution conditions. The principle of this method involves the complexation of both amylose and amylopectin, with complexation occurring *in situ* rather than prior to injection. This is possible by inclusion of a potassium iodide/iodine equilibrium within the acetic acid buffer, producing polyiodide ions that allow complexation. Determination of amylose content through spectrophotometric methods typically involves up to 15 minutes of reaction time for complexation. Using the CE method employed here, the complexation time is much reduced, and so its effect on the separation and detection of both amylose and amylopectin requires investigation.

2.3.2.1 Conversion of raw data

In the analysis of the separation data, the raw data was transformed following the treatment procedure in Chamieh et al. [123]. The migration time of analytes in CE is dependent on both the electrophoretic mobility (μ) of the analyte and the electroosmotic flow. Therefore, as a corrective procedure, migration time (t_m) was converted to μ so that it does not depend on the electroosmotic flow. The electroosmotic flow is visualised by the migration of a neutral species (t_{eof}) and intrinsically has a μ of 0. This transformation is shown in Equation 1,

$$\mu = \frac{l_d l_t}{V}\left(\frac{1}{t_m} - \frac{1}{t_{eof}}\right) \quad (1)$$

where l_d is the capillary length to the detector, l_t is the total capillary length and V is the voltage.

The absorbance was also corrected to account for the analyte velocity through the detection window, correcting absorbance as a function of time spent in the detection window and accounting for the transformation from time-scale to mobility-scale distributions of the x-axis. It is important to note that detection occurs during the separation and not after it (post-column) as is the case in HPLC. This is shown in Equations 2 to 6, where absorbance is first corrected for velocity,

$$\text{UV Signal} = \frac{\text{Absorbance}}{t_m} \tag{2}$$

Transformation to weight-distribution of electrophoretic mobilities $W(\mu)$ is then done,

$$W(\mu) = \frac{\text{UV Signal}}{\frac{d\mu}{dt_m}} \tag{3}$$

where $\frac{d\mu}{dt_m}$ is the derivative of μ with respect to t_m,

$$\frac{d\mu}{dt_m} = -\frac{l_d l_t}{V} \times \frac{1}{{t_m}^2} \tag{4}$$

Therefore,

$$\frac{d\mu}{dt_m} \propto \frac{1}{{t_m}^2} \tag{5}$$

Simplifying Equation 3 according to Equations 2 and 5,

$$W(\mu) = \text{Absorbance} \times t_m \tag{6}$$

Using Equation 6, raw absorbance data was corrected according to analyte velocity and transformed from time-scale absorbance to mobility-scale absorbance. These corrections are essential in determining molecular property based distributions. The transformations effect on data is shown in Figure 29, comparing the same data plotted in raw data form (Figure 29A) and after corrective transformations (Figure 29B).

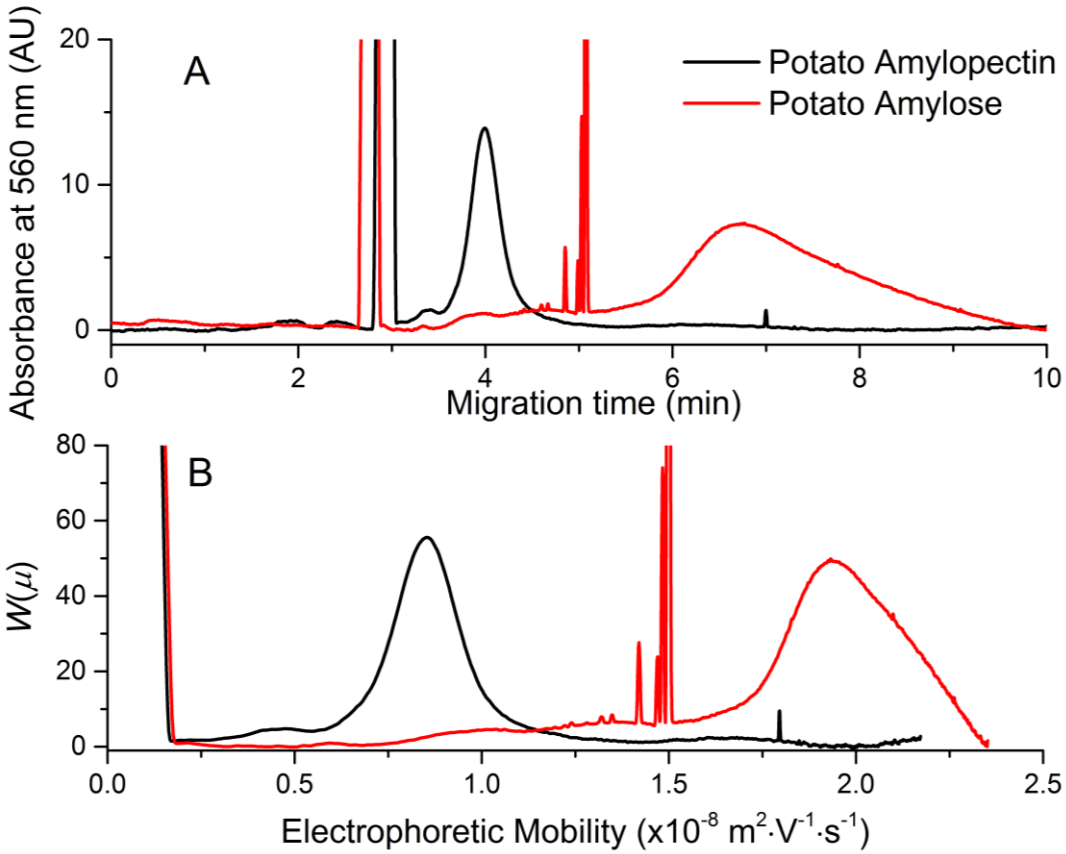

Figure 29 A) Electropherograms, and B) Weight-distributions of electrophoretic mobilities of amylose and amylopectin A) Before and, B) After correction and transformation

2.3.2.2 CE in the critical conditions

The separation of polymers in CE is limited to polymers that are charged or can be charged. When large polyelectrolytes are separated by CE, they are separated in the critical conditions. This is referred to as CE in the critical conditions (CE-CC). This is an analogy to liquid chromatography in the critical conditions (LC-CC) where conditions are sought in which a homopolymer is not separated by molar mass [100]. In CE-CC the separation of polyelectrolytes is independent of molar mass when the degree of polymerisation is greater than 10. This effect has been demonstrated experimentally in DNA[124], carboxymethyl celluloses[125], poly(styrene sulfonates)[126], and poly(acrylic acid)[127]. This effect is illustrated in Figure 30. Most polymer samples are not homogenous and are composed of many molecules with different molar masses, end groups, composition distributions and branching

characteristics. Currently the most commonly assessed molecular attribute of polymers is the heterogeneity of molar mass, calculated as the ratio of the weight-average molar mass and the number-average molar mass (dispersity). Typically these values are determined by size-exclusion chromatography [128]. A limitation of this approach is the inability to separate based on molecular attributes other than hydrodynamic volume [81]. Separation by CE-CC allows for separation by one or more of these characteristics, with no influence of molar mass, enabling the characterisation of complex polymers.

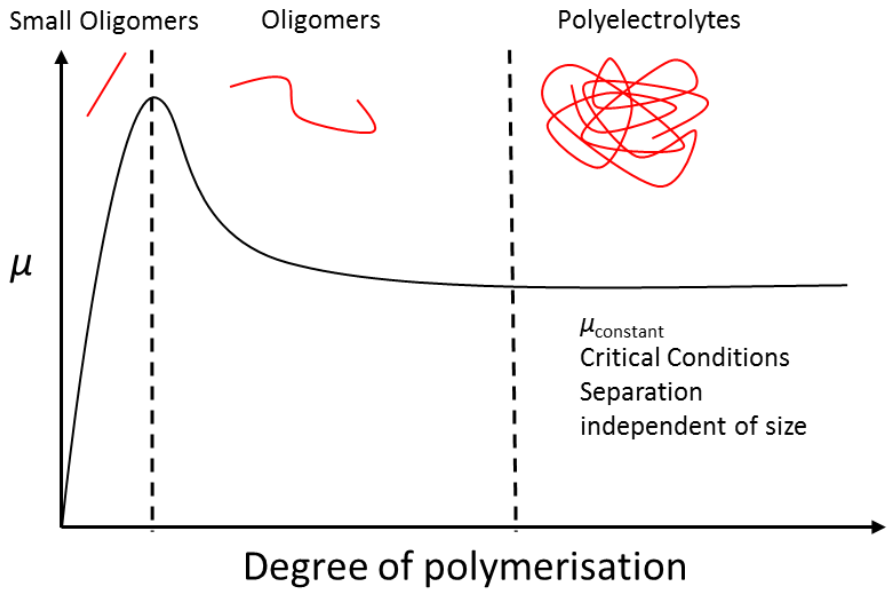

Figure 30 Evolution of μ with increasing size (adapted from Cottet et al. [126])

When separation takes place in the critical conditions, the electrophoretic mobility is sensitive to the structural and compositional features other than molar mass. The tendency of such features to manifest in distributions yields a distribution of electrophoretic mobilities dependent on the separation factors. This distribution can be used in the characterisation of heterogeneity of molecular characteristics within polyelectrolyte samples. Separation in the critical conditions has been shown experimentally in the separation by branching in poly(acrylic acid)[129] and dendrigraft polylysine[130] , by degree of acetylation in chitosan[131], and by composition in block copolymers[132]. In the separation by branching of poly(acrylic acid), greater branching yielded shorter migration times, corresponding to lower μ (Figure 31) [129]. Separation by branching in amylose and amylopectin has also been shown, where the more highly branched amylopectin yielded a faster migration in contrast to the less branched amyloseFigure 9 [105].

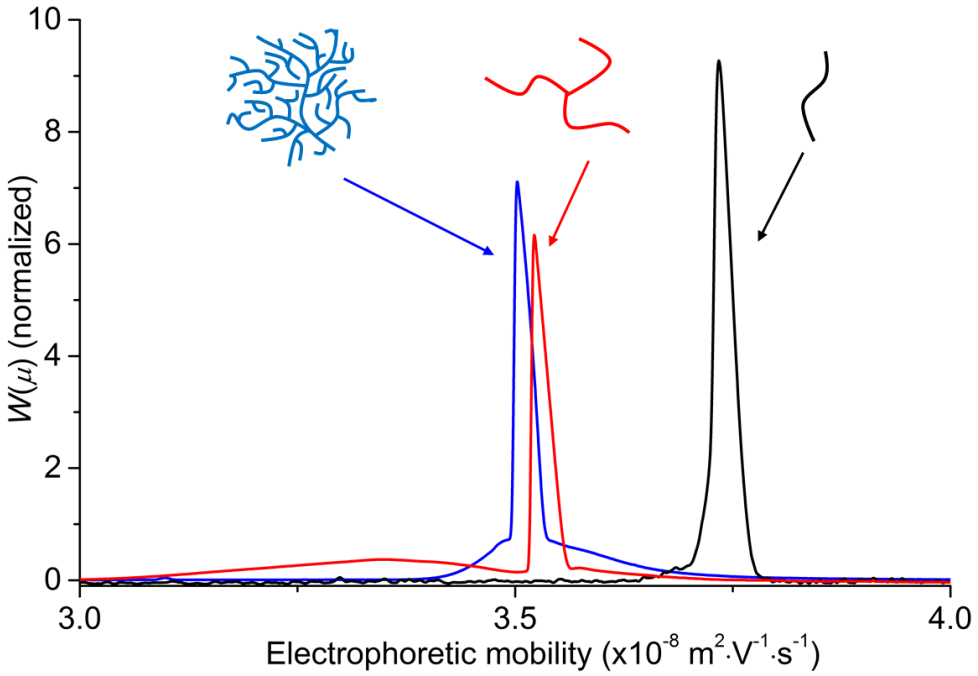

Figure 31 Weight-distributions of electrophoretic mobilities of poly(acrylic acid) illustrating separation by branching in CE-CC [112].

The broadness of the resulting electrophoretic mobility distributions can be assessed through the value of their dispersity [112]. The dispersity of distribution of electrophoretic mobilities can then be related to structural distributions dependent on the molecular attributes that are influencing the separation.

As previously mentioned, the extremely large molar mass of both amylose and amylopectin means that separation occurs in the critical conditions in which separation becomes independent of molar mass. Both amylose and amylopectin are glucose homopolymers, and differ only in their branching structure. Therefore, the separation of iodine bound amylose and amylopectin is expected to yield a separation by branching structures. With separation occurring as a function of branching structure, the determination of electrophoretic mobility distributions can be employed, allowing investigation into the inherent heterogeneity of branching in amylose and amylopectin, as well as into the overall heterogeneity of branching within starch. Investigating the heterogeneity of branching will be a valuable tool in understanding the digestive properties of starch. The calculation and determination of dispersity will be discussed in Section 2.3.3.

2.3.2.3 Pressure mobilisation to assess adsorption

In free solution CE, adsorption onto the untreated silica capillary walls is common in the analysis of proteins, leading to peak tailing and loss of resolution [133]. The kinetics of this phenomenon has been investigated in the literature [134], emphasising the importance of mitigating this effect through approaches such as capillary coatings [135, 136] or extreme pHs [137] to invert the coulombic forces. A simulation of this effect is presented in Figure 32, showing the tailing effect that is indicative of adsorption to the capillary wall. In some cases, this adsorption can also result in tailing that never returns to the baseline, significantly complicating analysis. This effect is not limited to only proteins [132], and can occur in any cases where coulombic forces are strong enough to create significant interaction between analytes and the capillary wall [132]. Adsorption of analytes to the capillary wall has a significant impact on the separation mechanism and subsequent detection of analytes. The way in which it impacts on the separation means that any information regarding the separation mechanism is lost or corrupted. This is especially important in reference to CE-CC, where separation becomes independent of molar mass, and separation occurs by other factors. The electrophoretic mobility distribution obtained in this type of separation would likely be corrupted by adsorption, and any subsequent characterisation would be made much more difficult to achieve accurately. Therefore, to ensure adsorption is not occurring, starch samples were tested using pressure mobilisation. In pressure mobilisation, the sample is injected into the capillary, and pushed through the capillary using only pressure. By applying only hydrodynamic pressure with no electric field, the interaction between the negatively charged silica capillary walls and the charged analytes can be investigated directly [116]. It is important to note that this is not a separation experiment, and as such there is no separation of the analytes.

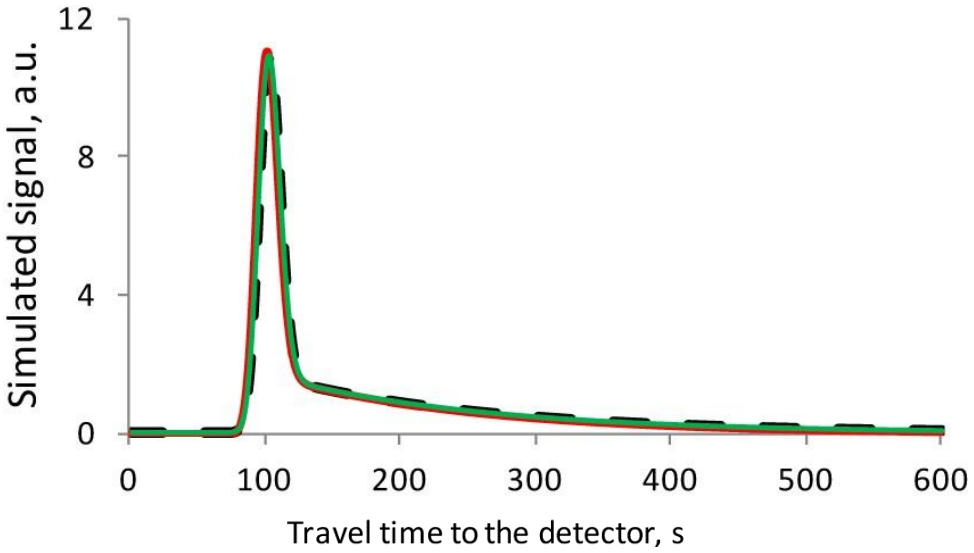

Figure 32 Signal simulation of pressure mobilisation experiment based on 1-dimensional (red) and 2-dimensional (dashed black line) models with adsorption and desorption rate constants of k_{ad} = 10 $(mM)^{-1} \cdot s^{-1}$ and k_{de} = 0.1 s^{-1} respectively. The best fit of 1-dimensional model into the 2-dimensional simulated data is shown by the green line. Taken from Cherney et al.[134]

In this work, the complexation of starch with iodine is essential in imparting charge and allowing detection of amylose and amylopectin components, therefore mixing in the background electrolyte was employed to ensure complexation occurred [138]. The procedure for this method is described in Section2.2.2.

Pressure mobilisation was applied to samples prepared in the optimal conditions as described in the Section 2.2.2 as these are the conditions that will be employed for subsequent analysis and characterisation of starch samples. In Figure 33, the results of pressure mobilisation on amylose and amylopectin standards are compared with the pressure mobilisation of pure DMSO. The absence of tailing seen relative to a pure DMSO marker indicate that any adsorption of the starch complex to the wall is negligible. The broader, symmetric peak observed is indicative of the presence of a larger component compared to the relatively sharp peak seen in pure DMSO and also observed in starch samples dissolved in DMSO. The relationship of peak width with diffusion coefficient supports this, and therefore the broad symmetrical peak was assigned as the iodine complexed starch components amylose and amylopectin. The symmetrical nature of the broad peak indicated that no adsorption was occurring.

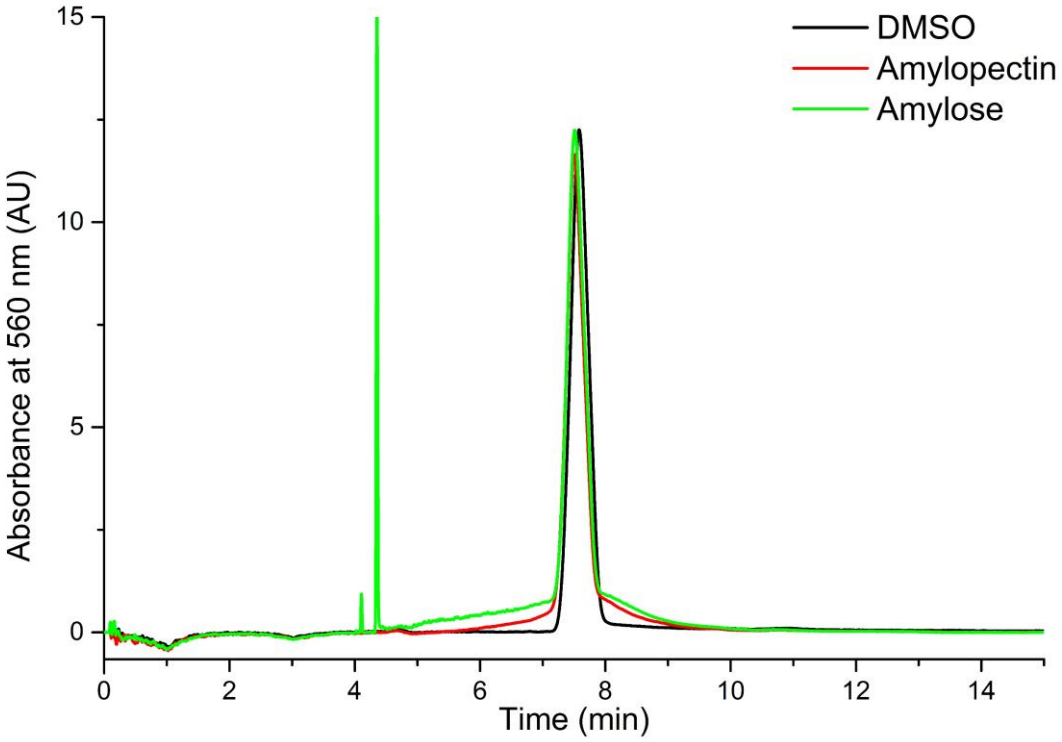

Figure 33 Elugram (pressure mobilisation) of DMSO and starches prepared in optimal conditions at 1 g·L^{-1}.

Pressure mobilisation was also done at different sample concentrations and in different dissolution solvents in a comparative study to investigate if the increased viscosity or addition of lithium bromide to the solvent had any significant effects on adsorption to the capillary wall. Again no significant signs of adsorption were observed, with no tailing of the peak occurring relative to a 50/50 DMSO/running buffer standard marker (Figure 34) at either 10 g·L^{-1} versus 1 g·L^{-1} or in 90 % DMSO versus anhydrous DMSO with 0.05 % LiBr. Similarly to the previous case, the broader symmetrical peak is indicative of the larger amylose and amylopectin species. The symmetrical nature of this peak revealed that no adsorption was occurring.

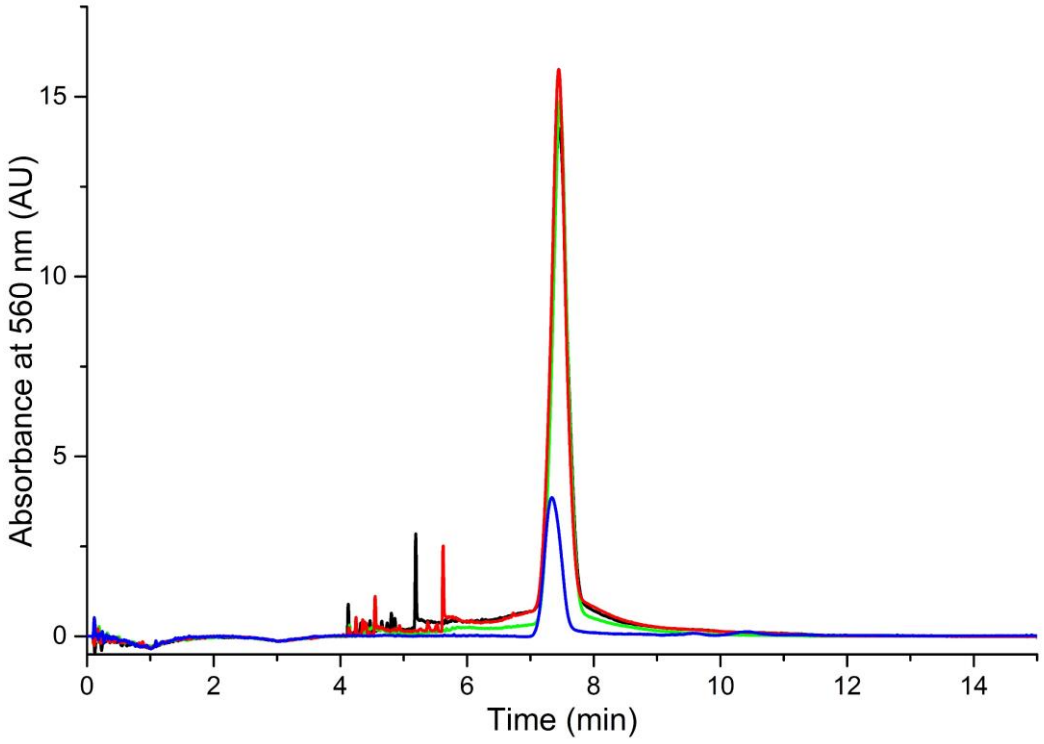

Figure 34 Elugram (pressure mobilisation) of Corn starch prepared at 10 g·L^{-1} in 90 % DMSO following Herrero-Martinez et al.[105] (Black), Rice starch prepared at 1 g·L^{-1} in the optimal conditions (Green) and 10 g·L^{-1} following Herrero-Martinez et al.[105] (Red) and running buffer with 50 % DMSO (Blue).

In the separation of amylose and amylopectin, the role of adsorption appeared to be insignificant and thus recovery is high, indicating that there is very little affinity between the iodine bound starch and glass. This in stark contrast to the characterisation of starch by SEC, where methodology is often plagued by low recovery as a result of adsorption to the organic stationary phases employed [81]. The absence of adsorption here means that the determination of distributions of electrophoretic mobilities relating to branching heterogeneity is possible. This will be discussed in Section 2.3.3.

2.3.2.4 Starch-iodine incubation

The nature of this separation and detection relies on the binding of amylose and amylopectin chains with iodine in solution to form a starch-iodide complex. In solution, potassium iodide and iodine form a triiodide ion that complexes strongly with starch, yielding a characteristic blue coloured helical complex. The UV-Vis spectra of amylose and amylopectin are different, with maxima at ~540 and ~620 nm, respectively. However, their absorbance bands overlap and thus through separation and subsequent individual detection a more accurate characterisation of these components can be achieved.

The I_3^-/starch complexation equilibrium is often used in the determination of amylose content. Measurements are traditionally done by simple colorimetric and spectrophotometric methods [74, 113, 139], often including equilibrium time for full complexation (typically 10 min). This approach is quick and simple, thus its high prevalence as an amylose determination technique. As part of this work, the impact of incubation time was studied *in situ* by pausing the separation within the capillary for a set amount of time. Samples were injected hydrodynamically (Section 2.2.2) and mixed with the background electrolyte by ramping the voltage up to 20 kV over 1 min and holding for 30 s and then down to - 0 kV. This mixing time allows for the sample to be adequately mixed with the iodine containing background electrolyte, while also removing any Li^+ and Br^- ions that could interfere with iodine binding [109, 110]. Incubation time was then determined by the time spent at 0 kV from the previous step, before the voltage was ramped back up to 20 kV at the conclusion of the incubation period.

At low concentrations of lithium bromide (0.05 %) the impact on complexation time yielded mixed results over the 1 to 10 min of incubation time tested (Figure 37). In Waxy corn (Figure 37A), a sample that should theoretically consist of primarily amylopectin, the separation yielded a single peak with 0 min of incubation as expected. However, with further incubation time, an extra peak was observed indicating a population of amylose within the sample. In this case then it was determined that some amylose is present in the sample and adequate time is required for complexation, indicating slower iodine binding kinetics for different amyloses. In Gelose 80 (Figure 37B), no significant changes in separation or detection were observed with varying incubation time, despite the much higher amylose content that is expected compared to the Waxy corn sample. These results are thus contradictory, and the reasons behind this conflict are not completely understood. One possible explanation is a difference in the type of amylose in each sample, with the amylose in Gelose 80 facilitating faster iodine binding and thus not requiring extended iodine incubation time.

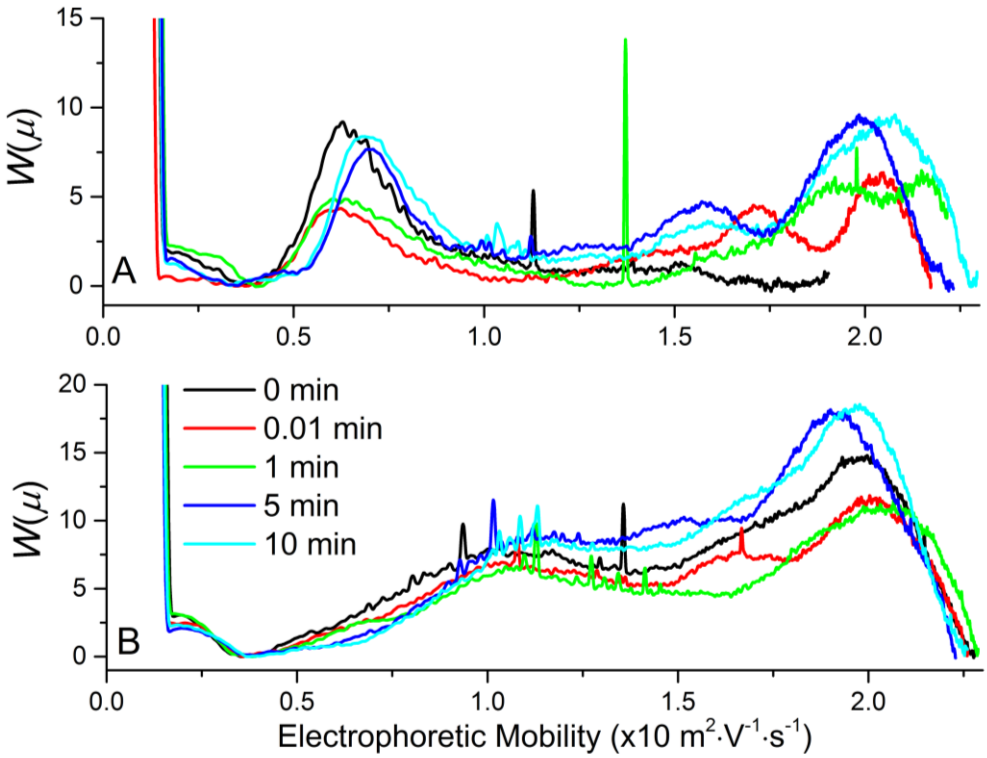

Figure 35 Weight-distributions of electrophoretic mobilities of A) Waxy Corn starch and B) Gelose 80 showing evolution of $W(\mu)$ with increasing incubation time in background electrolyte; samples were prepared in the optimal conditions at 1 g·L^{-1}.

At higher concentrations of lithium bromide (5 %), a significant effect of increasing incubation time was observed (Figure 36). Incubations times shorter than a minute showed a significant loss of signal, and as incubation time increased the separation underwent significant changes. At 5 min of incubation time, the appearance of four peaks versus two after an incubation time of 1 min indicates a new population has undergone iodine binding; however, after 10 min only 3 peaks were clearly observed. This indicates that a change in the iodine binding occurred. . The peak area was also found to increase with increasing incubation; however, after 10 min the peak area was reduced. This again indicates a shift in the nature of the iodine binding. Thus at higher lithium bromide concentrations a longer incubation time is required to facilitate complete complexation.

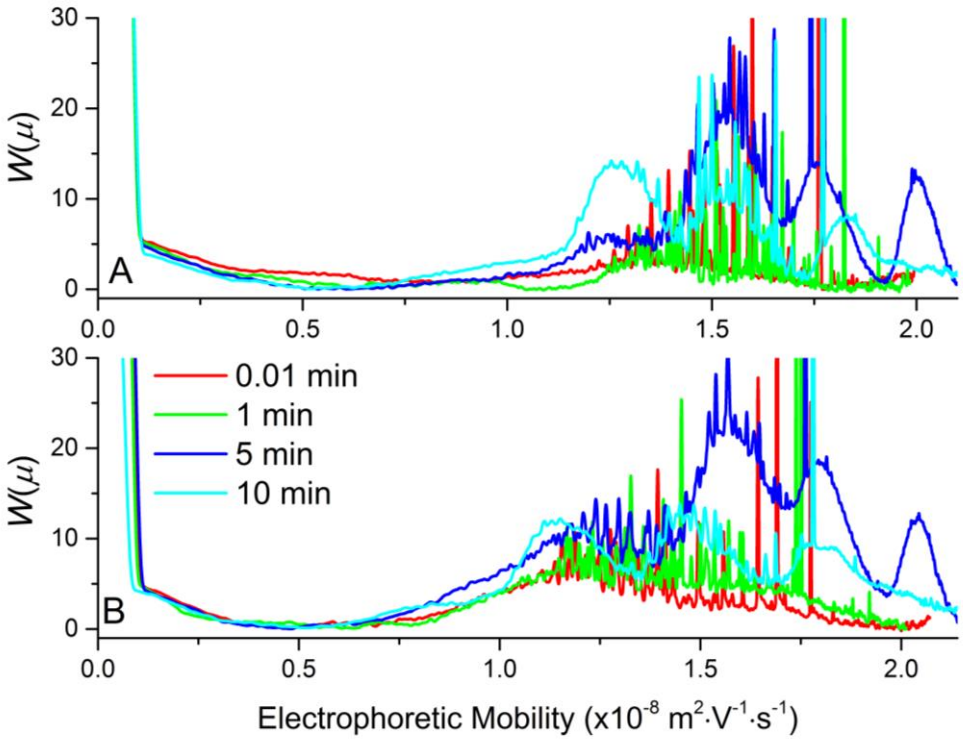

Figure 36 Weight-distributions of electrophoretic mobilities of: A) Potato amylose; and B) Gelose 80 showing evolution of $W(\mu)$ with increasing incubation time in the background electrolyte. Samples were prepared in the optimal conditions at 1 g·L^{-1}, with a LiBr concentration of 5 % w/w.

These higher lithium bromide concentrations are important in the dissolution of high amylose starches, and so the application of this method would require the addition of time for equilibrium in the running buffer to allow for a complete complexation. In this experiment, incubation was done up to 10 min in the two dissolution mixtures; however, at higher LiBr concentrations changes in separation were continuing to occur in the final time steps. Therefore, it is not clear if the complexation is complete. Further work will need to be done to determine how long is required for a full complexation with iodine to occur. Conversely, the presence of lithium bromide in solution may also result in incomplete starch-iodine complexation and so bias analysis of the sample. Therefore, in cases of samples with high amylose content, high LiBr concentrations should be used; however, methodology will need to be modified to account for the extended time required for complete iodine complexation and further potential impacts explored. Low LiBr concentrations also impacted the complexation time, and will also need to be explored further.

2.3.3 Characterisation

In the characterisation of starch, much work has been done in the analysis of molecular and structural characteristics including determination of molar mass, chain length and branch length distributions [85, 140, 141]. These characteristics are often expressed in terms of distributions, a result of the heterogeneous nature of natural polysaccharides such as starch. Starch is comprised of two macromolecules, amylose and amylopectin, with vastly different branching structures. The branching structure of these two macromolecules is not homogenous, and so we are presented with a distribution of structures in both amylose and amylopectin. Often in food analysis a quantitative measure of amylose content is made with no further investigation into its structural properties. In many cases where amylose content is a desired parameter, such as in food products or even industrial applications, the distribution of branching structures in these two components is likely to play a very important role.

2.3.3.1 Dispersity of electrophoretic mobility distributions

Currently the most commonly assessed molecular attribute of polymers is molar mass. The heterogeneity of molar mass can be assessed through the determination of its dispersity and is typically done by size-exclusion chromatography (SEC) [128]. The dispersity is calculated as the weight-average molar mass divided by the number-average molar mass. However, the characterisation of polymers by SEC is limited by its inability to separate polymers according to other molecular features such as branching or composition [81]. A number of methods for separation by other molecular attributes, such as copolymer composition and branching, also exist [142, 143]; however, heterogeneity of these attributes is not often quantified. In CE-CC the heterogeneity of these attributes can be assessed through the analysis of electrophoretic mobility distributions.

Methodology for the determination of dispersity from distributions of electrophoretic mobilities in CE has recently been published by our research team, exploring four different approaches to the calculation of dispersity [112]. Calculations in this work are based on the ratio of moments in a distribution, specifically the weight distribution of electrophoretic mobilities

with $W(\mu)$ representing the weight fraction of polyelectrolyte chains with electrophoretic mobility μ. A mass sensitive detection such as UV is required for this. The transformation of raw data to $W(\mu)$ is achieved using Equations 1 and 6.

Four approaches were explored in this work. The specifics of these calculations will not be discussed here, and the reader is referred to the cited publication [112] for further information. The equations used in the calculation of dispersities of electrophoretic mobilities (D) by these four approaches are presented in Equations 7, 8, 9 and 10, and the weight-average electrophoretic mobility (μ_w) and moment-average electrophoretic mobility (μ_m) calculated by Equations 11 and 12 respectively.

$$D(1,0) = D(W(\mu),1,0) = \frac{[\sum_z W(\mu_z)\mu_z(\mu_{z+1}-\mu_z)][\sum_z W(\mu_z)\mu_z{}^{-1}(\mu_{z+1}-\mu_z)]}{[\sum_z W(\mu_z)(\mu_{z+1}-\mu_z)]^2} \quad (7)$$

$$D(2,0) = D(W(\mu),2,0) = \frac{[\sum_z W(\mu_z)\mu_z{}^2(\mu_{z+1}-\mu_z)][\sum_z W(\mu_z)(\mu_{z+1}-\mu_z)]}{[\sum_z W(\mu_z)\mu_z(\mu_{z+1}-\mu_z)]^2} \quad (8)$$

$$D(3,0) = D(W(\mu),3,0) = \frac{[\sum_z W(\mu_z)\mu_z{}^3(\mu_{z+1}-\mu_z)][\sum_z W(\mu_z)\mu_z(\mu_{z+1}-\mu_z)]}{[\sum_z W(\mu_z)\mu_z{}^2(\mu_{z+1}-\mu_z)]^2} \quad (9)$$

$$SDev = D_\sigma = \left[\frac{\sum_z W(\mu_z)(\mu_z-\mu_w)^2(\mu_{z+1}-\mu_z)}{\sum_z W(\mu_z)(\mu_{z+1}-\mu_z)}\right]^{0.5} \quad (10)$$

$$\mu_w = \frac{[\sum_z W(\mu_z)\mu_z(\mu_{z+1}-\mu_z)]}{[\sum_z W(\mu_z)(\mu_{z+1}-\mu_z)]} \quad (11)$$

$$\mu_m = \frac{[\sum_z W(\mu_z)(\mu_{z+1}-\mu_z)]}{[\sum_z W(\mu_z)\mu_z{}^{-1}(\mu_{z+1}-\mu_z)]} \quad (12)$$

where μ_z is the electrophoretic mobility of the z^{th} molecule.

In the first approach (D(1,0)) an analogy with weight-average molar mass divided by number-average molar mass is employed. D(1,0) is calculated as the ratio of the first and zeroth order moments divided by the ratio of zeroth and negative first order moments of the distribution. In the second approach (D(2,0)) an analogy with z-average molar mass divided by weight-average molar mass is used, taking the ratio of the second and first order moments (z-average) divided by the ratio of first and zeroth order moments of the distribution. In the third approach (D(3,0)), dispersity is calculated as the ratio of third and second order moments divided by the ratio of second and first order moments of the distribution. In the final approach (Equation 10), the standard deviation is calculated as a measure of dispersity, taking the μ_w as a reference. The way these approaches calculate dispersity varies depending on the peak shape, and so all approaches should be compared in cases of non-symmetric distributions

(with a tail) or bimodal distributions (kurtosis). Herein these dispersities will be referred to as $D(1,0)$, $D(2,0)$, $D(3,0)$ and *SDev*, respectively.

The dispersity of amylose and amylopectin was calculated from the distribution of mobilities obtained by CE and used to assess the heterogeneity of branching. In the separation of amylose and amylopectin a clear separation of the two components is not always achieved, and may be a result of method limitations. Improved selectivity may help, or this may arise as a result of a continuous and overlapping distribution of both amylose and amylopectin in relation to their branching structures. Due to this, the results discussed here will be a measure of the whole $W(\mu)$ (dispersity of peaks from the beginning of the amylopectin peak to the end of the amylose peak). In cases where a clear separation was achieved, results were included to allow a comparison of the individual dispersities of amylose and amylopectin. All results presented in this section are taken from samples prepared using the optimal conditions mentioned in the previous sections (unless otherwise stated), using anhydrous DMSO with 0.05 % LiBr with shaking at 300 rpm and 80 °C in a thermomixer for at least 8 h. Samples are injected either cooled or hot, as will be specified in discussion.

Weight-distributions of electrophoretic mobilities from which dispersity values were calculated were normalised according to the total area under both the amylose and amylopectin peaks. This means that this data now represents a real distribution, whereas previous data was not normalised and therefore is not a real distribution but a corrected electropherogram. This allows for a visual comparison of dispersity to be made, complementing the calculated dispersity values. In the graphical representations of dispersity values, both y-axes were scaled from a respective value representative of the minimum amount of dispersity to the highest value of dispersity obtained. Scaling in this way allows for comparisons to be drawn between the different types of dispersity calculations.

2.3.3.2 Investigating heterogeneity of branching in starch

The dispersity within samples maintained at high temperature is discussed here. When sample solutions were maintained at the dissolution temperature, repeatability was drastically improved and the presence of aggregates reduced. Figure 37 shows the $W(\mu)$ of samples stored

at dissolution temperature. Investigating the calculated dispersity values in Figure 38, dispersity values were much higher than for any other polymers reported using this methodology in CE. In the case of branching in poly(sodium acrylate acid)(PNaA), dispersity values reported range from ~1.0000 for linear to ~1.0015 for a 3-arm star, with *SDev* values an order of magnitude smaller than those reported here [112].

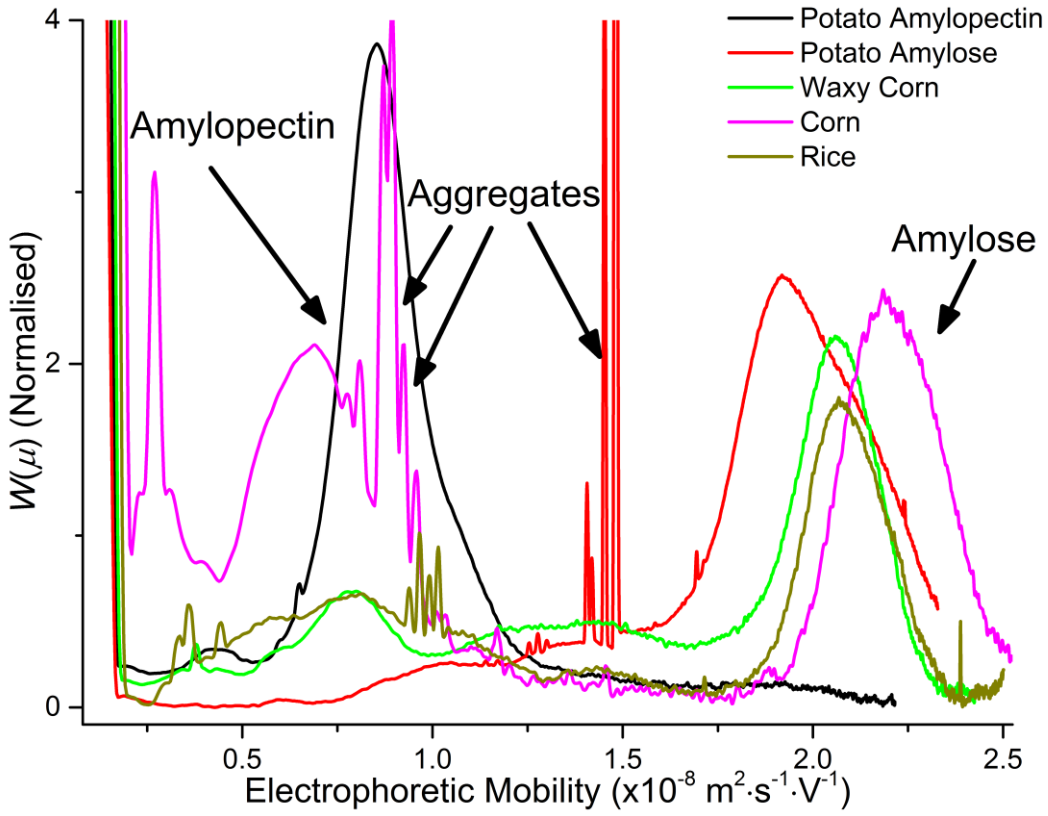

Figure 37 Normalised weight-distributions of electrophoretic mobilities of starch samples prepared in the optimal conditions at 1 g·L^{-1} and stored at dissolution temperature. The amylopectin peak is over the range 0.25 to 1.25 (× 10^{-8} m^2·V^{-1}·s^{-1}) and the amylose peak over the range of 1.5 to 2.5 (× 10^{-8} m^2·V^{-1}·s^{-1}). Dispersity values are in Figure 38

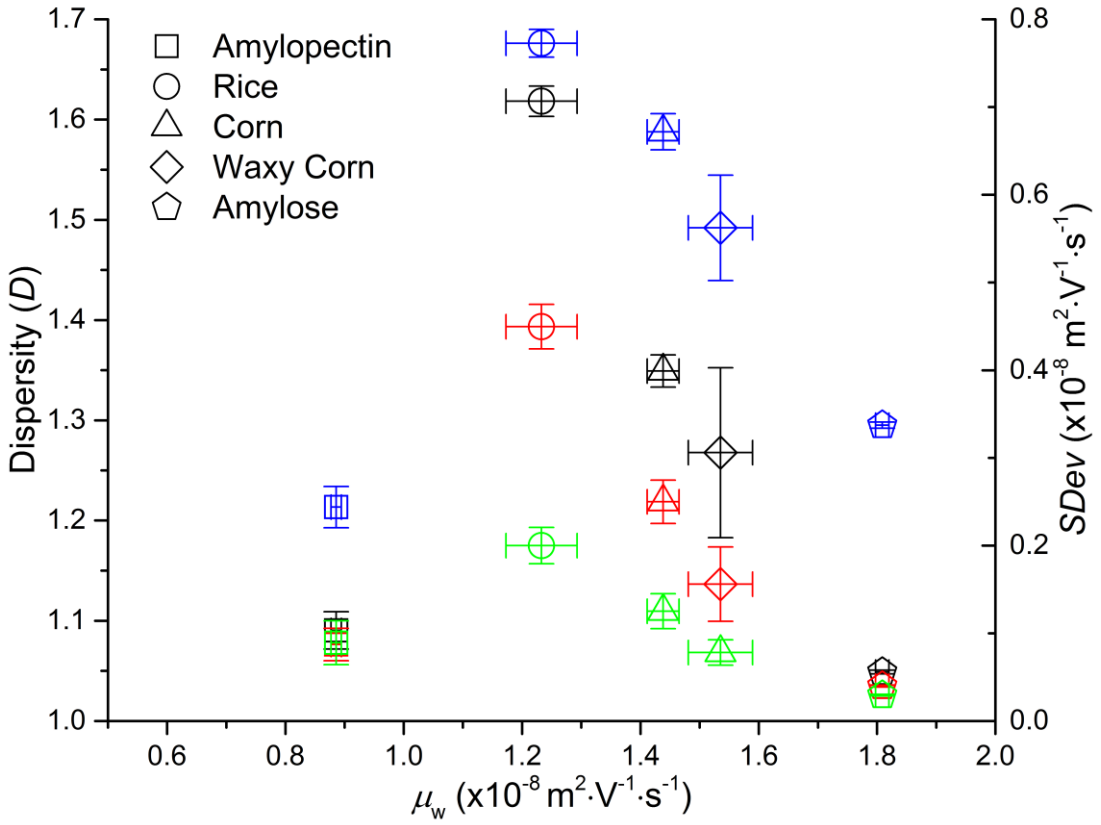

Figure 38 Dispersity values of the distributions in Figure 39 plotted against μ_w, Black - *D*(1,0), Red - *D*(2,0), Green - *D*(3,0), Blue – *SDev*. Error bars are the standard deviation of dispersity from triplicate CE experiments.

In Figure 38, potato amylose and potato amylopectin samples are compared to samples containing both amylose and amylopectin. When looking at the μ_w of these 'mixed' samples versus amylose and amylopectin, the values appeared to fall between the two. This is a result of μ_w being calculated as the average of both amylose and amylopectin. With contributions of both, μ_w should fall between amylose and amylopectin mobilities, weighed depending on the contributions of each component. In the case of the amylose and amylopectin samples, the dispersity reported was much higher than literature values [112]. Thus, the heterogeneity of branching in both amylose and amylopectin alone is already significantly higher than that in the small pool of synthetic polymers studied previously [112]. This could be explained by the non-random branching seen in starch biosynthesis compared to the random branching seen in statistical polymers. Therefore, the considerably higher dispersity values reported here for samples containing bimodal peaks in the form of amylose and amylopectin are expected. Thus, the heterogeneity of branching in amylose and amylopectin is extremely high.

In comparing different sample dispersities using the 4 approaches in calculation, conclusions can be drawn as to how heterogeneity of branching compares between samples, as well as how these approaches respond to the distributions used for calculation.

Investigating the difference in dispersity between samples in Figure 38, the comparison of heterogeneity of branching in amylose and amylopectin was explored. The heterogeneity of branching seen in the literature shows that as degree of branching increased in PNaA, dispersity increased [112]. However, when degree of branching continues to increase, a point is reached where branching is so great that the dispersity of branching decreases [112]. This can be explained as follows: when the degree of branching increases, the ways in which branching can occur differently is reduced; whereas in less branched polymers where branching can occur randomly then branching can occur in many more different ways. This phenomenon has also been observed in the local dispersity values of poly(alkyl acrylates) determined by multiple detection SEC from the ratio of the local weight-average molar mass (by light scattering) to the local number-average molar mass (by viscometry)[81]. In applying this theory to amylose and amylopectin, the highly branched nature of amylopectin versus the slightly branched nature of amylose would suggest that amylose may have a greater heterogeneity of branching structures. In the dispersity values of $D(1,0)$, $D(2,0)$ and $D(3,0)$ this trend was not observed and instead amylopectin exhibited a greater dispersity. This is likely attributed to the separation itself. In this experiment, the run time was not sufficient to allow for the amylose to completely migrate, evidenced by the peak at higher mobility not returning to the baseline. This led to an underestimated dispersity value for the incomplete peak. A difference is also introduced in the way in which these dispersities are calculated. Taking 0 as a reference for the same peak width, the dispersity values will depend on the distance of μ_w from this value, and so a more significant effect is observed in amylose than amylopectin. When the dispersity values of *SDev* in both amylose and amylopectin were compared, the opposite trend was observed, with amylose yielding a higher dispersity. As this approach takes μ_w as the reference peak width dispersity values do not depend on the distance from 0 [144], yielding a trend that matches the visual dispersity cues seen in Figure 31. Significant inaccuracy in the dispersity of amylose as a result of insufficient experimental run time was apparent; however, the importance of investigating all 4 approaches has been highlighted in this comparison.

In comparing those samples with both amylose and amylopectin present, all 4 approaches to dispersity yielded the same trend, with Rice starch having the greatest dispersity, followed by Corn starch and then Waxy corn starch. This gives a point of differentiation between samples; however, the specifics of how these types of dispersities behave when applied to these separations may still be investigated. In comparing the dispersities $D(1,0)$, $D(2,0)$ and $D(3,0)$, the relative difference between the sample dispersities increased when going from $D(3,0)$, to $D(2,0)$ and again to $D(1,0)$. In both corn and Rice starch, $D(3,0)$ was much lower than both $D(2,0)$ and $D(1,0)$. This indicates a tailing of the $W(\mu)$ towards higher μ in these samples, thus suggest lower branching in $W(\mu)$. No significant differences in the dispersity values of other samples were observed, indicating minimal tailing toward higher or lower μ and thus no bias to greater or lower branching in $W(\mu)$. In comparing the values of $D(1,0)$ to those of *SDev*, the values by *SDev* appeared to yield a smaller relative difference on a scaled axis, indicating a less precise measure in contrast to the greater spread of values seen in $D(1,0)$. This can also be said in general of calculations of *SDev* in comparison to those others presented. The spread of dispersity values by $D(1,0)$, $D(2,0)$ and $D(3,0)$ on a scaled axis, versus those of *SDev* on a scaled axis, was much greater. This indicates a greater precision of measurement in the use of these dispersity values versus those of *SDev*. This subsequently allowed for a greater degree of separation between different dispersity values to be obtained. However, the type of dispersity calculation employed cannot be selected based solely on its increased precision. This is because it is possible that these different types of calculations are actually measuring different sample attributes, and as such an increased precision may indicate a stronger or weaker difference between samples for that attribute. Examples of varying sample attributes that may manifest in the specific properties of the structural distributions of amylose and amylopectin are symmetrical or non-symmetrical distributions.

The trends discussed here in the comparison of dispersity calculations and dispersity by *SDev* have been observed in the separation of amylose and amylopectin, and as thus may only apply to such a system. In the application of this method to other samples, the same approach should be made where all approaches of dispersity are explored and compared, and conclusions are drawn based on that individual system.

Figure 39 shows the separation of amylose and amylopectin in cooled corn and Rice starch. As shown in Section 2.3.1.3, injection of cooled samples is not optimal, with poor repeatability and increased signs of aggregation. Despite this, dispersity information can still be obtained and used to investigate ideas of dispersity between amylose and amylopectin. In Figure 39, a clear separation of amylose and amylopectin was seen, allowing a measure of dispersity of each in this bimodal system.

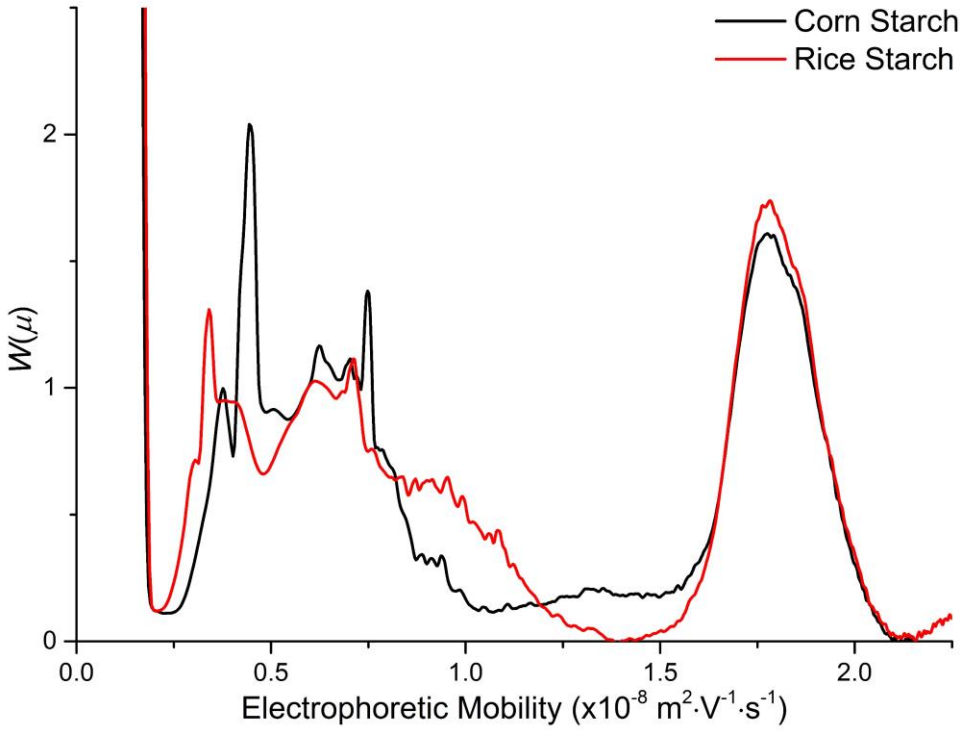

Figure 39 Normalised weight-distributions of μ of cooled samples prepared in the optimal conditions at 1 g·L^{-1}. The amylopectin peak is over the range of 0.25 to 1.25 (× 10^{-8} m^2·V^{-1}·s^{-1}) and the amylose peak over the range of 1.5 to 2.5 (× 10^{-8} m^2·V^{-1}·s^{-1}).Dispersity values are in Figure 40.

Figure 40 shows the dispersity values of amylose and amylopectin by $D(1,0)$, $D(2,0)$ and $D(3,0)$. The same trend was again observed as those of potato amylose and potato amylopectin (Figure 37 and Figure 38) where amylopectin yielded a higher dispersity than amylose. This is against the logic of how dispersity would be affected by increased branching and again suggests that the heterogeneity of branching is greater in amylopectin than in amylose. When looking at *SDev* dispersity values, the trend of higher dispersity in amylopectin continued in contrast0020to the previous results of potato amylose and amylopectin. This greater dispersity of amylopectin can again be visualised in the electrophoretic mobility distributions in Figure 39, whereby the amylopectin peak was significantly broader than that of amylose. Again, the

SDev values were in a narrow range of values, suggesting a lesser precision in this measurement as opposed to the values obtained for $D(1,0)$, $D(2,0)$ and $D(3,0)$.

Comparing the dispersity values of amylose and amylopectin between samples further allows for determination of a point of difference between samples. Dispersity values could also be further used with structural information obtained through other characterisation techniques to learn more about how heterogeneity of branching relates to other properties in the supramolecular structure of starch. Comparing the $D(1,0)$, $D(2,0)$ and $D(3,0)$ of amylose and amylopectin between samples in Figure 40 indicated no significant differences in dispersity, with large error range resulting in strong overlap of dispersity values. Despite this, with improvements to precision the determination of dispersity shows promise for indicating differences in the dispersity of both amylose and amylopectin components. In comparing the different dispersity values of each sample, no significant differences were observed between dispersity values for either amylose or amylopectin peaks of each sample, as had been seen for Corn and Rice starch in Figure 40. This is likely a result of the bimodality of $W(\mu)$, resulting in a significantly greater heterogeneity compared to that of a single peak system. Therefore, either significant tailing is not apparent in the individual amylose and amylopectin peaks, or the difference in dispersity values manifests on a smaller scale than is seen in the extremely high dispersity values in Figure 41 and is limited by the current error of these dispersity values. As these results are based on cooled samples, no solid conclusions about the samples could be made. However, a slight difference in dispersity values for amylopectin between the samples indicates the existence of different types of amylopectin in terms of branching. It is expected that precision will be improved in optimally prepared samples at high temperature as a result of the improved experimental repeatability.

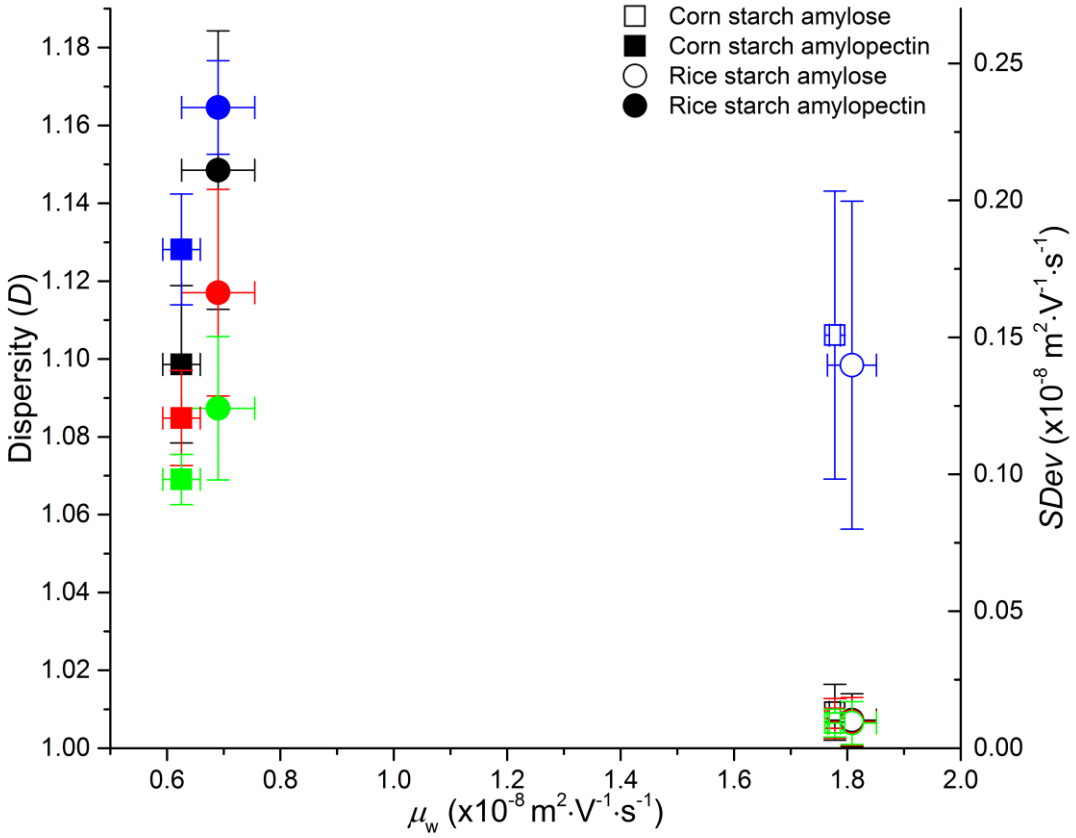

Figure 40 Dispersity values of the distributions in Figure 41 plotted against μ_w, Black - *D*(1,0), Red - *D*(2,0), Green - *D*(3,0), Blue – *SDev*. Error bars are the standard deviation of dispersity from triplicate CE experiments.

From these results , the dispersity values are a valuable and rich source of information in the characterisation of polymers. In the case of starch samples,these dispersity values allowed for extensive insight into the heterogeneity of branching within a sample, including not only the overall heterogeneity of branching but also the individual heterogeneities of branching in amylose and amylopectin. This could prove to be a powerful tool in the total characterisation of starch, and will be extremely relevant in the further investigation of other properties of starch such as digestibility.

2.3.3.3 Impact of sample temperature on dispersity values and repeatability

As discussed in Section 2.3.1.3, temperature plays an important role in the separation of amylose and amylopectin. By maintaining solutions at dissolution temperatures until injection time, repeatability was improved and the presence of aggregates was reduced. In this section the results of dispersity calculated from hot and cooled samples are explored.

Figure 41presents $W(\mu)$ of three different starches injected before and after cooling. The primary difference observed between hot and cooled samples from the $W(\mu)$s is in the total peak area, as well as slight variations in peak shape and position.

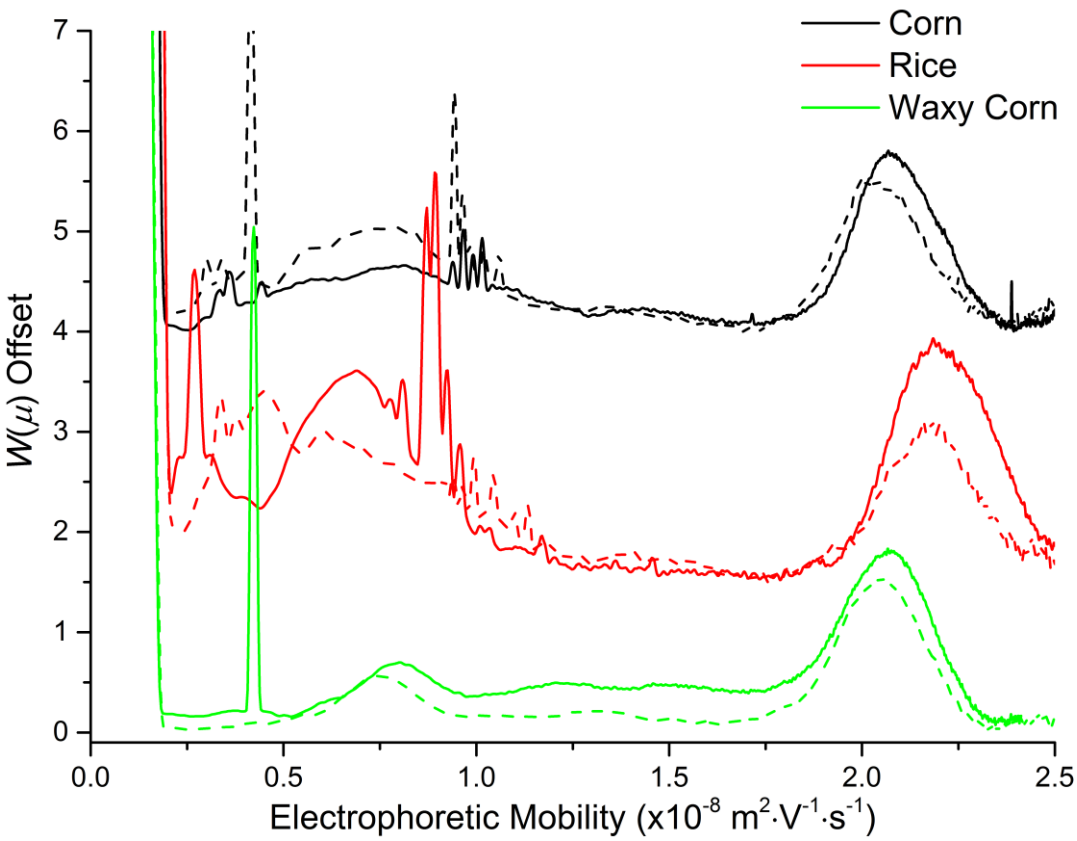

Figure 41 Normalised weight-distributions of electrophoretic mobilities of starch samples prepared in the optimal conditions at 1 g·L^{-1}, either injected after cooling (dashed line) or stored at dissolution temperature (solid line). The amylopectin peak is over the range of 0.5 to 1.25 (× 10^{-8} m^2·V^{-1}·s^{-1}) and the amylose peak over the range of 1.75 to 2.5 (× 10^{-8} m^2·V^{-1}·s^{-1}). Dispersity values are in Figure 42.

Figure 42 gives the dispersity values for these starches, including $D(1,0)$, $D(2,0)$, $D(3,0)$ and *SDev*. No significant trends were observed in $D(1,0)$, $D(2,0)$ or $D(3,0)$ with cooling. Dispersity values of Rice starch and Waxy corn starch did not differ significantly, and, in the case of Waxy corn starch, both dispersity values and μ_w were completely unchanged with cooling. Dispersity values of Corn starch decreased slightly with cooling; however, the error associated with these values makes the significance of this difference questionable. However, the significant shift to higher μ_w seen upon cooling in Corn starch indicates that the total apparent amount of branching decreases with cooling. In the *SDev* dispersities these trends were somewhat lost, with the margin of error in the measurements allowing overlap of both the hot and cooled values. Therefore no difference in dispersity was observed. The area taken

by these *SDev* dispersities was again very small, alluding again to a lesser sensitivity as opposed to the first three approaches of dispersity.

In looking at difference in μ_w between samples, the influence of bias based on the contributions of each peak in this bimodal system can be easily visualised. The higher μ_w values seen in Waxy corn starch correspond to the much greater peak area and peak width of amylose, whereas the lower mobilities seen in Rice starch correspond to the larger peak area and peak width of amylopectin. Therefore, along with dispersity giving insight into the overall heterogeneity of branching in these systems, the contribution to this dispersity reflected in the μ_w gives insight into the contributor to this dispersity.

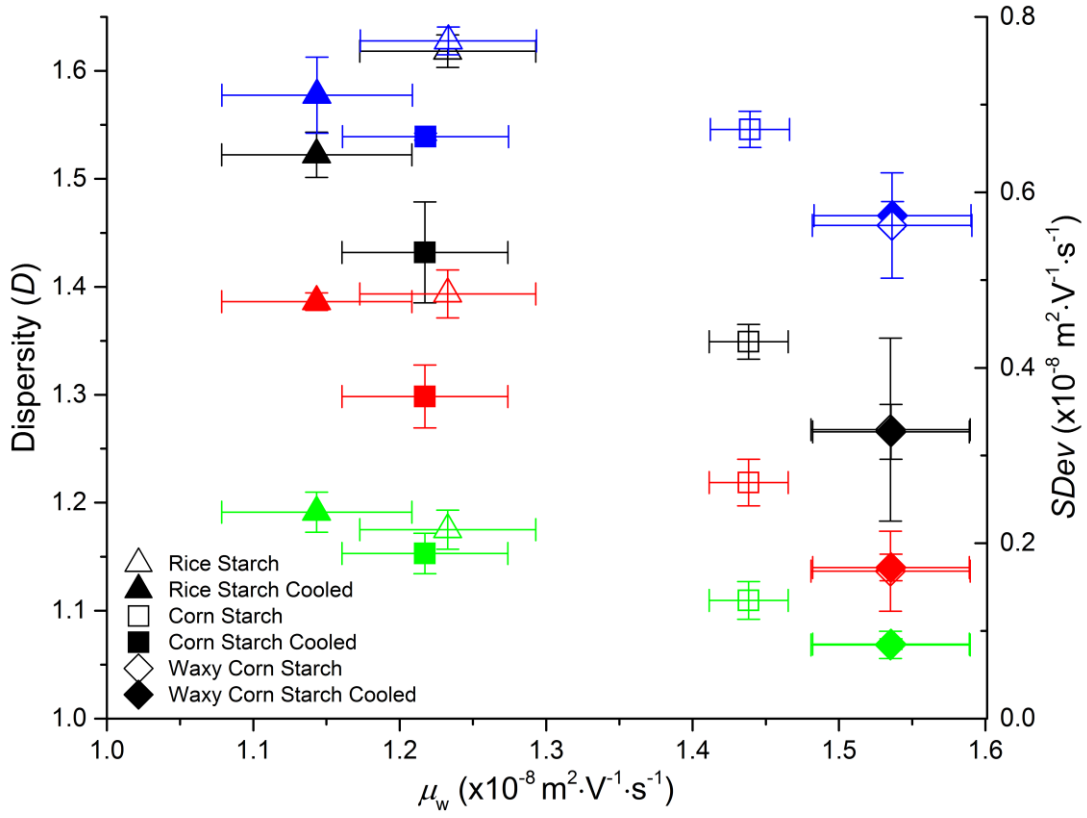

Figure 42 Dispersity values of the distributions in Figure 43 plotted against μ_w, Black - *D*(1,0), Red - *D*(2,0), Green - *D*(3,0), Blue – *Sdev*. Error bars are the standard deviation of dispersity from triplicate CE experiments.

In general, no significant effect on dispersity was observed as a result of cooling. The slight changes in dispersity with cooling were within the margin of error, and thus do not present any information of statistical significance. While dispersity was not observed to change with cooling, μ_w significantly shifted towards higher μ_w in a single case, indicating a reduction in the apparent amount of branching. This suggests an increasing contribution of amylose with

cooling, also possibly a partial loss of amylopectin in solution. Further, this investigation has allowed for insight into how slight changes in the separation data can impact dispersity values, highlighting the importance of repeatability and reproducibility in applying this dispersity methodology.

The repeatability of cooled samples was also explored. The use of cooled samples here is not optimal; however, conclusions may still be drawn in regards to the way dispersity values respond to variations in separations.

Figure 43 and Figure 44, respectively, show the $W(\mu)$ of corn and Rice starch and their calculated dispersities across two experiments. From Figure 43 it is immediately apparent that the repeatability between experiments has quite a significant margin of error in amylose, with a lesser impact observed in amylopectin.

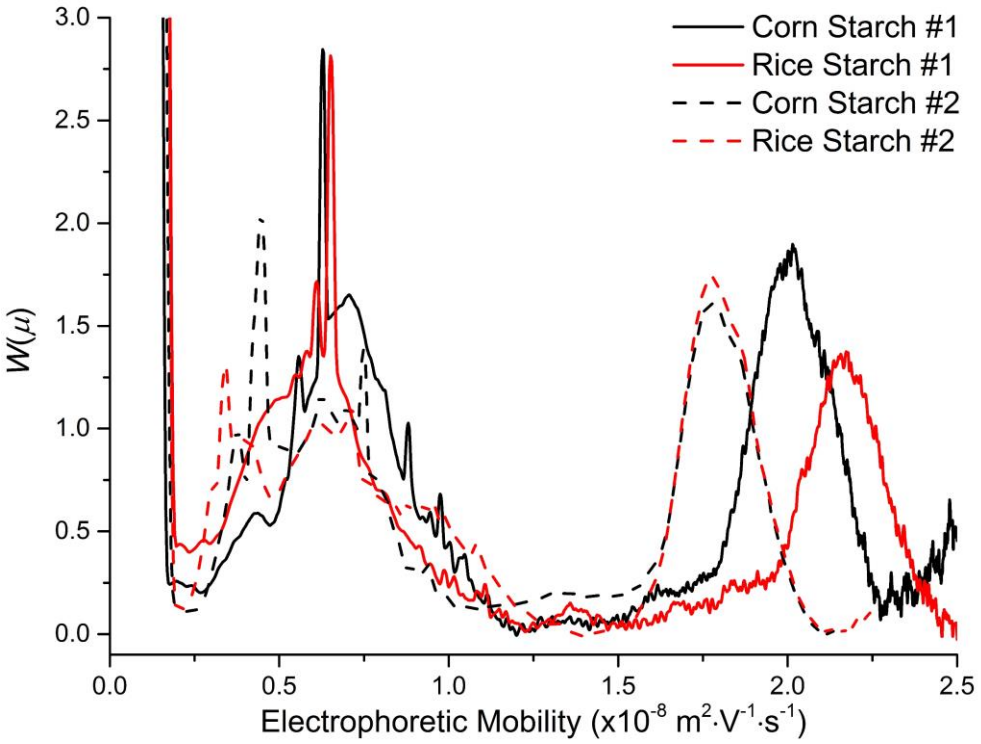

Figure 43 Normalised weight-distributions of electrophoretic mobilities of samples prepared in the optimal conditions at 1 g·L^{-1} and allowed to cool prior to injection. The amylopectin peak is over the range of 0.25 to 1.25 (× 10^{-8} m^2·V^{-1}·s^{-1}) and the amylose peak over the range of 1.5 to 2.5 (× 10^{-8} m^2·V^{-1}·s^{-1}). Dispersity values are in Figure 46.

In Figure 44, the dispersity values of $D(1,0)$, $D(2,0)$ and $D(3,0)$ and their associated errors brought the values between experiments within the same range, showing a level of repeatability. However, taking these error ranges into account also bring the dispersity values of both samples into very similar ranges, yielding a lack of differentiation between the two

samples. A similar trend was also seen in dispersities by *SDev*, whereby little differentiation was seen between samples as a result of error linked to the repeatability. Margin of error in weight-average mobilities also brings values of the samples within an acceptable range, showing a level of repeatability within the separation itself; however, this should not affect the calculation of and comparison of dispersities between samples.

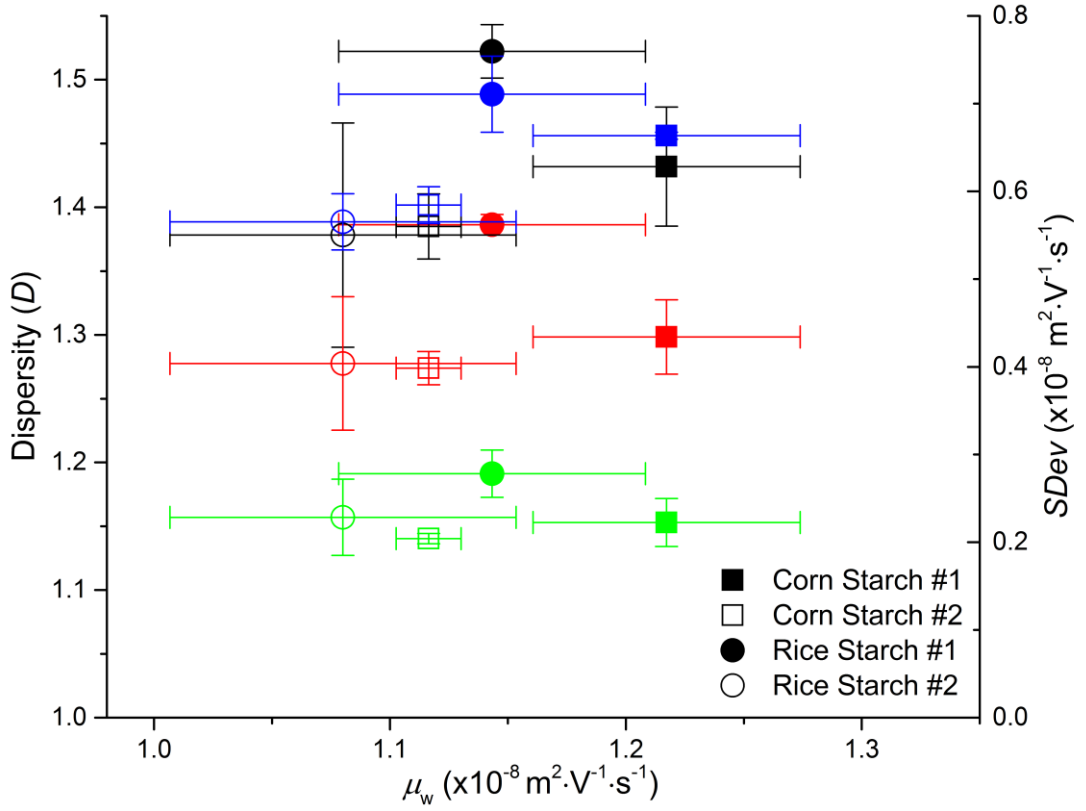

Figure 44 Dispersity values of the distributions in Figure 45 plotted against μ_w, Black - *D*(1,0), Red - *D*(2,0), Green - *D*(3,0), Blue – *Sdev*. Error bars are the standard deviation of dispersity from triplicate CE experiments.

The results presented here have been collected from samples which have been cooled before separation, and so the effects discussed here may not translate directly to those in optimally prepared samples maintained at dissolution temperatures.

2.4 Conclusion

CE was able to separate and analyse amylose and amylopectin in starch samples by taking advantage of iodine complexation. However, this chapter shows that the quality of dissolution plays an important role in the separation, and would thus also affect any quantitative analysis.

A number of parameters were investigated in the dissolution conditions presented by Herrero-Martinez et al. [105] to first investigate the effects and then to further optimise the method. The most significant aspect of improvement to dissolution conditions, and its subsequent effect on separation was starch concentration. Additionally, in dissolution procedures, some form of mixing is important. Magnetic stirring risks the degradation of starch molecules therefore shaking is recommended. Filtration of starch solutions results in significant loss of signal in both amylose and amylopectin, suggesting a significant sample loss. Degradation was also observed as a result of filtration. In relation to recommended practice in SEC, it may be better to filter the solvent prior to dissolution but not filter the starch solution itself prior to analysis [84]. This also applies to conventional amylose content determination methods that rely on spectrophotometric detection.

The optimal dissolution conditions of Schmitz et al. [108] with were compared to those of Herrero-Martinez et al. [105], taking into account concentration and filtration. The improved dissolution conditions resulted in a greater extent of dissolution of amylose. However, the presence of LiBr in the dissolution impacted the binding of iodine to amylose and amylopectin. Introducing an incubation time into the separation method unveiled that complexation was still occurring after 10 minutes of incubation when using 5 % LiBr. Therefore, method modifications will be necessary in the analysis of high amylose starches. Further work will also be required to investigate if a complete complexation is possible with such high LiBr concentrations.

Temperature is also essential in the complete dissolution of starch. Maintaining the solution at dissolution temperature right up to the injection improved repeatability and minimised the formation of aggregates. Initial experiments of storing both the buffer and samples at 60 °C in the CE system produced inconsistent results. Systems capable of an isolated temperature control for samples (Sciex MDQ CE system) have the potential to make experiments less tedious while maintaining the benefits of high solution temperature. Additionally, the separation of amylose and amylopectin is not always observed to be complete, and so further optimisation of the method is required to improve selectivity.

Based on my work certain dissolution conditions can be recommended as optimal in the dissolution of starch. Starch concentration in solution is suggested to be kept at a maximum of 1 $g.L^{-1}$. Filtration of starch solutions should also be avoided. Anhydrous DMSO

with the addition of LiBr should be employed as the solvent. This is especially important for high amylose starches. With the addition of LiBr some complexation time within the capillary is required to facilitate complete iodine binding of starch molecules. At high LiBr concentrations this complexation time should be no less than 10 minutes. High dissolution temperatures are also important, with a temperature of at least 80 °C recommended. Additionally, solution temperatures should be maintained at dissolution temperature until injection.

After establishing optimal conditions, the methodology of Thevarajah et al. [112] was applied in the determination of heterogeneity of branching in amylose and amylopectin. The results discussed in this chapter highlight the importance of investigating all approaches in the calculation of dispersity, as well as comparing them all in the characterisation of samples.. Extremely large dispersity values of $W(\mu)$ were found relative to what has been found in other polymers by this method [112] indicating a large degree of heterogeneity in branching structure. Additionally, different starch samples could be distinguished by their unique dispersity values. However, the significance of these differences is dependent on the error of dispersity values, closely linked to the repeatability of $W(\mu)$. . Identifying differences in dispersity between samples will indicate if the amount of branching and distributions of branching structures seen in different starches are unique, exemplifying the heterogeneous nature of starch structure. Thus, the determination of dispersity by this method is a powerful tool in understanding how the structures of amylose and amylopectin can influence both higher levels of structure as well as overall starch properties.

Chapter 3 Characterisation of the supramolecular structure of starch: Investigating short- and long-range crystalline structure

This chapter focuses on the characterisation of the supramolecular structure of starch (structural levels 3 to 5 of Figure 2). While the molecular structure of starch plays an important role in defining supramolecular structure, these higher levels of structure have a major influence on the physicochemical properties of starch. In this chapter the crystallinity of starch is investigated by Fourier-transform infrared (FTIR) spectroscopy and powder X-ray diffraction (XRD). Crystallinity in starch plays an important role in properties such as digestibility by influencing enzyme access, as well as texture through hydration states and dense helical structures. However, starch does not exist as a purely crystalline material and is rather semi-crystalline, consisting of both amorphous and crystalline phases. Small angle X-ray scattering is employed to investigate the semi-crystalline lamellar structure of starch, an important feature in understanding digestibility. The repeating crystalline and amorphous lamellae (structural level 4, Figure 2), and overarching repeating semi-crystalline and amorphous lamellae (structural level 5, Figure 2) have the potential to significantly influence the rate and extent of digestibility of starch.

3.1 Introduction

Starch is the major energy storage system in photosynthesising plants, and therefore is a highly abundant polysaccharide [19]. Starches have formed a major part of the human diet for thousands of years, with the rise of agriculture further increasing their contribution to the human diet [19, 145]. The use of starches is not limited to nutritional applications, but also finds widespread use in industrial applications such as pharmaceuticals, biodegradable plastics,

concrete and even detergents [19]. This diverse range of applications of starch arises from the ability to modify starches properties to suit these specific end uses, whether through genetic or chemical means.

Creating starches with the desired properties often requires modifications to the sample, with modifications by temperature, enzymatic or moisture treatments common [146]. However, obtaining the properties desired requires a deeper understanding of how the physicochemical properties can be used to predict the impact and outcomes of these treatments more reliably. Thus, characterisation of the physicochemical properties and the role they play in different processing and modification process is essential in optimising how we process starch.

In the food industry, the modifications of starches and their properties vary greatly, influenced heavily by consumer preferences [147]. This is extremely evident in the high degree of processing applied to the majority of starch based and starch containing foods. Processing in these cases is often done in the name of palatability and efficiency, creating products consumers will repeat purchase and that are commercially viable [147]. Processing often subjects products to modifications by heat, moisture and mechanical factors, inducing changes such as gelatinisation and retrogradation; irreversible changes to the underlying starch structure [147]. However, these modifications are not specific to creating the desired properties, and also play a role in other physicochemical properties. Due to its high contribution to the human diet, starch based food products are an ideal target in influencing the health of the global population. While processing conditions are often employed in the attempt to create desirable products, the impact they have on nutrition and health factors in the final products are significant [148, 149].

In this day and age, the digestibility of foods is becoming a major factor in the determination of 'healthy' foods. With rising rates of obesity and obesity related diseases, it is important to investigate ways in which the population health can be improved. Enhancing digestibility properties of food stuffs may be the answer. As discussed in the Chapter 1 the digestion profile of foods plays a role in many aspects of health. So understanding the digestion profile is an important step in creating healthier products. In obtaining a deeper understanding of this, the characterisation of structure is essential. It is expected that starch structure plays a significant role in the digestive properties of starch. As shown in Chapter 1, starch has a complex hierarchical structure, all levels of which can play a role in the efficacy of digestive

enzymes. By characterising these structural properties in starch products and relating them to their digestibility whether by *in vivo* or *in vitro* methods, relationships may be discovered which can then be used in the prediction of digestive properties. A predictive analytical based approach has the potential to significantly streamline the production and design of 'healthy' foods, removing the high costs and processing time associated with other approaches such as *in vivo* glycaemic index (GI) testing.

Due to the complex hierarchical structure of starch, characterisation is also complex. A range of methods and techniques already exist for the characterisation of starches [150]. However, their application is often limited to starches, rather than more complex whole food samples such as breakfast cereals. In this chapter, the application of published methods to rice flours produced from rice breeding programs is explored to understand how structural characteristics of starch relate to digestibility along with other properties. Additionally, the viability of applying these methods to the characterisation of starch in more complex breakfast cereals is also explored. In this characterisation the crystallinity of starch will be assessed by powder X-ray diffraction (XRD) [151], and the relative crystallinity determined by Fourier transform infrared (FTIR) spectroscopy [152]. The characteristics of lamellar structure will also be assessed by small angle X-ray scattering (SAXS) [153].

3.2 Materials

Milli-Q® quality (Millipore, Bedford, MA, USA) water was used throughout the analysis. FTIR grade potassium bromide (KBr) ≥99 % (221864) was obtained from Sigma Aldrich (Castle Hill, NSW, Australia) and stored in a desiccator with silica beads under vacuum. Three types of commercial maize starches with different amylose contents (waxy (3.4 % amylose), regular (24 % amylose) and Gelose 80 (83 % amylose)) [113], were obtained from Penford Australia Limited (Lane Cove, NSE, 2066, Australia). Crystallinity and amylose content for these samples is shown in Table A1. Amylose content was from Tan et al. [113], and determined by the spectrophotometric iodine binding method. Breakfast cereals, Uncle Tobys® Oats Traditional™, Kellogg's® Rice Bubbles® and Kellogg's® All Bran®, were purchased from Woolworths (Sydney, NSW, Australia), and ground using a Breville© BarVista coffee and spice grinder at low speed for 20 s. Laboratory sieves were used to obtain the fraction of sample with

particle size 500-1000 μm. *Doongara*, *Quest 19* and *I-Geo-Tze* rice samples were provided by the Department of Primary Industries (DPI), Yanco, NSW, Australia as part of a rice breeding program. There are 4 samples of each rice variety, grown in separate greenhouses with different growing temperatures. Two samples are grown at lower temperature denoted by head house 1 (HH1) and head house 6 (HH6), while the other two are grown at higher temperatures denoted by head house 3 (HH3) and head house 5 (HH5). Amylose content is shown in Table A1.

3.3 Results and discussion

3.3.1 FTIR spectroscopy in the determination of short-range order

3.3.1.1 Introduction

FTIR spectroscopy is a valuable tool in the analysis of molecular structure and composition, allowing analysis of the infrared absorbance of both liquid and solid samples [154]. FTIR spectra provide information on the fundamental molecular vibrations in the sample, allowing for extensive insight into both chemical and structural characteristics of samples. FTIR spectroscopy can be applied in the near infrared (NIR) range, 14000 – 4000 cm^{-1}, mid infrared (MIR) range, 4000 – 400 cm^{-1}, and the far infrared (FIR) range, 400 – 4 cm^{-1} each of which can be used to obtain different information.

NIR spectroscopy is commonly used in infrared analysis due to the wealth of information it offers, allowing the observation of overtones or combinations of the fundamental vibrations occurring in the MIR region [154]. The nature of the NIR region makes analysis difficult and often requires data processing such as derivation and deconvolution to allow for meaningful analysis. However, application of such processing techniques can often lead to inaccuracies in assessment. NIR is commonly used in the food industry, allowing for compositional analysis of fat, protein, moisture and sugars [155-157]. MIR spectroscopy provides an abundance of structural and compositional information on biological materials, with absorptions in this region arising from various chemical functional groups [158]. The variation

in absorptions between samples is often employed in routine sample identification, with the MIR region often being referred to as the 'fingerprint region' [158]. Limitations in the application of infrared analysis are often seen in chemically and structurally complex samples, for which overlapping peaks can mask critical information [159]. This is a significant problem in the analysis of biological samples, often requiring multivariate analysis due to the complex sample matrix. The presence of water, and its strong broad absorbance can also mask certain signals and influence others either directly or indirectly.

Along with the choice of region in infrared analysis, various modes can be applied to record FTIR spectra. Commonly used modes include attenuated total reflectance FTIR (ATR-FTIR) spectroscopy, and transmission mode FTIR spectroscopy. ATR-FTIR spectroscopy utilises total internal reflection within a cell (e.g. a diamond) to allow multiple reflectance of the beam onto a sample in close contact with the cell. Transmission mode FTIR spectroscopy is the oldest infrared method and employs the same principle of absorption of energy of infrared wavelengths as it passes through the sample, and can be employed in liquid, solid or gaseous forms. The absorption of energy at the wavelength at which the sample absorbs is then measured, and the resulting attenuated radiation plotted as a function of wavelength [154]. The use of ATR-FTIR spectroscopy is limited due to the heterogeneity and thickness of the sample. This is due to the limited penetration of the infrared radiation, although with suitable preparation this limitation can be managed. These same homogeneity issues can be found in sample preparation for transmission mode FTIR spectroscopy, and so care must be taken in the preparation of pellets for analysis.

Many methods have been published in which relative crystallinity of starch has been determined from the ratio of intensities of infrared peaks assigned to the amorphous and crystalline phases of starch. This is shown in Equation 11, where *CI* is the crystalline index, I_c is the height of the crystalline peak and I_a is the height of the amorphous peak.

$$CI = \frac{I_c}{I_a} \tag{11}$$

The peaks in the region 1100-900 cm^{-1} are sensitive to changes in starch structure, specifically those shown in Figure 45. These peaks have seen widespread use in the study of a range of starch samples, including monitoring retrogradation[160], enzymatic hydrolysis[163], and

acid hydrolysis residues[161]. The peaks of interest in the determination of *CI* values vary slightly between publications, though it is generally accepted that the peak at 1022 cm^{-1} is correlated with vibrational modes within the amorphous phase [161], due to its decrease with increasing crystallinity[161, 164]. Conversely, there is much debate on what infrared regions are characteristic of crystalline regions (Table 3). The peak at 1047 cm^{-1} is taken as the crystalline contribution [152, 161-163, 165], while the peak at 995 or 1000 cm^{-1} is also commonly employed[161, 162]. These peaks are observed to increase in samples with higher levels of crystallinity, and in the case of 995/1000 cm^{-1} was sensitive to hydration in crystalline regions[161]. However, the peak at 1047 cm^{-1} is not sensitive to the change in amorphous/crystalline ratio induced by acid hydrolysis. The peak at 995 cm^{-1} is more sensitive to crystalline regions[162], while also showing a better correlation with crystallinity measurements[166]. The peak at 995 or 1000 cm^{-1} was recognized as water sensitive and related to intramolecular hydrogen bonding of hydroxyl groups [152]. All of these works agree that assigning these peaks individually is unrealistic as a result of the highly coupled vibrational modes that play a significant role in spectral features. Additionally, signal intensity relies on many factors including the concentration and extinction coefficient of the corresponding species in the sample. By assuming the ratio of peak heights reflects the ratio of the corresponding species in the sample, in this case crystalline and amorphous phases, then it must be assumed that these factors are equal.

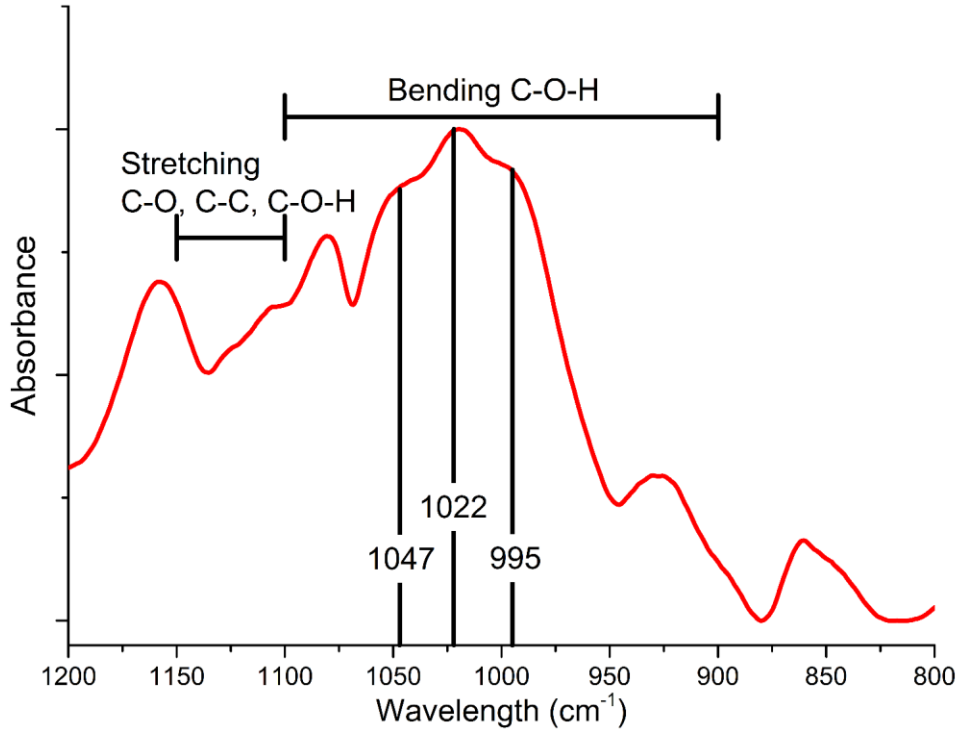

Figure 45 Transmission mode FTIR spectrum of *Doongara* rice flour (HH1) conditioned at 44 % RH showing the vibrations of interest, and characteristic bond vibrations

Table 3 Summary of infrared peaks of interest

Peak maximum (cm^{-1})	Peak Assignment	References	Comments
1022	Amorphous Regions	152, 161-163, 165	Widely accepted as representative of the amorphous region of starch when used in the determination of crystallinity by FTIR spectroscopy.
995	Crystalline Regions	162	More sensitive to change in amorphous/crystalline ratio.
1000	Water Dependent Crystalline Peak	161	Responds to changes in helices organisation in crystalline and semi-crystalline samples.
1047	Crystalline Regions	152, 161-163, 165	A combination of overlapping peaks 1053 cm^{-1} and 1040 cm^{-1} [167]. Peak splitting shown during gelatinisation of starch [162].

An in-depth study on the suitability of FTIR spectroscopy as a tool to characterise the degree of order in starch has investigated these peak ratios compared to data obtained by other analytical techniques including nuclear magnetic resonance spectroscopy (NMR), X-ray diffraction (XRD) and differential scanning calorimetry (DSC)[166]. FTIR spectroscopy is a tool that can quantitatively probe short range order; however, the assumption of a linear relationship between crystallinity and peak height ratios is overly simplistic. The relationship of these peaks with degree of order within starch is largely based on experimental observations of relationships of these peaks to chain conformation and helicity within starch samples [160, 167, 168]. The molecular reasoning behind these changes is not clearly understood, and the application of this method is not always straightforward. The closeness of the peaks used in the determination of *CI* leads to significant overlap, while hydration can also play a role in peak position [166]. The determination of peak height values introduces significant error due to subjective human determination of the peak position and height, especially complicated by the lack of defined peaks in most cases. Further error may be introduced by deconvolution processing to enhance the resolution between overlapping peaks, and raises concerns as to the parameters of these deconvolutions, the impact they may have, and how deconvolution is applied across samples.

In this section the viability of FTIR in determining differences in crystallinity between samples was assessed. The most common literature methodologies employ ATR mode infrared spectroscopy due to its simplicity and versatility; however, issues with baseline correction and a lack of quantitative parameters makes it less than ideal. In the determination of crystalline ratios, the peaks of interest are very close and often overlapping or convoluted. So in this work ways in which resolution could be improved were explored. This includes moving to transmission mode FTIR spectroscopy and thus a smaller sample concentration. Resolution at very low temperatures thought to also help in improving resolution was also explored.

3.3.1.2 Materials and methods

FTIR spectroscopy was performed on a Bruker Vertex 70 spectrometer (Advanced Materials Characterisation Facility, AMCF). FTIR spectra were acquired on all the samples with 64 scans, and the recording resolution was between 1 and 4 cm^{-1}; however, no differences are observed due to the change. FTIR spectroscopy measurements were done in either ATR or

transmission mode. Cold stage transmission mode FTIR spectra were recorded using a Specac variable temperature cell holder under vacuum, where specified. Transmission mode FTIR spectroscopy measurements were done using KBr pellets with a sample concentration of 2 % w/w (200 mg total mass). Powder for pressing was prepared by combining sample and KBr powder and grinding together into a fine powder using an agate mortar and pestle. Powder was then transferred to the die and spread with light tapping. Pellets were pressed using a PIKE Technologies CrushIR digital hydraulic press. The pressure sequence was: 3 tonnes followed by immediate release, 7 tonnes for 30 s, then ramp from 7 to 10 tonnes and hold for 2 min. Pressed pellets were analysed on the day of pressing and stored in a desiccator until analysis.

All starch and rice samples were conditioned to either 44 % or 90 % relative humidity (RH) for at least 1 week prior to analysis. Sample environments at 44 and 90 % RH were created by placing a saturated solution of potassium carbonate (K_2CO_3) or barium chloride ($BaCl_2$), respectively, in a desiccator and adequately sealing [169].

All FTIR spectra were processed with Bruker OPUS 7.5 [170]. All ATR-FTIR spectra were corrected by an extended ATR correction built into the OPUS 7.5 software. All FTIR spectra were baseline corrected by 1 step (minimum amount) in the software's interactive mode using a rubber band based correction algorithm. All FTIR spectra were then normalised to an absorbance range of 0 to 2.0 based on min-max calculations. Bandwidth reduction by Fourier self-deconvolution (FSD) was achieved through application of the inbuilt FSD functionality, with both Lorentzian and Gaussian line shapes investigated. The bandwidth and noise reduction were adjusted appropriately for each sample. Deconvolution parameters for samples are shown in Table A2. FTIR spectra were plotted with OriginLab OriginPro 9.0 [115].

CI values were calculated using Equation 11, substituting the crystalline peak height with the value of the crystalline peak specified, 1047 or 995 cm^{-1} and the height of the amorphous peak, 1022 cm^{-1}. *CI* values calculated for peaks at 1047 and 1022 cm^{-1} are referred to as CI_{1047} and the ratio of peaks at 995 and 1022 cm^{-1} as CI_{995}.

3.3.1.3 Investigating the viability of ATR-FTIR spectroscopy in the determination of crystallinity

3.3.1.3.1 Investigating ATR-FTIR spectroscopy viability in standard conditions

In the determination of *CI*, measurements are commonly made by ATR-FTIR spectroscopy. This is a simple, versatile and robust means of measuring FTIR spectra and is gaining traction as the *de facto* choice in infrared spectroscopy; however, ATR's limited penetration depth cannot probe bulk properties, which is especially important in the determination of crystallinity.

Different starch samples conditioned at 44 % RH were measured using an ATR accessory (Figure 46). Clear differences between samples were observed; however, the positions of the peaks of interest were not always clearly defined, making determination of crystalline values difficult. This was most evident in Gelose 80, where the expected peaks at 1022 and 995 cm^{-1} were clearly overlapping, forming a combined median peak. However, the high amylose content (82.9 %) and low crystallinity (15 %) of this sample could explain the apparent absence of this crystalline peak at 995 cm^{-1} and the shift of the amorphous peak. Regardless, the results presented here identified a major problem in this methodology: the lack of resolution between the peaks of interest, thus limiting the accuracy with which determinations could be made.

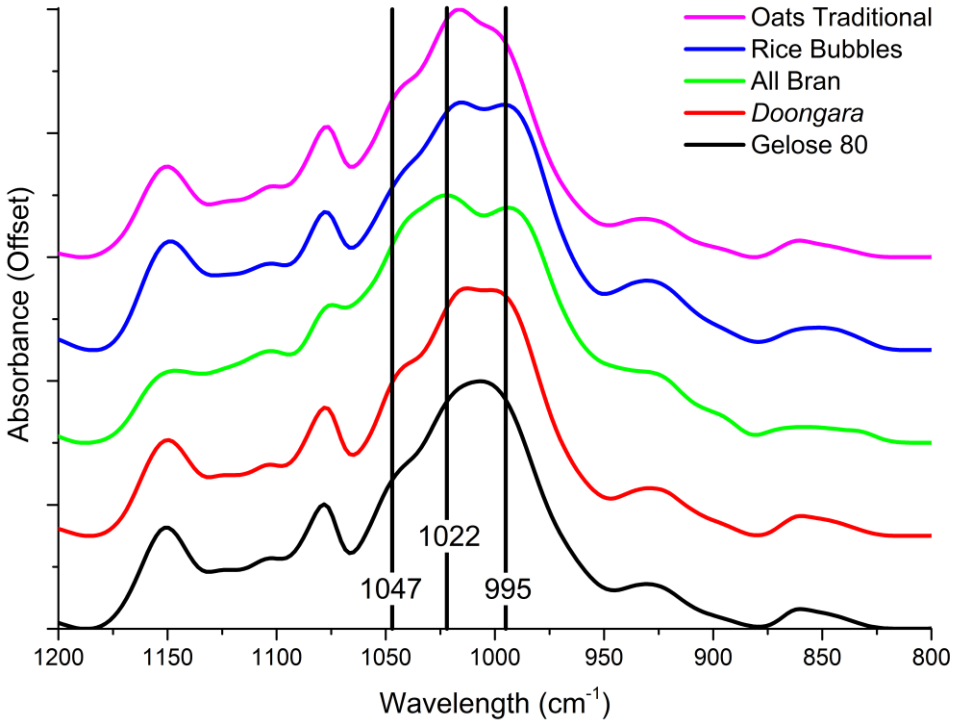

Figure 46 ATR-FTIR spectra of starches and starchy samples conditioned at 44 % RH

Investigating further the data obtained by ATR-FTIR spectroscopy, starch samples with known crystallinity values (Table A1) were qualitatively compared in terms of crystalline and amorphous FTIR spectral features (Figure 47). This comparison revealed slight variations between the low crystallinity Gelose 80 and the higher crystallinity Waxy maize. However, the difference observed between Waxy and Regular maizes was minor, suggesting a higher crystallinity than expected for the Regular maize. Again, strong overlap of peaks was evident, significantly impairing the determination of peak height for the peaks of interest, and thus increasing the underlying inaccuracy in such a measurement.

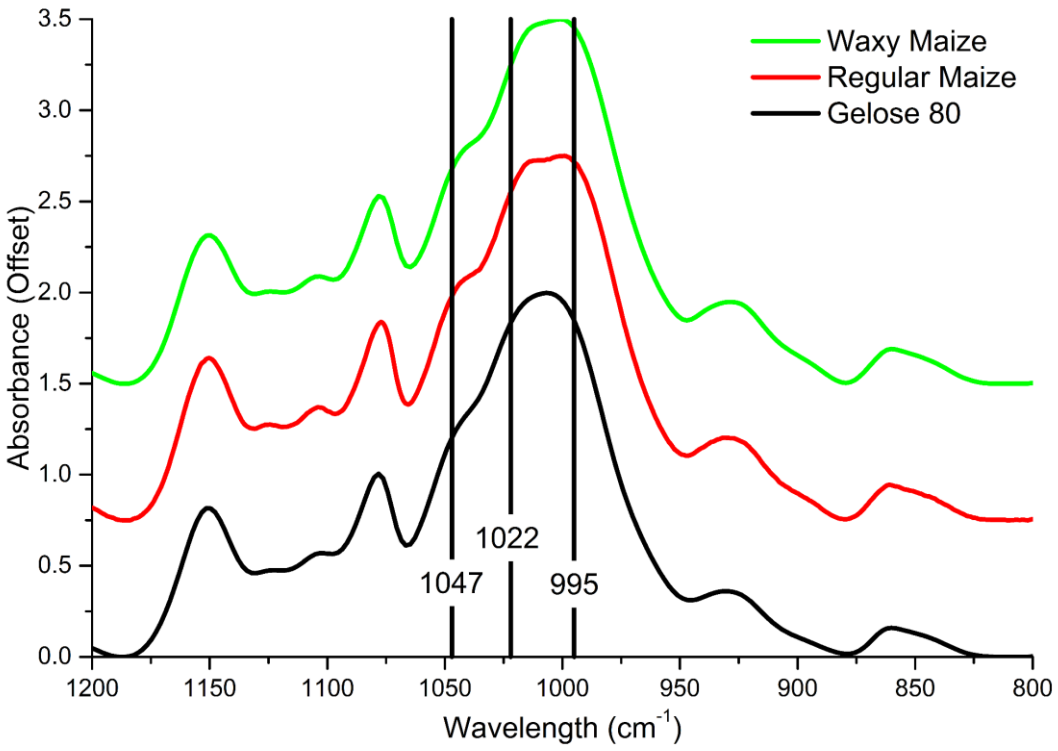

Figure 47 ATR-FTIR spectra of starches conditioned at 44 % RH

3.3.1.3.2 Investigating the sensitivity of ATR-FTIR spectroscopy to hydration based structural changes

As a result of the poor resolution of peaks seen using ATR-FTIR spectroscopy on samples conditioned to room temperature and humidity, the effects of hydration were explored, taking typical ATR-FTIR spectra of samples conditioned at 90 % RH. The peak at 995 cm^{-1} is sensitive to hydration in starch [161]. By varying hydration in starch, the ordered structure is altered. This can be observed by FTIR spectroscopy as changes in the height of the peaks at 995 and 1022 cm^{-1} whose ratio is used to calculate *CI*, CI_{995}. This was correlated with a phase transition from nematic to smectic phases [161]. Thus a difference could be observed in terms of crystallinity by this ratio. However, this work also noted that no changes were observed in the peak at 1047 cm^{-1}, despite its close links to order within starch systems. Taking into account the phase transition that should occur at higher hydration, and the subsequent impact on order within the system, samples were conditioned to 90 % RH and analysed by FTIR spectroscopy to investigate and confirm the ability to observe crystalline changes in these samples.

The ATR-FTIR spectrum of Gelose 80 conditioned at 90 % RH showed very little difference compared to that of the 44 % RH sample except for the formation of a sharp shoulder peak at 1047 cm^{-1} (Figure 48A). This is despite the suggestions that the peak at 1047 cm^{-1} is not affected by hydration [161]. Very slight differences were observed in the main peak at 1010 cm^{-1}, with slight shoulders forming that suggest two additional peaks; however, the severe overlap of these peaks complicates the determination of specific peak heights for *CI* calculations. In Regular maize (Figure 48B), a greater difference was observed with the peaks at 1047 and 1014 cm^{-1} becoming more pronounced with increased hydration and the peak at 995 cm^{-1} decreasing in resolution, becoming a shoulder to the main peak. Additionally, the relative ratio of peak intensities at 1022 and 995 cm^{-1} appeared to change as a result of hydration indicating a change in crystallinity as expected. Thus it was confirmed that changes to crystallinity could be observed by ATR-FTIR spectroscopy; however, the poor resolution of peaks remains a problem in *CI* calculations and an alternative approach is required to improve the resolution of these infrared peaks.

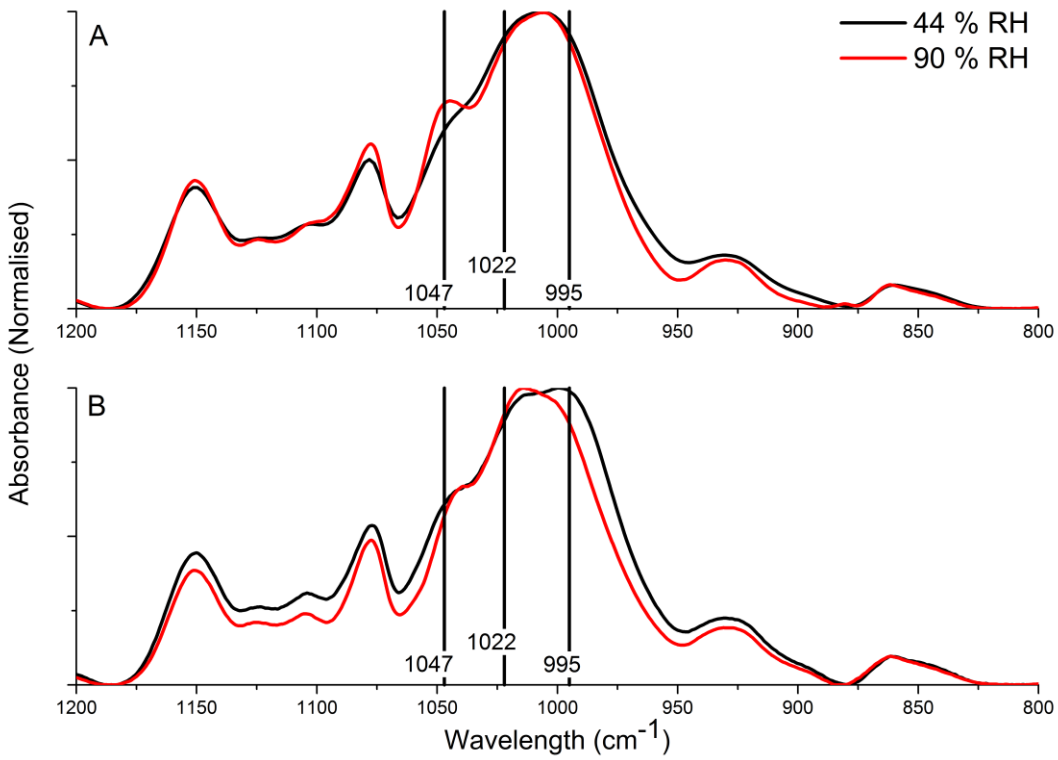

Figure 48 ATR-FTIR spectra of: A) Gelose 80 and B) Regular maize conditioned at 44 % or 90 % RH.

3.3.1.3.3 Intermediate conclusion

The resolution necessary to determine accurate peak positions and intensities is not available by ATR-FTIR spectroscopy. Severe overlap of the peaks of interest complicates the determination of crystalline ratios. Bandwidth reduction by Fourier self-deconvolution (FSD) may provide enhancements to the resolution of these peaks; however, some of these may arise from limitations of the methodology itself.

In the analysis of samples using ATR accessories, samples are often pressed against the crystal using a clamping type device to create and maintain good contact of the sample and crystal. However, in the case of powders, samples can be spread by the clamping mechanism resulting in poor contact. This can introduce background noise and other interference resulting in lower signal to noise ratios . Subsequently, this may lead to poor resolution of infrared peaks. The limited depth of penetration(0.1 to 5 μm [171]) compared to the size of starch granules (1 to 100 μm[41]) hinders a representative 'bulk' analysis. Finally, approaches to correcting the baseline and peak intensities of ATR-FTIR spectra may also play a role. Due to the mechanism of ATR a correction is required on raw ATR-FTIR spectra that aims to normalise intensities and adjust the baseline. This is usually not a significant contributor to skewing within the spectral profile.

Despite these limitations, a best attempt was made to determine *CI* values from raw FTIR spectra. The peak height was taken at the specific wavelengths of interest on raw spectra, and from the resolved peak maxima on FTIR spectra enhanced by FSD. Bandwidth reducing FSD approaches will be further discussed in Section 3.3.1.5.

Figure 49 shows the *CI* values of samples measured by ATR-FTIR spectroscopy, and compared to the crystallinity determinations by X-ray diffraction. Figure 49A shows the calculated CI_{995}, which are suggested to be a better indicator of crystallinity [151]. *CI* values from raw FTIR spectra show a linear correlation with increasing crystallinity; however, the *CI* values obtained from FSD processed FTIR spectra showed no apparent trend with crystallinity. In this case the type of peak shape used in FSD did not result in a difference in correlation with crystallinity. Figure 49B shows the CI_{1047} values. The correlations seen from CI_{1047} values of raw and Lorentzian FSD processed spectra suggest a negative correlation of *CI* with measured

crystallinity. CI_{1047} values from Gaussian FSD processed FTIR spectra yield a positive correlation; however this correlation was weak.

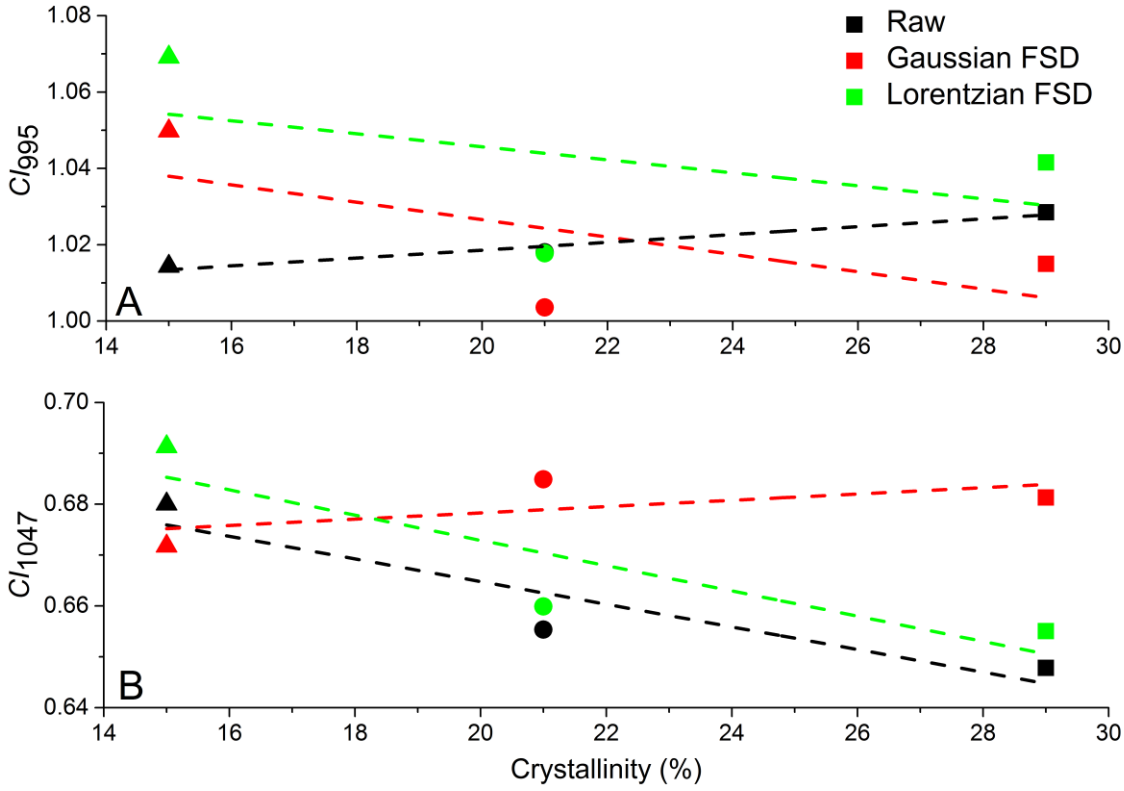

Figure 49 A - CI_{995} and B - CI_{1047} values of square - Gelose 80, circle – Regular maize, triangle - Waxy maize conditioned at 44 % RH and measured by ATR-FTIR spectroscopy plotted against crystallinity measured by X-ray diffraction [113]. Dotted lines are linear fits of *CI* calculated from black – raw data (A -R^2 = 0.98 and B - R^2 = 0.86), red – Gaussian FSD processed data (A - R^2 = 0.44 and B - R^2 = 0.41) and green – Lorentzian processed FSD data (A - R^2 = 0.22 and B - R^2 = 0.78. Fit parameters are in Table A5. Black circle that is not visible is located behind the green circle.

Therefore, ATR-FTIR spectroscopy is not a viable technique in the determination of *CI* values that correlate with crystallinity. This arises as a result of the poor resolution of peaks of interest complicating the determination of peak height. Further, when FSD was applied, *CI* values still did not correlate well with measured crystallinity, despite apparent decomposition into realistic and unique infrared peaks. An example of the effects of FSD is shown in Figure A3.

3.3.1.4 Exploring alternative FTIR approaches in the determination of crystallinity

3.3.1.4.1 Employing transmission mode FTIR spectroscopy in the determination of crystallinity

The poor resolution of the peaks of interest by ATR-FTIR spectroscopy complicates the determination of the crystalline ratios due to the uncertainty associated with the peak height determinations. In the previous results (Section 3.3.1.3) peaks at 1022 and 995 cm^{-1} did not appear as resolved peaks', rather as a single peak with a median peak maximum. As a result, different methodologies were assessed for their potential to enhance the resolution of the FTIR spectra especially in the region of interest.

Figure 50A shows the infrared spectrum of Gelose 80 in a KBr pellet recorded by transmission mode FTIR spectroscopy. A significant difference from the same sample analysed using ATR-FTIR spectroscopy was observed (Figure 48). A shift of the major peak from 1010 cm^{-1} in ATR-FTIR spectroscopy to 1022 cm^{-1} in transmission mode FTIR spectroscopy lined up this peak with the expected position of the amorphous peak. Significant effects on the other peaks of interest at 995 and 1047 cm^{-1} were also observed. By ATR-FTIR spectroscopy (Figure 50A, Black), the peaks at 1022 and 995 cm^{-1} were almost completely unresolved and rather formed a single peak in most cases. In contrast, these peaks appear more resolved in transmission mode FTIR spectroscopy (Figure 50A, Red), with the peak at 995 cm^{-1} appearing as a pronounced shoulder at the expected wavenumber. Improvements to the resolution of the peak at 1047 cm^{-1} were less pronounced; however, a significant increase in the prominence of this shoulder was evident in comparison to measurements by ATR-FTIR spectroscopy. This effect was also observed in Regular maize when compared with the original ATR-FTIR spectroscopy methodology (Figure 50B), suggesting that measurements made in transmission mode FTIR spectroscopy are likely to produce more accurate crystalline ratio values in the analysis of starch crystallinity.

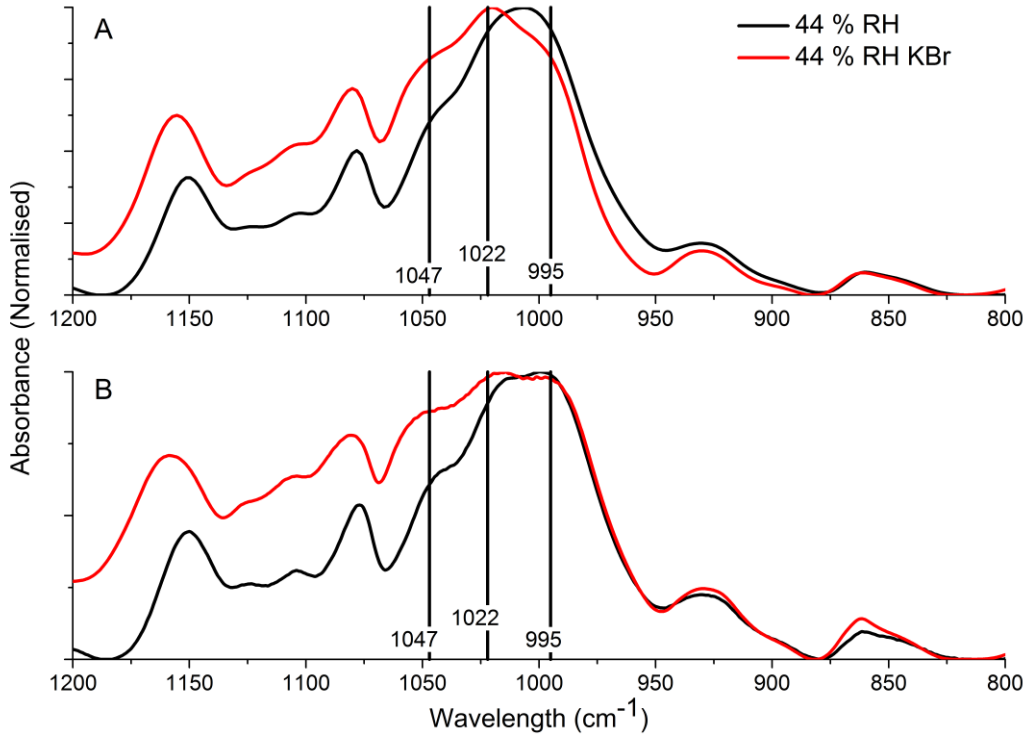

Figure 50 FTIR spectra of: A) Gelose 80 and B) Regular maize, conditioned at 44 % relative humidity. Measured by ATR –FTIR spectroscopy (black) or in KBr pellet by transmission mode FTIR spectroscopy (red).

The increased prominence of these peaks using KBr pellets in transmission mode FTIR spectroscopy allowed for an improved accuracy in the identification of the peaks of interest and their maximum intensities for use in *CI* calculations. This increased prominence was expected to enhance the responsiveness to FSD processing, as a better starting point is provided and better judgements may be made as to the accuracy of deconvoluted results. However, no greater resolution of peaks was observed after bandwidth reduction by FSD, in contrast to previous results by ATR-FTIR spectroscopy (Section 3.3.1.3), with significant overlap of peaks complicating the determination of peak maximum intensities.

3.3.1.4.2 Exploring cryogenic temperatures in enhancing resolution

Further improvements to the resolution of the peaks of interest were explored. Cryogenic temperatures have been used widely over the life of infrared technology with an extremely broad range of applications. The outcome of many of these studies was a reduced peak width and improved resolution [172, 173]. The cause of these effects on spectral features has been explored and explained by a number of phenomena that are known to be sensitive to

temperature and may influence spectral characteristics. A leading explanation for this phenomenon is the effect of temperature on intermolecular forces. When temperature is decreased significant energy is lost, affecting intermolecular forces in the sample and how they react to infrared radiation [154, 174]. Another effect observed at lower temperatures is that seen on non-fundamental peaks, where temperature can play a significant role in the depopulation of excited-state energy levels. This can translate to lower signal intensity for these non-fundamental peaks, which may lead to enhanced resolution of overlapping peaks [175].

While lower temperatures may yield an improvement in spectral resolution, cryogenic temperatures may also impact the sample itself.. In the analysis of polymers such as starch, the glass transition temperature (T_g) defines the point at which polymer chains lose their spatial mobility, and are essentially locked in a random configuration. In starch, the T_g varies with moisture content [176]; however, this transition still primarily occurs above room temperature (25 °C) with values from 30 to 90 °C reported [176]. Thus, the differences in structure between room temperature and cryogenic temperature as a result of glass transition are likely insignificant.

The resolution advantages found with cryogenic infrared measurement justified the application of this approach to the starch samples used in this project. This technique maintained the use of KBr pellets in transmission mode FTIR spectroscopy, preserving the benefits observed previously while also exploring the benefit of cryogenic temperatures. Figure 51A shows the transmission mode FTIR spectra of Gelose 80 at room temperature (25 °C) and at -170 °C. Cryogenic temperatures revealed slight improvements in the resolution of both shoulder peaks at 1047 and 995 cm^{-1}, as well as greater peak height relative to the most intense peak at 1022 cm^{-1}. This same effect was observed in other samples analysed: Regular maize and Waxy maize (Figure 51B and Figure 51C). However, these resolution improvements were minimal and still did not result in clearly resolved peaks. As was the case at room temperature, the improved peak resolution of shoulder peaks is likely to be beneficial in obtaining more accurate results through bandwidth reduction by FSD.

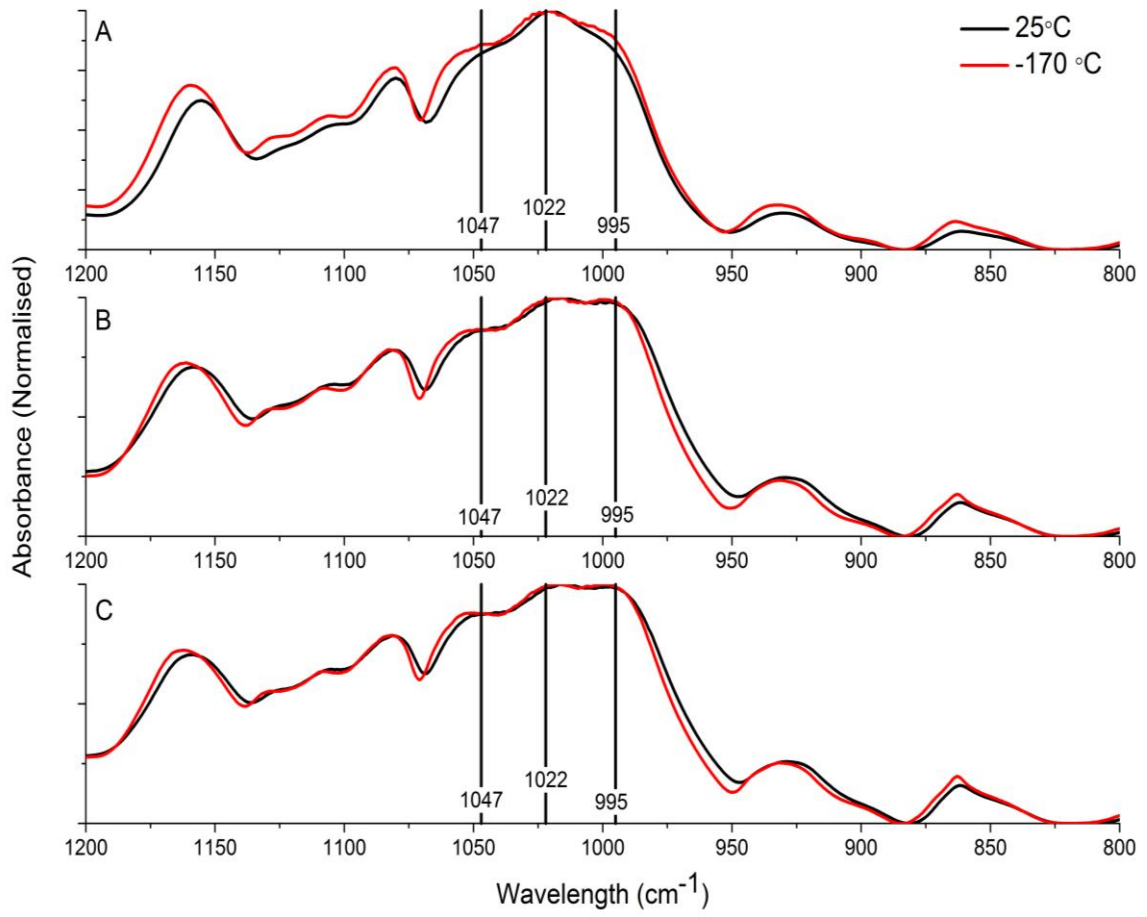

Figure 51 Transmission mode FTIR spectra of A) Gelose 80, B) Regular maize and C) Waxy maize, conditioned at 44 % relative humidity and measured at different temperatures.

3.3.1.4.2.1 Monitoring the effect of cooling

Under cryogenic conditions, starch infared spectra exhibited enhanced resolution of peak maxima associated with the determination of *CI* ratios. However, the effect of cooling, and how the kinetics of cooling play a role was unknown. Therefore further work was done exploring the effects of different paramaters in the cryogenic infrared analysis of starch including: the observation of changes over a temperature range, the effect of cooling for extended time, and the effect of thermal stresses by heating and cooling. In Figure 52A, the FTIR spectra of Gelose 80 are shown as it was cooled from room temperature (25 °C) to -170 °C. Doing so allowed for an investigation of the evolution of the peaks in the FTIR spectrum with respect to temperature, with the potential to identify more efficient temperature targets. The results presented in Figure 52A revealed that a very slight increases in peak height at 1047 cm^{-1} occured as the temperature decreased, with continuous changes down to -170 °C. No significant changes were observed in the peaks at 1022 and 995 cm^{-1}; however, across the entire

FTIR spectrum a slight increase in peak intensities was observed. These same effects were also observed in Waxy maize (Figure 52B). Similar to the results observed for Gelose 80, FTIR spectral resolution, particularly for the peaks of interest, was improved as temperature decreased. However, in the case of Waxy maize this improvement was observed in both the peak at 1047 cm^{-1} as well as in the clearer separation of the two peaks at 1022 and 995 cm^{-1}, yielding a greater distinction between these two peaks.These changes were again continuously observed as the temperature decreased with apparent increased resolution across the whole FTIR spectrum.

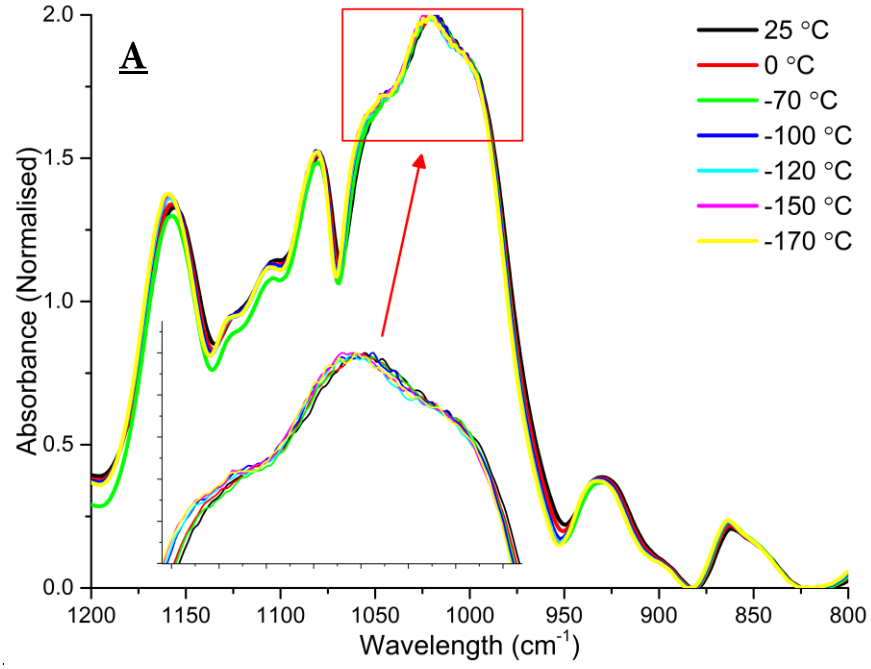

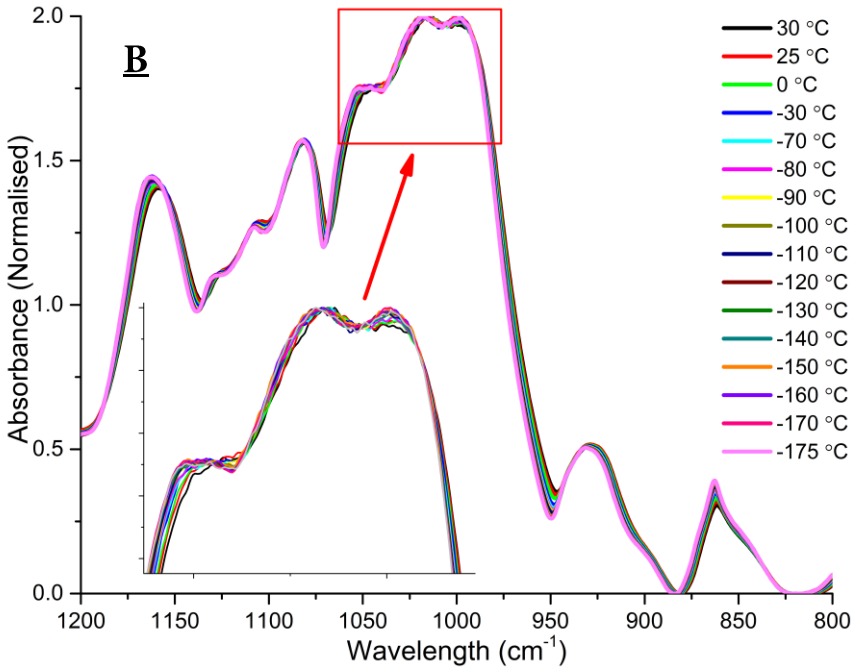

Figure 52 Transmission mode FTIR spectra of A) Gelose 80 and B) Waxy maize measured at different temperatures.

Thus as temperature is decreased continuous changes are observed, yielding a slight increase in peak intensities, while also enhancing the resolution of some overlapping or convoluted peaks. It was determined that there was no optimal temperature in regards to improved resolution. The change in temperature was instead found to continuously influence the FTIR spectra.

3.3.1.4.2.2 Monitoring the temperature equilibrium

A further investigation was made into the effect of prolonged cryogenic temperatures on sample spectra. Figure 53 shows the effects of prolonged cryogenic temperatures on the infrared spectrum of a Regular maize sample (44 % RH). Qualitatively there are no significant differences as a result of longer times spent at low temperature. The only difference was increased background noise in the peaks at 1022 and 995 cm^{-1}, which due the nature of noise, are unlikely to be repeatable between measurements. This same lack of significant change was observed across all the measured FTIR spectra, and indicates that the cooling time required to equilibrate sample temperature with the sample holder was insignificant, and additional waiting time was not required for cooling to be complete.

Secondly, prolonged exposure to low temperatures does not appear to have any effects on the sample that can be directly observed by infrared analysis. Thus no impact on the determination of crystalline ratio values should be observed.

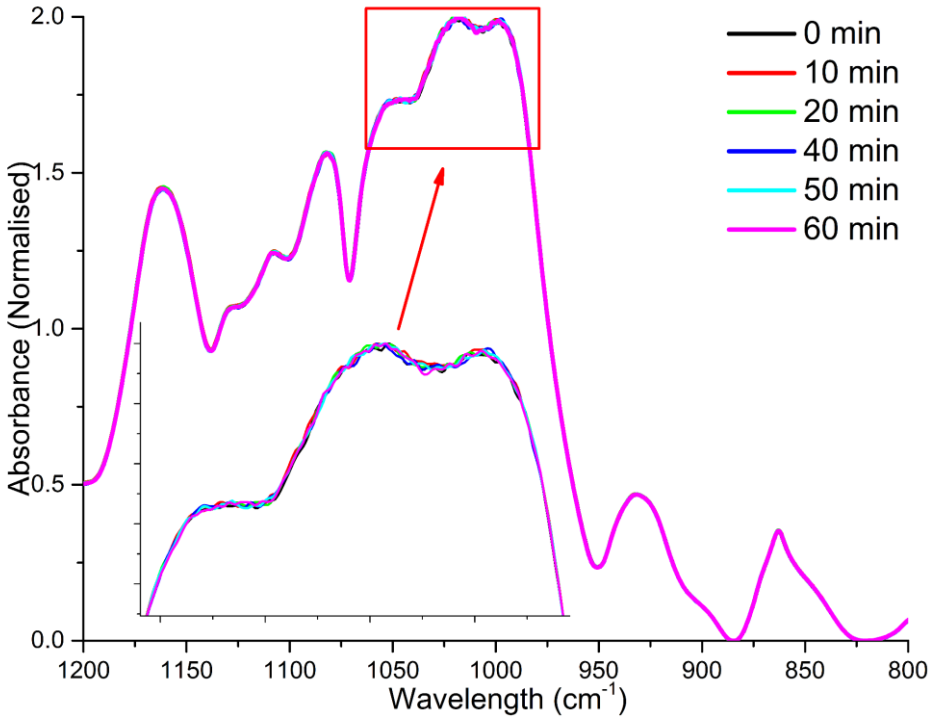

Figure 53 Transmission mode FTIR spectra of Regular maize, measured over time at cryogenic temperature (-170 °C)

3.3.1.4.2.3 Monitoring effect of cooling on structure and the role of humidity

The effects of thermal stress on both the sample and the KBr pellet as well as the potential of condensation occurring within the sample cell as a result of low temperatures were also explored. Any condensation occurring in the sample cell, despite the vacuum experiments are run under, would likely interfere with any FTIR spectra measurements. Figure 54 shows the testing of thermal stresses and potential condensation effects on Regular maize (44 % RH). From an initial measurement at 0 °C, the sample was cooled directly to -170 °C yielding the same spectral effects as discussed earlier. The sample was then heated to 50 °C and held at that temperature for 1 h before measurement. FTIR spectra measurements at 50 °C yielded a similar difference as those observed between room temperature (25 °C) and -170 °C; however, the decrease in resolution of peaks of interest was more apparent than at room temperature with the shoulder at 1047 cm^{-1} becoming much less pronounced from the main peak. Peak

heights at 1047 and 995 cm^{-1} also decreased at 50 °C, which would play a role in *CI* calculations. Thus, measurements at 50 °C were less ideal than those at room and cryogenic temperatures.

Following the conditioning at 50 °C, the sample was then re-cooled to -170 °C to investigate the impact of thermal stresses by thermal variation and the role of moisture. Most moisture should have been removed by the combination of a 50 °C sample temperature and vacuum, and thus should not be a contributing factor. Figure 54 revealed that no significant impact by cooling and reheating could be observed when compared to the initial measurement at -170 °C. Additionally it appeared that any moisture that may have been present did not play a significant role in the resulting FTIR spectra. Again, the increased intensity profile at lower temperatures was observed in both measurements at -170 °C.

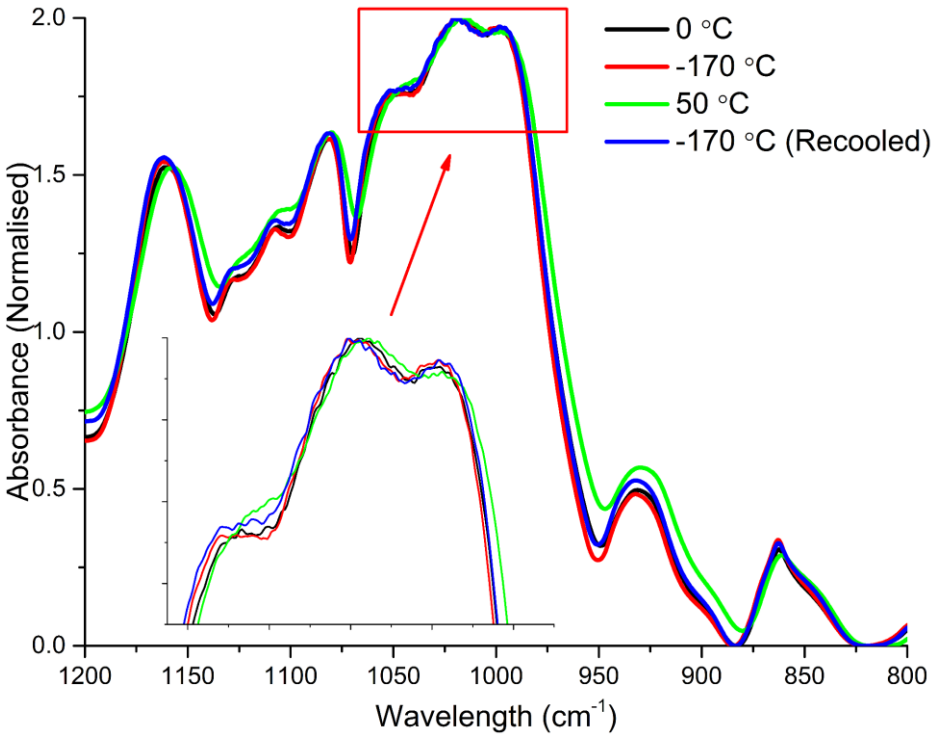

Figure 54 Tranmission mode FTIR spectra of Regular maize at different temperatures.

Therefore, moisture was not a factor in the change of spectral features relative to room temperature, and no apparent irreversible structural changes occurred as a result of cooling to cryogenic temperatures.

3.3.1.4.3 Intermediate conclusions

It is clear that in the case of infrared analysis of starch in the determination of crystallinity, severe overlap of the peaks of interest is likely to significantly impact the

calculation of *CI* values. This arises as a result of the difficulties associated with the accurate determination of peak positions and their subsequent peak height. Analysis of starch samples by transmission mode FTIR spectroscopy yielded improvements to the resolution of shoulder peaks not clearly observed by ATR-FTIR spectroscopy. Further improvements were seen by measurements at cryogenic temperatures, which may be helpful in further enhancing the reliability of bandwidth reduction by FSD. However, the extensive sample preparation involved in KBr pellet pressing for transmission FTIR spectroscopy and the time consuming procedure involved in cooling to cryogenic temperatures for cold stage measurements offsets the greatest advantage of infrared analysis: short analysis times. This factor is especially important for high throughput applications such as those desired here: fast crystallinity measurements on a wide range of food based samples. As a result, the measurement of FTIR spectra using transmission mode FTIR spectroscopy was determined to yield sufficient resolution to explore the crystallinity index values of samples.. *CI* values determined from cold stage infrared measurements will still be included for comparative purposes.

3.3.1.5 Exploring the determination of *CI* as a measure of crystallinity

In the determination of *CI* values by infrared analysis, the peak height of a crystalline peak, here 1047 or 995 cm^{-1}, is divided by the peak height of an amorphous peak, here 1022 cm^{-1} as described by Equation 11. As discussed previously (Section 3.3.1.1), the assignment of these bands and the subsequent *CI* have been experimentally determined, correlating known crystalline changes with changes in this peak height ratio. Here the merits of two approaches were explored, the ratio of 1047/1022 cm^{-1} peak heights (CI_{1047}) most commonly employed in the literature [161, 163, 166], along with the ratio of 995/1022 cm^{-1} peak heights (CI_{995}) suggested to be a more accurate approach in the determination of a *CI* value [162]. Results obtained from each ratio were compared with known crystallinity of samples determined by X-ray diffraction. This was done for confirmation of this method's sensitivity to crystalline structure and its viability in its determination.

For these determinations, bandwidth reduction by FSD of FTIR spectra was also investigated to determine any positive or negative effects this may have on the *CI* values.

Bandwidth reduction by FSD has the potential to significantly impact on spectral features when indiscriminately applied, and the degree of bandwidth reduction required is often at the discretion of the researcher. The built-in FSD process used assumes that the spectrum consists of well resolved lines that have been convoluted by the same type of line-broadening function. In bandwidth reduction processing, the aim is to recreate this line-broadening function through the variables of peak width and peak shape, with subsequent interferogram division of the defined function to remove the convolution seen in the original spectrum. There is also an additional apodisation function based noise reduction option available to improve the apparent signal-to-noise ratio.

3.3.1.5.1 Investigating the relationship between *CI* and crystallinity measured by XRD

In applying these software FSD processes to the FTIR spectra, both Lorentzian and Gaussian functions were explored, with the remaining parameters being individually tailored to each unique infrared spectrum as not all responded in the same manner. FSD was applied in such a way as to reach a point where the best resolution of peaks could be observed with minimal visible alterations from the original FTIR spectra, culminating in a very individualistic approach. This is likely to play a significant role in any *CI* values that are calculated, especially in the case of significant spectral alterations that may influence the peaks of interest. The parameters for each FSD are listed in Table A2. Results discussed in this section are from measurements of samples stored at 44 % RH for at least two weeks prior to analysis. *CI* values are in Tables A3 and A4.

Investigating the FTIR spectra obtained from samples by transmission mode FTIR spectroscopy, a correlation of *CI* with measured crystallinity was observed (Figure 55). In the determination of CI_{995} values, a positive but weak correlation of *CI* with measured crystallinity was observed in both raw and deconvoluted FTIR spectra (Figure 55A). However, the difference in *CI* between samples at 21 % and 30 % crystallinity was minimal, and likely within the margin of error, approximately 1 %. FSD of spectra values did not improve the linearity of the correlation.

In the calculations of CI_{1047}, an apparent linear trend was again observed between *CI* and measured crystallinity for both raw and FSD processed FTIR spectra (Figure 55B). In this case,

the trend was more linear than the correlation seen in CI_{995} values in raw FTIR spectra. FSD processed FTIR spectra revealed a similar trend to that CI_{995} values, with minimal differentiation in *CI* between samples at 21 % and 30 % crystallinity. These values are likely to be within margin of error of one another, as in the previous case. Additionally, FSD again did not yield an improvement to the linearity of the correlation.

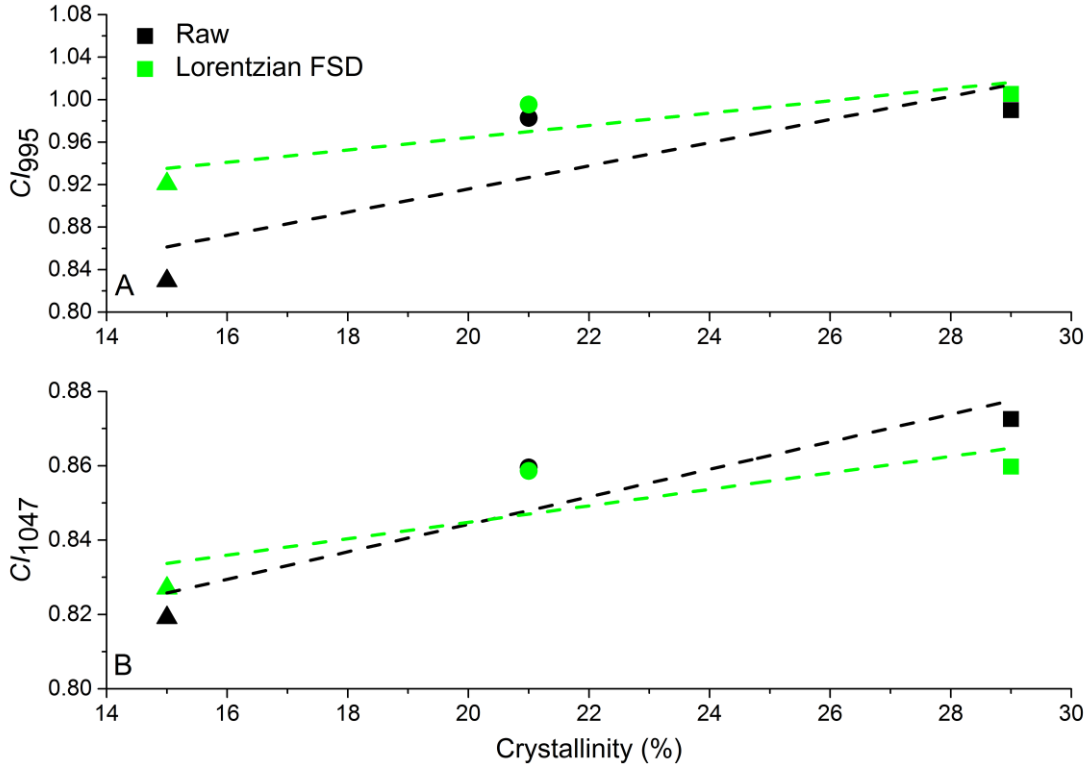

Figure 55 A- CI_{995} and B- CI_{1047} of square - Gelose 80, circle – Regular maize, triangle -Waxy maize, conditioned at 44 % RH and measured in KBr pellet by transmission mode FTIR spectroscopy plotted against crystallinity measured by XRD [113]. Dotted lines are linear fits of *CI* calculated from black – raw data (A - $R^2 = 0.71$ and B - $R^2 = 0.870$) and green – Lorentzian FSD processed data (A - $R^2 = 0.77$ and B - $R^2 = 0.70$). Fit parameters are in Table A5.

The correlation of *CI* with measured crystallinity was also explored in samples analysed by transmission mode FTIR spectroscopy at cryogenic temperatures (at least -170 °C) (Figure 56). In the CI_{995} values, an increasing *CI* with measured crystallinity was observed; however, only when calculated from the raw FTIR spectra. When calculations were made from the FSD processed FTIR spectra. this trend was lost, with the sample at 21 % measured crystallinity suggested to be more crystalline than one at a measured crystallinity of 30 %. This indicates that the bandwidth reduction by FSD had a significant impact on the spectral features in such a way as to alter the ratios of these peaks. Similar to previous cases, the differentiation in *CI*

between the samples at 21 % and 30 % crystallinity was minimal in the CI_{995} values from raw FTIR spectra.

Investigating the CI_{1047} values similarly yielded a positive correlation between *CI* and measured crystallinity. Figure 56B demonstrates this correlation, with both raw and deconvoluted FTIR spectra yielding very similar *CI* values; however, the FSD processed results still had a weaker linear correlation than the raw FTIR spectra. Compared to previous cases, these results gave a better linear correlation of *CI* with measured crystallinity, yielding a more significant distinction between *CI* values between samples of varying crystallinity.

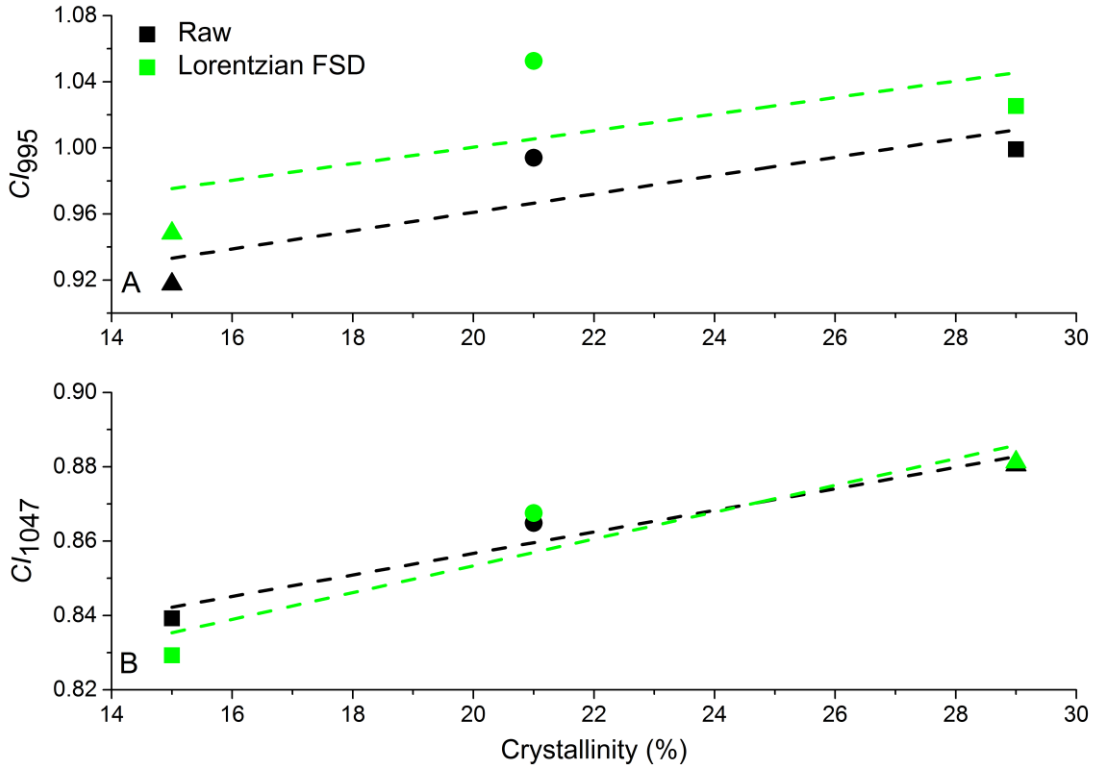

Figure 56 A- CI_{995} and B- CI_{1047} of Square - Gelose 80, circle – Regular maize and triangle - Waxy maize conditioned at 44 % RH and measured by transmission mode FTIR spectroscopy at cryogenic temperatures (-170 °C) plotted against crystallinity measured by XRD [113]. Dotted lines are linear fits of *CI* calculated from Black – Raw data (A – $R^2 = 0.730$ and B – $R^2 = 0.95$) and Green – Lorentzian FSD processed data (A – $R^2 = 0.42$ and B – $R^2 = 0.88$). Fit parameters are in Table A5.

A correlation of CI_{995} and CI_{1047} with measured crystallinity was observed at both room and cryogenic temperatures. However, CI_{1047} yielded a stronger and more consistent correlation with measured crystallinity. The measurements at low temperature produced a stronger correlation than the ones at room temperature, especially in the CI_{1047} values, as well as a greater consistency in correlation seen in the similar values obtained by FSD. *CI* values from FSD processed spectra, in most cases, reflected the trends found from raw FTIR spectra;

however, they exhibited a weaker linearity in the correlation. In some cases FSD had a significant effect on the determined *CI*, with different approaches yielding very different ratio values, as well as showing different trends in the correlation with measured crystallinity.

There was no indication that bandwidth reduction by FSD yields a more accurate correlation with measured crystallinity, with most linear fit coefficients being lower than in raw FTIR spectra results. Despite this, *CI* values from FSD processed FTIR spectra will be included in further results as a comparative tool. Despite the difficulties in finding peaks and peak height in the raw FTIR spectra, a reasonable correlation was seen between *CI* values and measured crystallinity. This indicates a link between the crystalline and amorphous peaks and the actual crystalline structure within the starch. This relationship may prove to be a useful tool in the relatively quick analysis of samples where general crystallinity information is desired, or as an estimate of crystallinity that may be correlated with other properties. However, upon preliminary investigation this method did not provide an accurate determination of crystallinity, and a large degree of inaccuracy is likely present in the logic of relating such a measurement to crystallinity in a semi-crystalline polymer sample such as starch.

3.3.1.5.2 Investigating the relationship of *CI* with amylose content

The semi-crystalline structure of starch is complex, with the formation of double helices and single helices playing a major role in the apparent crystallinity of a system, as well as the tendency for semi-crystalline lamellae to form on a larger length scale in native starch granules. In general, amylopectin contributes most significantly to the crystalline phase of starch, while amylose is the major contributor to the amorphous phase of starch. However, the formation of helices, overlap of phases and nature of branching all play a role in the structural order within the lamellae and the system as a whole. From this, a correlation of amylose content with crystallinity would be logical, whereby increasing amylose content would result in a greater fraction of amorphous phase and thus a lower crystallinity. In this section the *CI* values determined from the FTIR spectra obtained by transmission mode FTIR spectroscopy in standard starch samples is explored to assess the correlation of *CI* values with amylose content. A weak correlation of *CI* with measured crystallinity was observed in this work. A relationship

with amylose content would be a useful tool in the analysis and comparison of starch based samples.

Figure 57 shows the results of CI_{995}, comparing the CI_{995} values of the three maize starch samples shown previously (Figure 55 and Figure 56) to their amylose content. Initially, it was found that CI_{995} from raw FTIR spectra of the maize starches correlated with crystallinity (Figure 55A). A correlation of *CI* with amylose content indicated that amylose content has an influence on this *CI* value (Figure 57A). *CI* values from deconvoluted FTIR spectra showed a similar trend with amylose content, yielding similar correlation coefficients. The deconvoluted and raw results also indicated very different trend scales, with raw values giving a greater spread of values, and thus likely an inherently greater precision in the value.

The relationship between CI_{1047} and amylose content was also explored (Figure 57B). In previous cases, this ratio showed a stronger correlation with measured crystallinity than CI_{995} (Figure 55B). In this data, a similar correlation was seen where increasing amylose content decreased the *CI* value. This correlation was linear in raw FTIR spectra; however, in deconvoluted FTIR spectra the *CI* values at low amylose contents were very similar such as was the case with the previous crystallinity correlation (Figure 55B). These values are likely within margin of error, and so may not indicate any specific trends. This may be a result of bandwidth reduction by FSD destructively altering the peak ratios.

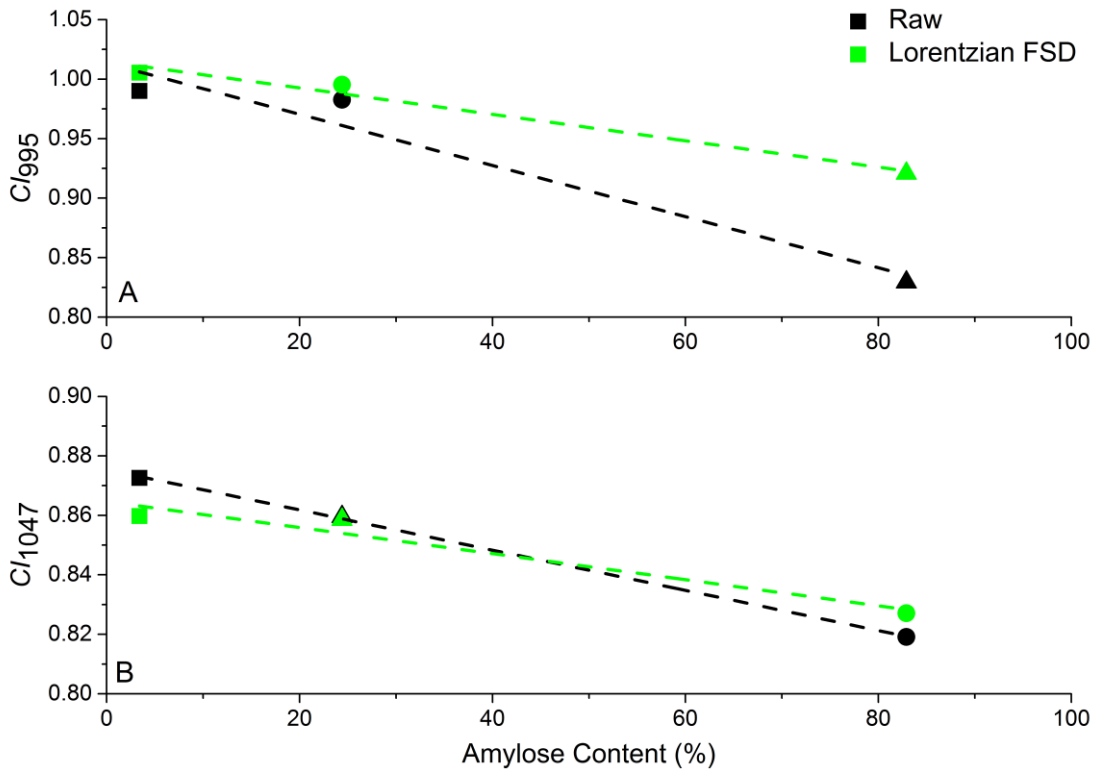

Figure 57 A- CI_{995} and B- CI_{1047} of square - Gelose 80, circle – Regular maize and triangle - Waxy maize conditioned at 44 % RH and measured by transmission mode FTIR spectroscopy in KBr pellet plotted against amylose content. Dotted lines are linear fits of *CI* calculated from Black – Raw data (A – $R^2 = 0.95$ and B – $R^2 = 1.00$) and Green – Lorentzian FSD processed data (A – $R^2 = 0.98$ and B – $R^2 = 0.95$). Fit parameters are in Table A6.

In the correlation of amylose content with calculated *CI* values, CI_{995} values yielded a strong linear correlation with amylose content in both raw and deconvoluted FTIR spectra in maize starches. CI_{1047} values yielded a more linear correlation of *CI* with amylose content. Bandwidth reduction by FSD did not significantly improve the linearity of the correlation compare to *CI* values from raw FTIR spectra

3.3.1.5.3 Intermediate conclusions

Results presented here suggest a significant trend between *CI*, measured crystallinity and amylose content, lending credit to the correlation of amorphous phase structure with amylose chains. As a fast measure of relative crystallinity between samples, this method shows promise in the analysis of similar samples, and may be extended to comparison of different samples. However, improvements to the resolution of peaks plays an important role in obtaining realistic crystalline ratios from the peaks commonly employed in the literature for the determination of these *CI* values. Improvements were observed as a result of measuring samples at cryogenic temperature; however, the time associated with this approach is

unrealistic in the analysis of large sample sets. In the analysis of simple KBr pellets, sample preparation time is still significant, especially in comparison to the processes required for ATR-FTIR measurements. This negates the primary benefit of infrared analysis, which is its speed and high throughput. Therefore, where crystallinity information is required, measurements of crystallinity be made by other methods such as powder X-ray diffraction or solid state NMR spectroscopy, that yield a more accurate and quantifiable determination of crystallinity.

3.3.1.6 Investigating *CI* as a measure of crystallinity in rice flours

The analysis of other starch based samples was possible by infrared spectroscopy, exhibiting the expected peaks for the determination of *CI*. In application to more complex samples, the influence of additional components within the sample matrix is likely to be a major factor. Rice is primarily composed of starch and water, and the influence of additional components is likely to be signficantly reduced, making the determination of *CI* values feasible. As determined earlier (Section 3.3.1.4.2), the use of cold-stage FTIR spectroscopy was inappropriate due to its minute improvements with signifcantly increased labour in methodology. Therefore the analysis of rice samples was done by transmission mode FTIR spectroscopy at room temperature, aiming to obtain the improved results that were previously observed.

Figure 58 presents the FTIR spectra of three rice samples. These rice samples were selected for their signifcant differences from one another, not only in variety, but also physicochemical and textural properties. Differences between the samples were minor; however, still observable. While the peak at 995 cm^{-1} yielded a greater peak height for the *Quest 19* sample than for the other samples, the peak at 1047 cm^{-1} had a lower apparent peak height for that sample than for the other samples. This would suggest in the calculation of crystalline ratios from these peaks that the *CI* by one ratio would yield a different trend of values between samples than would be seen by the ratio of the other. The ratio of choice in these *CI* ratios varies between publications with different experimental observations correlating these bands with crystalline features. Therefore, both ratios should be investigated in any further analysis.

This disparity in peak heights with no clear trend in relative intensities between samples was evident across the three rice samples analysed, and is investigated more in depth through the calculated *CI* values.

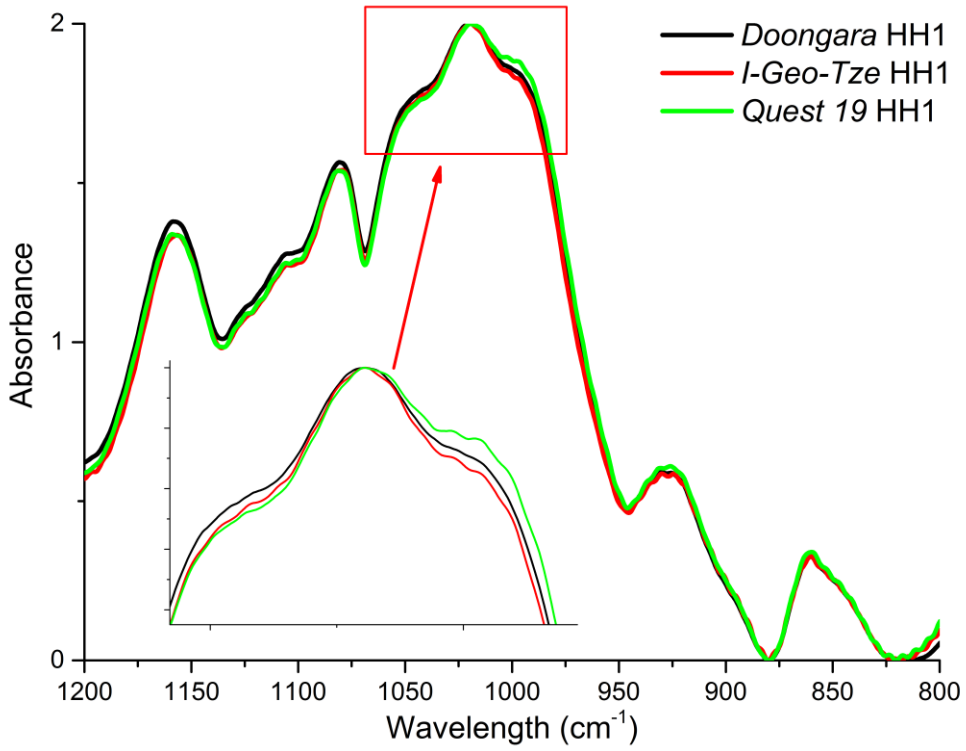

Figure 58 Transmission mode FTIR spectra of rice flours conditioned at 44 % RH.

Figure 59 shows the CI_{995} values of rice flours. In relating this peak ratio with amylose content, a monotonic trend was observed where *CI* decreased with amylose content. This indicates that increasing amylose content is decreasing the overall crystallinity of the system, fitting with common theories of the role of amylose in the semi-crystalline structure [150]. This trend appeared to be linear in these samples, with deconvoluted values also giving the same trend. A slight discrepancy between raw and deconvoluted values was seen in *Doongara*; however, this is likely within the margin of error. Overall, these results suggested that CI_{995} values shows some sensitivity to crystallinity or structural changes as a result of increasing amylose content in rice flours. However, this does not necessarily indicate a direct correlation, as differences in the rice varieties may also be a factor in this trend.

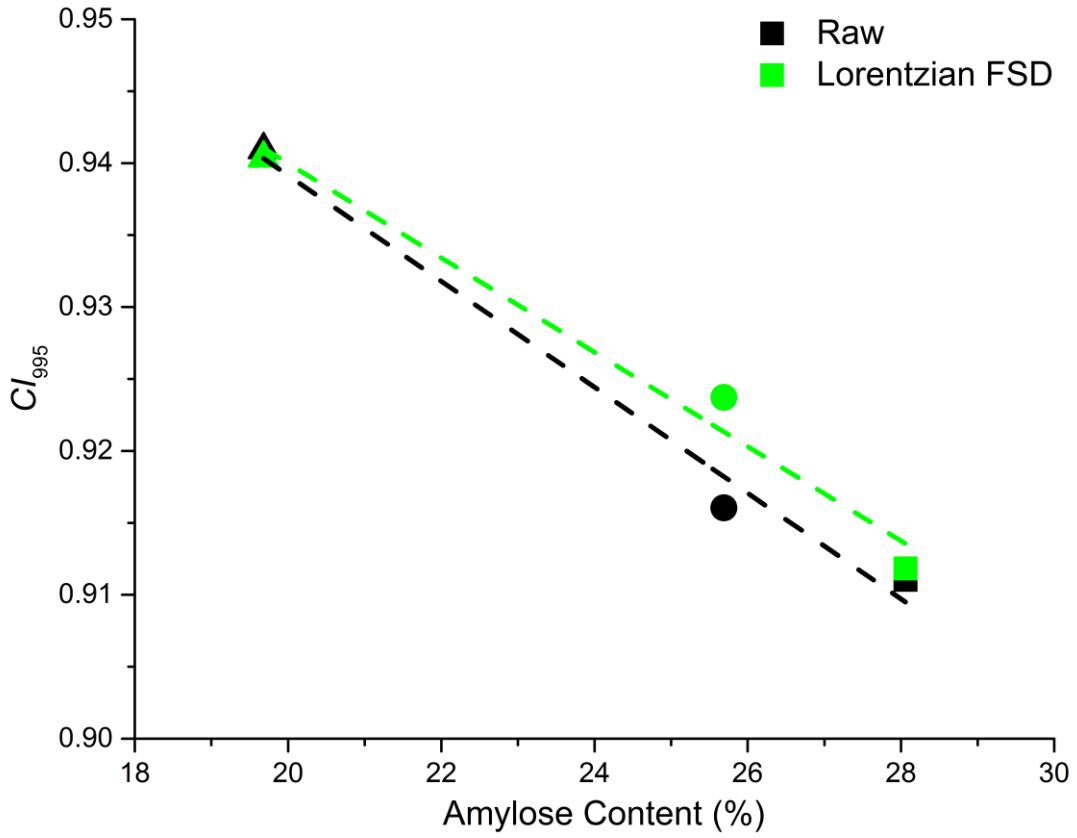

Figure 59 CI_{995} of rice flours measured by transmission mode FTIR at RT (25 °C) plotted against amylose content. Dotted lines are linear fits of *CI* calculated from Black – Raw data (R^2 = 0.99) and Green – Lorentzian FSD processed data (R^2 = 0.98). Fit parameters are in Table A6.

Figure 60 shows the CI_{1047} values of rice flours. In the analysis of maize starches earlier (Section 3.3.1.5.2), the most linear trend of *CI* with amylose content was observed in CI_{1047} values. However, in investigating rice flours by this approach, no clear trend was observed. Rather, a scattering of *CI* values with amylose content was observed. In addition, FSD appeared to also alter the *CI* values indicating a destructive change to the original FTIR spectra. Despite this, the relative difference in *CI* values between samples were unaffected by FSD processing. While no trend was observed in the CI_{1047} values, groupings may still provide limited information on samples.

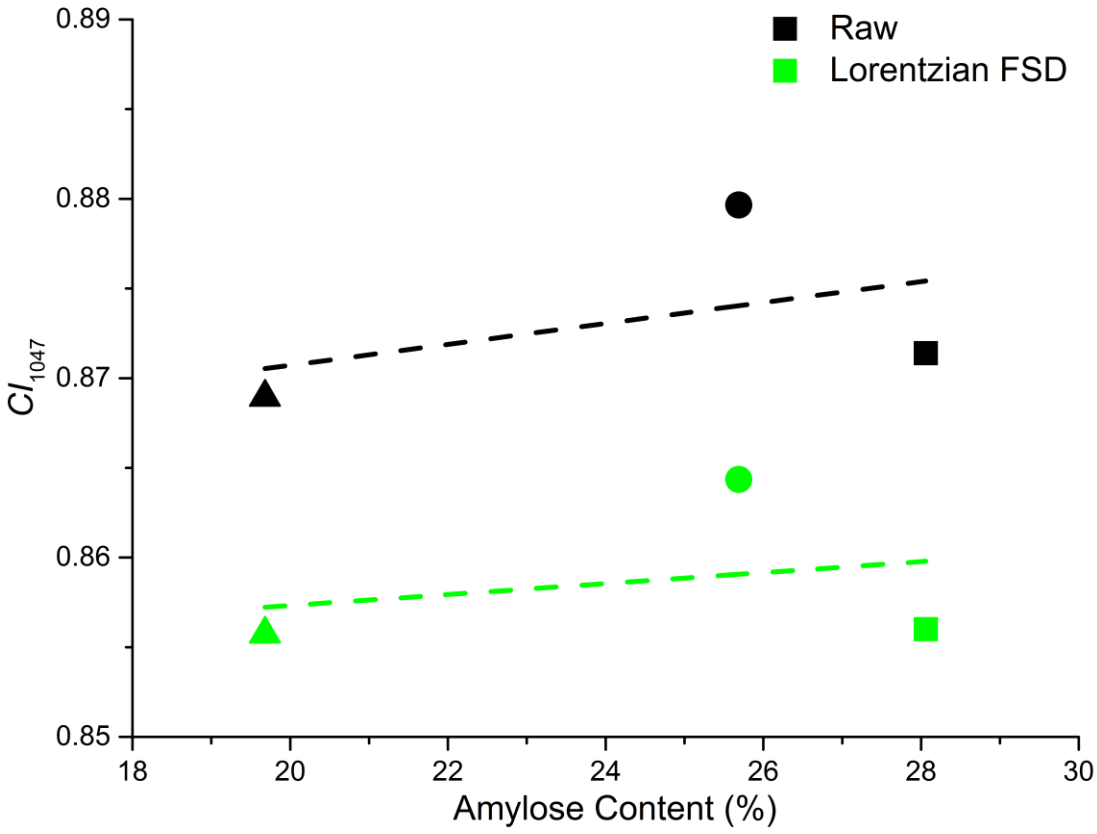

Figure 60 CI_{1047} of rice flours measured by transmission mode FTIR at RT (25 °C) plotted against amylose content. Dotted lines are linear fits of *CI* calculated from Black – Raw data (R^2 = 0.20) and Green – Lorentzian FSD processed data (R^2 = 0.07). Fit parameters are in Table A6.

In conclusion, information about crystallinity can be obtained from FTIR spectroscopy in the analysis of rice flours. CI_{995} yielded a trend with amylose content, logically suggesting decreasing crystallinity with increasing amylose content, while CI_{1047} values gave no such trend. This may indicate insensitivity to structure in certain cases, as previously both ratios correlated to a degree with crystallinity. As such, it is possible that the more complex structure of rice flour over starches influences the peak ratios. By determining the crystallinity of these rice flours, this may be explored. However, issues also arise from the determination of peak height, and this large source of error is likely to have the most significant impact on *CI* values.

3.3.1.7 Investigating *CI* as a measure of crystallinity in more complex samples

In the application of this method to more complex samples such as breakfast cereals, the limitations that arise are significant. Real food samples commonly contain a complex matrix of components including lipids, proteins and sugars. Depending on their molecular structures

these components can cause significant interference with starch peaks in infrared analysis. Figure 61 shows the FTIR spectra of breakfast cereals recorded by ATR-FTIR spectroscopy and conditioned at 44 % RH humidity, along with the infrared spectrum of a pure sucrose powder. This data revealed the overlap of absorption bands of sucrose with the region of the peaks of interest in starch. Sucrose is a common additive in breakfast cereals and one of the major sugars present [66], as such this is the most likely to create interference problems in starch analysis of such samples. Sugar content varies between the breakfast cereals presented here, and so the extent to which the sucrose will interfere is likely to vary. In general, the breakfast cereals analysed have a relatively low sucrose content with Oats Traditional containing less than 1 g per 100 g, and All Bran and Rice Bubbles less than 10 g per 100 g [66]. This low sucrose content results in a lesser interference. However, in applying this methodology to samples with higher sugar content, comparisons with those with lower levels becomes complicated due to the difference in interference effects and the problems associated with quantifying the degree of interference in analysis. This problem is likely exacerbated by the presence of other sugars, which is often the case. Further experiments would be required to confirm if these other common dietary sugars are likely to influence the starch FTIR spectra in a similar fashion.

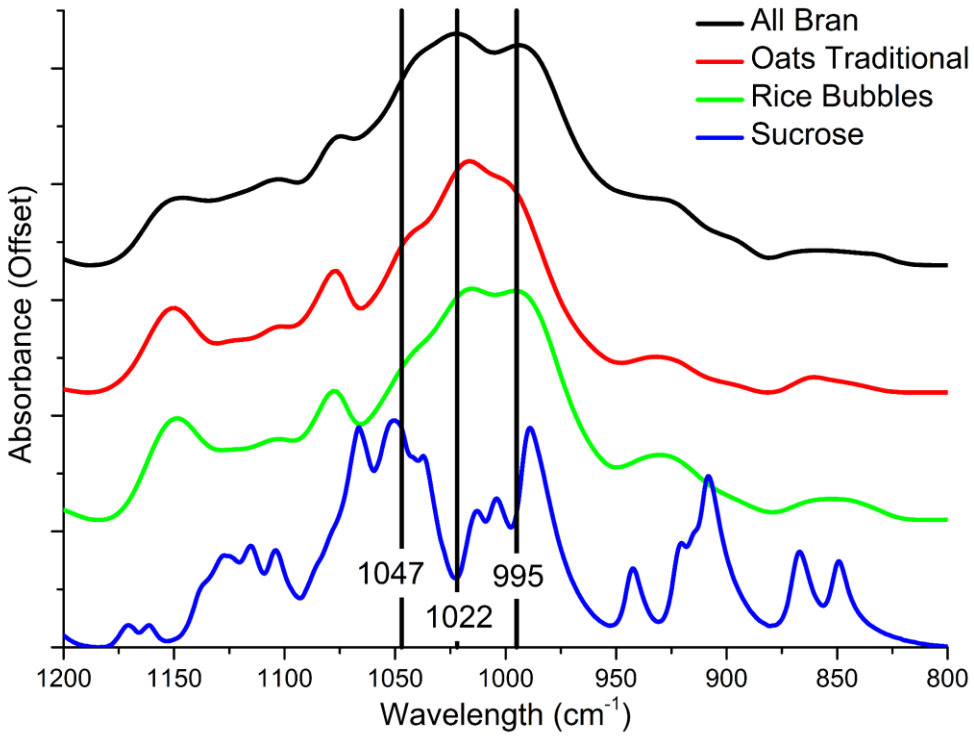

Figure 61 ATR-FTIR spectra of Australian breakfast cereals conditioned at 44 % relative humidity and of sucrose.

3.3.1.8 Conclusions

In the determination of crystallinity by FTIR spectroscopy, both CI_{995} and CI_{1047} values rely on the accurate determination of peak maxima from the FTIR spectra. Poor resolution of the peaks of interest in starch was apparent when measured using ATR-FTIR spectroscopy, making the method unsuitable for the determination of crystalline values. A better resolution of the peaks of interest could be obtained by employing transmission FTIR spectroscopy, with measurements at cryogenic temperatures (-170 °C) providing further improvements. This enhanced resolution allowed for a more accurate determination of peak maxima while also improving responsiveness to bandwidth reduction by FSD. However, the time involved in cryogenic measurements was significant, negating the analysis time advantage of infrared spectroscopy. Therefore, transmission FTIR spectroscopy measurements at room temperature were determined to be sufficient to explore *CI* values.

In exploring *CI* values, neither determination of *CI* (CI_{995} or CI_{1047}) was observed to yield a strong relationship with crystallinity. Both ratios showed a monotonic correlation with crystallinity, and trends were also observed with amylose content in both maize starches and rice flours. However, as a measure of crystallinity, the determination of a *CI* is not an accurate approach to crystallinity. Nevertheless, it may find use in quality control scenarios where only general relative values are required. As a research tool, it is not advisable to rely on such a technique. Where accurate crystallinity information is needed, techniques such as X-ray diffraction and solid state ^{13}C NMR spectroscopy are more suitable.

In applying FTIR spectroscopy to more complex samples such as breakfast cereals, the presence of other components in the samples matrix significantly influenced spectral features. Sucrose, one of the many sugars found in breakfast cereals, absorbs directly in the region of interest, and as such will influence peak intensities to variable degrees depending on its concentration. This severely limits the application of FTIR spectroscopy to complex samples such as breakfast cereals, as the error introduced by such interference is likely to destroy any information that may be obtainable from the FTIR spectra.

3.3.2 X-ray diffraction – Investigating long-range order

3.3.2.1 Introduction

X-ray diffraction (XRD) is a widely used technique in the analysis of crystalline structures, most notably in mineralogy for the determination of unit cells and subsequent identification or classification of minerals [177]. XRD collects X-rays emitted by electrons knocked out of inner energy shells by bombardment with electrons. When the geometry of incident X-rays satisfies Bragg's equation a peak in intensity occurs.

The quality of diffraction effects in XRD relies on the strict and undisturbed periodicity of atoms, with any deviation being evident in the resulting diffraction diagram. In minerals this long range order is strongly present. Thus very sharp and unique diffraction patterns are obtained [177]. However, in the case of sufficiently small crystals constructive interference may also occur, leading to peak broadening. This is especially evident in the case of semi-crystalline samples, where non-uniform crystallinity, as well as incomplete crystallinity leads to constructive interference diffractions yielding broad peaks. Amorphous or non-crystalline samples experience similarly broad diffraction peaks. In polymer applications where supramolecular structure is rarely perfectly crystalline, broad diffraction peaks will be observed. These broad peaks need to be considered in the characterisation of long range order. Thus in the analysis of semicrystalline samples describing both amorphous and crystalline contributions is appropriate.

X-ray diffraction has been widely applied to polymers such as starch, for both industrial and research purposes investigating changes in crystallinity, monitoring retrogradation and monitoring supramolecular structure during digestion [178-180]. For starch, XRD allows for characterisation of phases within the sample, yielding differentiation between amorphous and crystalline regions (Figure 2) through the observation of sharper crystalline diffraction peaks superimposed on a broad amorphous contribution. XRD can be used in the determination of crystallinity by characterisation of A/B type polymorphs within the starch [151]. Another crystal polymorph is also often observed, dubbed V-type crystalline, described as arising from single

amylose helices complexing with lipids [181]. In the case of A/B type polymorphs, there is a clear distinction in the diffraction patterns between the two crystalline arrangements. These different crystalline polymorphs influence digestibility, with B-type observed to be more resistant to enzymatic digestion compared to A-type granules [182].

In the quantification of crystallinity there are a number of approaches that can be employed. The majority of these rely on fitting or subtractive based approaches, identifying the amorphous and crystalline contributions as independent from one another in a long range arrangement. Early calculations of crystallinity in starch were based on a two phase system, consisting of a perfectly crystalline domain interspersed with amorphous regions [183]. This approach has remained common in crystallinity determinations [151, 184], although the application of curve fitting techniques is becoming more and more popular [151, 166, 185], with the availability of powerful processing hardware and advanced modelling functionalities. All of these techniques rely on the accurate decomposition of crystalline and amorphous contributions from the total intensity profile. The degree of crystallinity calculated is simply a percentage of crystalline peak areas with respect to the total peak areas. While long range crystallinity can be measured by this approach, XRD is only sensitive to perfectly regular or highly ordered arrangements. As a result, the contributions of short range order from irregular arrangements of single and double helices are not taken into account. Solid state ^{13}C NMR is a powerful tool in this respect, allowing for the determination of crystallinity from the amount of single and double helices as well as amorphous content [113, 186].

The fitting of amorphous and crystalline contributions to the X-ray diffractogram of native starch is complex. The amorphous background forms a major component of this fitting, playing a role in the fitting of crystalline peaks and thus influencing the end crystallinity values. In the traditional two phase approaches, the amorphous contribution is extended up to the crystalline diffraction peaks (Figure 62).

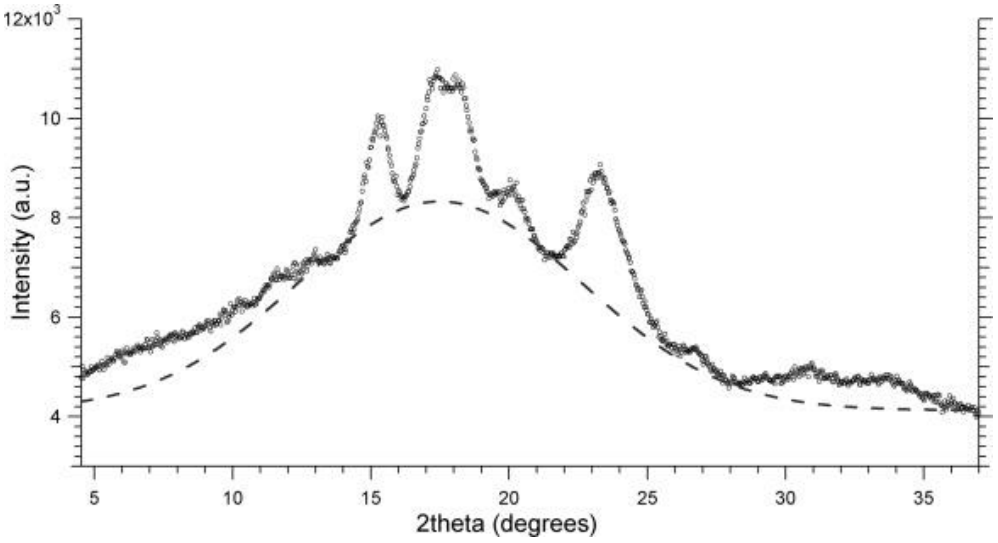

Figure 62 Amorphous background subtraction as part of the two phase method for determining crystallinity of starch by X-ray diffraction [151].

However, this approach does not take into account irregular crystalline components. One study aimed to take into account these irregular crystals by a peak fitting approach (Figure 63)[151]. The crystallinity of starch can be determined by a peak fitting approach that correlated well with double helix content as determined by ^{13}C NMR [151]. From this it was concluded that double helices exist also within irregular crystals. Therefore by this approach, it is possible to take into account the imperfect crystalline structures in the determination of crystallinity by XRD. Additionally, by this peak fitting approach the determination of different types of crystallites is possible, including the V-type crystallite formed by amylose, and their contribution to overall crystallinity could be made. Further information can also be obtained from the peak parameters, such as peak width, related to the size of the crystal where broader peaks are indicative of smaller crystals or dislocations in the crystal lattice.

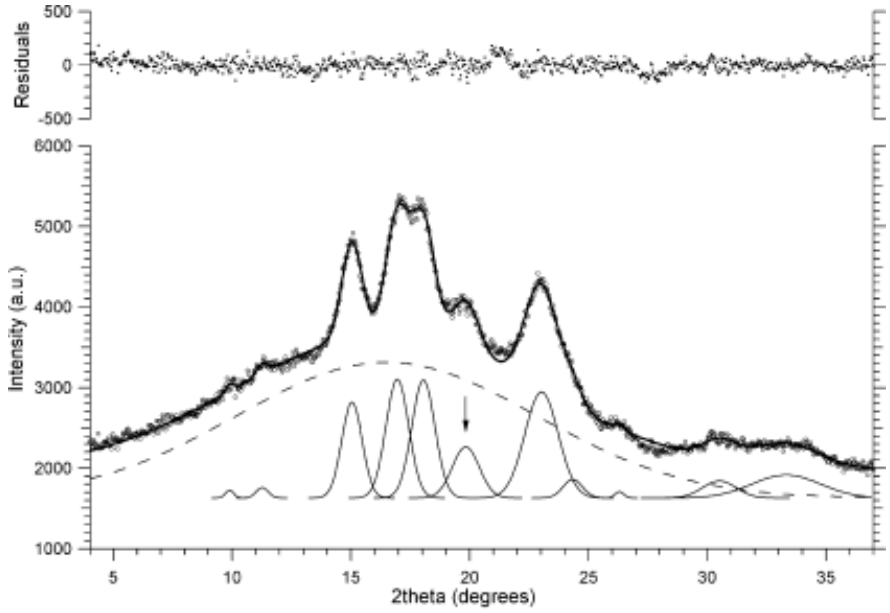

Figure 63 Decomposition of X-ray diffractogram into Gaussian amorphous and crystalline peak shapes [151].

Powder X-ray diffraction of starches in the determination of crystallinity promises to be a valuable tool in the analysis of the processing effects on starch structure. Peak fitting approaches yield a close correlation with the determination of double helices by ^{13}C NMR spectroscopy, and so were concluded to be a more accurate approach than the traditional two phase system concept [151]. Additionally, through peak fitting approaches, information on each diffraction peak can yield new information on the effects of processing on specific crystalline arrangements [151]. One such case is in the determination of V-type crystallinity which could yield information on amylose within the sample structure. The application of X-ray diffraction in the determination of crystallinity within rice samples, as well as within other starchy plant foods, has been extensively studied [151, 178, 179]. Further, this peak fitting method has potential in development for application to more complex food stuffs, such as breakfast cereals, in which a complex matrix including vitamins, minerals, sugars, lipids and proteins is likely to complicate analysis.

3.3.2.2 Materials and methods

Powder X-ray diffraction experiments were performed on a Bruker D8 advance diffractometer. Data was collected over the 2θ range from 4 to 39 ° at a step size of 0.02 ° with a 12 mm variable slit. Scan time was 4 s per step, with a total scan time of 2 h. Incident radiation was Cu Kα II with detection by a Bruker LYNXEYE silicon drift detector. Data was treated in

either Bruker TOPAS 3 [187] or WaveMetrics Igor Pro [188]software, as will be discussed in Section 3.3.2.3.

Samples were placed on a sample holder in powder form and levelled to a thin, flat layer. Analysis was then performed directly on this sample.

3.3.2.3 Determination of crystallinity by X-ray diffraction

3.3.2.3.1 Choices of peak fitting and data manipulation software packages

In employing a peak fitting approach for the determination of amorphous and crystalline contributions to total crystallinity, peak positions related to specific lattice arrangements need to be identified. A broad amorphous background is adjusted to best fit with crystalline peaks. Such an approach is inherently variable. With a multitude of peaks to be fitted and the parameters of the peaks themselves, there are a large number of factors to be taken into account with an infinite number of possible fitting parameters. Therefore, human input is almost always required to constrain the peak fitting software packages to realistic parameters expected for the system analysed. This variability can be exacerbated by the software used, and the algorithms employed in peak fitting. Most methods employ a non-linear least squares approach to minimise the chi-square; however, the specific algorithm used is not necessarily the same and so can yield differences in the end fitting parameters.

Here the determination of crystallinity by two different software packages is explored. Both packages employ a non-linear least squares approach to fitting, however, with different algorithms employed and different approaches to the parameter inputs. In addition to exploring the differences between software packages, the influence of sample holder background diffraction and subsequent subtraction is explored. In powder X-ray diffraction measurements, the sample setup is very important. Ideally sample thickness is sufficient to negate any possible penetration and therefore diffraction effects from the sample holder below the sample. In this work, however, as a result of small sample quantities, samples were levelled in a thin layer on the sample holder for analysis. This is likely not ideal, as diffraction effects

from the sample holder are likely to be a factor. So a sample holder background is also recorded. While diffraction effects from the sample holder will be seen in the sample measurements, the scale of interaction observed will occur as a function of sample thickness and so subtracting a full sample holder background is inaccurate. Thus the determinations of crystallinity will be made both with and without a sample background subtraction.

3.3.2.3.2 TOPAS software

First explored was the Bruker TOPAS software, a profile and structural analysis software with capabilities of peak fitting and refinement. Using TOPAS, emission correction for the Cu Kα II radiation were made and a background taken as a 1st order Chebychev function with a $1/x$ background function used to account for background air scatter at low angles. A broad amorphous peak was first fitted, then the remaining observable crystalline peaks added. The best possible fit was achieved by restricting peak positions according to a local visual range and expected positions based on experiment and theoretical literature values [151]. Gaussian peak shapes were used in fitting, as they yield a more realistic fitting in the determination of crystallinity [162]. Gaussian peaks are not available in TOPAS 3 so pseudo-Voigt peaks were employed with the Lorentzian contribution forced to 0. Fitting was done by a non-linear least squares routine based on the Newton-Raphson method with the Marquardt method [189] included for stability.

Figure 64 and Figure 65 show the fitting profile of Gelose 80 with and without background subtraction, respectively. The primary diffraction effects seen from the background was a small broad band from 7 to 14 ° (Figure A4). Subtraction of this background yielded an improved resolution of the small diffraction peaks in this region, and subsequently more realistic fitting of these peaks. Where background was not subtracted, these small diffraction peaks were less evident, making fitting more difficult and leading to broader bands than would be expected being preferentially fitted by the software. The apparent ratio of crystalline to amorphous peak area varied significantly with and without background subtraction (Table 4). This likely arose from the fitting software compensating for the lack of background subtraction by increasing the total area under the curve for the broad amorphous peak. The baseline function employed in this fitting procedure is based on a linear function between the start and end of the data analysed, allowing for a simple approach that can be

applied similarly between samples. In peak fitting by TOPAS, this linear baseline did not directly link the start and end points of the data set, with the most significant variation observed at lower angles. Additionally, the nature of the baseline did not appear to be similar between data sets, yielding different baseline treatments in each case. Despite this, a good fit of both background subtracted and non-background subtracted data was achieved. The peak fitted diffractograms of other samples analysed are in the appendices (Figures A5 to A8).

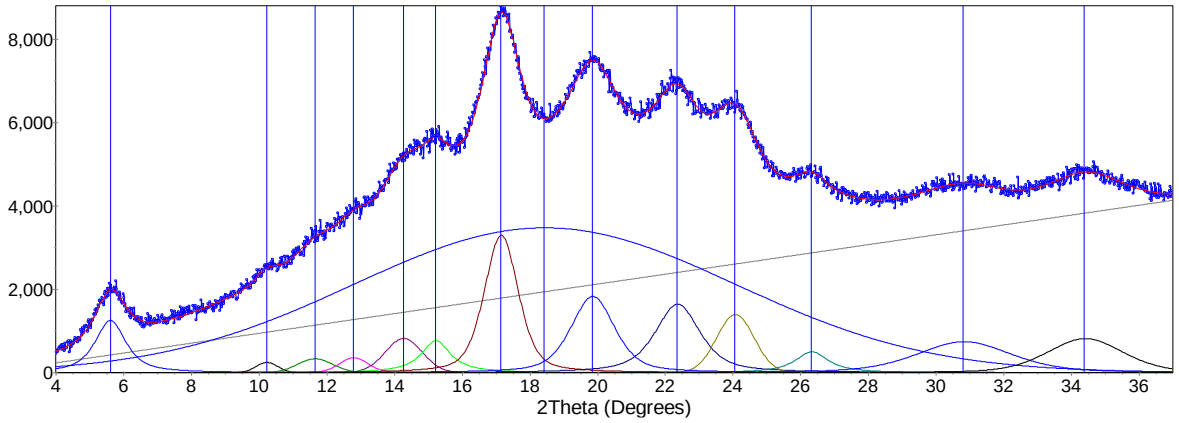

Figure 64 TOPAS software peak fitting of X-ray diffractogram of Gelose 80 conditioned at 44 % RH with sample holder background subtraction where fitted peaks are shown close to the x-axis with the broad (0 to 34 °) amorphous peak at 18 °, V-type peak at 20 ° and the remaining peaks being crystalline peaks. The baseline is shown as a linear curve from 4 to 37 °, and the sum of fitted peaks shown as the red line superimposed on the blue X-ray diffraction pattern.

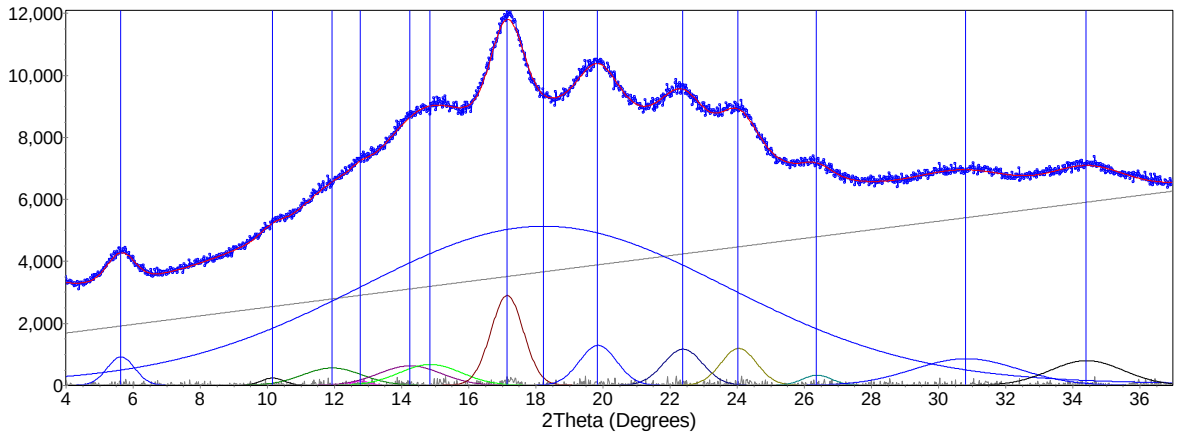

Figure 65 TOPAS software peak fitting of X-ray diffractogram of Gelose 80 conditioned at 44 % RH without sample holder background subtraction where fitted peaks are shown close to the x-axis with the broad (0 to 34 °) amorphous peak at 18 °, V-type peak at 20 ° and the remaining peaks being crystalline peaks. The baseline is shown as a linear curve from 4 to 37 °, and the sum of fitted peaks shown as the red line superimposed on the blue X-ray diffraction pattern.

3.3.2.3.3 Igor Pro software

Figure 66 and Figure 67 show the peak fitting of Gelose 80 using WaveMetrics Igor Pro software. This software package uses a Levenberg-Marquardt algorithm to search for

coefficient values that minimize the chi-squared. This is a form of non-linear least squares fitting. The fit is finished when the rate at which the chi-square values decreases is small enough. In Igor Pro, Gaussian peaks were interactively added allowing initial input of the expected parameters. Peak parameters were again constrained to realistic values based on visual cues, and theoretical expectations.

Figure 66 shows the peak fitting of Gelose 80 with the sample holder background subtracted. Using Igor Pro, peak fitting appeared to favour broader peak shapes at higher angles compared to those fitted by the TOPAS software. Again, the background subtracted data responded better to peak fitting at smaller angles as a result of the improved resolution of these peaks. This yielded a similar change in crystallinity with Igor Pro for both Waxy maize and Regular maize. However, for Gelose 80 with no background subtraction (Figure 67), the amorphous contribution exhibited an opposite trend from that seen with TOPAS for Gelose 80, with an apparent increase in crystalline peak area rather than an increase in amorphous background as seen previously (Figure 65). This subsequently yields a higher measure of crystallinity compared to the fitting in TOPAS. The baseline in peak fitting was again taken as a linear function between the start and end point of the data set. In the fitting by TOPAS, this linear baseline did not always line up with actual data set, possibly influence the fitting and therefore peak area contributions. In Igor Pro the linear baseline appeared to more closely relate to the start and end points of the data set, yielding a more repeatable approach to baseline determination. Again, a good fit of both background and non-background subtracted data sets was found using this software, with additional residual information easily available to determine the goodness of the fit. Peak fitted diffractograms of other samples are in the appendices (Figures A9 to A12).

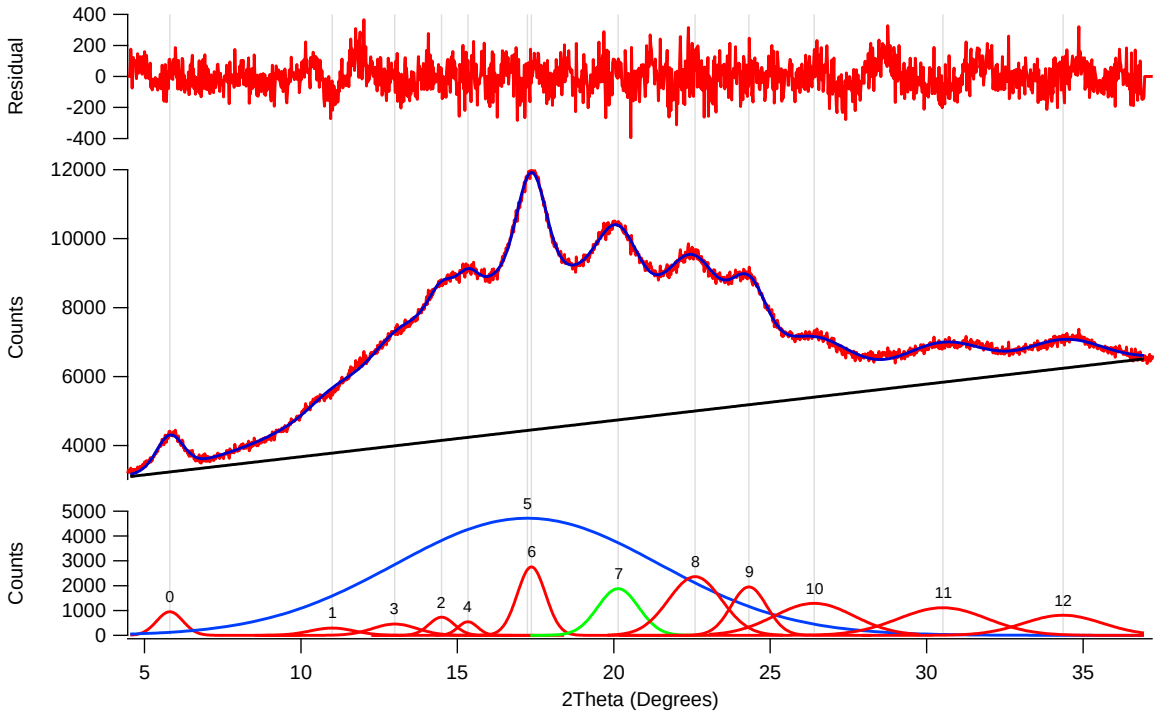

Figure 66 Igor Pro software peak fitting of X-ray diffractogram of Gelose 80 conditioned at 44 % RH with sample holder background subtraction. The bottom section shows the fitted peaks with Blue-Amorphous, Green – V-type and Red – crystalline peaks. The middle section shows the linear baseline used for fitting (black), the sum of fitted peaks (blue) and the original X-ray diffraction pattern (red). The top section shows the residuals of fitting.

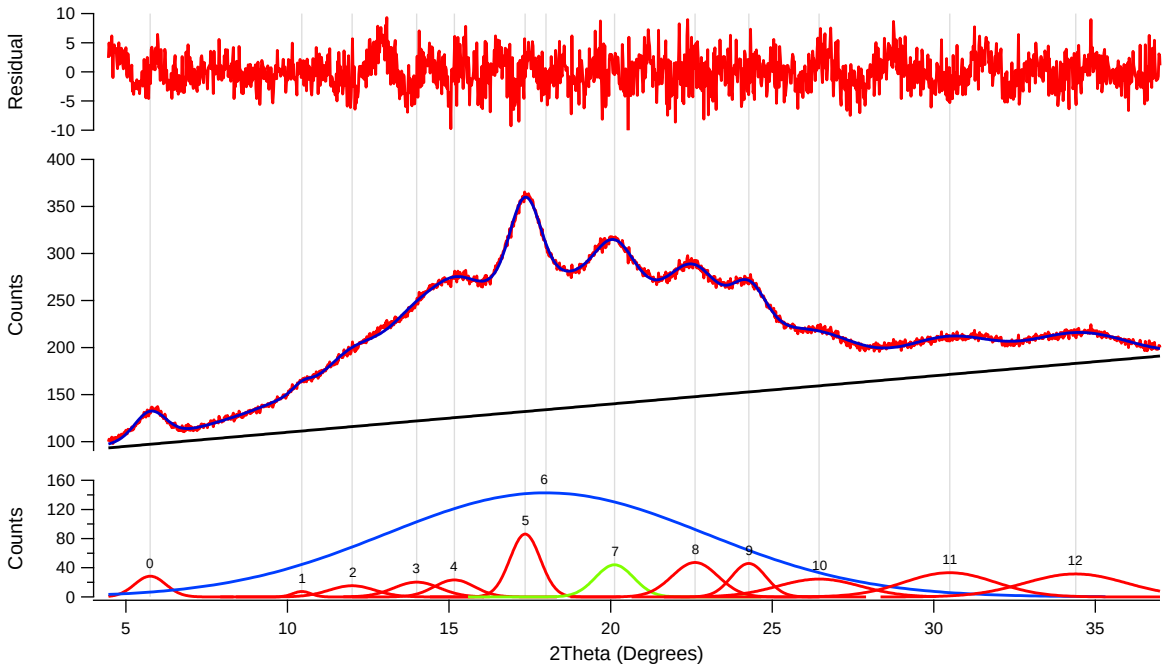

Figure 67 Igor Pro software peak fitting of X-ray diffractogram of Gelose 80 conditioned at 44 % RH without sample holder background subtraction. The bottom section shows the fitted peaks with Blue-Amorphous, Green – V-type and Red – crystalline peaks. The middle section shows the linear baseline used for fitting (black), the sum of fitted peaks (blue) and the original X-ray diffraction pattern (red). The top section shows the residuals of fitting.

3.3.2.3.4 Choice of the data processing software package

From the fitting by these 4 approaches, crystallinity values were calculated based on the ratio of crystalline area to total area. Calculation of V-type crystallinity was taken as the peak area contribution of the diffraction peak at 20 ° divided by the total area. These results are presented in Table 4.

Table 4 Percentage crystallinity (%) of starches determined by X-ray diffraction with and without background subtraction (BS) using different software packages

		TOPAS						Igor Pro					
		BS		No BS		Average		BS		No BS		Average	
Sample	Type	Crystallinity	V-Type	Crystallinity	V-Type	Crystallinity	V-Type	Crystallinity	V-Type	Crystallinity	V-Type	Crystallinity	V-Type
Gelose 80	B	29	4.8	19	1.9	24	3.4	27	2.6	32	3.9	29	3.3
Regular Maize	A	24	4.1	26	0.70	25	2.4	24	1.0	25	0. 86	25	0.92
Waxy Maize	A	27	3.4	29	0.11	28	1.8	30	0.3	31	0.06	30	0.17

In comparing the calculated crystallinity with and without the background subtraction, values of crystallinity were within 1 to 2 % of each other. This indicates that the background diffraction either does not play a significant role in total peak area, or the fitting software has appropriately taken the diffraction into account. However, this was observed only in Regular maize and Waxy maize, with the Gelose 80 showing a significant difference between background and non-background subtracted diffractograms. An absolute difference of 5 to 10 % crystallinity was found for Gelose 80, with the larger difference seen by peak fitting in TOPAS. This could be a result of background diffraction playing a more significant role in this more amorphous sample. Alternatively, fitting difficulties may arise from the type of crystalline polymorph. Gelose 80 varied the most significantly with and without background subtraction, and was the only starch tested with B-type crystalline structure. However, there is no strong evidence that the large variance between determinations with and without background subtraction is related to fitting issues of this polymorph type. The contribution of background diffraction in for the results here is expected to be between that of the full scale background subtraction and no background diffraction effects. So the average of the crystallinity values determined from these approaches was taken.

In comparing these measured crystallinities to those previously made on these samples [113] a close correlation was seen in Regular maize and Waxy maize, with published values of 21 and 29 % respectively [113], with a more significant overestimation found in Regular maize compared to published values [113]. However, this still indicates a good reproducibility despite the variation in software and data manipulations. In the case of Gelose 80, a large variation was seen between both the average crystallinity by both software packages, as well as with the published crystallinity of 15 % [113]. A relative deviation of up to 100 % has been found in this work, possibly related to the nature of this starch sample. Gelose 80 has a high amylose content and subsequently higher proportion of amorphous content that may not be appropriately taken into account in peak fitting approaches. The polymorph type may also be a factor, but there is no significant evidence to support this.

In investigating V-type crystallinity, a correlation with amylose content should be expected, and this general trend is seen in all approaches. However, the effect of background subtraction on the crystallinity value in TOPAS is significant in all samples with a relative variation ranging from 50 % in Gelose 80 to 3000 % in Waxy maize. In contrast, the calculated V-type crystallinity by peak fitting in Igor Pro yielded a consistent determination of V-type crystallinity in strong agreement with the expected trend.

The many variables involved in peak fitting can have a significant effect on the determination of crystallinity. The major factor found herein was in the subtraction of a sample holder background, yielding an unknown contribution to the diffraction peak area. Differences between software packages and the algorithms they employ in peak fitting also yielded differences in the determination of crystallinity. These variations were apparent in both the overall crystallinity and the V-type crystallinity. This highlights one of the main weaknesses in the peak fitting approaches, which is the extremely large number of ways in which peaks can be fitted. When peak fitting is properly employed, the associated error can be mitigated through prior knowledge of the crystalline system being analysed. However, this cannot completely account for the variation of processing by different software packages, and so a degree of error will still be associated with such measurements when comparing different packages. Despite this, a degree of reproducibility was found in this work when compared to previous work on the same samples using a similar approach [113]; however, no strong conclusions can be drawn indicating the reproducibility of this method. Therefore, in

agreement with literature [151] it was determined that the determination of crystallinity by X-ray diffraction is a viable technique in the characterisation of starch.

Both TOPAS and Igor Pro software packages performed similarly in the determination of total crystallinity, both with and without background subtraction. In the determination of V-type crystallinity, the Igor Pro software package gave results closer to the published values for these samples, and showed significantly less variation in the final value as a result of sample holder background subtraction. However, the sample preparation in these experiments was not optimal, and a thicker sample would likely aid in mitigating potential background diffraction. Where background diffraction is not significant, the performance of each of these software packages is likely to be different, and so from the data here it is difficult to indicate which one is the better software package. Both have their merits. The TOPAS software is an advanced software package, providing extensive control over the fitting parameters and is highly specialised for X-ray crystallography; however, this also makes peak fitting complicated, requiring extensive manual input in obtaining realistic fit parameters. The Igor Pro software is slightly more user friendly, offering a simpler interactive interface for peak fitting, while also featuring some more advanced functionality. In fitting XRD diffractograms for the determination of crystallinity, the Igor Pro software was more user friendly; however, for advanced crystallography a specialised software such as TOPAS is more appropriate.

3.3.2.4 Application to more complex samples

Interest in starch extends further than pure starch samples and characterisation of starch in complex food samples is becoming a bigger area of interest as obesity and other diet related diseases become a major factor in worldwide health. Characterisation of starch is complicated by the presence of a variety of other components within the sample matrix such as proteins, lipids and sugars. In the analysis by X-ray diffraction, these additional components can play a major role in the determination of crystallinity, dependent on their arrangements and quantities within the sample.

One such sample where these factors may play a role is breakfast cereals. Primarily grain based products, breakfast cereals have high starch content, with additional sugars commonly added to modify the product's palatability. In measuring the crystallinity of starch in such a product, the high sugar content is likely to significantly influence the diffractograms obtained.

Figure 68 shows the diffractogram of granular sucrose, yielding very strong and sharp diffraction peaks indicative of a highly crystallised system. In the analysis of starch in a system containing such a crystalline component, the difference in diffraction strength is likely to completely mask any underlying crystallinity in the starch. While longer scan times in pure starch would be helpful in improving peak intensities of the poorly diffracting semi-crystalline structure of starch, in samples containing components with a high degree of order this would likely not aid in resolving the starch peaks. Increasing scan time will result in decreasing the intensity of starch diffraction peaks relative to the more crystalline components, rather decreasing the diffraction peaks of starch with increasing scan time. Conversely, shortening scan times will likely show only the highly crystalline components with insufficient time for adequate resolution of starch peaks. Thus, subtractive approaches would likely not be viable in such complex starch systems with sugar based contributions, as the contributions from the highly order sugars is likely to destroy or irreversibly affect the starch contributions, resulting in an unrealistic starch diffraction pattern.

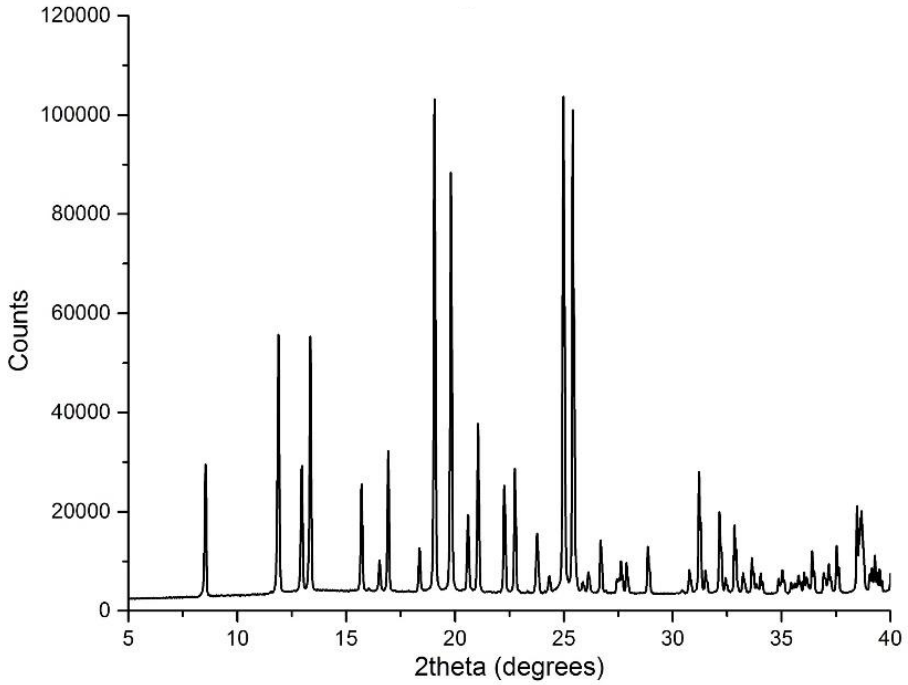

Figure 68 X-ray diffractogram of crystallized sucrose

3.3.2.5 Conclusions

This section determined that powder X-ray diffraction is a viable technique in the determination of crystallinity in starches, as has been previously determined [151]. However, the

influence of software and sample preparation is important. A sufficiently thick sample is ideal for analysis to negate any effects of background diffraction that cannot be accurately subtracted. While applying these methods to systems composed primarily of starch is realistic, application to complex systems containing other highly crystalline components such as sugars does not appear to be possible. Further investigation would be required to confirm this. Future work will involve determining the crystallinity of starch in rice flours by this methodology to better understand how starch structure relates to digestibility. Rice flours also represent a more complex sample. However, their relatively simple composition (primarily starch) means that interference should be minimised making accurate characterisation possible.

3.3.3 Investigating lamellar structure by small-angle X-ray scattering

3.3.3.1 Introduction

Small angle X-ray scattering (SAXS) is a fundamental method for the analysis of condensed matter, and is especially powerful for the analysis of biological samples which are not always crystalline. Scattering techniques provide information on the length scale of 1 to 100 nm, bridging the gap between crystallography and microscopy [153]. Compared to XRD, SAXS has a modest resolution that is not sufficient to reveal atomic structure; however, SAXS shows its strength in the measurement of sizes, shapes and interactions of larger nanoparticles and molecules. Detection of large scale spacing is achieved by bombarding the sample with intense, narrow X-ray beams, supplied by a synchrotron or lab based X-ray source, at the sample and detecting scattered X-rays relative to the primary beam. Small angle scattering techniques can also make use of neutrons as the incident radiation. This technique is referred to as small angle neutron scattering (SANS) and is a complementary technique to SAXS. In scattering techniques, the incident X-ray or neutron radiation is elastically scattered by a sample, and the resulting scattered radiation is analysed. The resulting scattering pattern provides information on the size, shape and orientation of components in the system. In contrast to other scattering techniques, small angle scattering is useful in structural

determinations at lower resolutions investigating short range order. Larger sizes can be explored by ultra-small angle scattering techniques approaching 10 μm length scales.

For scattering to occur a contrast difference between the atoms or molecules and their surroundings is required. The type of contrast is dependent on the type of radiation used. In SAXS, a measure of the variations in electron density distribution is measured. So in a semi-crystalline structure such as starch this contrast arises from the difference in scattering length densities between the two phases: crystalline and amorphous lamellae [153].

The coexistence of multiple phases and complexity of the sample matrix make the analysis of starch complicated. However, significant contributions to the characterisation of semi-crystalline lamellar structure in native starch have been achieved by employing small angle scattering techniques [153]. These lamellar structures are a result of amylopectin and its side chains interspersing with amylose chains yielding a repeating ordered and amorphous phase and an overall semi-crystalline phase (Figure 2, level 4 to 5). These lamellar structures are only detected by small-angle scattering in a hydrated state, likely explained by the liquid crystalline model for starch where amylopectin side chains are theorised to behave as liquid-crystalline polymer [190-192]. Thus, it is important to completely hydrate starch samples and in the comparison of samples to ensure a consistency in the degree of hydration.

In the analysis of the lamellar structure, care must be taken in the treatment of scattering data. In the case of isotropically scattering samples, the scattering data can be normalised to sample transmission, background subtracted, and then radially averaged to a 1 dimensional scattering curve. However, in orientated samples, sector averaging approaches are considered to be more appropriate [153].

SAXS patterns from hydrated native starch granules yield a broad scattering peak. The parameters of this peak relate to the structural characteristics of the semi-crystalline lamellae (Figure 69). The peak position is inversely related to the average total thickness of one crystalline and one amorphous lamella within the semi-crystalline lamellae. This is commonly referred to as the lamellar repeat distance [191]. The peak height is proportional to the amount of the ordered semi-crystalline structure with respect to the total amorphous and crystalline phases [193]. Peak width is related to the total length of repeat units in a semi-crystalline arrangement, with sharper peaks indicating a larger semi-crystalline arrangement[45].

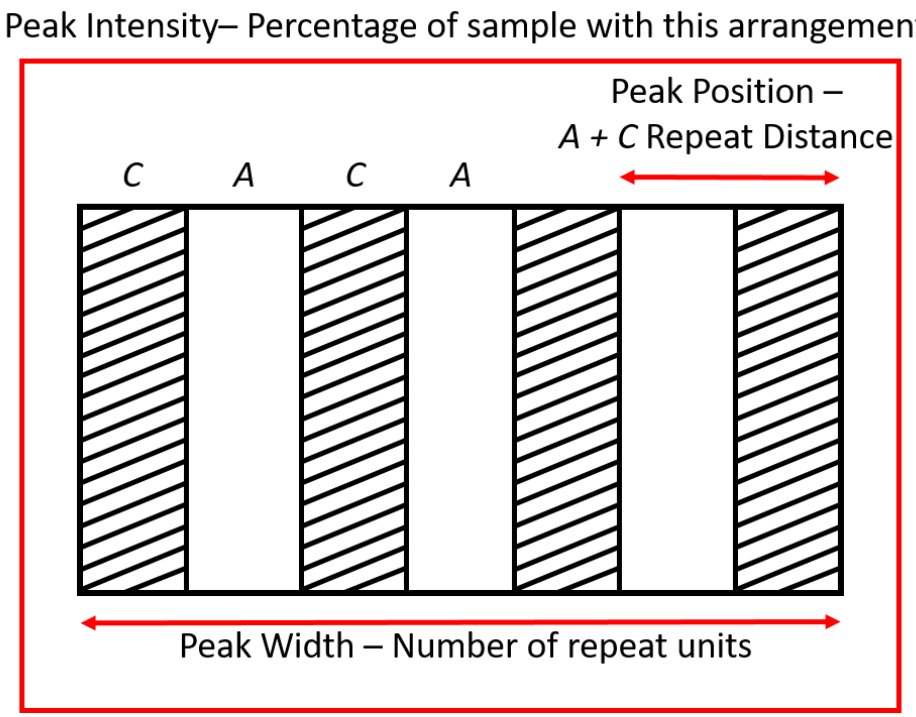

Figure 69 Graphical representation of the real space relationships of small angle X-ray scattering peak parameters [45, 191, 193], A - amorphous lamella and C - crystalline lamella.

In general, there are two approaches to extract peak parameters from SAXS data. One approach is based on iterative least squares based fitting of the observed intensity profile, and the other is based on correlation and interface distribution functions defined by a Fourier-transform intensity profile. In least squares based fitting methods, an appropriate model is required to describe the system. The simple paracrystalline model has been widely used in describing semi-crystalline systems and assumes three different electron densities, amorphous and crystalline for the repeating semi-crystalline lamellar structure, as well as the amorphous background [190]. However, this model is over simplistic in assuming that amylose exists only in the amorphous background, as the role of amylose in crystallites differs between type A and type B crystallites crystal structures [194]. This simplistic approach also does not account for deviations from an ideal lamellar structure, with inclusion of additional parameters allowing to account for such deviations [195, 196]. These approaches allow for an enhanced ability to fit scattering data; however, additional scattering information is required through other methods such as neutron contrast methods [153]. In the class of methods based on correlation functions, intensity data is Fourier transformed and the resulting function interpreted in terms of lamellar morphology to obtain structural parameters [196-199].

These methods have been compared, and consistent differences are observed between the approaches [153]. However, both approaches yielded meaningful results even when the lamellar peak was not clearly defined [200]. Empirical methods such as graphical methods and fitting of equations that describe the SAXS peak and account for underlying diffuse or interfacial scattering can also be used in determining height, position and width of SAXS peaks. The latter fitting approaches employs a power-law function to describe the underlying diffuse scattering at low ***q***, a Gaussian/Lorentzian peak to the fit the lamellar peak and a Gaussian peak for the second order reflection peak [46].

SAXS is a valuable tool in the analysis of lamellar structures in starch [153]. SAXS provides information on the repetition length of the semi-crystalline lamellae, as well as the distribution and composition of semi-crystalline components with respect to amorphous contributions. It has proven useful in the observation of the processes of starch swelling, gelatinisation, retrogradation and annealing [201-204]. Investigation into structure changes during digestion of starch granules by SAXS is an important tool in the determination of major factors affecting enzyme activity [180]. Trends in peak parameters can give insight into the processes involved, such as the tendency of peak height to decrease with increasing amylose content [45, 193, 205]. The most accepted theory accounts for this by a decrease in the electron density difference between crystalline and amorphous regions of the lamellae, closely related to overall crystallinity [153]. Thus, SAXS can have widespread applications into the study of lamellar and semi-crystalline structure in starch, and is especially valuable in assessing how processing and/or other structure influencing factors may alter this level of structure.

3.3.3.2 Materials and methods

Samples were packed into quartz glass tubes of; 80 mm length, 2 mm outer diameter, and 0.01 mm wall thickness (Hilgenberg GmbH, Malsfeld, Germany). Packed samples were hydrated with excess water, levelled above the packed sample for at least 12 h prior to analysis. Packed mark tubes were then sealed using paraffin wax to maintain sample integrity while they are under vacuum during the experiments.

Small angle X-ray scattering experiments were performed on a Bruker NANOSTAR SAXS system, employing 3 pinhole collimation for focussing. The instrument source is a copper rotating anode, yielding a Cu Kα radiation wavelength of 1.541 Å. The instrument is

fitted with a VANTEC1000 2D detector (resolution 68 μm). The scattering vector, $\boldsymbol{q}$ in the range of 0.01 to 0.35 $Å^{-1}$, was used in analysis. Optics and sample chamber were under vacuum to minimise air scatter effects. Scattering files were radially averaged using the Bruker NANOSTAR software package. One dimensional scattering files were water background subtracted and normalised according to transmission relative to a capillary filled with water using the ATSAS software package [206].

Data fitting used the WaveMetrics Igor Pro software [188] and National Institute of Standards and Technology (NIST) Center for Neutron Research macros [207]. The fitting function was a power law function, with an additional Gaussian and Lorentzian peak describing the main reflection, and a Gaussian peak to describe the secondary peak [46]. Fitting parameters were iteratively calculated, with the goodness of fit determined by the best achievable chi-square value.

3.3.3.3 Small angle X-ray scattering of maize starch standards

In the characterisation of lamellar structures in starch, starch standards characterised by other methods were investigated. These samples Waxy maize, Regular maize and Gelose 80 significantly structurally differ and thus should allow for a relatively simple investigation to the application of scattering methods to starch systems.

Figure 70 shows the scattering patterns of Waxy maize, Regular maize and Gelose 80. Differences between the samples were qualitatively observed, with peak height and peak width varying significantly between the samples. Notably, when relating peak intensities to amylose content, a trend of decreasing peak height was observed with increasing amylose content (Waxy maize – 3.4 %, Regular maize – 24.4 %, Gelose 80 – 82.9 %). This effect is similar to what has been seen in other starches[45, 193, 205]. Further differences between samples in peak width and slight differences in peak position were also evident, and may yield insight into structural influences due to not only amylose content, but also other structural characteristics such as degree of branching or crystallinity.

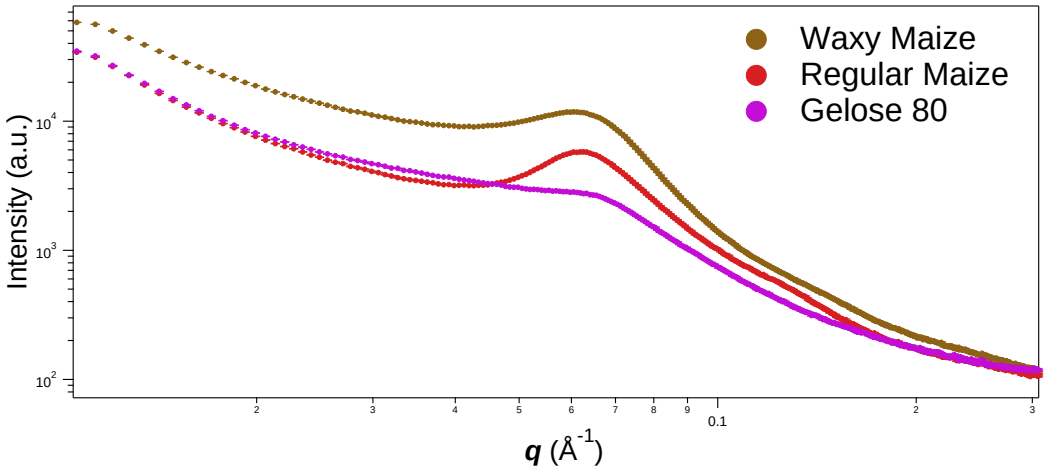

Figure 70 SAXS curves of starches known to differ significantly from one another

With the trends observed initially in the scattering patterns of the maize samples presented here, data was fitted to obtain the peak parameters. This fitting allowed for a means with which to compare to other known structural characteristics of these samples. Figure 71 shows the height of the main peak in the scattering pattern against the amylose content. As seen from the scattering pattern, a monotonic trend of decreasing peak height with increasing amylose content was observed. This correlates well with the aforementioned observations [153]and indicates an effect of amylose content on the semi-crystalline makeup of the starch granule. In larger sample sets, such trends may reveal groupings or alternate correlations that may indicate more as to how individual samples respond to treatments in this overall semi-crystalline structure.

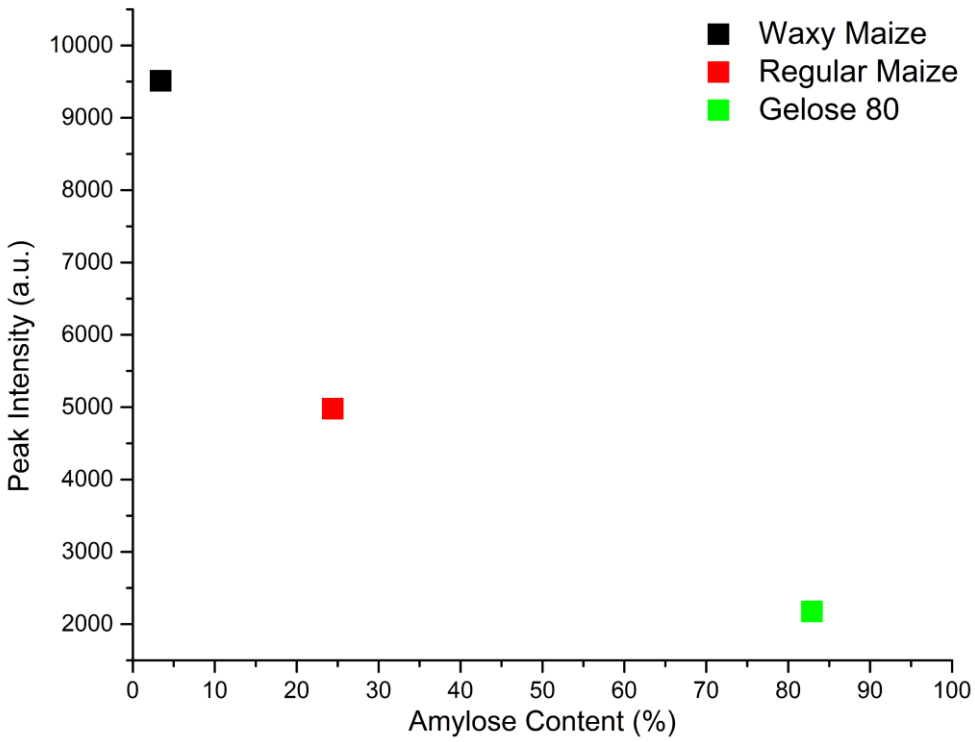

Figure 71 SAXS main peak height of maize starches plotted against amylose content. Error bars (1 standard deviation) fall inside the data point marker and cannot be seen.

Figure 72 shows the peak position of the fitted curves against the amylose content. Upon initial investigation no apparent trend appeared. However, in examining this data in relation to the scattering patterns in Figure 72, a discrepancy between the apparent peak position and the peak position of the calculated curve was observed. Specifically, the peak position increased with amylose content when qualitatively assessed from the scattering pattern; however, that trend did not appear in the fitted peaks. This highlights one of the difficulties of this approach, in that mathematically fitting data is not always straightforward, and in an effort to reduce the chi-square error unrealistic parameters may be calculated (Figure A13). The most significant discrepancy was seen in Gelose 80, the high amylose maize starch. This sample had the highest peak position based on visual observation; however, fitting yields a peak position much lower than either other samples. Fitting of this scattering pattern yielded difficulties arising from the broadness of the peak, and from the lack of a second reflection usually seen around a $\boldsymbol{q}$ value of 0.11 $Å^{-1}$, likely explaining the apparent inaccuracy in the fitted peak parameters. While the fitted data indicated no monotonic trend in peak position with amylose content, qualitative comparisons seemingly revealed an increasing peak position with amylose content. As discussed in the introduction (Section 3.3.3.1), the peak position gives insight into the repeat

distance of amorphous plus crystalline subunits in the lamellar structure. The correlation with amylose content suggests a modification of this repeat distance, possibly arising from amylose contributions to the amorphous lamellae. While the trend here is not clear, in applying this to larger sample sets, groupings could give insight into the influences of other processes on this repeat distance within semi-crystalline lamellar structures.

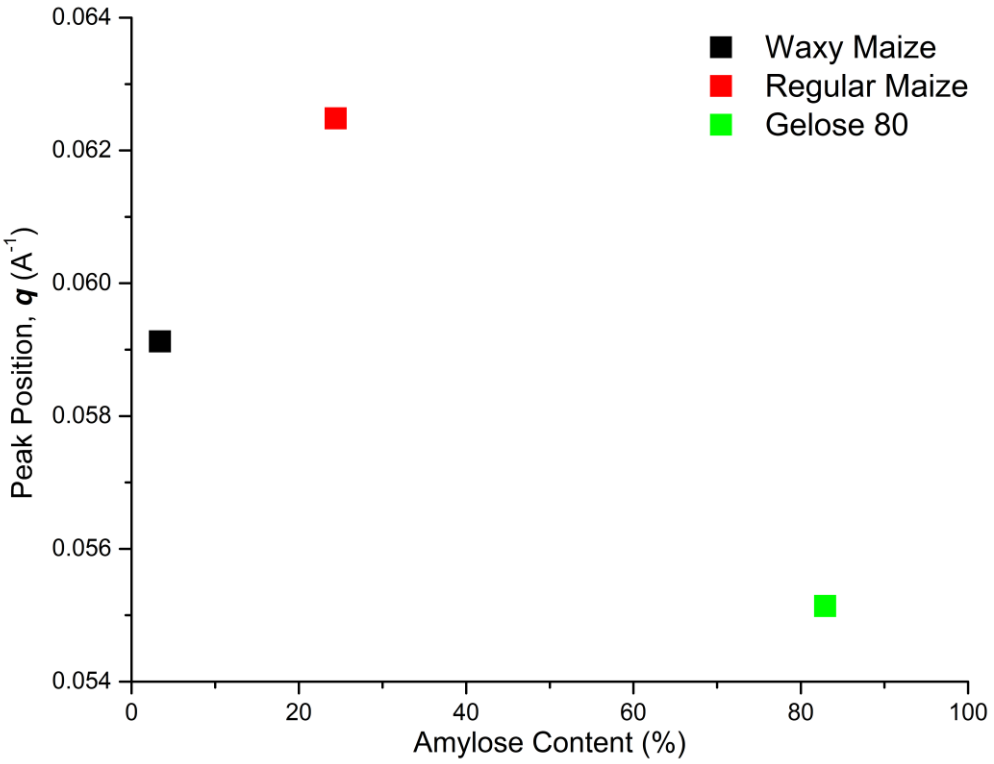

Figure 72 SAXS main peak position of maize starches plotted against amylose content. Error bars (1 standard deviation) fall inside the data point marker and cannot be seen.

Figure 73 shows the peak width of fitted curves against amylose content in maize starches. The peak width is related to the size of semi-crystalline lamellar structures. A clear trend was observed in the form of increasing peak width with increasing amylose content. This is logical if it is assumed that amylose content contributes primarily to the amorphous phase. The increased amorphous content would likely lead to an increase in the size of the amorphous lamellae within the semi-crystalline lamella. This trend was also clearly observed in the scattering patterns in Figure 72. Again, this information is valuable in investigating the impact of different factors on lamellar structure. Peak fitting yielded realistic peak width values with qualitative observations from scattering patterns.

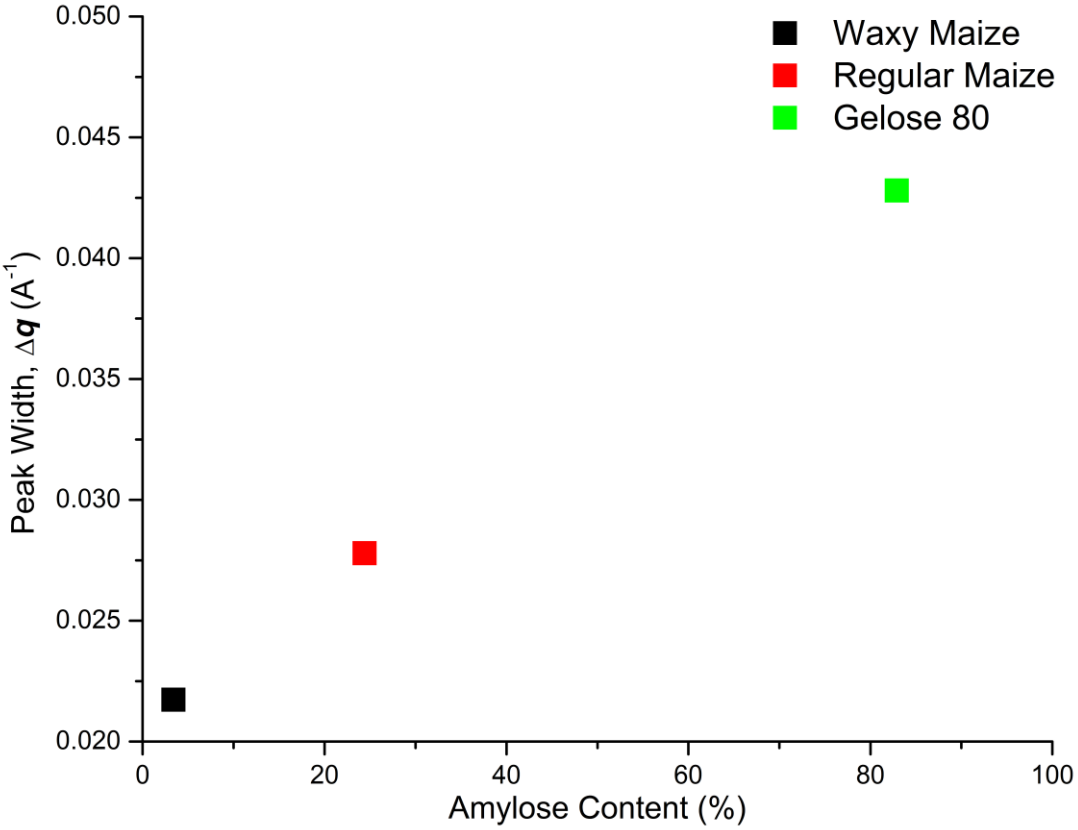

Figure 73 SAXS main peak width of maize starches plotted against amylose content. Error bars (1 standard deviation) fall inside the data point marker and cannot be seen.

SAXS experiments were also attempted on more complex samples. The investigation of semi-crystalline structure of starch in rice flours by SAXS is in Section 4.2. Similar to the results presented here, the peak parameters were determined by a peak fitting approach and used to understand how semi-crystalline features relate to other properties of these rice flours. The application of SAXS to breakfast cereals was also explored in this work, however was limited as a result of sample preparation. Hydration of breakfast cereals within the capillary used for SAXS experiment was extremely difficult, and the packing of externally hydrated samples was complicated due to the gelation of most samples. As a result of inconsistent packing, these samples were excluded from analysis.

3.3.3.4 Conclusions

SAXS is extremely valuable as a characterisation technique. Trends of peak parameters with varying starch properties such as amylose content had been reported previously [153]. The results presented show very similar trends to those seen in the literature [153], logical when

viewing amylose as a primarily amorphous contribution in starch samples. This view may be overly simplistic, and this trend may not occur in all samples; however, extensive knowledge may still be obtained from the scattering data. In fitting data, complications can arise in the case of peaks difficult to fit, or of peaks that vary from the original model. However, reasonably accurate determinations may still be made from such an approach and the modularity of this approach allows for enhancements to be made to improve fitting.

While general trends were observed here with amylose content, application to larger samples sets may yield additional trends such as groupings. Groupings can provide further information when related to other structural and processing factors, unlocking further possibilities in the characterisation and understanding of different processes on starch structure. In Chapter 4, the SAXS data of different rice samples grown at different temperatures is explored, potentially providing insight into the effects of these growing conditions on specific characteristics of different rice varieties.

3.4 Concluding remarks

In this chapter, levels 3 to 6 of starch structure were characterised (Figure 2). As a measure of crystallinity, the determination of *CI* values from peak height ratios in FTIR spectroscopy is not ideal. As a concept, using ATR-FTIR spectroscopy to characterise crystallinity was sound in the trade-off of accuracy with increased throughput. However, ATR-FTIR spectroscopy does not provide sufficient resolution of peaks to accurately determine the peak ratios. Transmission FTIR spectroscopy gave an improved resolution of the bands of interest, with cryogenic temperatures yielding slight resolution enhancements. *CI* values calculated in this setup yielded a correlation with measured crystallinity by XRD in both the *CI* ratios explored. However, the sample preparation time associated negates the short analysis time advantage of FTIR, especially in the case of cryogenic measurements. No substantial evidence was found to suggest that FSD enhances the determination of *CI* values relative to those taken from raw spectra. The use of FTIR spectroscopy in the determination of crystallinity is not a viable technique in the characterisation of starch structure; however, FTIR spectroscopy may find a use in quality control or high throughput applications where accuracy is not so important. Where accuracy is required such as for characterisation, techniques more

sensitive to crystalline structure should be employed such as XRD or solid state ^{13}C NMR spectroscopy.

In the determination of crystallinity, XRD is a powerful technique employed widely in the characterisation of crystalline structures. The determination of crystallinity in starch by XRD has been shown in the literature by many different methods. In the application of fitting methods, the algorithms and software employed play an important role in the entire fitting process. However, in most cases the difference between different software packages and fitting algorithms is negligible as most are based on very similar fitting methodologies. Further the influence of sample holder background is important, with interference occurring as a function of sample thickness, the degree of interference is variable and unknown. Sample holder background was significant relative to the sample diffraction in this case, therefore in the future a sufficiently thick sample should be employed to minimise the background diffraction effects. This would mean a sample amount of 1 g or greater, corresponding to a sample thickness of at least a few millimetres.

In assessing the lamellar structure of starch by SAXS, the peaks observed can be analysed by a variety of approaches. In this work scattering patterns were fitted to determine the peak parameters of the system. These peak parameters relate to real space structural features on the lamellar length scale and this allows for insight into the semi-crystalline structure of starch. In relating these peak parameters with amylose content, trends were observed that correlate well with the literature [153]. With the methods shown to be applicable to the starch standards here, it is expected that application to rice flours studied in this work is viable. The application of this technique to breakfast cereals was limited in this work as a result of non-satisfactory sample preparation and these samples were therefore excluded. In future investigations very interesting and novel observations may be made in the analysis of breakfast cereals by SAXS.

In this chapter, the characterisation of different levels of starch structure was explored by a variety of different techniques. Through the characterisation of the crystallinity and lamellar structure, a picture of the supramolecular conformations within starch granules is observed that is likely to be extremely relevant to digestibility profiles of starches. Both XRD and SAXS are powerful techniques in the analysis of these features; however, the application of FTIR spectroscopy lacks the selectivity to crystallinity required for accurate characterisation.

Chapter 4 Investigation of starch structure in rice and discussion on its role in digestibility

4.1 Relationship between starch structure and digestibility in rice

The digestibility of starchy grain based food products is influenced heavily by the morphology, molecular and supramolecular structure of starch [41, 184, 208-210]. These properties are in turn influenced significantly by a wide array of factors, including geographical and seasonal variations. Rice breeders aim to design rice varieties with desirable qualities for consumers, while maintaining consistency in the face of such environmental influences.

Amylose content is considered one of the most important properties of milled rice, a determinant in the end quality of a grain [211, 212]. Amylose content is linked to the digestibility of rice, with decreasing digestibility found in varieties with higher amylose content (Figure 74)[11, 208]. The variation seen in amylose content across rice varieties has been linked to genetic mutations within the *waxy* gene [213-216], and has been taken advantage of in the development of new products. However, while this may be used to develop rice products with tuneable amylose content, amylose content is also dependent on a number of other factors. Variations have been linked with environmental factors, especially temperature during seed development [211, 213-215], resulting in additional factors that must be taken into account in grain development.

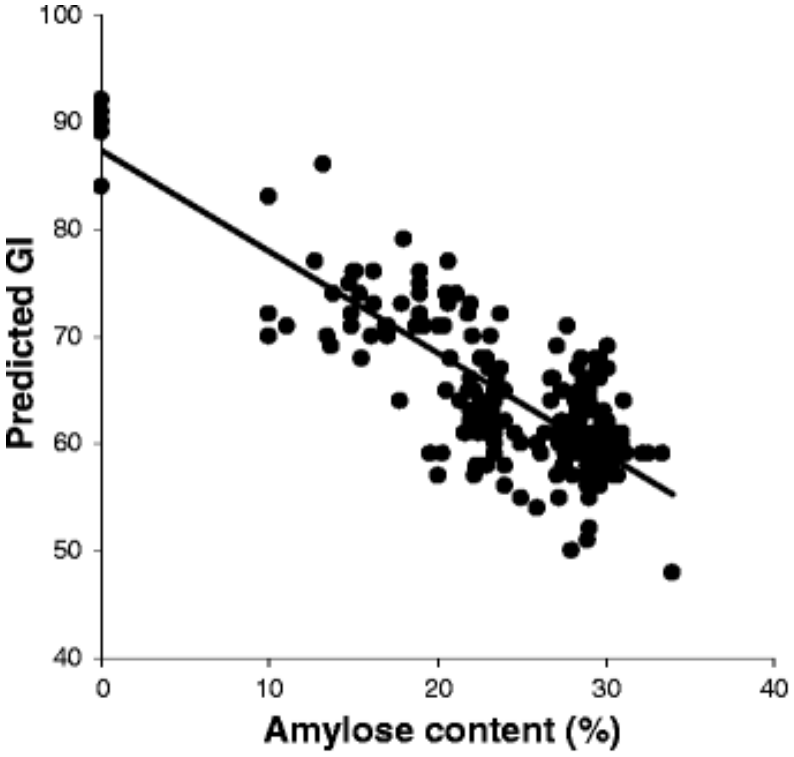

Figure 74 Correlation (R^2 = 0.73) between amylose content and predicted GI (in vitro) using 235 different samples. Taken from Fitzgerald et al.[11]. Article does not specify if amylose content is obtained on filtered samples.

Despite this, the relationship between amylose content, the expression of the *waxy* gene and the link between amylose and digestibility have enabled breeders to enhance the development cycle, providing a greater control over desired rice properties and traits.

In the development of rice varieties, breeding programs go through thousands of varieties. Knowledge of underlying processes and how environmental influences affect quality parameters is important in guiding this development cycle, producing high quality varieties in an economical and efficient way. In this, the role of starch structure is important. While environmental influences will affect structural properties, these structural properties directly influence the properties and traits associated with grain quality. In an effort to enhance the development cycle, tools need to be developed to further probe the structure of starch in rice and understand how it relates to rice properties. By characterising starch structure and correlating it with rice properties, new relationships may be discovered and employed in the development cycle, further optimising the processing involved in rice breeding. An especially important property of rice is its digestibility.

In the face of rising obesity rates and other diet related diseases, new products need to be developed to improve population health. The digestibility of foods is especially important

in this regard, with reduced digestibility and higher resistant starch or fibre content found to be beneficial to digestive health and weight management (Section 1.3.1). By characterising starch structure and relating it to the digestive profile, correlations may be found that can be employed in the development of future products. The high cost and time required for *in vivo* glycaemic index (GI) trials make them impractical as a determinant of digestibility in breeding programs, highlighting the potential impact of structural characterisation and measurement of biochemical properties as tools in rice breeding programs. Links between these properties and the digestibility are poorly understood; however, further characterisation promises to develop a deeper understanding of the underlying processes.

The information obtained by SAXS on the lamellar structure of rice samples is discussed here, relating it to their measured amylose content. Additionally, lamellar features will be related to the average degree of branching (*DB*) previously measured by ^{1}H NMR spectroscopy [217]. The determination of heterogeneity of branching by CE discussed in Chapter 2 will also be further discussed in its potential to predict digestibility.

4.2 Characterising starch structure in rice and investigating how it relates to digestibility

4.2.1 Comparing structural properties with literature GI values

In this work, rice flours of three difference varieties (*Doongara*, *I-Geo-Tze* and *Quest 19*), grown at higher or lower temperature, were characterised. Growing conditions influence rice grain properties and quality [213]. This is contrary to the desires of rice breeders, who in designing better products, also need a consistent product. This is especially important on the agricultural side, where different growing locations may be more ideal for agricultural activity, however, may not be ideal growing conditions for desired grain quality traits. This section explores the relationship of lamellar structure as investigated by SAXS of rice flours, with

factors such as growing temperature and properties such as amylose content and average degree of branching. An investigation into GI values is also concluded from database GI values on rice flours [218] investigated by Toutounji[217].

Toutounji [217] compiled the GI values of 38 rice varieties from the international GI database [218], and classified them according to their notation as either high or low amylose content. On average, rices with low amylose content (<24 %) had a higher GI value 72 ± 12 compared to those with a higher amylose content (>25 %) with a GI value of 51 ± 5. In exploring the impact of this on the samples analysed here, this suggests that *I-Geo-Tze* with the highest amylose content grown at high (28 %) and low (28 %) temperatures would have a lower GI than *Doongara* (26 % and 18 %) and *Quest 19* (20 % and 12 %). However, the correlation of amylose content with predicted GI is low (Figure 74, correlation coefficient 0.75). Therefore, it is likely that other structural factors, especially those related to the amylose content, will also play a role in the digestibility of rice grains.

4.2.2 How lamellar structure relates to amylose content

While amylose content appears to correlate with digestibility, the amylose content itself is likely not the only factor in this link. Varying amylose contents and spatial arrangements play a significant role in the supramolecular structure of starch, further influencing enzyme efficacy and access in digestion. Amylose in the supramolecular structure of starch contributes primarily to the amorphous phases of starch in both the bulk amorphous and semi-crystalline phases. However, amylose is also capable of forming ordered conformations that can influence digestion in the form of single helices. The branching seen in amylose may also influence semi-crystalline structures, thus influencing the access pathways during digestion.

The lamellar structure of the three rice varieties grown at different temperatures was investigated by SAXS using the methodology described in Section 3.3.3 with a single measurement made for each sample (Figures A14 to A16). From this scattering information, a comparison of lamellae features was made between the different rice varieties by their growing temperature and amylose content. Amylose content was determined using a modified

version of the colorimetric method (AACCI approved method 61-03.01[139, 212]) at DPI (Yanco, NSW, Australia).

In SAXS of starch, the peak intensity relates to the total sample fraction within the semi-crystalline arrangements and is closely linked to the crystallinity of a sample [153]. A trend of decreasing peak intensity with increasing amylose content was observed in both *Doongara* and *Quest 19* varieties (Figure 75). This is in agreement with the assumption that amylose contributes primarily to the amorphous phase of starch structure. In *I-Geo-Tze* all values of amylose content and peak intensity appeared consistent, indicating a degree of consistency in semi-crystalline structure with varying growing temperatures. This correlation of amylose content with peak intensity is consistent with what has been observed in plant starches [45, 153, 193, 205]. This is the first such observation in rice flours. This trend strongly indicates the contributions of amylose to amorphous phases. Extrapolating this information, the digestibility in relation to amylose content may be a result of its influence on amorphous structures, suggesting that a more amorphous structure may be more resistant to digestion.

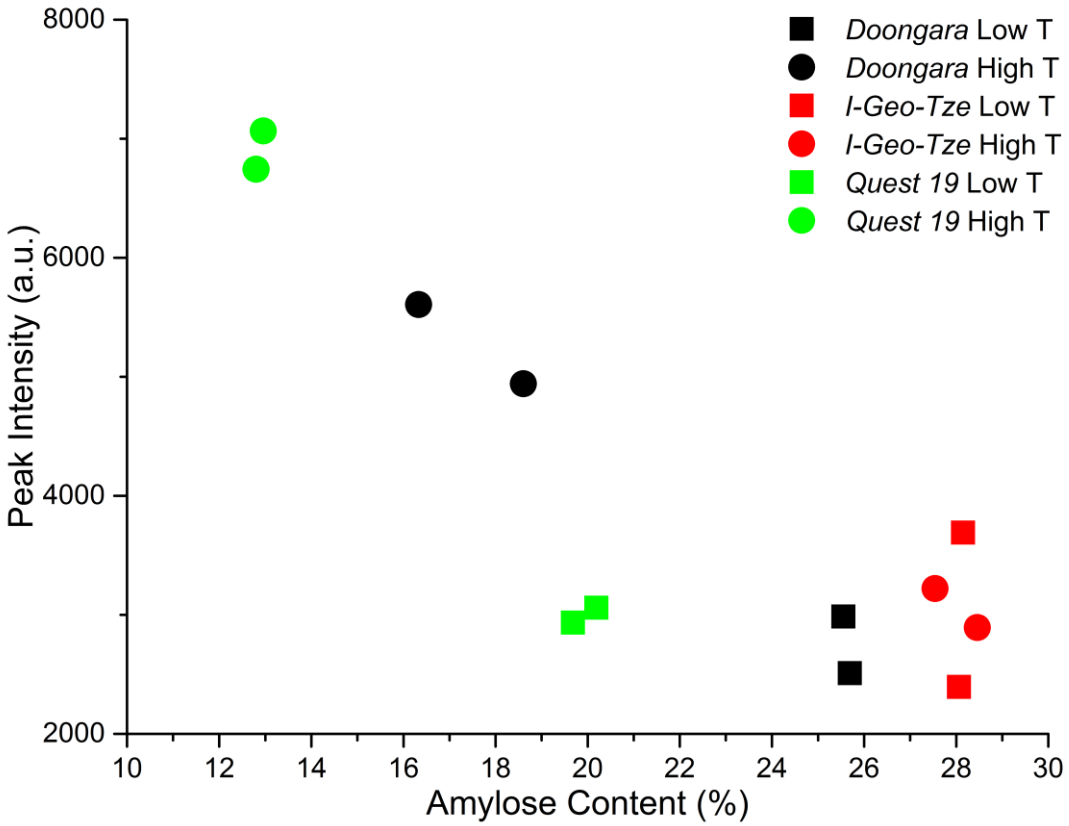

Figure 75 SAXS peak intensity plotted against amylose content of rice flours from rice grains grown at higher or lower temperature (*T*). Two replicates grown in different head houses are shown for each temperature. Error bars were calculated by fitting software as an estimated standard deviation of the fit coefficient. Error bars fall inside the data point marker and cannot be seen.

Investigating the peak width in SAXS of starch reveals information on the number of repeat amorphous plus crystalline lamellae in a semi-crystalline lamellar structure. In contrast to the overall contributions of semi-crystalline structure obtained from peak intensity, this metric reveals the size of the semi-crystalline lamellae. The peak width is dependent on the average total thickness of one crystalline and one amorphous lamella and the total number of crystalline and amorphous lamellae that make up the semi-crystalline lamellae. In Figure 76, a general trend of increasing peak width with increasing amylose content was observed; however, this was a weak association, and rather each variety exhibited different behaviours with changing amylose content and growing temperature. In *Doongara*, while amylose content varies between different temperatures, no change in the peak width was observed, indicating that while amylose content may change the number of repeat units or size of repeat units in the semi-crystalline lamellae, the overall size was not altered. However, in *Quest 19*, a clear change in the peak width was observed, with the scattering data yielding an increased peak width with increasing amylose content as a result of growing at low temperatures. This

suggests that in this variety, the increased growing temperature and subsequently reduced amylose content play a role in reducing the size of the semi crystalline lamellae. This may be linked to the repeat distance of the crystalline and amorphous lamellae, where changes in the amylose content could directly affect the amorphous contributions of the semi-crystalline lamellae. Investigating the effect of temperature and amylose content on peak width in *I-Geo-Tze* revealed no clear trends. Variation in peak width between samples was observed; however, a consistent relationship with temperature or amylose content was not observed and rather may arise from other factors such as natural heterogeneity.

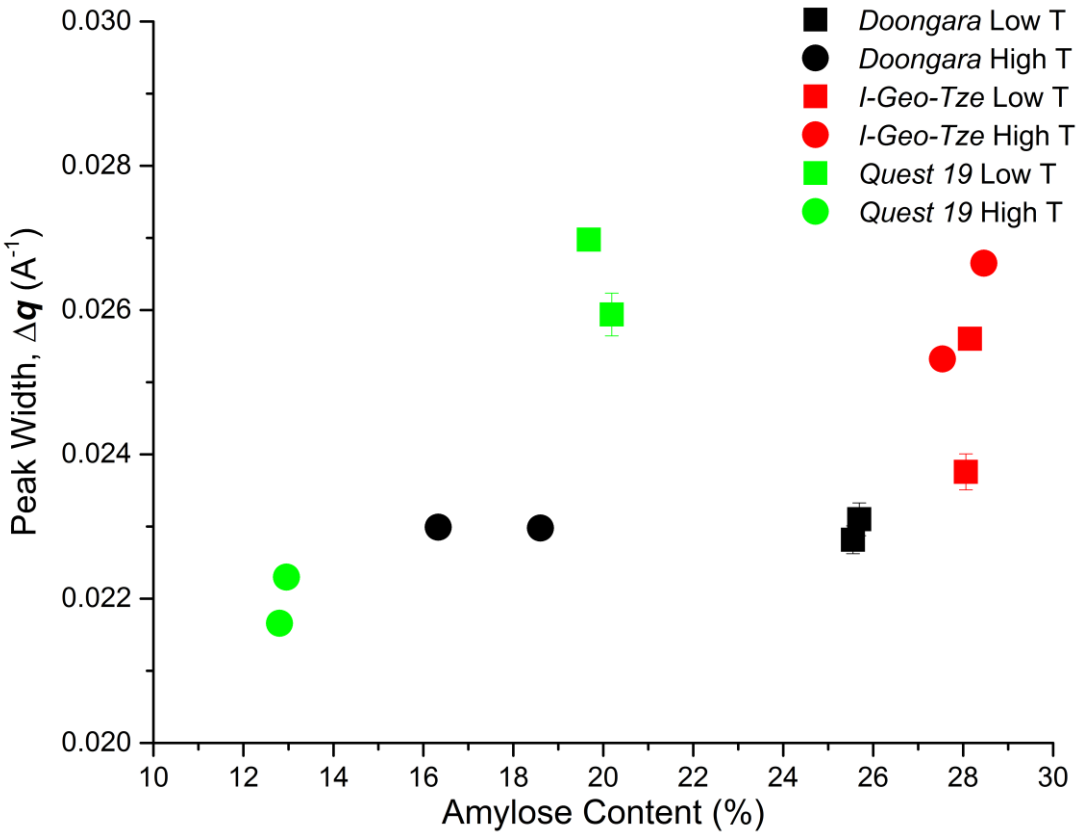

Figure 76 SAXS peak width plotted against amylose content of rice flours from rice grains grown at higher or lower temperature (*T*). Two replicates grown in different head houses are shown for each temperature. Error bars (1 standard deviation) of some points fall inside the data point marker and cannot be seen.

The semi-crystalline lamellar repeat distance represents the combined size of one crystalline plus one amorphous lamella within the semi-crystalline lamellae and can be investigated through the peak position in SAXS. The reciprocal relationship of peak position with the repetition length means that shifts to higher $\boldsymbol{q}$ values correlate to shorter distances between two consecutive crystalline regions, likely to play a significant role in the digestibility

through a seemingly more ordered semi-crystalline lamellar structure. The peak position of rice flours was investigated in their relationship with amylose content and temperature. While investigating the individual varieties revealed some trends, an overall trend was not observed (Figure 77).

In the *Quest 19* variety, a shift in the peak position to lower $\boldsymbol{q}$ values was observed with decreasing amylose content as a result of growing at higher temperatures. This shift suggests an increase in the repetition length, despite the decrease in amylose content which would be expected to result in a decrease in size of the amorphous component. Therefore, it is posited that the increased repetition length is related to other effects of growing temperature on the size of the crystalline lamellae. The role of decreasing amylose content is not clearly understood. It is hypothesised that the decreasing amylose content leads to a decrease in the total amount of the amorphous component. This is supported by the apparent increase in semi-crystalline structure seen in Figure 75 with the increase in repeat distance justified by a non-changing amorphous lamella, and increasing crystalline lamella size. Alternatively, the reduced amylose content could have resulted in a decrease in the size of amorphous lamella, in which case the apparent increase in lamellar repeat distance would then suggest a significant increase in the size of the crystalline lamella. Therefore, it was determined that a physical increase in the size of the crystalline lamellae was most probable. This would contribute to a more ordered structure, possibly influencing the digestive characteristics. This same trend was not observed in the *Doongara* variety, for which low temperature samples yielded consistent peak positions, while high temperature samples gave inconsistent results, suggesting two different effects on the repeat distance. In exploring these values, further repeats of SAXS measurements with repeat sample preparation would be required to determine if any statistically significant trend can be observed between the size of repeat units with amylose content or growing temperature for this variety. In investigating the shift in peak position in *I-Geo-Tze*, any effects of amylose content are unlikely due to the consistency of amylose content between the samples. However, a change in peak position was still observed, and did not appear to be related to growing temperature. Therefore, if these variations are statistically significant, other factors are likely at play and further work may be beneficial in identifying the other factors that influence structure and digestibility.

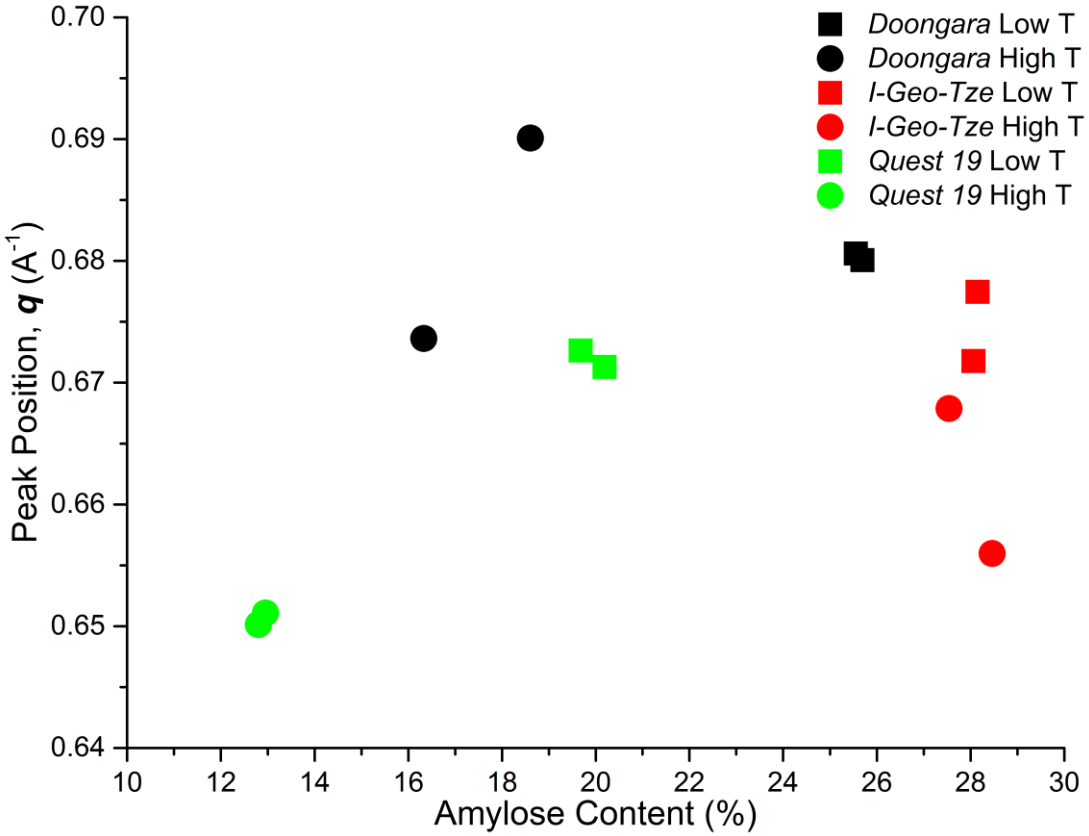

Figure 77 SAXS peak position plotted against amylose content of rice flours from rice grains grown at higher or lower temperature (*T*). Two replicates grown in different head houses are shown for each temperature. Error bars (1 standard deviation) fall inside the data point marker and cannot be seen.

In investigating the relationship of the lamellar structure with the amylose content, observations may be made on its influence on the semi-crystalline structure by investigating the parameters of the SAXS peak parameters. In these rice samples, peak intensity decreases with increasing amylose content, and is likely a result of increased amorphous phase contributions due to the increase amylose within the system. This effect is consistent with that found in plant starches [153] but is the first time it has been found in rice flours. In investigating peak width, any trends between amylose content and the size of semi-crystalline lamellae was dependant on the variety and so likely arises from factors other than amylose content. Growing temperature also did not directly influence the size of the semi-crystalline lamellae, instead playing a role mainly through its influence on amylose content. Further to this, no specific trends were observed in peak position shifts, related to the thickness of a repeat unit, outside of an apparent increase in thickness with increased amylose content in the *Quest 19* variety. In relating peak parameters to amylose content and growing temperature, trends were observed that correlate well with the knowledge of the general role of amylose in supramolecular

structure. However, variations in these trends were also observed between rice varieties, indicating that factors other than amylose content and temperature also play a role. Thus further investigation of other properties is essential in understanding what factors influence semi-crystalline structure, and how these changes translate into digestibility.

Before confidently assigning these trends, further work is also required in investigating the repeatability of these measurements. Due to the highly heterogeneous nature of natural samples, properties can vary significantly within a sample. Therefore, to confirm any relationships, repeat SAXS measurements with repeat sample preparation must be made, especially when taking into consideration the similarity of values obtained here for peak width and peak position.

4.2.3 How the lamellar structure relates to the average degree of branching

The average degree of branching *(DB)* of starch in rice was measured by ^{1}H NMR spectroscopy as another characterisation approach to understanding the influence of growing conditions on starch structure is rice, and how it can influence starch structure. This work was done by Toutounji[217] on the same rice samples investigated in this work.

A general trend was observed where 2 out of the 3 rice varieties grown at higher temperatures showed a reduced amylose content and increased *DB* compared to those grown at lower temperature (Figure 78). However, as in Section 4.2.2, *I-Geo-Tze* maintains a consistent structure with growing temperature and amylose content, showing no significant variation in *DB* measurements. The relationship of amylose content with growing temperature has been demonstrated previously [213-215]; however, the relationship of *DB* with amylose content was a new observation by Toutounji[217].

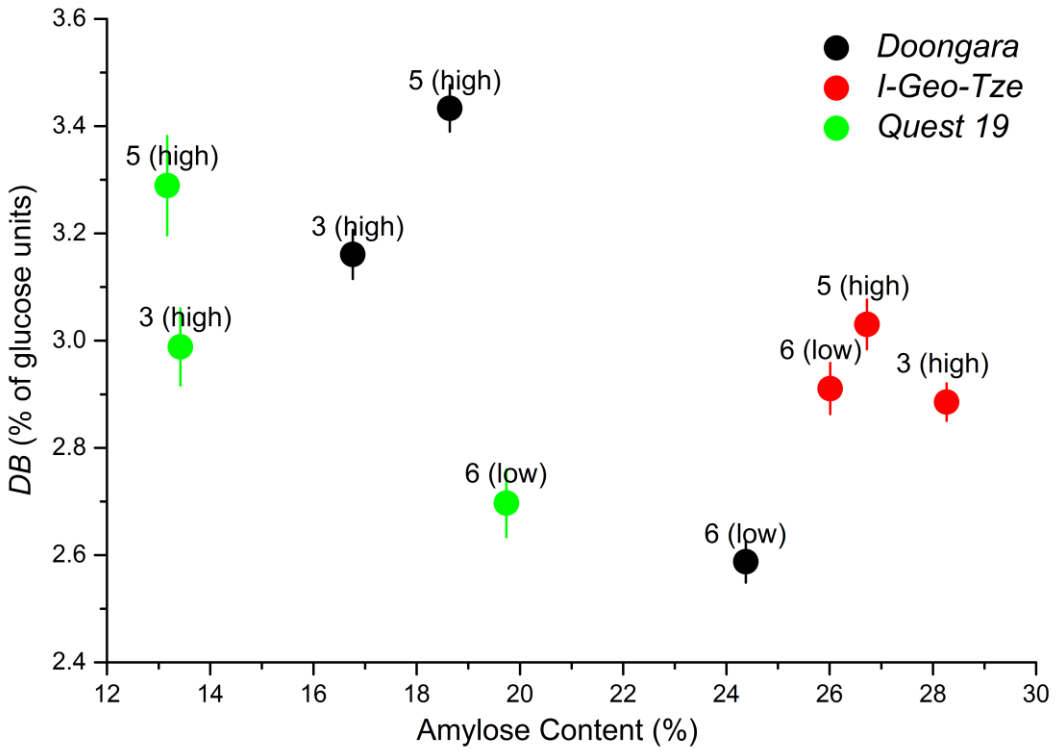

Figure 78 *DB* plotted against amylose content of rice flour samples grown at higher or lower temperature, adaptation from Toutounji[217]. Two replicates grown in different head houses are shown for each temperature (second low T not shown). Error bars are calculated as the standard deviation of three repeat experiments and preparations.

These observations of increased *DB* with decreasing amylose content likely arise from the difference in branching between amylose and amylopectin within starch. With a reduced contribution of less branched amylose with respect to highly branched amylopectin, the average degree of branching within the sample intuitively increases. In investigating the relative *DB* between varieties, the difference between higher and lower temperature in two varieties was significant. The results revealed that a higher amylose content is linked to a lower average *DB*, in agreement with the low branching nature of amylose. However, in the case of *I-Geo-Tze*, where amylose content was highest, the *DB* in all measurements was higher than the low temperature *DB* measurements in *Doongara* and *Quest 19*. This result indicated a greater amount of branching in either amylose or amylopectin, thus contributing to a greater average degree of branching.

In comparing the *DB* with the lamellar structure of these rice varieties, insights into the influence of branching in the semi-crystalline structure of starch can be gained. Peak intensity correlated with *DB*, indicating a decreasing amount of semi-crystalline structure with decreasing *DB* (Figure 81). This likely arises from the involvement of amylose in the

amorphous phase, and suggested that in these samples amylose was contributing more to the bulk amorphous phase rather than the amorphous component of the semi-crystalline structure. However, this trend was observed only for *Doongara* and *Quest 19* varieties. *I-Geo-Tze* showed minimal variation in both peak intensity and *DB*, supporting the relationships of *DB* and amylose content with total semi-crystalline structure.

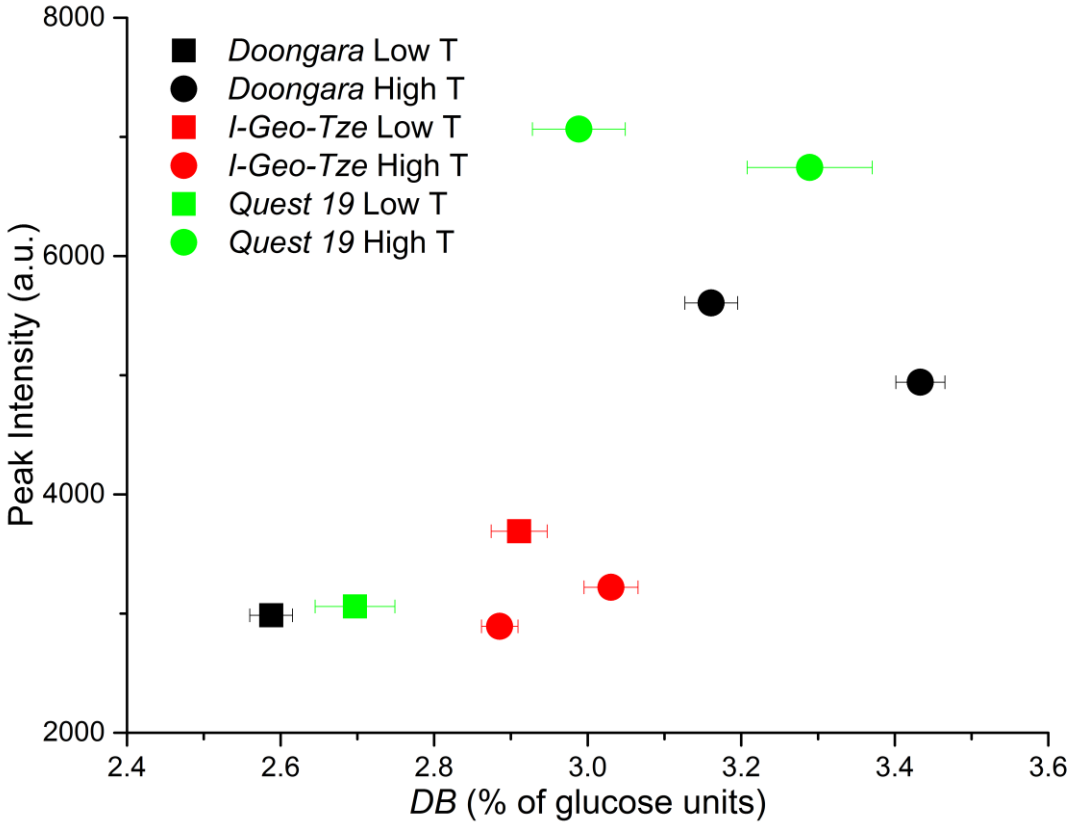

Figure 79 SAXS peak intensity plotted against *DB* (values adapted from Toutounji [217]) of rice flour samples grown at higher or lower temperature (*T*),. Two replicates grown in different head houses are shown for each temperature (second low T not shown). Error bars for *DB* are calculated as the standard deviation of three repeat experiments and preparations. Error bars for peak intensity were calculated by fitting software as an estimated standard deviation of the fit coefficient. This error bar falls inside the data point marker and cannot be seen.

Peak width did not appear to show any specific correlation with *DB* (Figure 82); however when explored in relation to peak intensity (Figure 81) some observations may be made about the individual samples. In *Doongara*, with increasing *DB* the peak width did not change. This confirms what was observed for *Doongara* in Figure 81, indicating that the decreasing relative amount of semi-crystalline structure arises from an increase in the amount of background amorphous phase as a result of the increasing content of the lesser branched amylose. For *Quest 19* the peak width increased with decreasing *DB*, indicating that lesser branched components are increasing the size of the semi-crystalline lamellae. In relating this to amylose

content, this suggests that the increasein this lesser branched component is contributing primarily to the amorphous component of the semi-crystalline lamellae. This is in stark contrast to what was seen for *Doongara*. The peak width of *I-Geo-Tze* did not vary significantly, consistent with the minimal variation seen in *DB,* indicating an inherent consistency in this product in terms of starch structure and how it is affected by growing temperature.

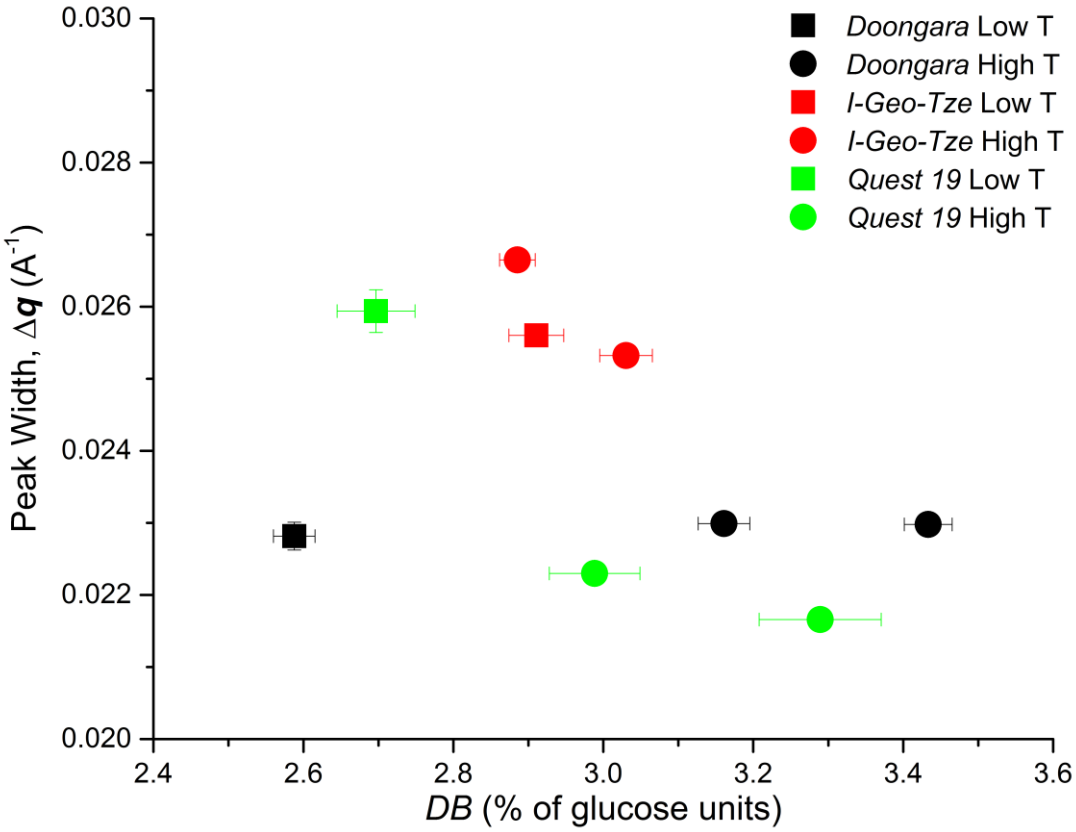

Figure 80 SAXS peak width plotted against *DB* (values adapted from Toutounji[217]) of rice flour samples grown at higher or lower temperature (*T*). Two replicates grown in different head houses are shown for each temperature (second low T not shown). Error bars for *DB* are calculated as the standard deviation of three repeat experiments and preparations. Error bars for peak intensity were calculated by fitting software as an estimated standard deviation of the fit coefficient. This error bar falls inside the data point marker and cannot be seen.

Peak position did not have any significant overall correlation with *DB* (Figure 83); however some observations may be made from observations obtained from the other peak parameters (Figure 82 and Figure 81). For *Doongara*, the lack of variation in peak position suggests that the size of one repeat unit is unchanged with the changing *DB*. This supports the previous information in Figure 81 and Figure 82 for *Doongara*, indicating that the decrease in *DB* and related increase in amylose content are creating a greater amount of bulk amorphous phase rather than affecting the amorphous component of the semi-crystalline lamellae. For *Quest 19*, the peak position increased with decreased *DB*, indicating a decreasing size of the

crystalline plus amorphous repeat unit with decreasing *DB*. This may correlate with the changing proportions of amylose and amylopectin within the sample, as when amylose content increase, then the amylopectin content decreases. Such a case may then favour a greater amount of amorphous phase. Investigations into the relation of the *DB* to the peak intensity (Figure 81) and peak width (Figure 82) suggest that with decreasing *DB*, and intuitively increasing amylose content, the amount of semi-crystalline structure decreases. The size of the semi-crystalline lamellae also increased with decreasing *DB*. . Figure 83 then reveals that while the semi-crystalline lamellae size is increasing with decreasing *DB*, the repeat distance is decreasing (increasing peak width). This indicates that the change in size of the semi-crystalline lamellae is not a result of increased amorphous contributions, but likely an increase in the number of alternating repeat units. For *I-Geo-Tze* an apparent variation in peak position with growing temperature was observed, but not with *DB*. In other cases the results from *I-Geo-Tze* produced highly consistent values (Section 4.2). Therefore, it is expected that this variation likely results from another factor that is not currently known; however, this result may be statistically insignificant and experimental repeats are required.

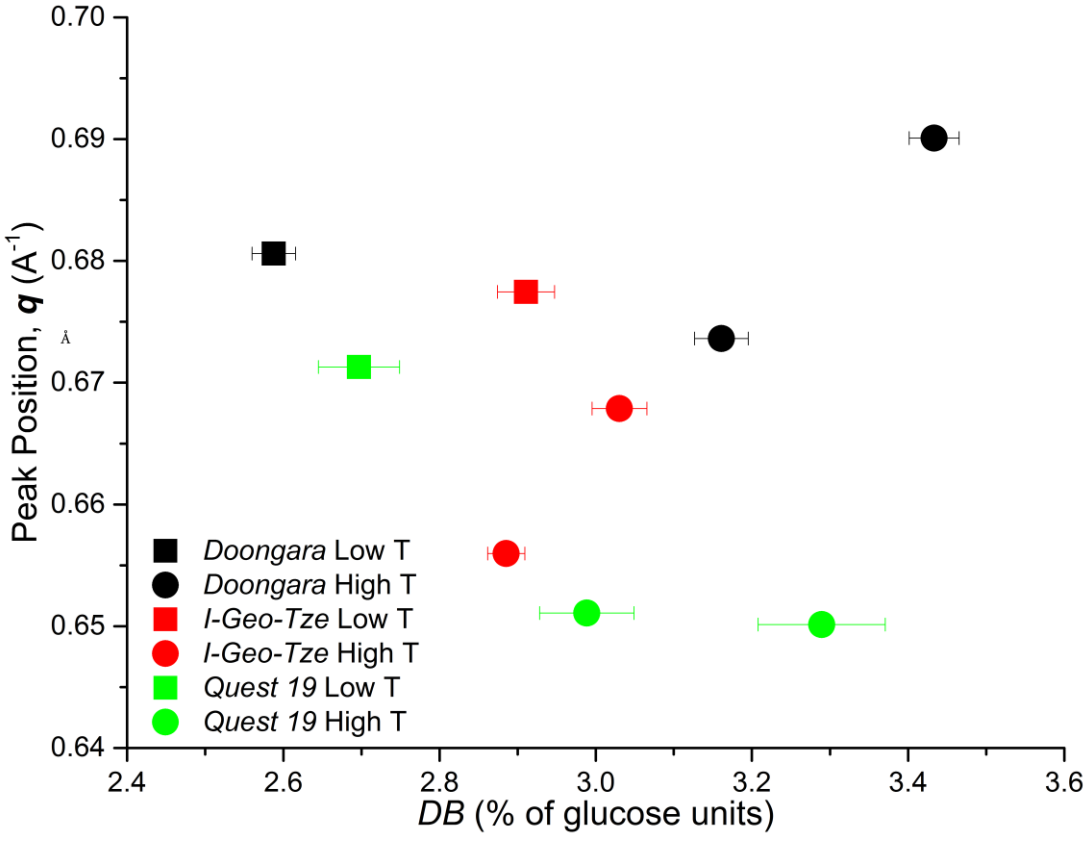

Figure 81 SAXS peak position plotted against *DB* (values adapted from Toutounji [217]) of rice flour samples grown at higher or lower temperature (*T*). Two replicates grown in different head houses are shown for each temperature (second low T not

shown). Error bars for *DB* are calculated as the standard deviation of three repeat experiments and preparations. Error bars for peak intensity were calculated by fitting software as an estimated standard deviation of the fit coefficient. This error bar falls inside the data point marker and cannot be seen.

In conclusion, a relationship between the average degree of branching and semi-crystalline structure is observed in relation to amylose content. This observation confirms the knowledge of the contribution of amylose to amorphous phases, and its lower branching than seen in amylopectin. However, while the amylose content has been linked with decreased digestibility, long chains of amylopectin have also been attributed to increased resistance to enzyme digestion [208, 219] indicating the potential importance of investigating branching in the digestibility of starch samples. As was discussed in the Section 4.2.2, a determination of error in these measurements is necessary to confirm or unveil any trends. Further work is therefore required to investigate links between the *DB* and the different levels of lamellar structure. In uncovering such a relationship between the *DB* and the semi-crystalline lamellar structure, this information could be used in determining impact of these features on digestibility, providing a potential screening method in early generations of breeding programs towards creating healthier products.

4.2.4 The heterogeneity of branching and its impact on digestibility

In the Section 4.2.3, the average degree of branching was discussed in relation to the growing conditions of rice samples and their lamellar structure. However, while information may be gained on branching within the sample, this measurement is only an average and is inclusive of both amylose and amylopectin components. This convolutes the contributions of the two components to this value and further characterisation is required to obtain a deeper understanding of what this values means in terms of the starch structure and its properties

In Chapter 2 the determination of heterogeneity of branching in starch standards was explored. The dispersity was calculated for the whole sample allowing for an overview of the overall heterogeneity of branching structures. This is similar to the nature of *DB* measurements which does not differentiate the contributions from amylose and amylopectin; however, *DB* does not assess heterogeneity, instead yielding only an average. Heterogeneity of branching provides another angle with which to view the branching in starch and promises to be a

valuable parameter in the determination of digestibility. Assessing the heterogeneity of branching will also complement the determination of *DB*. By determining the heterogeneity of branching, what changes in *DB* relate to in terms of amylose and amylopectin may be determined, allowing to discriminate the primary factor affecting the *DB*. Such an example could determine whether an increase in *DB* is linked to increasing branching in amylose or in amylopectin.

The branching in amylose and amylopectin and its effect on the semi-crystalline structure of starch is likely to be a major factor in both digestibility and other quality parameters of rice. For example, by understanding and determining the heterogeneity of branching in starch, the correlation of amylose content with GI may be better understood. The ability to differentiate different types of amylose and amylopectin will be a powerful tool, allowing for an understanding of the effect of different types of branching structures on digestibility. However, obtaining this information requires further development in the complete separation of amylose and amylopectin to obtain accurate information on their individual branching dispersity. Taking into account both amylose content and the heterogeneity of branching will allow for another avenue with which to predict digestibility, and is likely to provide a more accurate prediction than the amylose content alone. In relating this work to that in Figure 76, it is expected that the determination of amylose content from $W(\mu)$ by capillary electrophoresis will yield a more precise amylose content than traditional UV-Vis absorption methods, as well as a more accurate determination as a result of the separation of the amylopectin from amylose. Reproducing Figure 76 using this determination of amylose content is expected to yield an improved correlation with digestibility. The heterogeneity of branching may also be taken into account to further improve the correlation. By taking into account the heterogeneity of branching in amylose and the bias towards higher or lower branching the determined amylose content can be adjusted to remove bias in how different branching structures influence digestibility. For example, the amylose content from $W(\mu)$ may be adjusted by dividing or multiplying by the μ_w or μ_m to account for the different types of amyloses. Such an approach would be an extremely valuable approach in predicting the digestibility of starchy foods.

Chapter 5 Conclusions and Future Research

5.1 Predicting the digestibility of starch through structural characterisation

The aim of this work was to develop methods that allow the characterisation of starch structure in rice and breakfast cereals, and to determine the relationship of these features to digestive properties. The molecular characterisation of starch was achieved by capillary electrophoresis in the critical conditions (CE-CC). CE-CC allowed for the investigation of the heterogeneity of branching structures within starch, as well as the reliable quantification of amylose content. Supramolecular characterisation was achieved by spectroscopic techniques investigating long and short range crystallinity within the semi-crystalline starch by X-ray diffraction (XRD) and Fourier transform infrared (FTIR) spectroscopy, respectively. The supramolecular structure was also further probed in a preliminary study by small angle X-ray scattering (SAXS), investigating the repeating semi-crystalline structure of starch within the granule. The characterisation techniques employed and the level of structure they were used to investigate is illustrated in Figure 82.

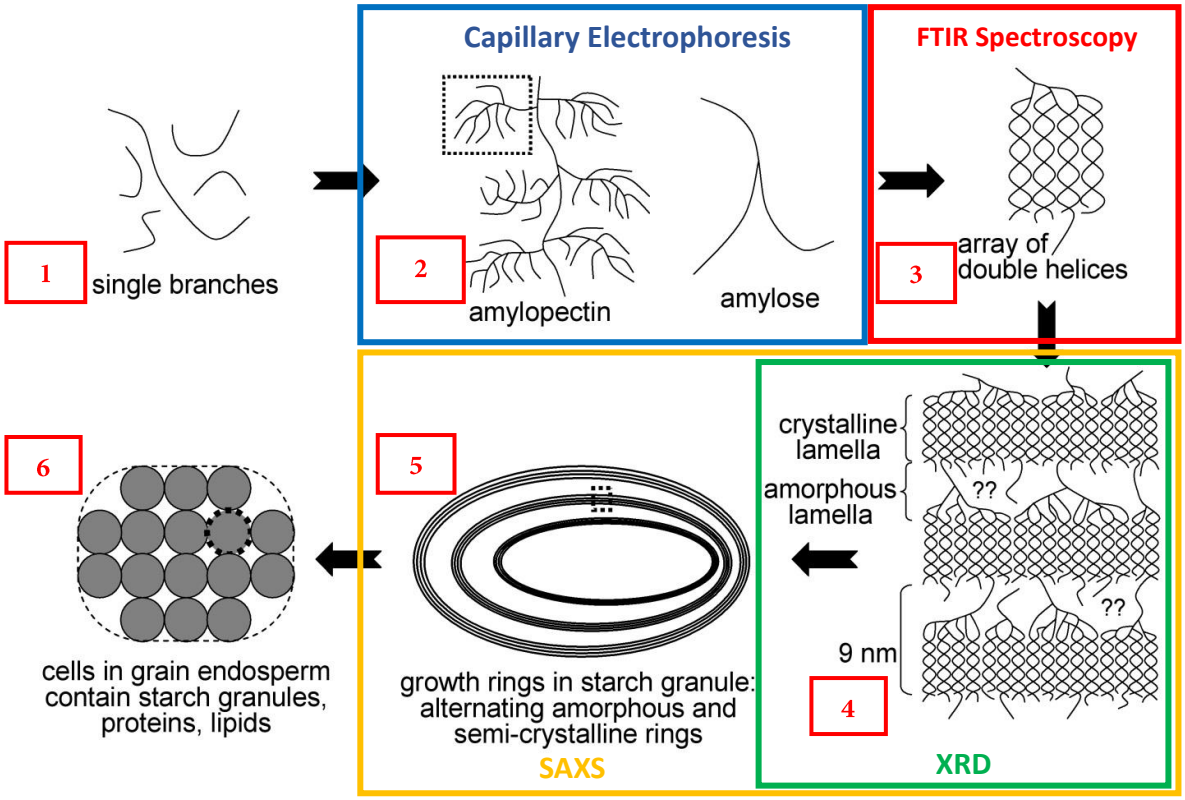

Figure 82 The six structural levels (numbered) of starch shown with the techniques used to characterise these levels (adapted from Gaborieau and Castignolles [42])

5.1.1 CE-CC for the molecular characterisation of starch

5.1.1.1 Conclusions

Amylose and amylopectin are traditionally measured by colorimetric and spectrophotometric approaches in solutions containing both. This introduces interference and inaccuracy as a result of overlapping absorbance bands. Separation overcomes these limitations and allows a more accurate quantification and characterisation of these components.

In Chapter 2, capillary electrophoresis (CE) was employed for the separation of amylose and amylopectin as a means to quantify and characterise these components within starch samples [105]. The dissolution of starch in the work of Herrero-Martinez et al.[105] employed non ideal conditions, and so optimal dissolution conditions of Schmitz et al.[108] were also investigated and the effect of improved dissolution on separation and characterisation

explored. Three parameters were investigated: sample concentration, dissolution solvent and temperature. The high sample concentrations employed in the work of Herrero-Martinez et al.[105] was a major factor in the aggregation observed. By reducing the concentration, a reduction in signs of aggregation was observed, an essential hurdle to overcome for accurate analysis. The effects of the apparent improved dissolution conditions were also observed, with the use of anhydrous DMSO containing LiBr and high temperatures found to increase the amount of amylose being detected. High storage temperatures also improved the repeatability of the separation, likely a result of the greater extent of starch dissolution. Filtration is commonly employed in chromatography out of necessity, protecting sensitive equipment from large particulates; however, this is not necessary in CE. Filtration of starch samples is detrimental to analysis, resulting in a partial to complete loss of both amylose and amylopectin from the suspension.

The separation of amylose and amylopectin by CE-CC occurs as a result of factors other than molar mass. Due to the simple composition of starch, a homopolymer of glucose, it is posited that the main separation factor in starch is its branching structures, indicated by the observed separation of amylose from amylopectin. This separation also allows insight into the heterogeneity of branching of the individual components. The development of a new methodology by Thevarajah et al. [112] allowed for investigations into the heterogeneity of these separation factors through the determination of dispersity of electrophoretic mobility distributions. Calculated dispersity values were significantly higher than those reported for other application of this method investigating branching heterogeneity of polymers [112], emphasising the large degree of heterogeneity within starch. However, limitations in the determination of branching heterogeneity arise in both the separation and the definition of amylose and amylopectin themselves. Incomplete separation of amylose from amylopectin meant that an accurate determination of branching heterogeneity in each component individually was not possible, a possible indication of a lack of clear distinction between the two structures. Therefore, in this work, dispersity values were calculated on the whole sample (from the combination of both amylose and amylopectin peaks).

In summary, the separation of amylose and amylopectin by iodine binding in CE is a powerful tool in the analysis of amylose and amylopectin in starch samples. By obtaining a complete dissolution, the amylose content can be more accurately quantified. Due to

separation occurring in the critical conditions, further characterisation can be done by analysis of distributions of μs yielded by separation. The application of the dispersity methodology to such distributions allows for insight into the heterogeneity of branching within starch samples. Heterogeneity of branching is expected to play a significant role in properties of starch such as a digestibility. Thus, this method would be an invaluable tool in any such study.

5.1.1.2 Future Research

Future work will involve improving the selectivity of the CE method, through means such as increasing the capillary length while maintaining the strength of the electric field. This will provide further insight into the separation, indicating whether amylose and amylopectin are two truly different components, or if a continuum of branching structures exists. In the event of a complete separation, the accurate quantification of these components through development of a calibration curve can be achieved, along with determination of individual dispersity values for both amylose and amylopectin. The characterisation of branching structures and amylose content in rice flours will also be explored. This will likely require adjustment of the CE method as the dissolution of the starch in rice flour is likely to be more challenging than that of pure starch. In exploring the difficulties of dissolution in more complex samples, alternative solvents may also be employed. Ionic liquids are highly polar compounds and have shown great promise in the dissolution of polysaccharides, and are already widely used in the dissolution of celluloses [220].;However, the use of some ionic liquids at high dissolution temperatures may result in starch degradation [220] and would require appropriate hardware to main these dissolution temperatures for CE experiments. While ionic liquids that are viable at room temperature do exist, there is a lack of property data available, and they are not always shown to be stable [221].

An alternative technique in the separation of amylose from amylopectin is asymmetric flow field-flow fractionation (AsFlFFF), shown to have great potential in the characterisation of starch [222, 223]. AsFlFFF is attractive as a starch characterisation technique due to its large size range (2 to >800 nm), low shear forces and the fact that filtering is often not required [222]. By employing AsFlFFF with multi angle light scattering (MALS) and refractive index (RI) detectors the molar mass and root-mean-square radius can be measured directly [223]. The

determination of weight-average molar mass and molar mass distributions may also become possible. Both CE and AsFlFFF have the potential to yield different types of sample information, and thus could serve as complementary techniques in obtaining a complete characterisation of amylose and amylopectin in starch. This has potential to improve research areas such as rice breeding and food development where amylose content forms an important metrics in quality and properties. In current correlations of GI with amylose content, outliers in the data are poorly understood and result in poor correlation coefficients. By characterising the branching structure of amylose, a better correlation of amylose content with GI than is shown in Figure 76 may be made. By accounting for the bias of amylose in a sample towards higher or lower branching, amylose content may be adjusted to serve as a better predictor for digestibility. Further characterisation of starch structure promising to help in better understanding what else may influence quality and properties.

5.1.2 Approaches to characterising the supramolecular structure in starch

5.1.2.1 Conclusions

To characterise the supramolecular structure of starch, a number of approaches were explored in assessing semi-crystalline structural features. The crystallinity of starch is an important factor in many of the desired properties of starch products such as in food products where it can influence digestibility through the formation of enzyme resistant structures. FTIR spectroscopy was investigated as a fast and simple approach to characterising crystallinity in starch samples.. This approach, based on observations of vibrational bands, is not a direct investigation of crystallinity. As such the relationship of these measurements to real world structural order is unclear. The peaks of interest related to crystalline and amorphous phases were poorly resolved. Therefore avenues were explored to improve resolution.

Attenuated total reflection FTIR (ATR-FTIR) measurements had poor resolution of the peaks of interest with significant overlap of peaks. Transmission FTIR measurements yielded an improved resolution of the peaks of interest, though poor resolution of peaks was still apparent. The use of cryogenic temperatures in transmission FTIR measurements improved

the resolution further; however, these improvements were not significant. The use of cryogenic temperatures also negatively impacted the greatest asset of infrared analysis in this application: the fast and simple nature of measurements. Bandwidth reduction by Fourier self-deconvolution (FSD) of spectra was also explored, slightly improving the resolution of the peaks of interest.

Crystalline index values were calculated as the ratio of infrared peak heights of a crystalline and an amorphous peak and compared with previously determined crystallinity by X-ray diffraction [113].A monotonic relationship of *CI* with measured crystallinity was found indicating a dependency of these ratios on crystalline structure. However, this relationship was weak and highly variable, depending on the peak ratio used and spectral enhancement by FSD. While the use of infrared analysis has some sensitivity to crystalline structure, in the fine characterisation of starch structure this is not a viable approach. However, this approach may find some use in areas where a quick measurement and general estimate of crystallinity is required. Techniques such as X-ray diffraction and solid state ^{13}C NMR spectroscopy would be more suitable where accurate characterisation is required.

X-ray diffraction is viable in probing the crystalline structure of semi-crystalline materials. The amorphous phases in these systems contribute to band broadening and a lower overall signal-to-noise, complicating analysis and requiring the development of models to interpret data. In the determination of crystallinity within the semi-crystalline structure of starch peak fitting approaches allow for more accurate characterisation than traditional two phase approaches by accounting for irregular crystal structures. As a result, peak fitting approaches have become more common place. Most software based peak fitting is based on the same algorithms; however, operator influence can still bias results leading to inaccurate analysis in some cases. The influence of different software packages was explored. Software had a minimal effect on the determination of both A- and B-type crystallinity both with and without a sample holder background subtraction, except in the case of high amylose samples. This is hypothesised to arise from the nature of the sample, which is highly amorphous, impacting on the quality of fitted peaks.. It was also hypothesised that the type of polymorph may impact on fitting, however no significant evidence was found to support this. Calculated crystallinity values aligned well with previously published results [113], except in the case of the high amylose sample, reporting a higher crystallinity. This may be a result of sample changes

with storage such as retrogradation, or may also arise from flaws in the experimental procedure.

In the determination of V-type crystallinity by XRD, both software and background subtraction were found to influence V-type crystallinity values. The Igor Pro software package yielded more realistic crystallinity values when compared to previously determined crystallinity values. Igor Pro software was also more consistent both with and without background subtraction than the TOPAS software.

Therefore, it was determined that in some case software has the potential to influence results and must therefore be explored with respect to other approaches to confirm the model and obtain realistic values. However, while differences between software packages were explored here, there are also other factors that play a role. Determined crystallinity values that varied from those previously determined suggests an issue of reproducibility, despite the tendency of such approaches to produce highly repeatable values. Thus experimental procedure and sample changes are likely the major factors biasing results. Diffraction experiments in this work were performed on a thin sample layer. In XRD, an infinitely thick sample is ideal to minimise background interaction and so this may have played a role in the results here. About 1 g of sample is expected to be sufficient, provided sample thickness is at least a few millimetres, to minimise background interference. Additionally, sample changes such as retrogradation are likely to influence the crystallinity values and this cannot be ruled out.

Therefore, it was determined that in the characterisation of crystallinity and crystalline polymorphs, peak fitting approaches by XRD yield a relatively quick and highly repeatable analysis. While XRD lacks sensitivity to imperfect crystalline domains, a good view of crystalline structure can be obtained by this approach, providing valuable information with which to understand and relate to other structural characteristics.

SAXS yields insight into the semi-crystalline lamellar structure of starch and its features. The method was confirmed on starch standards, observing similar correlation of altered semi-crystalline lamellar features with changing amylose content as reported in the literature [153].

The SAXS methodology was then applied to rice flours provided by the NSW Department of Primary Industries, representing a selection of rice varieties grown at different temperatures and known to differ significantly in their physicochemical properties. Increasing

growing temperature has been shown to decrease amylose content of rice grains [213, 224], and this has also been observed in the samples studied. Similar to the analysis of starches, the analysis of rice flours revealed a correlation of lamellar structure with amylose content. With increasing amylose content, a decrease in the total semi-crystalline structure was observed, suggesting a significant contribution of amylose to amorphous phases. In exploring the relationship of amylose content with other lamellar features, no clear trends were observed outside of varietal correlations.

The average degree of branching has been shown to vary with amylose content, reflecting the changing ratio of slightly branched amylose and highly branched amylopectin. However, this correlation did not appear consistent across varieties, with the highest amylose content variety yielding a higher *DB* than other low amylose content varieties. This indicates an inherent difference in amylose and/or amylopectin structure can occur between varieties thus highlighting the importance of characterisation in understanding digestion. In correlating *DB* with the lamellar structure, the observed relationship of *DB* with amylose content suggests a correlation of *DB* with the relative proportions of semi-crystalline structure as was observed in the correlation of amylose content with lamellar structure.

5.1.2.2 Future Research

The size scales over which crystallinity manifests means that it can directly impact the accessibility of digestive enzymes. Thus, crystallinity is an important factor in digestibility. Future work on the characterisation of crystallinity in starch should focus on the use of XRD as a crystallinity characterisation technique and be applied to understanding the digestibility of starches and starch based products.

^{13}C CP-MAS NMR spectroscopy is also a powerful tool in the characterisation of starch, shown to be capable of probing short range order [225]. Using this approach NMR spectra can be decomposed into amorphous (single chain) and ordered (single and double helical components) spectral contributions allowing for the investigation of single-helix V-type and double-helix (A or B-type) conformations [113, 186]. NMR spectroscopy and XRD are complementary tools in the characterisation of crystallinity in starch [151] and both should be explored in further characterisation of starch. In relation to the rice varieties studied,

characterisation of crystallinity could also further help to understand the impact of growing temperatures and subsequent impact on functional and structural properties.

While amylose content correlated with changes in semi-crystalline lamellar structure, further characterisation is required. Future work could involve expanding the analysis of semi-crystalline structure to a wider variety of rice samples. This would allow for a deeper insight into the influence of growing temperature on semi-crystalline structure as well as a better understanding of other structural features of starch. Along with expanding the analysis, repeat experiments would be essential in generating statistically significant analysis outcomes and so should also be undertaken in future work.

Characterisation of crystallinity and semi-crystalline lamellar structure in starch and starch based samples in conjunction with known amylose content would allow for a better understanding of the relationship of amylose content to amorphous and crystalline structure, and lamellar features. With different branching structures evident across varieties, further characterisation promises to uncover the influence of these branching properties on other structural levels. A deeper understanding of the semi-crystalline structure will allow for insight into the role of branching on the different components of the semi-crystalline structure of starch, with potential to gain a better understanding of digestibility.

5.2 The larger context

In this project, the structure of starch was characterised in rice in an effort to understand how growing conditions and other physicochemical properties can influence both molecular and supramolecular structure. This work aimed to develop knowledge and tools to not only characterise starch structure, but also to elucidate how these structural features relate to digestibility.

In vivo measurements of digestibility are the current market standard for digestibility in the form of the internationally recognised glycaemic index (GI) value. However, *in vitro* methods also show promise, providing a more controlled and standard measurement of digestibility. Generating statistically significant data from *in vivo* digestibility trials would require large testing groups to account for the significant person-to-person variability, thus

incurring prohibitively high costs and long analysis times. This makes *in vivo* methods unrealistic in research and development applications for food, and opens the door to the development of robust and simple *in vitro* digestion methods to further our understanding of digestibility.

In developing products with better digestive properties while also maintaining the sensory quality that consumers expect, the development of tools to characterise structure and predict digestibility promises to fast track progress. Development cycles such as in rice breeding programs typically produce thousands of varieties or candidates during a single cycle, all of which need to be assessed in their suitability to fulfilling the desired properties. As such, fast and effective techniques and methods are required. By understanding the link between starch structure and digestibility, the development of tools to improve the efficiency of these development cycles could allow a greater push to the development of healthier consumer products. This could yield far reaching benefits in the health of the global population, a valuable approach in combatting rising obesity rates and other diet related diseases.

In conclusion, a better understanding of how starch structure relates to the digestibility of starchy grain based foods would be beneficial in developing healthier foods, and exploring the digestibility of products where digestibility trials are not possible. This has large implications for consumers, health advisors and the food industry alike, and could prove beneficial in the improvement of public health and prevention and management of diet related diseases such as obesity and diabetes.

Appendices

Starch sample information

The basic available information for some of the samples used in this research project including amylose content and crystallinity measured by XRD is shown in Table A1. Rice sample variety name is followed by a head house number (HH) that indicates what temperature it was grown at. Samples are grown at lower temperature are identified by the label HH1 or HH6 while samples grown at higher temperature are identified by the label HH3 or HH5.

Table A1 Amylose content determined by colorimetric method and crystallinity determined by XRD of some samples investigated in this thesis

Sample	Amylose content (%)	Crystallinity by XRD (%)
Penford Waxy Maize[a]	3.4	29
Penford Regular Maize[a]	24.4	21
Penford Gelose 80[a]	82.9	15
Doongara HH1[b]	25.69	
Doongara HH3[b]	16.33	
Doongara HH5[b]	18.60	
Doongara HH6[b]	25.55	
I-Geo-Tze HH1[b]	28.06	
I-Geo-Tze HH3[b]	28.46	
I-Geo-Tze HH5[b]	27.54	
I-Geo-Tze HH6[b]	28.15	
Quest 19 HH1[b]	19.68	
Quest 19 HH3[b]	12.96	
Quest 19 HH5[b]	12.79	
Quest 19 HH6[b]	20.19	

[a]Values determined and published in Tan et al [113], [b]values determined by collaborators at Department of Primary Industries by iodine binding method

Additional information from capillary electrophoresis

Figures A1 and A2 show the weight-distributions of electrophoretic mobilities of filtered Rice and Corn starch solutions respectively. These samples were prepared as described in the figure caption and repeatedly injected over time. This was done to investigate the aggregation effects with storage time at room temperature after filtration.

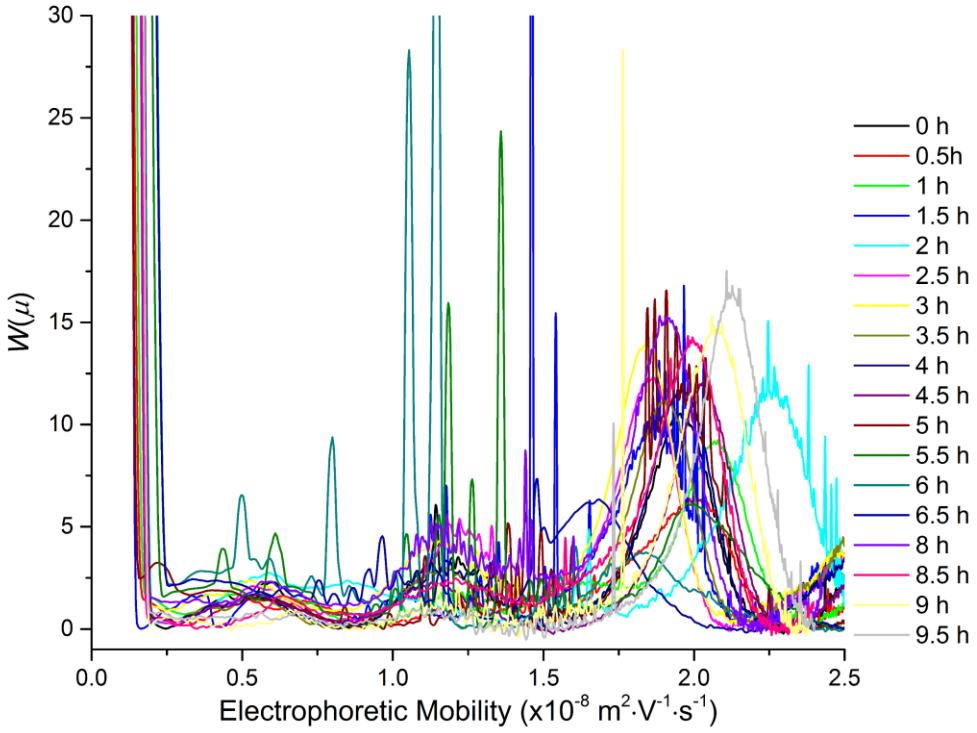

Figure A1 Weight-distributions of electrophoretic mobilities of filtered Rice starch prepared at 10 g·L^{-1} in 90 % DMSO by magnetic stirring at room temperature, showing the evolution of $W(\mu)$ of filtered Rice starch with sample aging. Peak mobility and area are shown in Figure 27

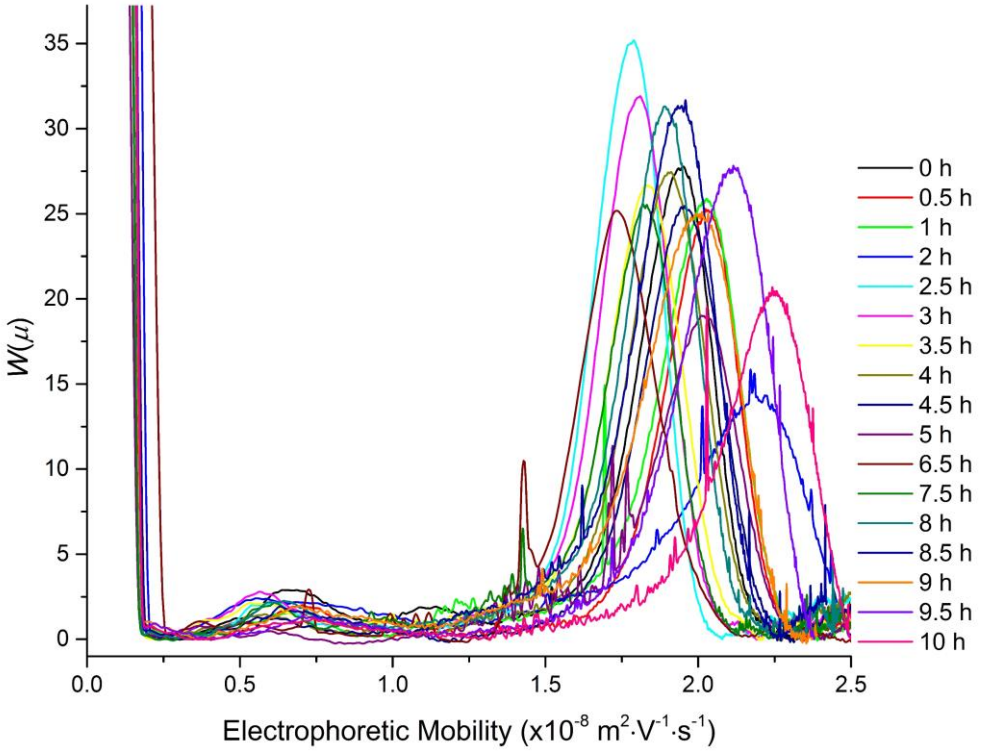

Figure A2 Weight-distributions of electrophoretic mobilities of filtered Corn starch prepared at 10 g·L^{-1} in 90 % DMSO by magnetic stirring at room temperature, showing the evolution of $W(\mu)$ of filtered Corn starch with sample aging. Peak mobility and area are shown in Figure 30

Additional information from FTIR spectroscopy

FSD of FTIR spectra

Figure A3 shows an example of the effects of Fourier self-deconvolution on the ATR-FTIR spectra of Gelose 80 using Bruker Opus 7.5 software. The graph illustrates the effect of both Gaussian and Lorentzian line shapes options compared to the raw spectrum.

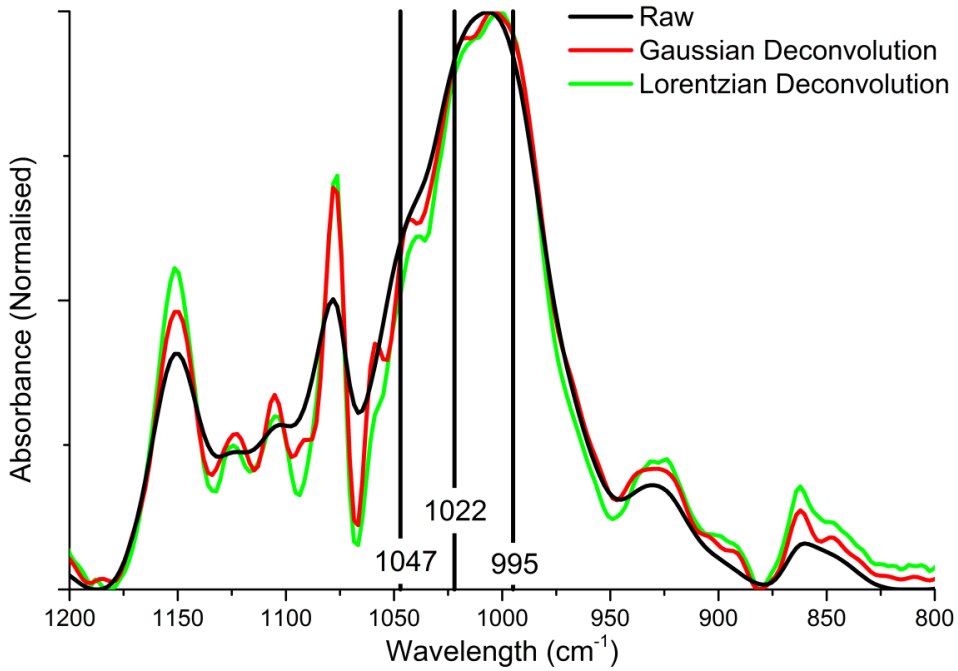

Figure A3 ATR-FTIR spectra of Gelose 80 conditioned at 44 % RH and RT (25 °C) showing raw and FSD processed spectra. FSD parameters are shown in table A2

Table A2 shows the final FSD parameters applied to each spectrum that was processed as part of this work. Bandwidth refers to the peak width of the function used for FSD and noise reduction refers to the additional apodisation based noised reduction applied. The following codes are used in the tables below: HH – Head house sample was grown in denoted by a number (HH1), ATR – Attenuated total reflectance FTIR, KBr – transmission mode FTIR spectroscopy, and Cold stage – Transmission mode FTIR spectroscopy at -170 °C. All samples were conditioned to 44 % relative humidity.

Table A2 FSD parameters for FTIR measurements

		Gaussian		Lorentzian	
Sample	**Technique**	**Bandwidth**	**Noise reduction**	**Bandwidth**	**Noise reduction**
***Doongara* HH1**	**ATR**	93.903	0.29	7.66555	1
	KBr	-	-	37.9737	0.1
Gelose 80	**ATR**	93.903	0.3	7.66555	1
	KBr	-	-	34.2713	0.14
	Cold stage	-	-	50.2202	0.07
Regular Maize	**ATR**	702.19	0.11	24.3051	0.19
	KBr	-	-	21.3602	0.22
	Cold stage	-	-	45.9482	0.08
Waxy Maize	**ATR**	93.903	0.29	17.2475	0.32
	KBr	-	-	16.0439	0.2
	Cold stage	-	-	27.436	0.1

***I-Geo-Tze* HH1**	**KBr**	-	-	24.3032	0.18
***Quest 19* HH1**	**KBr**	-	-	27.436	0.15

Crystalline index values

Table A3 shows the CI_{995} values calculated from FTIR spectra as the ratio of peak heights at 995 and 1022 cm^{-1}. All samples were conditioned to 44 % RH.

Table A3 CI_{995} values of samples calculated from FTIR spectra with and without spectral enhancement

	Raw			Gaussian	Lorentzian		
Samples	**ATR**	**KBr**	**KBr cold stage**	**ATR**	**ATR**	**KBr**	**KBr cold stage**
***Doongara* HH1**	0.9920	0.9160	-	0.9894	1.0054	0.9237	-
Gelose80	1.0143	0.8294	0.9175	1.0498	1.0692	0.9208	0.9484
Waxy Maize	1.0285	0.9901	0.9992	1.0150	1.0415	1.0054	1.0253
Regular Maize	1.0180	0.9828	0.9941	1.0036	1.0178	0.9954	1.0526
***I-Geo-Tze* HH1**	-	0.9110	-	-	-	0.9118	-
***Quest 19* HH1**	-	0.9409	-	-	-	0.9404	-

Table A4 shows the CI_{1047} values calculated from FTIR spectra as the ratio of peak heights at 1047 and 1022 cm^{-1}. All samples were conditioned to 44 % RH.

Table A4 CI_{1047} values of samples calculated from FTIR spectra with and without spectral enhancement

	Raw			Gaussian	Lorentzian		
Samples	**ATR**	**KBr**	**KBr cold stage**	**ATR**	**ATR**	**KBr**	**KBr cold stage**
***Doongara* HH1**	0.6695	0.8797	-	0.6919	0.6660	0.8644	-
Gelose80	0.6800	0.8191	0.8392	0.6718	0.6913	0.8271	0.8293
Waxy Maize	0.6478	0.8726	0.8805	0.6813	0.6551	0.8597	0.8813
Regular Maize	0.6554	0.8596	0.8649	0.6849	0.6599	0.8586	0.8675
***I-Geo-Tze* HH1**	-	0.8714	-	-	-	0.8560	-
***Quest 19* HH1**	-	0.8689	-	-	-	0.8557	-

Linear fits of *CI* data

CI values of both CI_{995} *and* CI_{1047} calculated from spectra of different starch samples were fitted with linear equations to establish any correlation with crystallinity measured by XRD (Table A3) or amylose content (Table A4). Linear fits are in the form of $y = mx + b$, and the variables given in the tables as slope (m) and intercept (b). The goodness of fit is given as the R-squared (coefficient of determination) value of the fit.

Table A5 Table of parameters for linear fits of *CI* of different starch samples plotted against crystallinity by XRD

	CI_{995}					CI_{1047}				
Name	Figure	Treatment	Slope	Intercept	R^2	Figure	Treatment	Slope	Intercept	R^2
Maize starches by ATR-FTIR spectroscopy	Figure 49A	Raw	0.9980	0.0010	0.9651	Figure 49B	Raw	0.7093	-0.0022	0.8618
	Figure 49A	Gaussian	1.0721	-0.0023	0.4403	Figure 49B	Gaussian	0.6659	0.0006	0.4123
	Figure 49A	Lorentzian	1.0798	-0.0017	0.2169	Figure 49B	Lorentzian	0.7225	-0.0025	0.7845
Maize starches by transmission mode FTIR spectroscopy	Figure 55A	Raw	0.6978	0.0109	0.7131	Figure 55B	Raw	0.7703	0.0037	0.8690
	Figure 55A	Lorentzian	0.8485	0.0058	0.7718	Figure 55B	Lorentzian	0.8005	0.0022	0.7041
Maize starches by transmission mode FTIR spectroscopy at cryogenic temperatures	Figure 56A	Raw	0.8500	0.0056	0.7268	Figure 56B	Raw	0.7988	0.0029	0.9516
	Figure 56A	Lorentzian	0.9002	0.0050	0.4242	Figure 56B	Lorentzian	0.7812	0.0036	0.8839

Table A6 Table of parameters for linear fits of *CI* of different starch samples plotted against amylose content

	CI_{995}					CI_{1047}				
Name	Figure	Treatment	Slope	Intercept	R^2	Figure	Treatment	Slope	Intercept	R^2
Rice flours by transmission mode FTIR spectroscopy	Figure 59	Raw	1.0128	-0.0037	0.9854	Figure 60	Raw	0.8591	0.0006	0.2017
	Figure 59	Lorentzian	1.0056	-0.0033	0.9777	Figure 60	Lorentzian	0.8512	0.0003	0.0726
Maize starches by transmission mode FTIR spectroscopy	Figure 57A	Raw	1.0135	-0.0022	0.9536	Figure 57B	Raw	0.8754	-0.0007	0.9995
	Figure 57A	Lorentzian	1.0148	-0.0011	0.9777	Figure 57B	Lorentzian	0.8647	-0.0004	0.9494

Additional information from XRD experiments

XRD diffractogram of sample holder used for background subtraction

Figure A2 shows the X-ray diffractogram of the sample holder used in XRD analysis of starch samples. This diffractogram was used as the background in data where background subtraction was applied.

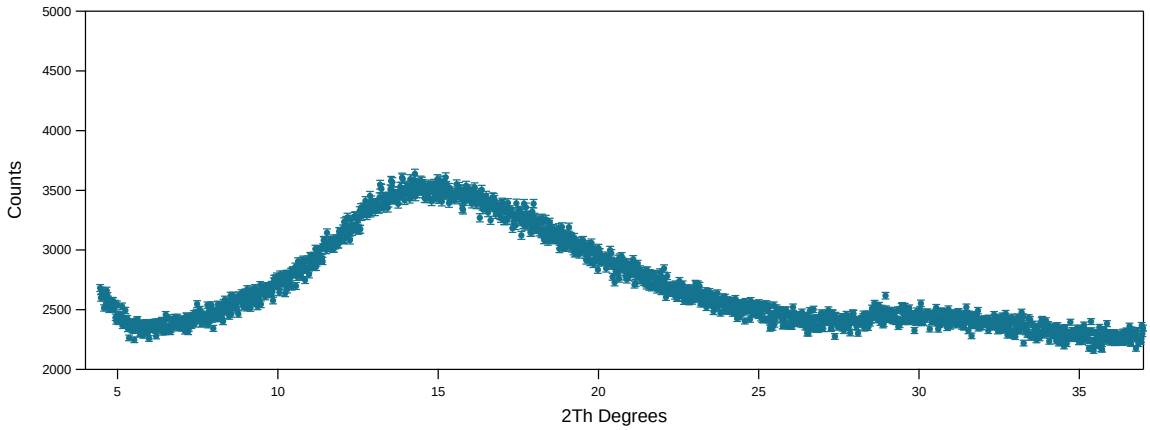

Figure A4 X-ray diffractogram of sample holder used for sample measurements (taken as a background measurement)

XRD diffractograms fitted using TOPAS software

Figures A5 to A8 show the additional X-ray diffractograms of samples fitted using the TOPAS software package. Fitted peaks are pseudo-Voigt peak shapes with the Lorentzian contribution forced to 0, and a linear baseline is employed that is controlled independently by the fitting software. These fitted diffractograms were used to calculate crystallinity values discussed in Section 3.3.2.3.4.

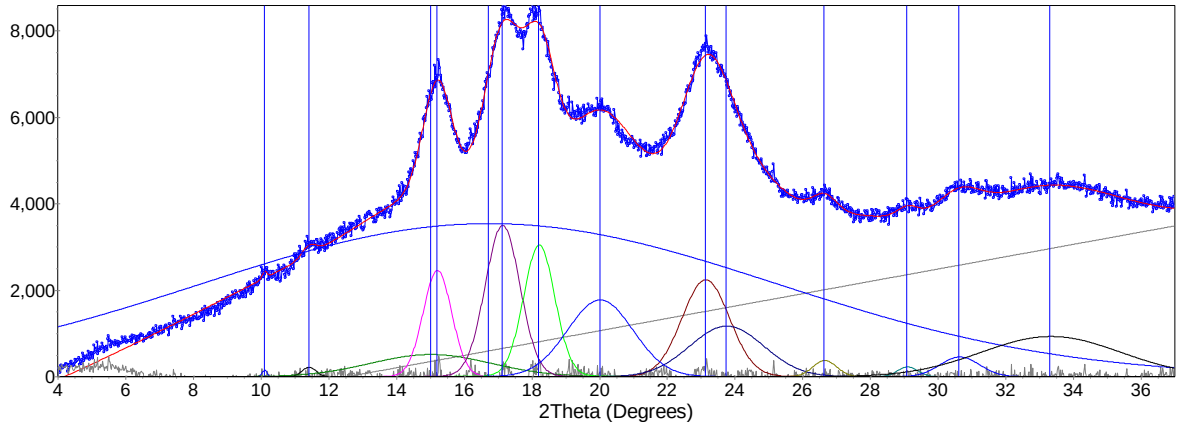

Figure A5 TOPAS software peak fitting of X-ray diffractogram of Regular maize conditioned at 44 % RH with sample holder background subtraction where fitted peaks are shown close to the x-axis with the broad (0 to 37 °) amorphous peak at 17 °, V-type peak at 20 ° and the remaining peaks being crystalline peaks. The baseline is shown as a linear curve from 4 to 37 °, and the sum of fitted peaks shown as the red line superimposed on the blue X-ray diffraction pattern

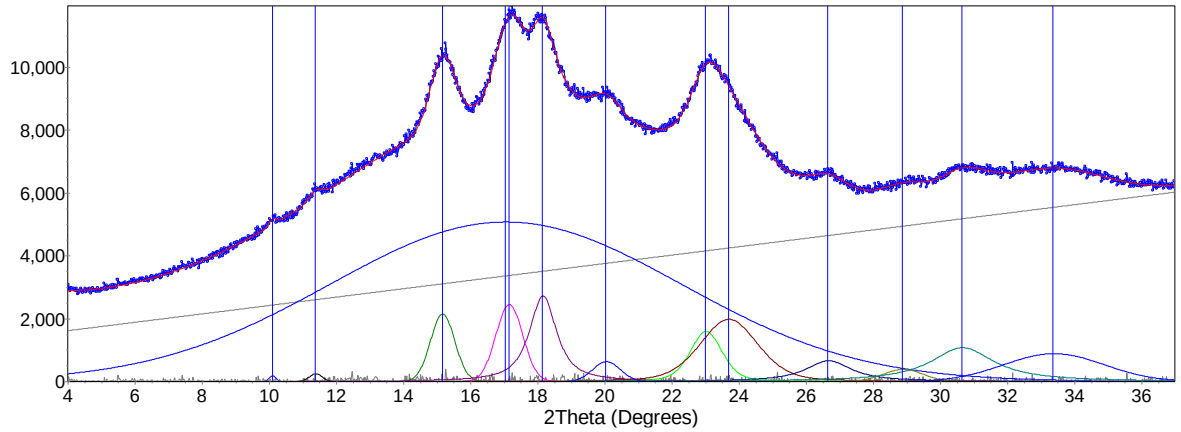

Figure A6 TOPAS software peak fitting of X-ray diffractogram of Regular maize conditioned at 44 % RH without sample holder background subtraction where fitted peaks are shown close to the x-axis with the broad (0 to 32 °) amorphous peak at 17 °, V-type peak at 20 ° and the remaining peaks being crystalline peaks. The baseline is shown as a linear curve from 4 to 37 °, and the sum of fitted peaks shown as the red line superimposed on the blue X-ray diffraction pattern

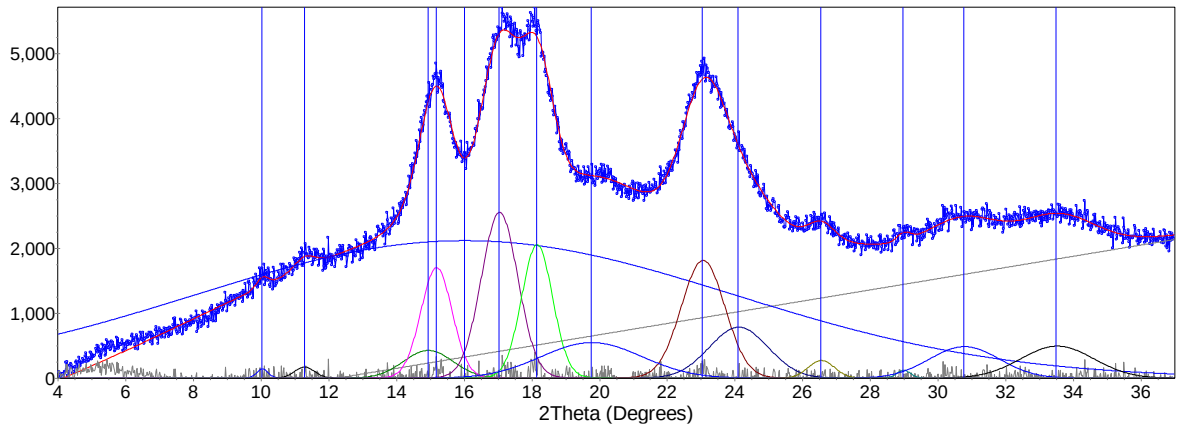

Figure A7 TOPAS software peak fitting of X-ray diffractogram of Waxy maize conditioned at 44 % RH with sample holder background subtraction where fitted peaks are shown close to the x-axis with the broad (0 to 37 °) amorphous peak at 16 °, V-type peak at 20 ° and the remaining peaks being crystalline peaks. The baseline is shown as a linear curve from 4 to 37 °, and the sum of fitted peaks shown as the red line superimposed on the blue X-ray diffraction pattern

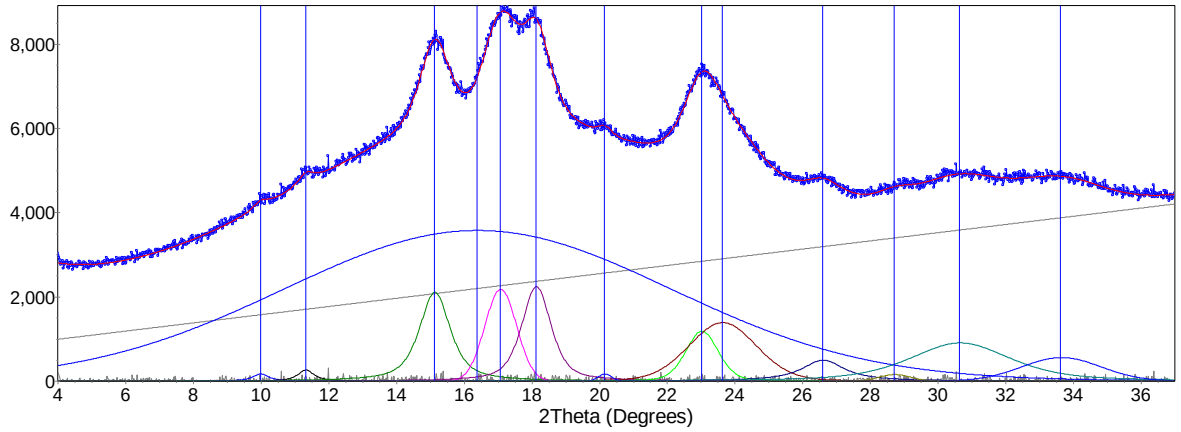

Figure A8 TOPAS software peak fitting of X-ray diffractogram of Waxy maize conditioned at 44 % RH without sample holder background subtraction where fitted peaks are shown close to the x-axis with the broad (0 to 32 °) amorphous peak at 16 °, V-type peak at 20 ° and the remaining peaks being crystalline peaks. The baseline is shown as a linear curve from 4 to 37 °, and the sum of fitted peaks shown as the red line superimposed on the blue X-ray diffraction pattern

XRD diffractograms fitted using Igor Pro software

Figures A9 to A12 show the additional X-ray diffractograms of samples fitted using the WaveMetrics Igor Pro software package. Fitted peaks are Gaussian peak shapes, and a linear baseline is employed with a degree of control given for manual input of baseline parameters allowing for an optimised fit. These fitted diffractograms were used to calculate crystallinity values discussed in Section 3.3.2.3.2.

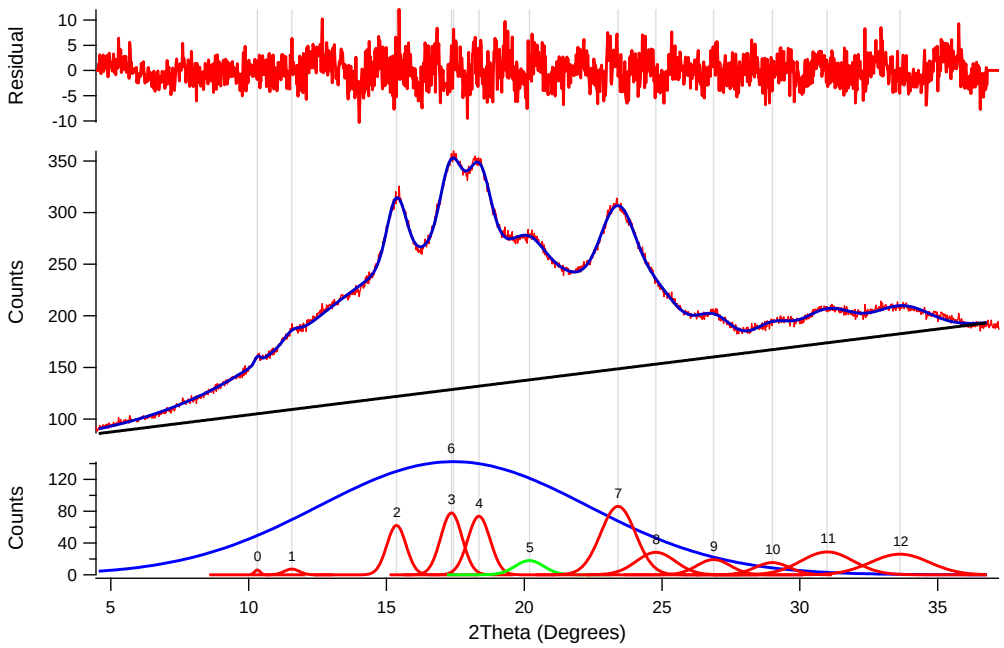

Figure A9 Igor Pro software peak fitting of X-ray diffractogram of Regular maize conditioned at 44 % RH with sample holder background subtraction. The bottom section shows the fitted peaks with Blue-Amorphous, Green – V-type and Red – crystalline peaks. The middle section shows the linear baseline used for fitting (black), the sum of fitted peaks (blue) and the original X-ray diffraction pattern (red). The top section shows the residuals of fitting

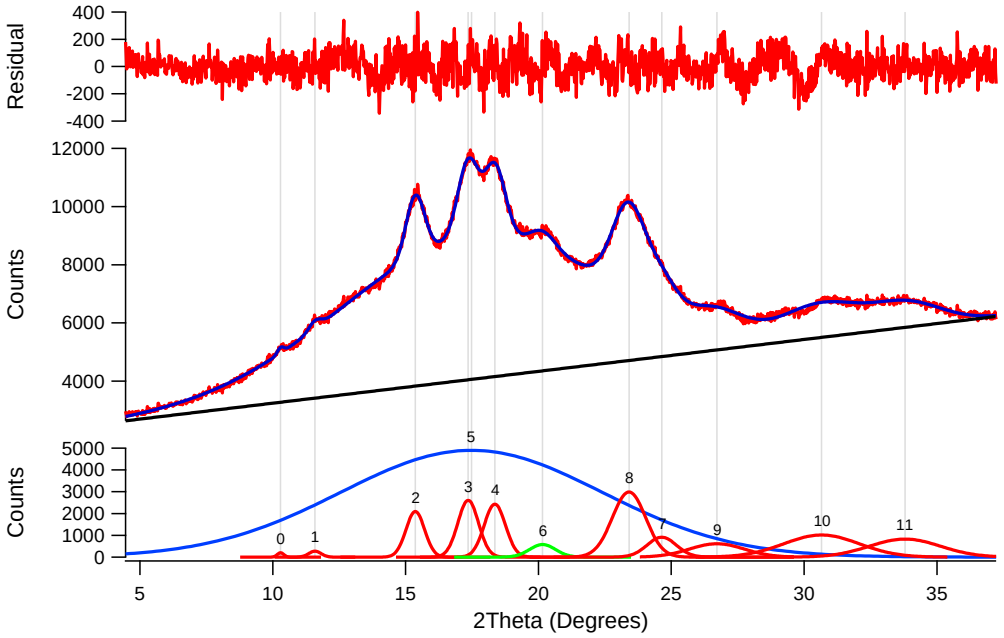

Figure A10 Igor Pro software peak fitting of X-ray diffractogram of Regular maize conditioned at 44 % RH without sample holder background subtraction. The bottom section shows the fitted peaks with Blue-Amorphous, Green – V-type and Red – crystalline peaks. The middle section shows the linear baseline used for fitting (black), the sum of fitted peaks (blue) and the original X-ray diffraction pattern (red). The top section shows the residuals of fitting

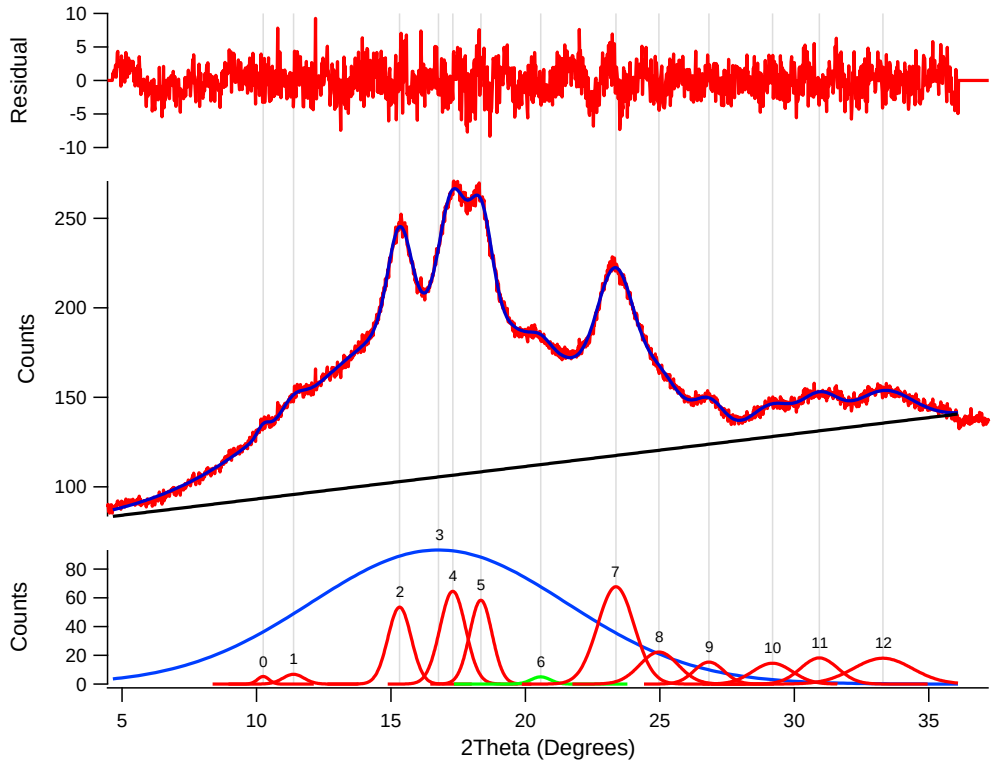

Figure A11 Igor Pro software peak fitting of X-ray diffractogram of Waxy maize conditioned at 44 % RH with sample holder background subtraction. The bottom section shows the fitted peaks with Blue-Amorphous, Green – V-type and Red – crystalline peaks. The middle section shows the linear baseline used for fitting (black), the sum of fitted peaks (blue) and the original X-ray diffraction pattern (red). The top section shows the residuals of fitting

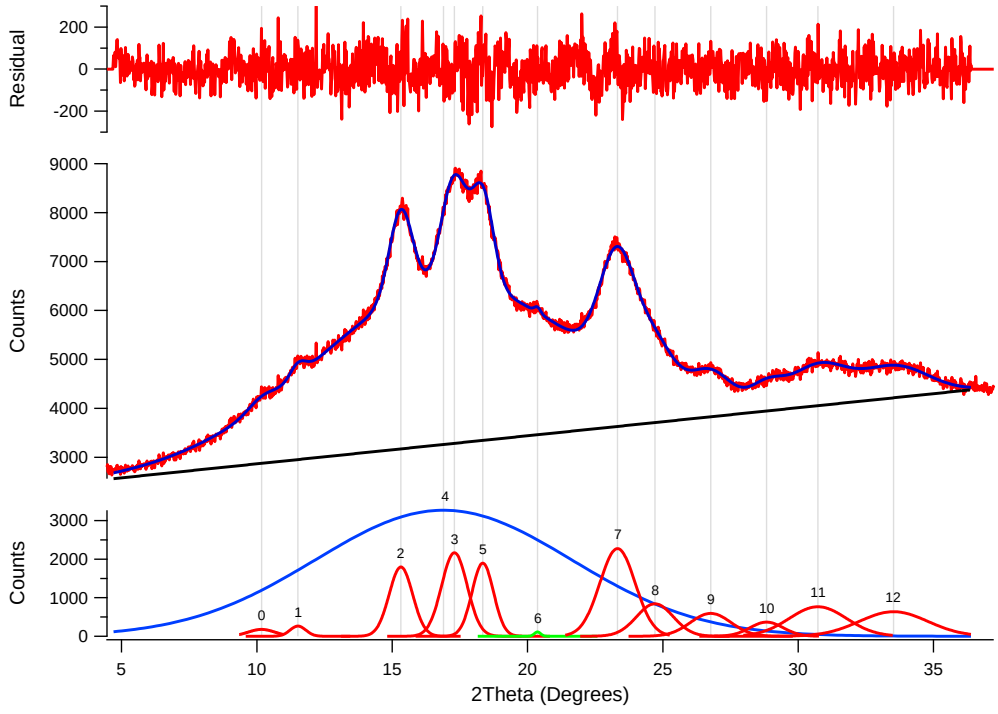

Figure A12 Igor Pro software peak fitting of X-ray diffractogram of Waxy maize conditioned at 44 % RH without sample holder background subtraction. The bottom section shows the fitted peaks with Blue-Amorphous, Green – V-type and Red – crystalline peaks. The middle section shows the linear baseline used for fitting (black), the sum of fitted peaks (blue) and the original X-ray diffraction pattern (red). The top section shows the residuals of fitting

Additional information from SAXS experiments

SAXS curve of Gelose 80 fitted using Igor Pro software

Figure A11 shows an example of the results of peak fitting of SAXS curves. This particular graph demonstrates the possibility of unrealistic peak parameters through peak fitting as a result of the algorithm aiming to minimise chi-squared values. In this case, the peak position clearly appears to be biased towards a lower q introducing error to the peak position parameter as well as influencing peak width and intensity parameters.

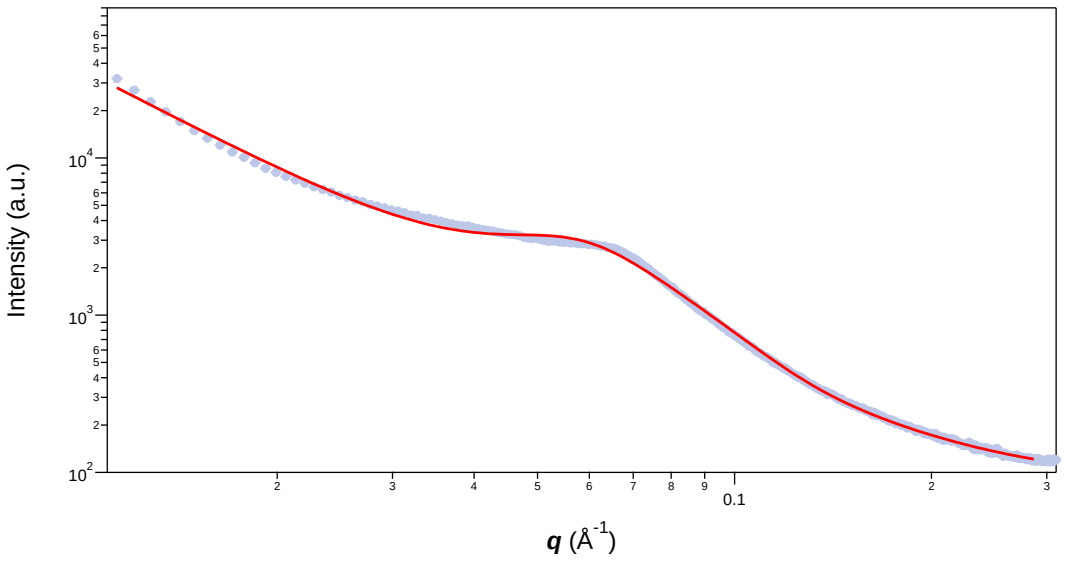

Figure A13 Peak fitted SAXS data of Gelose 80 where red - fitted peak and grey - the original scattering curve

SAXS curves of rice flours samples

Figures A14 to A16 show the SAXS curve of three different rice varieties, each presenting four different samples of that variety grown at lower or higher temperature identified by their head house number (see table A1). These SAXS curves have been fitted, and the fitted peak parameters discussed in Section 4.2.

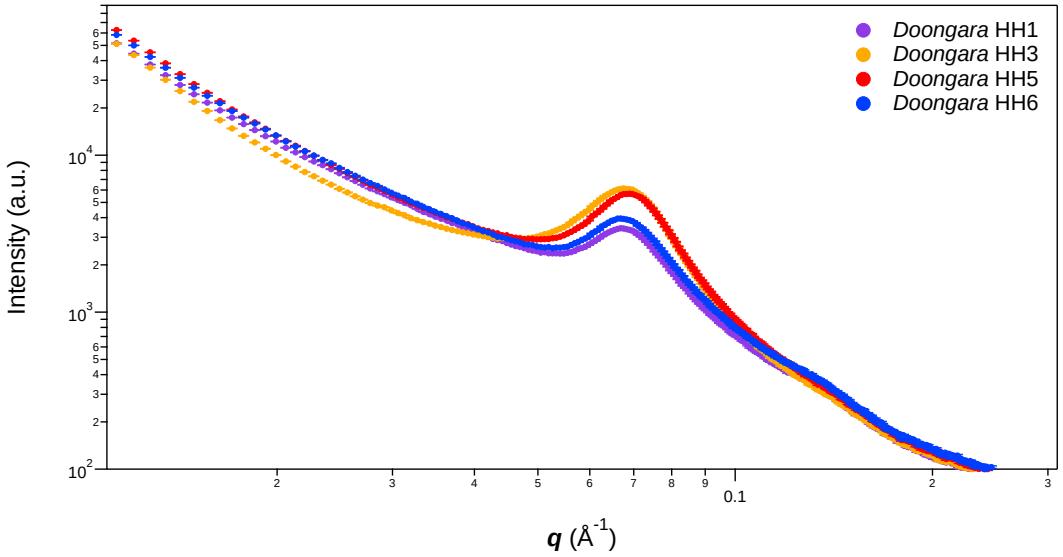

Figure A14 SAXS curves of *Doongara* rice variety grown at different temperatures, denoted by their head house number

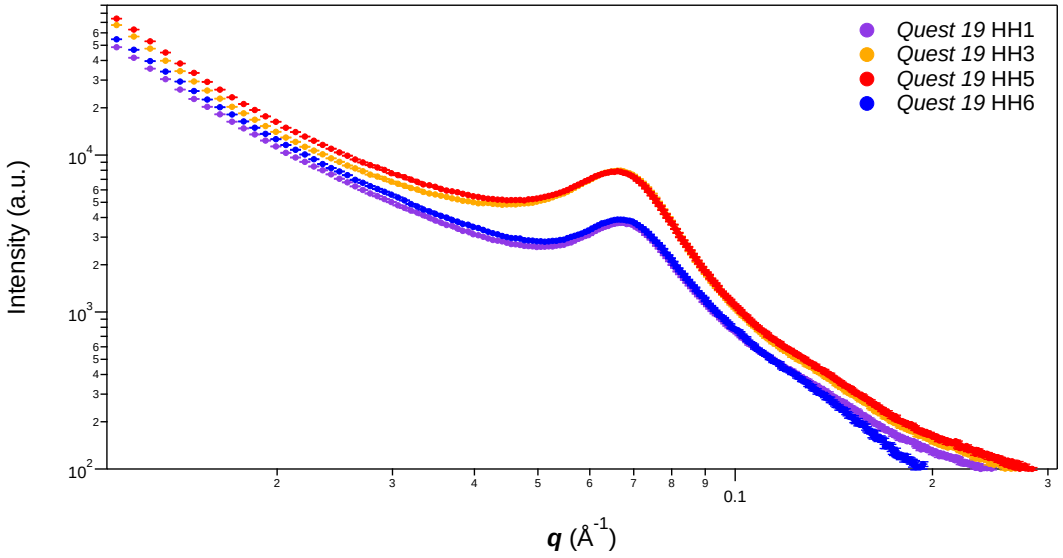

Figure A15 SAXS curves of *Quest19* rice variety grown at different temperatures, denoted by their head house number

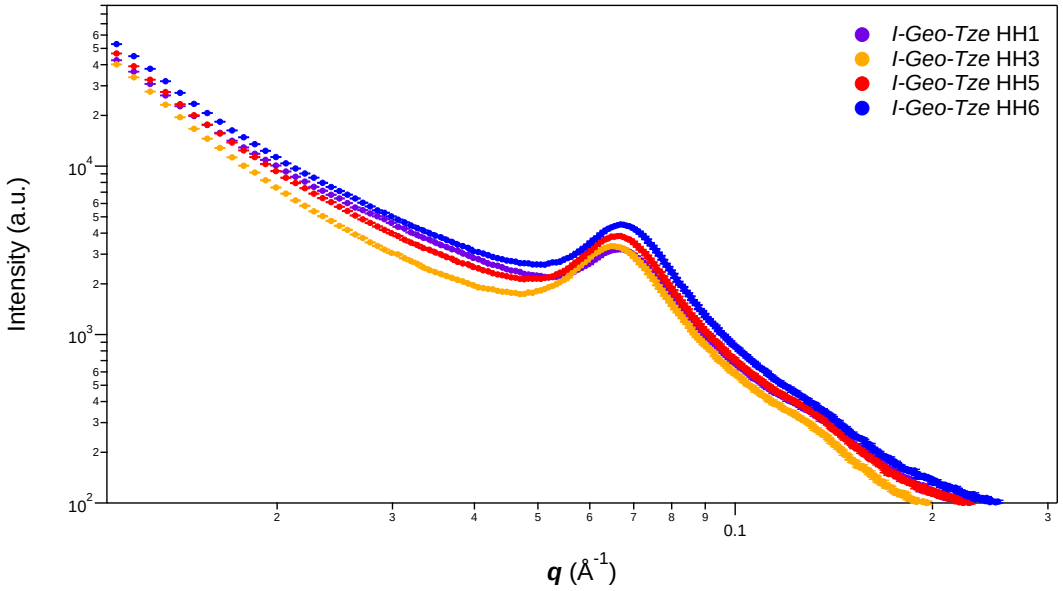

Figure A16 SAXS curves of *I-Geo-Tze* rice variety grown at different temperatures, denoted by their head house number

References

1. Juliano, B.O., *Rice: Overview*, in *Encyclopedia of Food Grains (Second Edition)*, J. Faubion, et al., Editors. 2016, Academic Press: Oxford. p. 125-129.
2. Woods, J. and Walker, K., *Choosing breakfast: How well does packet information on Australian breakfast cereals, bars and drinks reflect recommendations?* Nutrition & Dietetics, 2007, **64**(4): p. 226-233.
3. World Health Organisation, *Obesity: preventing and managing the global epidemic*, in *WHO Technical Report Series*. 2000: Geneva.
4. The Organisation for Economic Co-operation and Development (OECD), *Obesity Update* 2014: http://www.oecd.org/health/obesity-update.htm.
5. Hill, J.O. and Melanson, E.L., *Overview of the determinants of overweight and obesity: current evidence and research issues.* Medicine & Science in Sports & Exercise, 1999, **31**(11): p. S515.
6. Markwald, R.R., Melanson, E.L., Smith, M.R., Higgins, J., Perreault, L., Eckel, R.H., and Wright, K.P., *Impact of insufficient sleep on total daily energy expenditure, food intake, and weight gain.* Proceedings of the National Academy of Sciences, 2013, **110**(14): p. 5695-5700.
7. Wolever, T.M.S., *Dietary carbohydrates and insulin action in humans.* British Journal of Nutrition, 2000, **83**(S1): p. S97-S102.
8. Cummings, J.H., Roberfroid, M.B., Andersson, H., Barth, C., Ferro-Luzzi, A., Ghoos, Y., MGibney, M., Hermonsen, K., James, W.P.T., Korver, O., Lairon, D., Pascal, G., and Voragen, A.G.S., *A new look at dietary carbohydrate: chemistry, physiology and health.* European Journal of Clinical Nutrition, 1997, **51**(7): p. 417-423.
9. Cummings, J.H. and Stephen, A.M., *Carbohydrate terminology and classification.* European Journal of Clinical Nutrition, 2007, **61**(S1): p. S5-S18.
10. Bornhorst, G.M. and Singh, R.P., *Gastric Digestion In Vivo and In Vitro: How the Structural Aspects of Food Influence the Digestion Process.* Annual Review of Food Science and Technology, 2014, **5**(1): p. 111-132.
11. Fitzgerald, M.A., Rahman, S., Resurreccion, A.P., Concepcion, J., Daygon, V.D., Dipti, S.S., Kabir, K.A., Klingner, B., Morell, M.K., and Bird, A.R., *Identification of a Major Genetic Determinant of Glycaemic Index in Rice.* Rice, 2011, **4**(2): p. 66-74.
12. Waters, A.M. and Dixon, T., *A growing problem: trends and patterns in overweight and obesity among adults in Australia, 1980 to 2001*, in *AIHW Bulletin 8. Cat. no. AUS 36*. 2003, Australian Institute of Health and Welfare: Canberra.
13. American Medical Association. *AMA Adopts New Policies on Second Day of Voting at Annual Meeting*. 2013 [cited 2015]; Available from: http://www.ama-assn.org/ama/pub/news/news/2013/2013-06-18-new-ama-policies-annual-meeting.page.
14. Australian Bureau of Statistics, *4364.0.55.001 - Australian Health Survey: First Results, 2011 - 12*, Australian Bureau of Statistics, Editor. 2012, Commonwealth of Australia.
15. Booth, M.L., Wake, M., Armstrong, T., Chey, T., Hesketh, K., and Mathur, S., *The epidemiology of overweight and obesity among Australian children and adolescents, 1995-97.* Australian and New Zealand Journal of Public Health, 2001, **25**(2): p. 162-168.
16. Skidmore, P., *Macronutrient intakes and their role in obesity.* Nutrition Bulletin, 2007, **32**: p. 4-13.

17. Gross, L.S., Li, L., Ford, E.S., and Liu, S., *Increased consumption of refined carbohydrates and the epidemic of type 2 diabetes in the United States: an ecologic assessment.* The American Journal of Clinical Nutrition, 2004, **79**(5): p. 774-779.
18. Ao, Z., Quezada-Calvillo, R., Sim, L., Nichols, B.L., Rose, D.R., Sterchi, E.E., and Hamaker, B.R., *Evidence of native starch degradation with human small intestinal maltase-glucoamylase (recombinant).* FEBS Letters, 2007, **581**(13): p. 2381-2388.
19. Avérous, L. and Halley, P.J., *Chapter 1 - Starch Polymers: From the Field to Industrial Products*, in *Starch Polymers*, L. Avérous and P.J. Halley, Editors. 2014, Elsevier: Amsterdam. p. 3-10.
20. Englyst, H.N., Kingman, S.M., and Cummings, J.H., *Classification and measurement of nutritionally important starch fractions.* European Journal of Clinical Nutrition, 1992, **46(S2)**: p. S33-50.
21. Nugent, A.P., *Health properties of resistant starch.* Nutrition Bulletin, 2005, **30**(1): p. 27-54.
22. Sanz, T., Martínez-cervera, S., Salvador, A., and Fiszman, S.M., *Resistant starch content and glucose release of different resistant starch commercial ingredients: effect of cooking conditions.* European Food Research and Technology 2010, **231**(5): p. 655-662.
23. Phillips, J., Muir, J.G., Birkett, A., Lu, Z.X., Jones, G.P., O'Dea, K., and Young, G.P., *Effect of resistant starch on fecal bulk and fermentation-dependent events in humans.* The American Journal of Clinical Nutrition, 1995, **62**(1): p. 121-30.
24. Scheppach, W., Luehrs, H., and Menzel, T., *Beneficial health effects of low-digestible carbohydrate consumption.* British Journal of Nutrition, 2001, **85**(3): p. S23-S30.
25. Topping, D.L. and Clifton, P.M., *Short-Chain Fatty Acids and Human Colonic Function: Roles of Resistant Starch and Nonstarch Polysaccharides.* Physiological Reviews, 2001, **81**(3): p. 1031-1064.
26. McCance, R.A. and Lawrence, R.D., *The carbohydrate content of foods*. 1929, London: Her Majesty's Stationary Office.
27. Jenkins, D.J., Wolever, T.M., Taylor, R.H., Barker, H., Fielden, H., Baldwin, J.M., Bowling, A.C., Newman, H.C., Jenkins, A.L., and Goff, D.V., *Glycemic index of foods: a physiological basis for carbohydrate exchange.* The American Journal of Clinical Nutrition, 1981, **34**(3): p. 362-6.
28. Salmeron, J., Ascherio, A., Rimm, E.B., Colditz, G.A., Spiegelman, D., Jenkins, D.J., Stampfer, M.J., Wing, A.L., and Willett, W.C., *Dietary fiber, glycemic load, and risk of NIDDM in men.* Diabetes Care, 1997, **20**(4): p. 545-50.
29. Liu, S., Willett, W.C., Stampfer, M.J., Hu, F.B., Franz, M., Sampson, L., Hennekens, C.H., and Manson, J.E., *A prospective study of dietary glycemic load, carbohydrate intake, and risk of coronary heart disease in US women.* The American Journal of Clinical Nutrition, 2000, **71**(6): p. 1455-1461.
30. Mayer, J., Vitale, J.J., and Bates, M.W., *Mechanism of the Regulation of Food Intake.* Nature, 1951, **167**(4249): p. 562-563.
31. Feskens, E.J.M. and Du, H., *Dietary glycaemic index from an epidemiological point of view.* International Journal of Obesity, 2006, **30**(S3): p. S66-71.
32. Lehmann, U. and Robin, F., *Slowly digestible starch – its structure and health implications: a review.* Trends in Food Science & Technology, 2007, **18**(7): p. 346-355.
33. Brand-Miller, J.C., Holt, S.H., Pawlak, D.B., and McMillan, J., *Glycemic index and obesity.* The American Journal of Clinical Nutrition, 2002, **76**(1): p. 281S-285S.
34. Byrnes, S.E., Miller, J.C.B., and Denyer, G.S., *Amylopectin starch promotes the development of insulin resistance in rats.* The Journal of Nutrition, 1995, **125**(6): p. 1430-7.

35. Pawlak, D.B., Kushner, J.A., and Ludwig, D.S., *Effects of dietary glycaemic index on adiposity, glucose homoeostasis, and plasma lipids in animals.* The Lancet, 2004, **364**(9436): p. 778-85.
36. Wolever, T.M., Jenkins, D.J., Ocana, A.M., Rao, V.A., and Collier, G.R., *Second-meal effect: low-glycemic-index foods eaten at dinner improve subsequent breakfast glycemic response.* The American Journal of Clinical Nutrition, 1988, **48**(4): p. 1041-7.
37. Wolever, T.M. and Mehling, C., *Long-term effect of varying the source or amount of dietary carbohydrate on postprandial plasma glucose, insulin, triacylglycerol, and free fatty acid concentrations in subjects with impaired glucose tolerance.* The American Journal of Clinical Nutrition, 2003, **77**(3): p. 612-621.
38. Slavin, J. and Green, H., *Dietary fibre and satiety.* Nutrition Bulletin, 2007, **32**: p. 32-42.
39. Willis, H.J., Eldridge, A.L., Beiseigel, J., Thomas, W., and Slavin, J.L., *Greater satiety response with resistant starch and corn bran in human subjects.* Nutrition Research, **29**(2): p. 100-105.
40. Nilsson, A.C., Östman, E.M., Holst, J.J., and Björck, I.M.E., *Including indigestible carbohydrates in the evening meal of healthy subjects improves glucose tolerance, lowers inflammatory markers, and increases satiety after a subsequent standardized breakfast.* The Journal of Nutrition, 2008, **138**(4): p. 732-9.
41. Buléon, A., Colonna, P., Planchot, V., and Ball, S., *Starch granules: structure and biosynthesis.* International Journal of Biological Macromolecules, 1998, **23**(2): p. 85-112.
42. Gaborieau, M. and Castignolles, P., *Caractérisation de l'amidon et de ses matériaux composites.* Les Annales des falsifications de l'expertise chimique et toxicologique (Société des Experts Chimistes de France) 2009, **9710**: p. 23-32.
43. Copeland, L., Blazek, J., Salman, H., and Tang, M.C., *Form and functionality of starch.* Food Hydrocolloids, 2009, **23**(6): p. 1527-1534.
44. Pérez, S., Baldwin, P.M., and Gallant, D.J., *Chapter 5 - Structural Features of Starch Granules I*, in *Starch (Third Edition)*, J. BeMiller and R. Whistler, Editors. 2009, Academic Press: San Diego. p. 149-192.
45. Chanvrier, H., Uthayakumaran, S., Appelqvist, I.A., Gidley, M.J., Gilbert, E.P., and Lopez-Rubio, A., *Influence of storage conditions on the structure, thermal behavior, and formation of enzyme-resistant starch in extruded starches.* Journal of Agricultural and Food Chemistry, 2007, **55**(24): p. 9883-90.
46. Blazek, J. and Gilbert, E.P., *Effect of enzymatic hydrolysis on native starch granule structure.* Biomacromolecules, 2010, **11**(12): p. 3275-89.
47. Zhou, Z., Robards, K., Helliwell, S., and Blanchard, C., *Composition and functional properties of rice.* International Journal of Food Science & Technology, 2002, **37**(8): p. 849-868.
48. Arendt, E. and Zannini, E., *Rice*, in *Cereal Grains for the Food and Beverage Industries*. 2013, Woodhead Publishing: Cambridge, Sawston.
49. Ricegrowers' Association of Australia Inc. *About the Rice Industry* http://www.rga.org.au/the-rice-industry.aspx. [cited 13/02/16].
50. Ricegrowers' Association of Australia Inc. *Rice and the environment* http://www.rga.org.au/the-rice-industry/rice-and-the-environment.aspx. [cited 13/02/16].
51. Ricegrowers' Association of Australia Inc. *Rice Community* http://www.rga.org.au/the-rice-industry/rice-community.aspx. [cited 13/02/16].
52. Bhattacharya, K.R. and Ali, S.Z., *Agronomy, production and trade of rice*, in *An Introduction to Rice-grain Technology*, K.R. Bhattacharya and S.Z. Ali, Editors. 2015, WPI Publishing. p. 10-37.

53. Sun Rice. *Australian Rice Varieties* https://www.sunrice.com.au/media/6661/australian_rice_varieties_v2.pdf. [cited 13/02/16].
54. Strocchi, A. and Levitt, M.D., *Measurement of starch absorption in humans.* Canadian Journal of Physiology and Pharmacology, 1991, **69**(1): p. 108-110.
55. Rewthong, O., Soponronnarit, S., Taechapairoj, C., Tungtrakul, P., and Prachayawarakorn, S., *Effects of cooking, drying and pretreatment methods on texture and starch digestibility of instant rice.* Journal of Food Engineering, 2011, **103**(3): p. 258-264.
56. Rashmi, S. and Urooj, A., *Effect of processing on nutritionally important starch fractions in rice varieties.* International Journal of Food Sciences and Nutrition, 2003, **54**(1): p. 27-36.
57. Chiu, Y.-T. and Steward, M.L., *Effect of variety and cooking method on resistant starch content of white rice and subsequent postprandial glucose response and appetite in humans.* Asia Pacific Journal of Clinical Nutrition, 2013, **22**(3): p. 372-379.
58. Tamura, M., Singh, J., Kaur, L., and Ogawa, Y., *Impact of the degree of cooking on starch digestibility of rice – An in vitro study.* Food Chemistry, 2016, **191**: p. 98-104.
59. Li, J., Han, W., Xu, J., Xiong, S., and Zhao, S., *Comparison of morphological changes and in vitro starch digestibility of rice cooked by microwave and conductive heating.* Starch - Stärke, 2014, **66**(5-6): p. 549-557.
60. Miller, J.B., Pang, E., and Bramall, L., *Rice: a high or low glycemic index food?* The American Journal of Clinical Nutrition, 1992, **56**(6): p. 1034-6.
61. Zhou, Z., Robards, K., Helliwell, S., Blanchard, C., and Baxterb, G., *Rice Ageing. I. Effect of Changes in Protein on Starch Behaviour.* Starch - Stärke, 2003, **55**(3-4): p. 162-169.
62. Baxter, G., Zhao, J., and Blanchard, C., *Salinity alters the protein composition of rice endosperm and the physicochemical properties of rice flour.* Journal of the Science of Food and Agriculture, 2011, **91**(12): p. 2292-2297.
63. Zhou, Z., Robards, K., Helliwell, S., and Blanchard, C., *Effect of storage temperature on cooking behaviour of rice.* Food Chemistry, 2007, **105**(2): p. 491-497.
64. Zhou, Z., Robards, K., Helliwell, S., and Blanchard, C., *Effect of the addition of fatty acids on rice starch properties.* Food Research International, 2007, **40**(2): p. 209-214.
65. Zhou, Z., Robards, K., Helliwell, S., and Blanchard, C., *Effect of storage temperature on rice thermal properties.* Food Research International, 2010, **43**(3): p. 709-715.
66. Toutounji, M.R., Van Leeuwen, M.P., Oliver, J.D., Shrestha, A.K., Castignolles, P., and Gaborieau, M., *Quantification of sugars in breakfast cereals using capillary electrophoresis.* Carbohydrate Research, 2015, **408**: p. 134-141.
67. Fast, R.B., *Chapter 2: Manufacturing Technology of Ready-to-Eat Cereals*, in *Breakfast Cereals and How They Are Made*. 2000, AACC International, Inc. p. 17-54.
68. Kulp, K. and Ponte, J.G., *Ready-to-Eat Breakfast Cereals*, in *Handbook of Cereal Science and Technology*, P.J. Whalen, J.L. DesRochers, and C.E. Walker, Editors. 2000, CRC Press: New York.
69. Food Standards Australia New Zealand (FSANZ), *Standard 1.3.2 - Vitamin and Minerals*, in *Australia New Zealand Food Standards Code*. 2014, Food Standards Australia New Zealand (FSANZ): Canberra.
70. Food Standards Australia New Zealand (FSANZ), *Standard 2.1.1 - Cereals and Cereal Products*, in *Australia New Zealand Food Standards Code*. 2014, Food Standards Australia New Zealand (FSANZ): Canberra.
71. American Dietetic Association, *Position of the American Dietetic Association: Health Implications of Dietary Fiber.* Journal of the American Dietetic Association, 2008, **108**(10): p. 1716-1731.

72. Eyaru, R., Shrestha, A.K., and Arcot, J., *Effect of various processing techniques on digestibility of starch in Red kidney bean (Phaseolus vulgaris) and two varieties of peas (Pisum sativum).* Food Research International, 2009, **42**(8): p. 956-962.
73. Vasanthan, T., Gaosong, J., Yeung, J., and Li, J., *Dietary fiber profile of barley flour as affected by extrusion cooking.* Food Chemistry, 2002, **77**(1): p. 35-40.
74. Knutson, C.A., *A simplified colorimetric procedure for determination of amylose in maize starches.* Cereal Chemistry, 1986, **63**(2): p. 89-92.
75. Knutson, C.A., *Evaluation of variations in amylose-iodine absorbance spectra.* Carbohydrate Polymers, 1999, **42**: p. 65-72.
76. Takeda, Y., Hizukuri, S., and Juliano, B.O., *Structures of rice amylopectins with low and high affinities for iodine.* Carbohydrate Research, 1987, **168**(1): p. 79-88.
77. Zhu, T., Jackson, D.S., Wehling, R.L., and Geera, B., *Comparison of amylose determination methods and the development of a dual wavelength iodine binding technique.* Cereal Chemistry, 2008, **85**(1): p. 51-58.
78. Nollet, L.M.L., *Liquid chromatography in food analysis*, in *Encyclopedia of Analytical Chemistry*. 2006, John Wiley & Sons, Ltd.
79. Gilbert, R.G., Gidley, M.J., Hill, S., Kilz, P., Rolland-Sabaté, A., Stevenson, D.G., and Cave, R.A., *Characterizing the size and molecular weight distribution of starch: Why it is important and why it is hard.* Cereal Foods World, 2010, **55**(3): p. 139-143.
80. Hasjim, J., Lavau, G.C., Gidley, M.J., and Gilbert, R.G., *In vivo and in vitro starch digestion: Are current in vitro techniques adequate?* Biomacromolecules, 2010, **11**(12): p. 3600-3608.
81. Gaborieau, M. and Castignolles, P., *Size-exclusion chromatography (SEC) of branched polymers and polysaccharides.* Analytical and Bioanalytical Chemistry, 2011, **399**(4): p. 1413-1423.
82. Berek, D., *Size exclusion chromatography – A blessing and a curse of science and technology of synthetic polymers.* Journal of Separation Science, 2010, **33**(3): p. 315-335.
83. Suortti, T., Gorenstein, M.V., and Roger, P., *Determination of the molecular mass of amylose.* Journal of Chromatography A, 1998, **828**(1–2): p. 515-521.
84. Hoang, N.-L., Landolfi, A., Kravchuk, A., Girard, E., Peate, J., Hernandez, J.M., Gaborieau, M., Kravchuk, O., Gilbert, R.G., Guillaneuf, Y., and Castignolles, P., *Toward a full characterization of native starch: Separation and detection by size-exclusion chromatography.* Journal of Chromatography A, 2008, **1205**(1–2): p. 60-70.
85. Charoenkul, N., Uttapap, D., Pathipanawat, W., and Takeda, Y., *Simultaneous determination of amylose content & unit chain distribution of amylopectins of cassava starches by fluorescent labeling/HPSEC.* Carbohydrate Polymers, 2006, **65**(1): p. 102-108.
86. Kärkkäinen, J., Lappalainen, K., Joensuu, P., and Lajunen, M., *HPLC-ELSD analysis of six starch species heat-dispersed in [BMIM]Cl ionic liquid.* Carbohydrate Polymers, 2011, **84**(1): p. 509-516.
87. Zhong, F., Yokoyama, W., Wang, Q., and Shoemaker, C.F., *Rice starch, amylopectin, and amylose: Molecular weight and solubility in dimethyl sulfoxide-based solvents.* Journal of Agricultural and Food Chemistry, 2006, **54**(6): p. 2320-2326.
88. Dona, A., Yuen, C.-W.W., Peate, J., Gilbert, R.G., Castignolles, P., and Gaborieau, M., *A new NMR method for directly monitoring and quantifying the dissolution kinetics of starch in DMSO.* Carbohydrate Research, 2007, **342**(17): p. 2604-2610.
89. Gérard, C., Barron, C., Colonna, P., and Planchot, V., *Amylose determination in genetically modified starches.* Carbohydrate Polymers, 2001, **44**(1): p. 19-27.
90. Oliver, J.D., Gaborieau, M., Hilder, E.F., and Castignolles, P., *Simple and robust determination of monosaccharides in plant fibers in complex mixtures by capillary*

electrophoresis and high performance liquid chromatography. Journal of Chromatography A, 2013, **1291**: p. 179-186.
91. Kobayashi, S., Schwartz, S.J., and Lineback, D.R., *Rapid analysis of starch, amylose and amylopectin by high-performance size-exclusion chromatography.* Journal of Chromatography A, 1985, **319**: p. 205-214.
92. Foret, F., Krivankova, L., and Bocek, P., *Capillary zone electrophoresis*. 1993, Weinheim and New York: VCH.
93. Bosserhoff, A. and Hellerbrand, C., *Chapter 5 - Capillary Electrophoresis*, in *Molecular Diagnostics (Second Edition)*, G.P. Patrinos and W.J. Ansorge, Editors. 2010, Academic Press: San Diego. p. 59-73.
94. Kalsoom, U., Guijt, R.M., Boyce, M.C., Townsend, A.T., Haselberg, R., and Breadmore, M.C., *Direct electrokinetic injection of inorganic cations from whole fruits and vegetables for capillary electrophoresis analysis.* Journal of Chromatography A, 2016, **1428**: p. 346-51.
95. Hadley, M., Gilges, M., Senior, J., Shah, A., and Camilleri, P., *Capillary electrophoresis in the pharmaceutical industry: applications in discovery and chemical development.* Journal of Chromatography B: Biomedical Sciences and Applications, 2000, **745**(1): p. 177-188.
96. Stover, F.S., *Applications of capillary electrophoresis for industrial analysis.* ELECTROPHORESIS, 1990, **11**(9): p. 750-756.
97. Zhang, Z., Zhang, F., and Liu, Y., *Recent Advances in Enhancing the Sensitivity and Resolution of Capillary Electrophoresis.* Journal of Chromatographic Science, 2013, **51**(7): p. 666-83.
98. Breadmore, M.C., Tubaon, R.M., Shallan, A.I., Phung, S.C., Abdul Keyon, A.S., Gstoettenmayr, D., Prapatpong, P., Alhusban, A.A., Ranjbar, L., See, H.H., Dawod, M., and Quirino, J.P., *Recent advances in enhancing the sensitivity of electrophoresis and electrochromatography in capillaries and microchips (2012-2014).* Electrophoresis, 2015, **36**(1): p. 36-61.
99. Oliver, J.D., Sutton, A.T., Karu, N., Phillips, M., Markham, J., Peiris, P., Hilder, E.F., and Castignolles, P., *Simple and robust monitoring of ethanol fermentations by capillary electrophoresis.* Biotechnology and Applied Biochemistry, 2015, **62**(3): p. 329-342.
100. Thevarajah, J.J., Gaborieau, M., and Castignolles, P., *Separation and Characterization of Synthetic Polyelectrolytes and Polysaccharides with Capillary Electrophoresis.* Advances in Chemistry, 2014, **2014**: p. Article ID 798503.
101. Quigley, W.W.C. and Dovichi, N.J., *Capillary Electrophoresis for the Analysis of Biopolymers.* Analytical Chemistry, 2004, **76**(16): p. 4645-4658.
102. Grant, L.A., Ostenson, A.M., and Rayas-Duarte, P., *Determination of amylose and amylopectin of wheat starch using high performance size-exclusion chromatography (HPSEC).* Cereal Chemistry, 2002, **79**(6): p. 771-773.
103. Suortti, T. and Pessa, E., *Gel permeation chromatographic determination of starches using alkaline eluents.* Journal of Chromatography A, 1991, **536**: p. 251-254.
104. Roger, P., Baud, B., and Colonna, P., *Characterization of starch polysaccharides by flow field-flow fractionation–multi-angle laser light scattering–differential refractometer index.* Journal of Chromatography A, 2001, **917**(1–2): p. 179-185.
105. Herrero-Martínez, J.M., Schoenmakers, P.J., and Kok, W.T., *Determination of the amylose–amylopectin ratio of starches by iodine-affinity capillary electrophoresis.* Journal of Chromatography A, 2004, **1053**(1–2): p. 227-234.
106. Brewster, J.D. and Fishman, M.L., *Capillary electrophoresis of plant starches as the iodine complexes.* Journal of Chromatography A, 1995, **693**(2): p. 382-387.
107. Hong, M., Soini, H., and Novotny, M.V., *Affinity capillary electrophoretic studies of complexation between dextrin oligomers and polyiodides.* Electrophoresis, 2000, **21**(8): p. 1513-1520.

108. Schmitz, S., Dona, A.C., Castignolles, P., Gilbert, R.G., and Gaborieau, M., *Assessment of the Extent of Starch Dissolution in Dimethyl Sulfoxide by 1H NMR Spectroscopy.* Macromolecular Bioscience, 2009, **9**(5): p. 506-514.
109. El-Kafrawy, A., *Investigation of the cellulose/LiCl/dimethylacetamide and cellulose/LiCl/N-methyl-2-pyrrolidinone solutions by 13C NMR spectroscopy.* Journal of Applied Polymer Science, 1982, **27**(7): p. 2435-2443.
110. Spange, S., Reuter, A., Vilsmeier, E., Heinze, T., Keutel, D., and Linert, W., *Determination of empirical polarity parameters of the cellulose solvent N,N-dimethylacetamide/LiCl by means of the solvatochromic technique.* Journal of Polymer Science Part A: Polymer Chemistry, 1998, **36**(11): p. 1945-1955.
111. Snape, C.E., Morrison, W.R., Maroto-Valer, M.M., Karkalas, J., and Pethrick, R.A., *Solid state ^{13}C NMR investigation of lipid ligands in V-amylose inclusion complexes.* Carbohydrate Polymers, 1998, **36**(2–3): p. 225-237.
112. Thevarajah, J.J., Sutton, A.T., Maniego, A.R., Whitty, E.G., Cottet, H., Castignolles, P., and Gaborieau, M., *Quantifying the heterogeneity of chemical structures in complex charged polymers through the dispersity of their distributions of electrophoretic mobilities or of compositions.* Analytical Chemistry, 2016, **88**(3): p. 1674-1681.
113. Tan, I., Flanagan, B.M., Halley, P.J., Whittaker, A.K., and Gidley, M.J., *A Method for Estimating the Nature and Relative Proportions of Amorphous, Single, and Double-Helical Components in Starch Granules by 13C CP/MAS NMR.* Biomacromolecules, 2007, **8**(3): p. 885-891.
114. Agilent Technologies, *Chemstation A10.01*: Waldbronn, Germany.
115. OriginLab Corporation, *OriginPro 9.0*: Northhampton, MA, US.
116. Thevarajah, J.J., Bulanadi, J.C., Wagner, M., Gaborieau, M., and Castignolles, P., *Towards a less biased dissolution of chitosan.* Analytica Chimica Acta, 2016, **935**: p. 258-268.
117. Castignolles, P., Gaborieau, M., Hilder, E.F., Sprong, E., Ferguson, C.J., and Gilbert, R.G., *High-resolution separation of oligo(acrylic acid) by capillary zone electrophoresis.* Macromolecular Rapid Communications, 2006, **27**(1): p. 42-46.
118. de Gennes, P.-G., *Scaling Concepts in Polymer Physics*. 1st ed. 1979, Ithaca, United States: Cornell University Press. 319.
119. Han, J.-A. and Lim, S.-T., *Structural changes of corn starches by heating and stirring in DMSO measured by SEC-MALLS-RI system.* Carbohydrate Polymers, 2004, **55**(3): p. 265-272.
120. Langhorst, M.A., Stanley, F.W., Cutie, S.S., Sugarman, J.H., Wilson, L.R., Hoagland, D.A., and Prud'homme, R.K., *Determination of nonionic and partially hydrolyzed polyacrylamide molecular weight distributions using hydrodynamic chromatography.* Analytical Chemistry, 1986, **58**(11): p. 2242-2247.
121. Roger, P., Tran, V., Lesec, J., and Colonna, P., *Isolation and characterisation of single chain amylose.* Journal of Cereal Science, 1996, **24**(3): p. 247-262.
122. You, S. and Lim, S.-T., *Molecular characterization of corn starch using an aqueous HPSEC-MALLS-RI system under various dissolution and analytical conditions.* Cereal Chemistry Journal, 2000, **77**(3): p. 303-308.
123. Chamieh, J., Martin, M., and Cottet, H., *Quantitative analysis in capillary electrophoresis: Transformation of raw electropherograms into continuous distributions.* Analytical Chemistry, 2015, **87**(2): p. 1050-1057.
124. Stellwagen, N.C., Gelfi, C., and Righetti, P.G., *The free solution mobility of DNA.* Biopolymers, 1997, **42**(6): p. 687-703.
125. Oudhoff, K.A., Buijtenhuijs, F.A., Wijnen, P.H., Schoenmakers, P.J., and Kok, W.T., *Determination of the degree of substitution and its distribution of carboxymethylcelluloses by capillary zone electrophoresis.* Carbohydrate Research, 2004, **339**(11): p. 1917-24.

126. Cottet, H., Gareil, P., Theodoly, O., and Williams, C.E., *A semi-empirical approach to the modeling of the electrophoretic mobility in free solution: application to polystyrenesulfonates of various sulfonation rates.* Electrophoresis, 2000, **21**(17): p. 3529-40.
127. Gaborieau, M., Causon, T.J., Guillaneuf, Y., Hilder, E.F., and Castignolles, P., *Molecular weight and tacticity of oligoacrylates by capillary electrophoresis–mass spectrometry.* Australian Journal of Chemistry, 2010, **63**(8): p. 1219-1226.
128. Gilbert, R.G., Hess, M., Jenkins, A.L., Jones, G.R., Kratochvil, P., and Stepto, R.F.T., *Dispersity in Polymer Science.* Pure Applied Chemistry, 2009, **81**(2): p. 351-353.
129. Maniego, A.R., Ang, D., Guillaneuf, Y., Lefay, C., Gigmes, D., Aldrich-Wright, J.R., Gaborieau, M., and Castignolles, P., *Separation of poly(acrylic acid) salts according to topology using capillary electrophoresis in the critical conditions.* Analytical and Bioanalytical Chemistry, 2013, **405**(28): p. 9009-9020.
130. Ibrahim, A., Koval, D., Kašička, V., Faye, C., and Cottet, H., *Effective charge determination of dendrigraft poly-l-lysine by capillary isotachophoresis.* Macromolecules, 2013, **46**(2): p. 533-540.
131. Mnatsakanyan, M., Thevarajah, J.J., Roi, R.S., Lauto, A., Gaborieau, M., and Castignolles, P., *Separation of chitosan by degree of acetylation using simple free solution capillary electrophoresis.* Analytical and Bioanalytical Chemistry, 2013, **405**(21): p. 6873-6877.
132. Sutton, A.T., Read, E., Maniego, A.R., Thevarajah, J.J., Marty, J.-D., Destarac, M., Gaborieau, M., and Castignolles, P., *Purity of double hydrophilic block copolymers revealed by capillary electrophoresis in the critical conditions.* Journal of Chromatography A, 2014, **1372**: p. 187-195.
133. Camilleri, P., *History and Development of Capillary Electrophoresis*, in *Capillary Electrophoresis: Theory and Practice*, P. Camilleri, Editor. 2005, CRC Press. p. 1-22.
134. Cherney, L.T., Petrov, A.P., and Krylov, S.N., *One-dimensional approach to study kinetics of reversible binding of protein on capillary walls.* Analytical Chemistry, 2015, **87**(2): p. 1219-25.
135. Pei, L. and Lucy, C.A., *Insight into the stability of poly(diallydimethylammoniumchloride) and polybrene poly cationic coatings in capillary electrophoresis.* Journal of Chromatography A, 2014, **1365**: p. 226-233.
136. Pei, L. and Lucy, C.A., *Polymerized phospholipid bilayers as permanent coatings for small amine separations using mixed aqueous/organic capillary zone electrophoresis.* Journal of Chromatography A, 2012, **1267**: p. 80-88.
137. Camilleri, P., *Separation of peptides and proteins*, in *Capillary Electrophoresis: Theory and Practice*, P. Camilleri, Editor. 1997, CRC Press: Essex, United Kingdom.
138. Thevarajah, J.J., Bulanadi, J.C., Wagner, M., Gaborieau, M., and Castignolles, P., *Towards a less biased dissolution of chitosan.* Analytica Chimica Acta, 2016: p. In Press (Corrected Proof).
139. AACCI. Approved Methods of Analysis, *11th ed. Method 61-03.01, Amylose Content of Milled Rice*. 2011, AACC International: St. Paul, MN, U.S.A.
140. Fredriksson, H., Silverio, J., Andersson, R., Eliasson, A.C., and Aman, P., *The influence of amylose and amylopectin characteristics on gelatinization and retrogradation properties of different starches.* Carbohydrate Polymers, 1998, **35**(3-4): p. 119-134.
141. Gidley, M.J., Hanashiro, I., Hani, N.M., Hill, S.E., Huber, A., Jane, J.-L., Liu, Q., Morris, G.A., Rolland-Sabaté, A., Striegel, A.M., and Gilbert, R.G., *Reliable measurements of the size distributions of starch molecules in solution: Current dilemmas and recommendations.* Carbohydrate Polymers, 2010, **79**(2): p. 255-261.
142. Uliyanchenko, E., van der Wal, S., and Schoenmakers, P.J., *Challenges in polymer analysis by liquid chromatography.* Polymer Chemistry, 2012, **3**(9): p. 2313-2335.

143. Philipsen, H.J.A., *Determination of chemical composition distributions in synthetic polymers.* Journal of chromatography. A, 2004, **1037**(1-2): p. 329-350.
144. Thevarajah, J.J., Van Leeuwen, M.P., Cottet, H., Castignolles, P., and Gaborieau, M., *Determination of the distributions of the degrees of acetylation of chitosan.* International Journal of Biological Macromolecules, 2017, **95**: p. 40-48.
145. Schwartz, D. and Whistler, R.L., *Chapter 1 - History and future of starch*, in *Starch (Third Edition)*, J. BeMiller and R. Whistler, Editors. 2009, Academic Press: San Diego. p. 1-10.
146. Shrestha, A.K. and Halley, P.J., *Chapter 5 - Starch modification to develop novel starch-biopolymer blends: State of art and perspectives*, in *Starch Polymers*, P.J. Halley and L. Avérous, Editors. 2014, Elsevier: Amsterdam. p. 105-143.
147. Mason, W.R., *Chapter 20 - Starch use in foods*, in *Starch (Third Edition)*, J. BeMiller and R. Whistler, Editors. 2009, Academic Press: San Diego. p. 745-795.
148. Reddy, M.B. and Love, M., *The impact of food processing on the nutritional quality of vitamins and minerals*, in *Impact of Processing on Food Safety*, L.S. Jackson, M.G. Knize, and J.N. Morgan, Editors. 1999, Springer US: Boston, MA. p. 99-106.
149. Svihus, B., Uhlen, A.K., and Harstad, O.M., *Effect of starch granule structure, associated components and processing on nutritive value of cereal starch: A review.* Animal Feed Science and Technology, 2005, **122**(3–4): p. 303-320.
150. Wang, T.L., Bogracheva, T.Y., and Hedley, C.L., *Review article. Starch: as simple as A, B, C?* Journal of Experimental Botany, 1998, **49**(320): p. 481-502.
151. Lopez-Rubio, A., Flanagan, B.M., Gilbert, E.P., and Gidley, M.J., *A novel approach for calculating starch crystallinity and its correlation with double helix content: A combined XRD and NMR study.* Biopolymers, 2008, **89**(9): p. 761-768.
152. van Soest, J.J.G., Tournois, H., de Wit, D., and Vliegenthart, J.F.G., *Short-range structure in (partially) crystalline potato starch determined with attenuated total reflectance Fourier-transform IR spectroscopy.* Carbohydrate Research, 1995, **279**: p. 201-214.
153. Blazek, J. and Gilbert, E.P., *Application of small-angle X-ray and neutron scattering techniques to the characterisation of starch structure: A review.* Carbohydrate Polymers, 2011, **85**(2): p. 281-293.
154. Stuart, B., *Infrared Spectroscopy : Fundamentals and Applications*. 2004, Hoboken, NJ, USA: Wiley.
155. Reddy Gangidi, R. and Proctor, A., *Chapter 8 - Meat and Meat Products*, in *Infrared Spectroscopy for Food Quality Analysis and Control*, D.-W. Sun, Editor. 2009, Academic Press: San Diego. p. 179-214.
156. Fagan, C.C., O'Donnell, C.P., Rudzik, L., and Wüst, E., *Chapter 10 - Milk and dairy products*, in *Infrared Spectroscopy for Food Quality Analysis and Control*, D.-W. Sun, Editor. 2009, Academic Press: San Diego. p. 241-273.
157. Jespersen, B.M. and Munck, L., *Chapter 11 - Cereals and Cereal Products*, in *Infrared Spectroscopy for Food Quality Analysis and Control*, D.-W. Sun, Editor. 2009, Academic Press: San Diego. p. 275-319.
158. Lin, M., A Rasco, B., G Cavinato, A., and Al-Holy, M., *Chapter 6 - Infrared (IR) spectroscopy—near-infrared spectroscopy and mid-infrared spectroscopy*, in *Infrared Spectroscopy for Food Quality Analysis and Control*, D.-W. Sun, Editor. 2009, Academic Press: San Diego. p. 119-143.
159. Taylor, D.L., Thevarajah, J.J., Narayan, D.K., Murphy, P., Mangala, M.M., Lim, S., Wuhrer, R., Lefay, C., O'Connor, M.D., Gaborieau, M., and Castignolles, P., *Real-time monitoring of peptide grafting onto chitosan films using capillary electrophoresis.* Analytical and Bioanalytical Chemistry, 2015, **407**(9): p. 2543-2555.

160. Wilson, R.H., Kalichevsky, M.T., Ring, S.G., and Belton, P.S., *A fourier-transform infrared study of the gelation and retrogradation of waxy-maize starch.* Carbohydrate Research, 1987, **166**(1): p. 162-165.
161. Capron, I., Robert, P., Colonna, P., Brogly, M., and Planchot, V., *Starch in rubbery and glassy states by FTIR spectroscopy.* Carbohydrate Polymers, 2007, **68**(2): p. 249-259.
162. Lopez-Rubio, A., Flanagan, B.M., Shrestha, A.K., Gidley, M.J., and Gilbert, E.P., *Molecular rearrangement of starch during in vitro digestion: Toward a better understanding of enzyme resistant starch formation in processed starches.* Biomacromolecules, 2008, **9**(7): p. 1951-1958.
163. Sevenou, O., Hill, S.E., Farhat, I.A., and Mitchell, J.R., *Organisation of the external region of the starch granule as determined by infrared spectroscopy.* International Journal of Biological Macromolecules, 2002, **31**(1–3): p. 79-85.
164. Rubens, P. and Heremans, K., *Pressure–temperature gelatinization phase diagram of starch: An in situ Fourier transform infrared study.* Biopolymers, 2000, **54**(7): p. 524-530.
165. Dhital, S., Shrestha, A.K., Flanagan, B.M., Hasjim, J., and Gidley, M.J., *Cryo-milling of starch granules leads to differential effects on molecular size and conformation.* Carbohydrate Polymers, 2011, **84**(3): p. 1133-1140.
166. Warren, F.J., Gidley, M.J., and Flanagan, B.M., *Infrared spectroscopy as a tool to characterise starch ordered structure—a joint FTIR–ATR, NMR, XRD and DSC study.* Carbohydrate Polymers, 2016, **139**: p. 35-42.
167. Goodfellow, B.J. and Wilson, R.H., *A Fourier transform IR study of the gelation of amylose and amylopectin.* Biopolymers, 1990, **30**(13-14): p. 1183-1189.
168. Cael, S.J., Koenig, J.L., and Blackwell, J., *Infrared and raman spectroscopy of carbohydrates: Part III: raman spectra of the polymorphic forms of amylose.* Carbohydrate Research, 1973, **29**(1): p. 123-134.
169. Greenspan, L., *Humidity fixed points of binary saturated aqueous solutions.* Journal of Research of the National Bureau of Standards - A. Physics and Chemistry, 1977, **81A**(1): p. 89-96.
170. Bruker Optik GmbH, *Opus 7.5*: Rudolf-Plank-Straße, Ettlingen, Germany.
171. Subramanian, A. and Rodriguez-Saona, L., *Chapter 7 - Fourier Transform Infrared (FTIR) Spectroscopy*, in *Infrared Spectroscopy for Food Quality Analysis and Control*, D.-W. Sun, Editor. 2009, Academic Press: San Diego. p. 145-178.
172. Hermann, T.S. and Harvey, S.R., *Infrared spectroscopy at sub-ambient temperatures: I. Literature review.* Applied Spectroscopy, 1969, **23**(5): p. 435-450.
173. Caspary, R., *Infrared spectroscopy at low temperature for the improved resolution of spectra.* Applied Spectroscopy, 1968, **22**(6): p. 694-696.
174. Holland-moritz, K. and Siesler, H.W., *Infrared spectroscopy of polymers.* Applied Spectroscopy Reviews, 1976, **11**(1): p. 1-55.
175. Hermann, T.S., Harvey, S.R., and Honts, C.N., *Infrared spectroscopy at sub-ambient temperatures: II. Pure molecules.* Applied Spectroscopy, 1969, **23**(5): p. 451-460.
176. Zeleznak, K. and Hoseney, R., *The Glass Transition in Starch.* Cereal Chemistry, 1987, **64**(2): p. 121-124.
177. Stanjek, H. and Häusler, W., *Basics of X-ray Diffraction.* Hyperfine Interactions, 2004, **154**(1-4): p. 107-119.
178. Ribotta, P., Cuffini, S., León, A., and Añón, M., *The staling of bread: an X-ray diffraction study.* European Food Research and Technology, 2004, **218**(3): p. 219-223.
179. Ji, Y., Zhu, K., Zhou, H., and Qian, H., *Study of the retrogradation behaviour of rice cake using rapid visco analyser, Fourier transform infrared spectroscopy and X-ray analysis.* International Journal of Food Science & Technology, 2010, **45**(5): p. 871-876.

180. Shrestha, A.K., Blazek, J., Flanagan, B.M., Dhital, S., Larroque, O., Morell, M.K., Gilbert, E.P., and Gidley, M.J., *Molecular, mesoscopic and microscopic structure evolution during amylase digestion of maize starch granules.* Carbohydrate Polymers, 2012, **90**(1): p. 23-33.
181. Morrison, W.R., Law, R.V., and Snape, C.E., *Evidence for inclusion complexes of lipids with v-amylose in maize, rice and oat starches.* Journal of Cereal Science, 1993, **18**(2): p. 107-109.
182. Dhital, S., Shrestha, A.K., and Gidley, M.J., *Relationship between granule size and in vitro digestibility of maize and potato starches.* Carbohydrate Polymers, 2010, **82**(2): p. 480-488.
183. Nara, S., Mori, A., and Komiya, T., *Study on relative crystallinity of moist potato starch.* Starch - Stärke, 1978, **30**(4): p. 111-114.
184. Chung, H.-J., Liu, Q., Lee, L., and Wei, D., *Relationship between the structure, physicochemical properties and in vitro digestibility of rice starches with different amylose contents.* Food Hydrocolloids, 2011, **25**(5): p. 968-975.
185. Teng, A., Witt, T., Wang, K., Li, M., and Hasjim, J., *Molecular rearrangement of waxy and normal maize starch granules during in vitro digestion.* Carbohydrate Polymers, 2016, **139**: p. 10-19.
186. Paris, M., Bizot, H., Emery, J., Buzaré, J.Y., and Buléon, A., *Crystallinity and structuring role of water in native and recrystallized starches by 13C CP-MAS NMR spectroscopy: 1: Spectral decomposition.* Carbohydrate Polymers, 1999, **39**(4): p. 327-339.
187. Bruker AXS GmbH, *TOPAS 3*: Karlsruhe, Germany.
188. WaveMetrics Inc., *Igor Pro 6.37*: Lake Oswego, OR, USA.
189. Marquardt, D.W., *An algorithm for least-squares estimation of nonlinear parameters.* Journal of the Society for Industrial and Applied Mathematics, 1963, **11**(2): p. 431-441.
190. Cameron, R.E. and Donald, A.M., *A small-angle X-ray scattering study of the annealing and gelatinization of starch.* Polymer, 1992, **33**(12): p. 2628-2635.
191. Waigh, T.A., Jenkins, P.J., and Donald, A.M., *Quantification of water in carbohydrate lamellae using SANS.* Faraday Discussions, 1996, **103**: p. 325-337.
192. Waigh, T.A., Kato, K.L., Donald, A.M., Gidley, M.J., Clarke, C.J., and Riekel, C., *Side-chain liquid-crystalline model for starch.* Starch - Stärke, 2000, **52**(12): p. 450-460.
193. Yuryev, V.P., Krivandin, A.V., Kiseleva, V.I., Wasserman, L.A., Genkina, N.K., Fornal, J., Blaszczak, W., and Schiraldi, A., *Structural parameters of amylopectin clusters and semi-crystalline growth rings in wheat starches with different amylose content.* Carbohydrate Research, 2004, **339**(16): p. 2683-91.
194. Saibene, D. and Seetharaman, K., *Amylose involvement in the amylopectin clusters of potato starch granules.* Carbohydrate Polymers, 2010, **82**(2): p. 376-383.
195. Koberstein, J.T. and Stein, R.S., *Small-angle x-ray scattering measurements of diffuse phase-boundary thicknesses in segmented polyurethane elastomers.* Journal of Polymer Science: Polymer Physics Edition, 1983, **21**(10): p. 2181-2200.
196. Strobl, G.R. and Schneider, M., *Direct evaluation of the electron density correlation function of partially crystalline polymers.* Journal of Polymer Science: Polymer Physics Edition, 1980, **18**(6): p. 1343-1359.
197. Schmidt-Rohr, K., *Simulation of small-angle scattering curves by numerical Fourier transformation.* Journal of Applied Crystallography, 2007, **40**(1): p. 16-25.
198. Verma, R., Marand, H., and Hsiao, B., *Morphological changes during secondary crystallization and subsequent melting in poly(ether ether ketone) as studied by real time small angle X-ray scattering.* Macromolecules, 1996, **29**(24): p. 7767-7775.
199. Vonk, C., *Investigation of non-ideal two-phase polymer structures by small-angle X-ray scattering.* Journal of Applied Crystallography, 1973, **6**(2): p. 81-86.

200. Wang, Z.-G., Hsiao, B.S., and Murthy, N.S., *Comparison of intensity profile analysis and correlation function methods for studying the lamellar structures of semi-crystalline polymers using small-angle X-ray scattering.* Journal of Applied Crystallography, 2000, **33**(3 Part 1): p. 690-694.
201. Salman, H., Blazek, J., Lopez-Rubio, A., Gilbert, E.P., Hanley, T., and Copeland, L., *Structure–function relationships in A and B granules from wheat starches of similar amylose content.* Carbohydrate Polymers, 2009, **75**(3): p. 420-427.
202. Vermeylen, R., Goderis, B., Reynaers, H., and Delcour, J.A., *Gelatinisation related structural aspects of small and large wheat starch granules.* Carbohydrate Polymers, 2005, **62**(2): p. 170-181.
203. Bayer, R.K. and Baltá-Calleja, F.J., *Nanostructure of Potato Starch, Part I: Early Stages of Retrogradation of Amorphous Starch in Humid Atmosphere as Revealed by Simultaneous SAXS and WAXS.* International Journal of Polymeric Materials and Polymeric Biomaterials, 2006, **55**(10): p. 773-788.
204. Vermeylen, R., Goderis, B., and Delcour, J.A., *An X-ray study of hydrothermally treated potato starch.* Carbohydrate Polymers, 2006, **64**(2): p. 364-375.
205. Sanderson, J.S., Daniels, R.D., Donald, A.M., Blennow, A., and Engelsen, S.B., *Exploratory SAXS and HPAEC-PAD studies of starches from diverse plant genotypes.* Carbohydrate Polymers, 2006, **64**(3): p. 433-443.
206. Petoukhov, M.V., Franke, D., Shkumatov, A.V., Tria, G., Kikhney, A.G., Gajda, M., Gorba, C., Mertens, H.D.T., Konarev, P.V., and Svergun, D.I., *New developments in the ATSAS program package for small-angle scattering data analysis.* Journal of Applied Crystallography, 2012, **45**(2): p. 342-350.
207. Kline, S., *Reduction and analysis of SANS and USANS data using IGOR Pro.* Journal of Applied Crystallography, 2006, **39**(6): p. 895-900.
208. Zhu, L.-J., Liu, Q.-Q., Wilson, J.D., Gu, M.-H., and Shi, Y.-C., *Digestibility and physicochemical properties of rice (Oryza sativa L.) flours and starches differing in amylose content.* Carbohydrate Polymers, 2011, **86**(4): p. 1751-1759.
209. Frei, M., Siddhuraju, P., and Becker, K., *Studies on the in vitro starch digestibility and the glycemic index of six different indigenous rice cultivars from the Philippines.* Food Chemistry, 2003, **83**(3): p. 395-402.
210. Benmoussa, M., Moldenhauer, K.A.K., and Hamaker, B.R., *Rice amylopectin fine structure variability affects starch digestion properties.* Journal of Agricultural and Food Chemistry, 2007, **55**(4): p. 1475-1479.
211. Bergman, C.J., Bhattacharya, K.R., and Ohtsubo, K., *Chapter 15: Rice end-use quality analysis*, in *Rice: Chemistry and Technology*. 2004, American Association of Cereal Chemists, Inc. p. 415-472.
212. Juliano, B.O. *The chemical basis of rice grain quality*. in *Proceedings of the workshop on chemical apsects of rice grain quality*. 1979. Los Banos, Laguna, Philippines: International Rice Research Institute.
213. Ward, R.M., *Potential impact of temperature and carbon dioxide levels on rice quality*,Doctor of Philosophy thesis, The University of Sydney, Sydney, Australia, 2007
214. Chen, M.-H., Bergman, C., Pinson, S., and Fjellstrom, R., *Waxy gene haplotypes: Associations with apparent amylose content and the effect by the environment in an international rice germplasm collection.* Journal of Cereal Science, 2008, **47**(3): p. 536-545.
215. Sano, Y., *Differential regulation of waxy gene expression in rice endosperm.* Theoretical and Applied Genetics, 1984, **68**(5): p. 467-73.
216. Hirano, H.Y., Eiguchi, M., and Sano, Y., *A single base change altered the regulation of the Waxy gene at the posttranscriptional level during the domestication of rice.* Molecular Biology and Evolution, 1998, **15**(8): p. 978-87.

217. Toutounji, M.R., *Molecular characterisation of breakfast cereals and rice to understand their digestibility*,Master of Science (Honours) thesis, University of Western Sydney, Sydney, Australia, 2015
218. Brand-Miller, J.C. *The International Glycemic Index (GI) Database*. 2012 [cited August 2015]; Available from: http://www.glycemicindex.com/foodSearch.php.
219. Syahariza, Z.A., Sar, S., Hasjim, J., Tizzotti, M.J., and Gilbert, R.G., *The importance of amylose and amylopectin fine structures for starch digestibility in cooked rice grains.* Food Chemistry, 2013, **136**(2): p. 742-749.
220. El Seoud, O.A., Koschella, A., Fidale, L.C., Dorn, S., and Heinze, T., *Applications of ionic liquids in carbohydrate chemistry: A window of opportunities.* Biomacromolecules, 2007, **8**(9): p. 2629-2647.
221. Marsh, K.N., Boxall, J.A., and Lichtenthaler, R., *Room temperature ionic liquids and their mixtures—a review.* Fluid Phase Equilibria, 2004, **219**(1): p. 93-98.
222. Nilsson, L., *Starch and other polysaccharides*, in *Field-Flow Fractionation in Biopolymer Analysis*, R.S.K. Williams and D.K. Caldwell, Editors. 2012, Springer Vienna: Vienna. p. 165-185.
223. Wahlund, K.-G., Leeman, M., and Santacruz, S., *Size separations of starch of different botanical origin studied by asymmetrical-flow field-flow fractionation and multiangle light scattering.* Analytical and Bioanalytical Chemistry, 2011, **399**(4): p. 1455-1465.
224. Ahmed, N., Tetlow, I.J., Nawaz, S., Iqbal, A., Mubin, M., Nawaz ul Rehman, M.S., Butt, A., Lightfoot, D.A., and Maekawa, M., *Effect of high temperature on grain filling period, yield, amylose content and activity of starch biosynthesis enzymes in endosperm of basmati rice.* Journal of the Science of Food and Agriculture, 2015, **95**(11): p. 2237-2243.
225. Gidley, M.J. and Bociek, S.M., *Molecular organisation in starches: a 13C CP/MAS NMR study.* Journal of the American Chemistry Society, 1985, **107**: p. 7040-7044.